Supramolecular chemistry from small molecules to cavitands: Predictive and experimental approaches

by

Nandini Sarkar

B.S., University of Delhi, 2013
M.S., Indian Institute of Engineering Science and Technology, 2015

AN ABSTRACT OF A DISSERTATION

submitted in partial fulfillment of the requirements for the degree

DOCTOR OF PHILOSOPHY

Department of Chemistry
College of Arts and Sciences

KANSAS STATE UNIVERSITY
Manhattan, Kansas

2020

Abstract

We used the hydrogen-bond propensity (HBP) protocol for predicting if a co-crystal would form or not for six different target molecules in combination with 25 potential co-formers each. The correct outcome was successfully predicated 92-95% of the time, which indicates that for a series of small molecules, HBP is a very reliable indicator for determining if a co-crystal will form.

In order to examine if hydrogen and halogen-bonded systems can mimic each other, we conducted co-crystallization experiments using eight targets in combination with 25 co-formers. Molecular electrostatic potential surface (MEPS) calculations were used to guide the experimental space. The results suggested that in all the cases, hydrogen and halogen-bonds mimic each other. Validation studies of MEPS gave a prediction accuracy range of 64-84%.

Three different factors, hydrogen-bond propensity (HBP), hydrogen-bond coordination (HBC), and hydrogen-bond energies (HBE), were evaluated to predict the experimental outcomes of attempted co-crystallizations between two known drug molecules, Nevirapine and Diclofenac, and a series of potential co-formers. HBP gave the correct result in 26 out of 30 cases, whereas the HBC method predicted the correct outcome in 22 out of 30 cases. Finally, HBE gave the correct result in 23 out of 30 experiments. In those cases, where the crystal structure of a co-crystal of either Nevirapine or Diclofenac was known, we also examined how well the three methods predicted which primary hydrogen-bond interactions were present in the crystal structure. HBP correctly predicted 6 out of 6 cases, HBC could not predict any of the synthon formations correctly, and HBE successfully predicted 1 out of 6 cases.

Three different factors, hydrogen-bond propensity (HBP), hydrogen-bond energy (HBE), and molecular complementarity (MC), were used for predicting co-crystallization outcomes of seven active pharmaceutical ingredients (APIs) in combination with 42 potential co-formers. Validation studies indicate that individually the methods did not offer high accuracy. Hence, we implemented a combination of methods using Venn diagrams. The results suggested that the combination of MC and HBP method yielded the highest accuracy of 80%.

In order to ease the complexity of the predictive approaches, we designed CoForm, an automatic app for predicting co-crystallization outcomes. CoForm was used to predict co-crystallization outcomes for Loratadine and Desloratadine in combination with 42 generally regarded as safe (GRAS) list co-formers. The predictive abilities of CoForm were compared to commercially available tools such as HBP and MC. The results indicate that CoForm delivered a success rate of 80% for both Loratadine and Desloratadine in comparison to HBP 76% and 54%, respectively, and MC 39% and 22%, respectively.

Six cavitands were synthesized to explore the guest encapsulation via cavity inclusion, using five solvents (xylene, dichloromethane, ethyl acetate, acetonitrile, and dimethyl sulfoxide) with varying dipole moment as a potential guest. Cavity inclusion studies indicated that the cavitands could encapsulate a guest in five different orientations, with stoichiometries 1:1 to 1:2. A selectivity study showed that the cavitands were more selective towards DMSO, which also had the highest dipole moment.

Finally, cavitands were used as molecular containers for fragrant compounds and heterocyclic-N-oxides. In both cases, the host interacted with guests in 1:2 stoichiometry, as indicated by NMR titrations and TGA analysis. The host-guest interaction of cavitands with fragrant compounds lowered the volatility of the fragrant compounds from 5-10 mins to over a month.

Supramolecular chemistry from small molecules to cavitands: Predictive and experimental approaches

by

Nandini Sarkar

B.S., University of Delhi, 2013
M.S., Indian Institute of Engineering Science and Technology, 2015

A DISSERTATION

submitted in partial fulfillment of the requirements for the degree

DOCTOR OF PHILOSOPHY

Department of Chemistry
College of Arts and Sciences

KANSAS STATE UNIVERSITY
Manhattan, Kansas

2020

Approved by:

Major Professor

Christer B. Aakeröy

Abstract

We used the hydrogen-bond propensity (HBP) protocol for predicting if a co-crystal would form or not for six different target molecules in combination with 25 potential co-formers each. The correct outcome was successfully predicated 92-95% of the time, which indicates that for a series of small molecules, HBP is a very reliable indicator for determining if a co-crystal will form.

In order to examine if hydrogen and halogen-bonded systems can mimic each other, we conducted co-crystallization experiments using eight targets in combination with 25 co-formers. Molecular electrostatic potential surface (MEPS) calculations were used to guide the experimental space. The results suggested that in all the cases, hydrogen and halogen-bonds mimic each other. Validation studies of MEPS gave a prediction accuracy range of 64-84%.

Three different factors, hydrogen-bond propensity (HBP), hydrogen-bond coordination (HBC), and hydrogen-bond energies (HBE), were evaluated to predict the experimental outcomes of attempted co-crystallizations between two known drug molecules, Nevirapine and Diclofenac, and a series of potential co-formers. HBP gave the correct result in 26 out of 30 cases, whereas the HBC method predicted the correct outcome in 22 out of 30 cases. Finally, HBE gave the correct result in 23 out of 30 experiments. In those cases, where the crystal structure of a co-crystal of either Nevirapine or Diclofenac was known, we also examined how well the three methods predicted which primary hydrogen-bond interactions were present in the crystal structure. HBP correctly predicted 6 out of 6 cases, HBC could not predict any of the synthon formations correctly, and HBE successfully predicted 1 out of 6 cases.

Three different factors, hydrogen-bond propensity (HBP), hydrogen-bond energy (HBE), and molecular complementarity (MC), were used for predicting co-crystallization outcomes of seven active pharmaceutical ingredients (APIs) in combination with 42 potential co-formers. Validation studies indicate that individually the methods did not offer high accuracy. Hence, we implemented a combination of methods using Venn diagrams. The results suggested that the combination of MC and HBP method yielded the highest accuracy of 80%.

In order to ease the complexity of the predictive approaches, we designed CoForm, an automatic app for predicting co-crystallization outcomes. CoForm was used to predict co-crystallization outcomes for Loratadine and Desloratadine in combination with 42 generally regarded as safe (GRAS) list co-formers. The predictive abilities of CoForm were compared to commercially available tools such as HBP and MC. The results indicate that CoForm delivered a success rate of 80% for both Loratadine and Desloratadine in comparison to HBP 76% and 54%, respectively, and MC 39% and 22%, respectively.

Six cavitands were synthesized to explore the guest encapsulation via cavity inclusion, using five solvents (xylene, dichloromethane, ethyl acetate, acetonitrile, and dimethyl sulfoxide) with varying dipole moment as a potential guest. Cavity inclusion studies indicated that the cavitands could encapsulate a guest in five different orientations, with stoichiometries 1:1 to 1:2. A selectivity study showed that the cavitands were more selective towards DMSO, which also had the highest dipole moment.

Finally, cavitands were used as molecular containers for fragrant compounds and heterocyclic-N-oxides. In both cases, the host interacted with guests in 1:2 stoichiometry, as indicated by NMR titrations and TGA analysis. The host-guest interaction of cavitands with fragrant compounds lowered the volatility of the fragrant compounds from 5-10 mins to over a month.

Table of Contents

List of Figures

List of Tables

List of Schemes

Glossary of terms

Hydrogen-bond Coordination (HBC): It is a structure informatics-based model which indicates how many coordination numbers a hydrogen-bond donor and acceptor can form.

Hydrogen-bond Energy (HBE): It is simple model based on molecular electrostatic potential surfaces (MEPS) to calculate the interaction energies between a hydrogen-bond donor and acceptor.

Hydrogen-bond Propensity (HBP): It is the probability of formation of a hydrogen-bond interaction based on structure informatics of more than a million structures present in Cambridge Structural Database (CSD).

Molecular Complementarity (MC): It is a structure informatics-based model, which indicates if a given pair of molecules have complementary shape and size to result in a dense structure with minimum volume.

Acknowledgements

This work was carried out at the Department of Chemistry, Kansas State University during years 2015-2020. These years were the most demanding, frustrating and stressful of my life, but at the same time, they have been the most rewarding, exciting and unforgettable. During this journey I have met a lot of great people, who I want to express my sincere gratitude.

First and foremost, I want to express my deepest gratitude to my supervisor, Prof. Christer B. Aakeröy, for providing me with the opportunity to be a part of his group and introducing me into the exciting world of supramolecular chemistry. I am grateful for all the advice, support, patience, and encouragement throughout my five years of PhD. I am thankful for his continuous motivation and attention that have helped me shape into a better researcher, presenter and writer. I am fortunate to be a part of his group and could not have asked for a better mentor. Finally, all of this work could not have been possible without Dr. Aakeröy's sense of humor and his ability to lighten the mood in a high stress environment.

I would also like to thank my Ph.D. advisory committee; Professor Larry Erickson for accepting to be a part of my committee at the very last moment, Professor Tendai Gadzikwa for her immense support and guidance. Professor Paul Smith and Professor Bret Flanders for their invaluable time and encouragement.

I would also like to extend a special thank you to Professor Eric Matta and Dr. Emily McLaurin for helping me widen my knowledge in Chemistry.

I also wish to extend my deepest gratitude to Dr. Victor Day, Marijana Đaković, and Dr. Abhijeet Sinha for all the crystal structures mentioned in this thesis and for their patience and valuable inputs.

I also want to acknowledge Dr. Yasmin Patell, for being a very supportive teaching mentor and a caring friend, Dr. Simon Sham (for helping me with NMR), Mr. Ron Jackson (for fixing broken instruments and talks), Mr. Tobe Eggers (for fixing broken instruments), Mr. Michael Hinton (for

teaching me lab skills), Mr. Jim Hodgson (for fixing broken glassware), Ms. Mary Dooley and Ms. Kimberly Ross for making my research life smooth at K-State.

My deepest gratitude to all the present and past Aakeröy group members for always being there as friends, family and colleagues. I will cherish all our wonderful times and memories. A special thank you to Dr. Janaka for being my mentor and a great friend. Thank you to my two pillars in the Chemistry Department; Dr. Bhupinder Sandhu and Ayyappan Elangovan for always being there and helping me in every step.

My heartful gratitude to my parents and brother for their endless support and providing me with this opportunity to study abroad. This would not be possible without you! Your immense sacrifices and understanding have helped me overcome any obstacle in life and made me a better person.

I want to thank my partner Joy for supporting and collaborating with me whenever possible. I would also like to thank my friends in Manhattan for being a family away from home and making this journey enjoyable.

Finally, I would like to thank Phi Lambda Upsilon (PLU), Graduate student council (GSC), International Coordinating Council (ICC), and Indian Student association (ISA) for giving me an opportunity to serve the K-State community.

Dedication

To my mother, father and brother!

For their continuous love and support…

Preface

Research carried out in Kansas State University for this dissertation led to the following publications in scientific journals:

1. Sarkar, N.; Sinha, A. S.; Aakeröy, C. B. Systematic Investigation of Hydrogen-Bond Propensities for Informing Co-Crystal Design and Assembly. *CrystEngComm* **2019**. https://doi.org/10.1039/C9CE01196J.

2. Sarkar, N..; Aakeröy, C. B.. Evaluating hydrogen-bond propensity, hydrogen-bond coordination and hydrogen-bond energy as tools for predicting the outcome of attempted co-crystallization. *Supramolecular Chemistry* **2019**, DOI: 10.1080/10610278.2019.1693043.

3. Sarkar, Mitra, Aakeröy, et al. CoForm: An Automated Technique for Predicting Co-crystals. Patent Application filed April 2019. Patent Pending.

Chapter 1 – Introduction

1.1. Structure-property relationship

A relationship between structure and property was investigated in the pioneering research by Wiener[1,2], where the boiling points varied with molecular bulk and branching[3]. Since then the study of structure-property relationships has played an essential role in all fields including chemistry, environmental studies, biology, biochemistry, and engineering. The crystal structure of a compound is dependent on the crystallization process which yields crystals of different sizes and morphologies that can impact its solubility, and physical and chemical stability[4].

The importance of structure-property relationship is identified specifically in pharmaceutics as in the case of antiviral compound ritonavir. Ritonavir, marketed as Norvir in 1996, is a semi-solid capsule for treatment of Acquired Immunodeficiency Syndrome (AIDS)[5]. In 1998, several capsules of Norvir failed the dissolution experiment, upon examination a new structural arrangement (polymorph) was identified[6]. The new polymorph had completely different properties compared to Norvir's original form. This led to Norvir being removed from the market, resulting in huge loss of money and time, Figure 1.1.

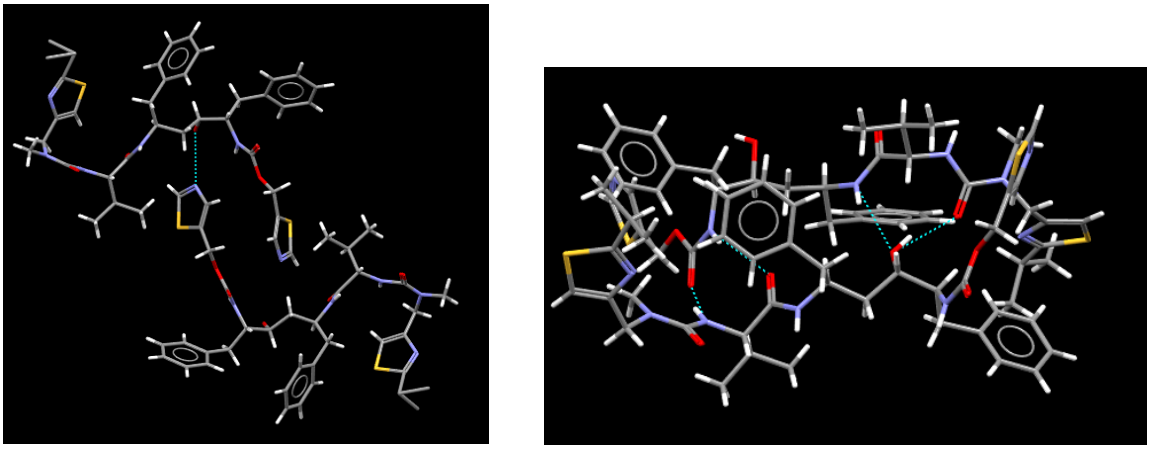

Figure 1.1. Different structural arrangement of Norvir, Form I (left), Form II (right)[5].

In order to achieve the desired properties in a compound either covalent modification or supramolecular syntheses via non-covalent interactions needs to be carried out.

1.2. Covalent *vs* supramolecular syntheses

Covalent synthesis involves making or breaking of a covalent bond in a reaction to isolate products with desired yield[7]. Covalent synthesis has been carried out over many years by organic chemists to understand the structure, reactivity, and pathways to produce better yields, Figure 1.2.

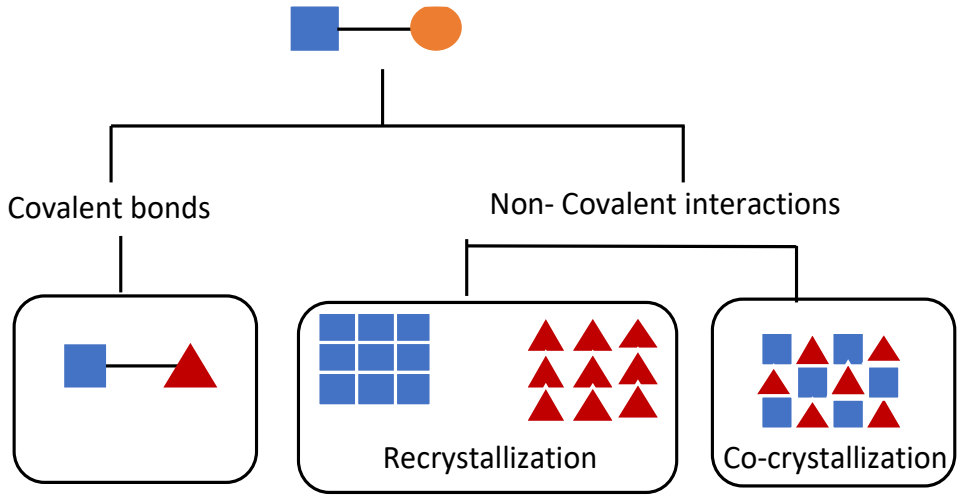

Figure 1.2. Covalent vs supramolecular syntheses.

Supramolecular synthesis, on the other hand, is a newer concept which is defined as the chemistry of non-covalent bonds. Supramolecular chemistry grew exponentially after the Nobel Prize in Chemistry 1987 was awarded to three of the pioneers, Charles Pedersen, Jean-Marie Lehn and Donald Cram[8]. The most common representative of a supramolecular system is a crystal lattice that is held together by weak non-covalent interactions between the molecules[9] some non-covalent interactions that play a role in supramolecular chemistry are hydrogen-bonds, halogen-bonds, π-π and van der waal's interactions, Table 1.1.

Table 1.1. Strength of intermolecular interactions.

Type of interactions	Strength (kJ/ mol)
Covalent bond	100-4400
Hydrogen bond	10-70
Halogen bond	5-180
π-π interaction	0-50
Van der Waal's interaction	<5

Crystal engineering involves strategies to organize different molecules in solid-state[10]. In a supramolecular synthesis the structure of a solid is dependent on the supramolecular synthon which is defined as[11], *a structural unit within a supermolecule which can be formed and/or assembled by known or conceivable synthetic operations involving intermolecular interactions*. Supramolecular interactions can be categorized as homomeric interactions, that occur within the individual molecules leading to re-crystallization; and heteromeric interactions which occur between different molecules leading to co-crystallization[12,13], Figure 1.2.

1.3. Co-crystallization

There is an extensive debate on the definition of co-crystals however, for the scope this dissertation we will define co-crystals as *solids that are crystalline single-phase materials composed of two or more different molecular compounds in a stoichiometric ratio*[14,15,16]. Co-crystallization is an attempt to bring forward a target with a potential partner, generally known as *co-former* within one periodic crystalline lattice via heteromeric interactions. The probability of formation of a co-crystal is around 1% since it is competing with a natural phenomenon of formation of homomeric interactions i.e. recrystallization, Figure 1.2.

The characterization of co-crystals is done by IR spectroscopy, TGA, DSC, single crystal X-ray crystallography, and powder X-ray diffraction[17,18,19]. The ability to form co-crystal is dependent on various factors such as solvent, stoichiometry, temperature, pressure, etc. Co-crystals are formed by breaking the homomeric interactions and subsequently replacing them with heteromeric interactions. The homomeric and heteromeric interactions are particularly non-covalent interactions, Table 1.1. In this dissertation we will focus on hydrogen and halogen bonds.

1.3.1. Hydrogen-bond based co-crystals

Hydrogen-bonds are the most commonly used intermolecular interactions for formation of co-crystals[20,21,22,23,24] due to their directionality and strength. Hence, even after a century of investigations it is still of utmost interest, which is reflected by the proposed change in the definition of hydrogen-bonds in 2011. A hydrogen bond (HB) is defined as[25] an *attractive interaction between a hydrogen atom from a molecule or a molecular fragment, X−H···A in which*

X is more electronegative than H, and an atom or a group of atoms in the same or different molecule, in which there is evidence of bond formation.

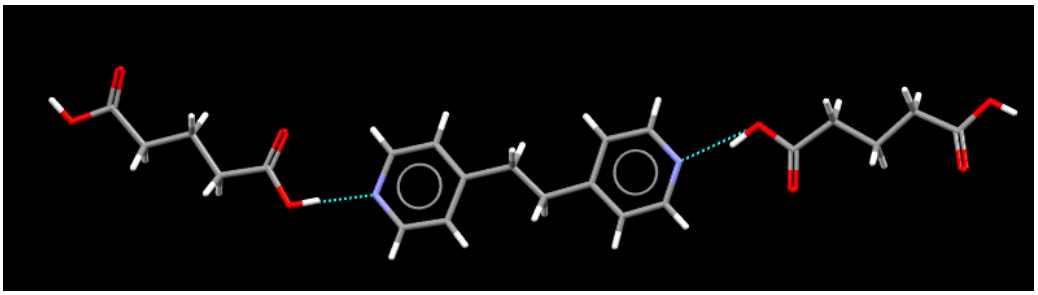

Figure 1.3. An example of a binary co-crystal between glutaric acid and 1,2-bis(4-pyridyl)ethane[26].

1.3.2. Halogen-bond based co-crystals

Halogen bonding is a non-covalent interaction, which is comparable in strength to hydrogen-bonds (~5-180 kJ/mol) and it has gained increasing importance in crystal engineering because of its effectiveness as a structure-directing force[27,28]. A halogen bond is defined as[29] *a net attractive interaction between an electrophilic region on a halogen atom X belonging to a molecule or a molecular fragment R–X (where R can be another atom, including X, or a group of atoms) and a nucleophilic region of a molecule, or molecular fragment, A–Z*[30,31,33], Figure 1.4.

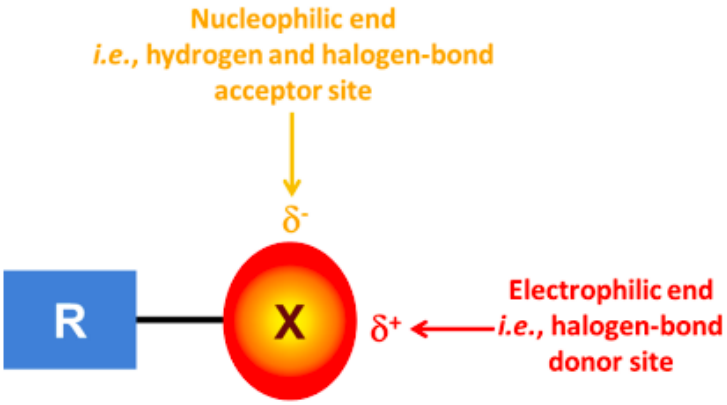

Figure 1.4. Representation of anisotropic distribution of electron density around covalently bound halogen atom[31,33].

An interesting feature of the halogen-bond is that the strength of this interaction can be effectively increased by "activating" the halogen atom ("σ-hole" activation) with electron withdrawing substituents or by introducing an *sp*-hybridized carbon next to the halogen atom[32,33].

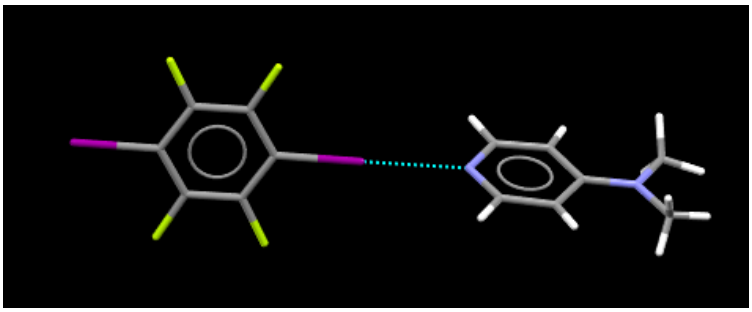

Figure 1.5. An example of a binary co-crystal between bis(N,N-dimethylpyridin-4-amine) 1,2,4,5-tetrafluoro-3,6-diiodobenzene[34].

1.4. Applications of co-crystallization

Co-crystallization and co-crystal-based approaches have been used to alter the physical properties of compounds relevant in pharmaceutics[35], energetic materials[36], agrochemicals[37], nutraceuticals[38], organic semiconductors[39], optoelectronic materials[40], ferroelectric materials[41,42], charge transfer complexes[43], non-linear optics[44,45], and liquid crystals[46]. Furthermore, co-crystallization can be applied in solid state solvent free synthesis[47], separation and purification processes[48], chiral resolution[49], and crystallization of non-solid compounds[50] to facilitate manufacturing processes.

1.4.1. Drug discovery and development timelines

Drug discovery and development timelines are risky, lengthy, and expensive. Typically, an investigation of more than 10,000 compounds is needed in order to deliver a single drug to the marketplace at the cost of approximately 1 billion dollars, Figure 1.6. What happens if a potentially useful drug fails to satisfy some critical characteristic physical demand, e.g., sufficient aqueous solubility and chemical stability[51,52]?

Figure 1.6. Drug discovery and development timeline.

There are various approaches that have been developed to improve bioavailability of the drugs such as particle size reduction, solid dispersion, complexation, salt formation, nanoparticles, self-emulsifying drug delivery system (SEDDS), addition of co-solvents, nano-suspension and emulsion and cocrystal formation[53,54]. Each technique has its own merits and demerits. Amongst all these techniques, co-crystallization is unique since it does not affect the pharmacological properties of the drug but may improve the drugs' bioavailability and also improve several of its physicochemical characteristics, such as melting point, tabletability, solubility, stability, bioavailability and permeability[55,56].

1.4.2. Agrochemical co-crystals

Agrochemicals such as pesticides, herbicides, insecticides, and fungicides, are important for crop production since they help in controlling pest for better quality and quantity of crops. The high solubility of many such chemicals in water make them susceptible to runoff in ground water where they cause environmental damage. Co-crystallization can be used to alter the physical properties of such chemicals by decreasing the water solubility, hygroscopicity, thermal stability, filterability and flowability and thereby affecting the overall usability and efficacy of a given agrochemical. Recent study by Bhupinder et al. shows the effect of co-crystallization in decreasing the water solubility of urea, commonly used as a pesticide[37], Figure 1.7.

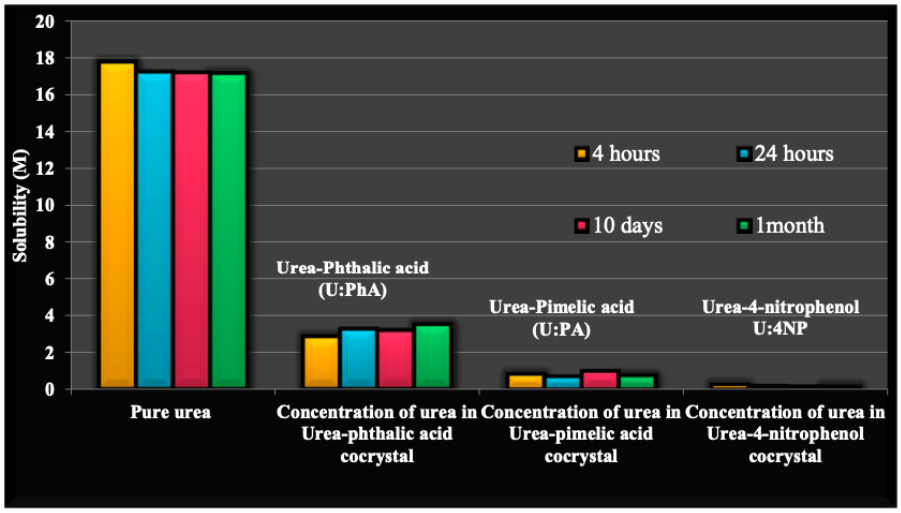

Figure 1.7. Solubility profile of urea and urea co-crystals[37].

1.5. Will it co-crystallize?

Co-crystal synthesis can be performed via several methods which includes slow solvent evaporation, slurry methods, liquid assisted grinding, melt, solution crystallizations, sonochemical methods[60], spray drying techniques, and co-sublimation techniques. Among all these methods, liquid assisted grinding has been reported to be the most cost-effective, green, and reliable method for discovery of new co-crystals[61].

In order to successfully make a co-crystal, the choice of an optimal co-former represents a key challenge, and the selection is typically driven by extensive screening experiments which can be both time consuming and costly. In order to facilitate the selection process and to reduce the amount of experimental work that is needed before a co-crystal can be made, there has been a growing interest in developing predictive methods that can help to narrow and inform the experimental search space. Various co-crystal prediction methodologies based on molecular electrostatic potentials[62,63], hydrogen bond energies (HBE)[64], pKa[65,66], Hansen solubility parameters[67], and lattice energy comparisons[68] are reported. Since more than a million small molecule crystal structures are available in the Cambridge Structural Database (CSD)[64,69,70,71], structure-informatics methods have considerable potential for being uniquely valuable for informing and guiding the screening efforts. Galek *et al* introduced hydrogen-bond propensity as a predictive tool[70,71] and Fábián used molecular shape and polarity to predict co-crystallization.[72,73]

1.6. Host-guest chemistry

Supramolecular chemistry has been developed for small, low molecular weight compounds (200-600 g/mol) to larger supramolecular building blocks with molecular weight (1000-1500 g/mol). Nature shows examples of elaborate complexes of proteins and nucleic acids to carry out transformations in the living cell, and these systems have been mimicked by synthetic chemistry as prototypes for *supramolecular machines*[74]. The first supramolecular host was a crown ether which was synthesized accidently by Pedersen[75]. Since then Lehn, Cram, and Pedersen carried out pioneering work on inclusion chemistry of molecular hosts such as crown ethers, cryptands, cavitands, and carcerands[76]. The synthesis of other scaffold such as spherands, pillararenes[77], cyclophanes, cryptophanes, calixarenes[78], cavitands[79,80], cyclodextrins[81], cucurbiturils[82] and more have been discovered in past few decades. These receptors can have high affinity and selectivity in binding due to the presence of pre-organized binding pockets. In a binding event, several non-covalent interactions play roles as the driving forces. Hence, they are good candidates to study the importance of structure-property relationships in molecular recognition. Figure 1.8 shows an example of different host-guest binding via non-covalent interactions.

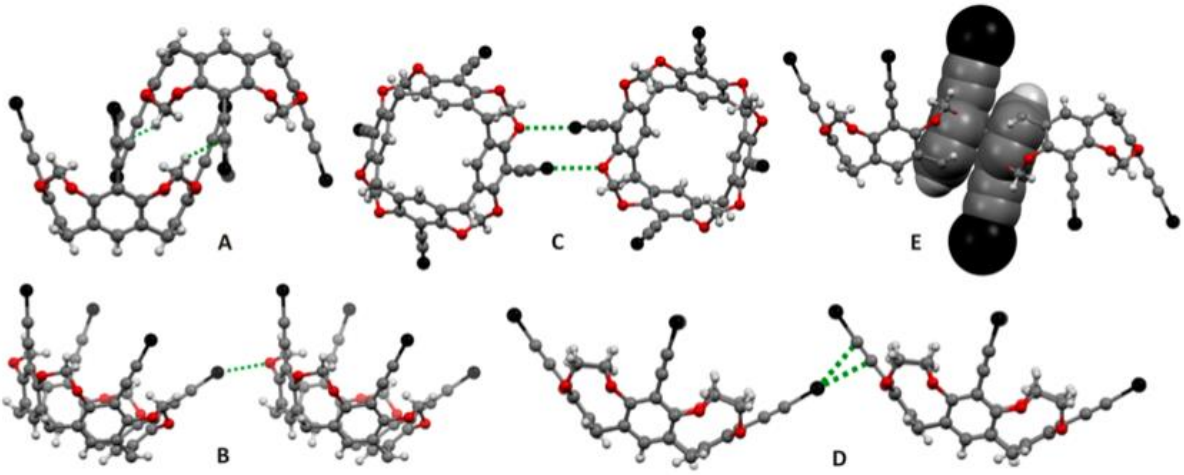

Figure 1.8. Weaker intermolecular binding motifs A = CH···π, B = X···O, C = $(X\cdots O)_2$, D = X···π, E = π···π previously observed in tetrahaloethynyl cavitands-ligand crystals[83].

1.7. Goals of the thesis

Over the past two decades the emergence of pharmaceutical co-crystals to develop better drugs with enhanced physiochemical properties has helped the pharmaceutical industry[84,85,86,87,88,89,90,91].

In 2013 (with updates from 2016 & 2018), USFDA (United States Food and Drug Administration) and in 2014, EMA (European Medical Agency) recognized co-crystals as a drug product.[54,92] To deliver pharmaceutical co-crystals with high value in minimum time, a systematic and reliable approach to the design of co-crystallization experiments is important. The significant step in designing co-crystallization experiments is identification of potential co-formers which might interact with the active pharmaceutical ingredient (API). First this thesis will explore the design, development, and evaluation of predictive methodologies that can guide the experimental space with high reliability. The second goal of this thesis is to employ the understanding of supramolecular synthetic strategies from small molecules to larger molecular receptors in order to probe molecular recognition events in solution.

This dissertation will focus on the following goals:

Chapter 2 describes a systematic investigation of hydrogen-bond propensity (HBP) for informing co-crystal design and assembly of 150 combinations of targets and co-formers, in comparison to experimentally observed outcomes.

Chapter 3 explores molecular electrostatic potential surface (MEPS) based selectivity for hydrogen and halogen bonded systems with similar molecular backbone.

Chapter 4 evaluates hydrogen-bond propensity (HBP), hydrogen-bond energy (HBE), and hydrogen-bond coordination (HBE) to predict co-crystal screening outcomes of two known drug molecules, Nevirapine and Diclofenac.

Chapter 5 focuses on validation studies of HBP, HBE and molecular complementarity (MC) for predicting co-crystallization outcomes of seven compounds that are larger and flexible, in combination with 42 GRAS list co-formers.

Chapter 6 will focus on design and development of CoForm, an automatic app for predicting co-crystallization outcomes, in comparison to commercially available tools, for Loratadine and Desloratadine in combination with 42 GRAS list co-formers.

Chapter 7 explores design and synthesis of functionalized cavitands for molecular recognition via cavity inclusion, of a series of solvent molecules with increasing dipole moment.

Chapter 8 describe synthesis of cavitands functionalized with hydrogen-bond donor and acceptor groups. The binding ability of these cavitands will be tested towards volatile fragrant compounds and heterocyclic-N-oxides.

1.8. References

(1) Wiener, H. Structural Determination of Paraffin Boiling Points. *J. Am. Chem. Soc.* **1947**, *69* (1), 17–20. https://doi.org/10.1021/ja01193a005.

(2) Wiener, H. Correlation of Heats of Isomerization, and Differences in Heats of Vaporization of Isomers, Among the Paraffin Hydrocarbons. *J. Am. Chem. Soc.* **1947**, *69* (11), 2636–2638. https://doi.org/10.1021/ja01203a022.

(3) Seybold, P. G.; May, M.; Bagal, U. A. Molecular Structure: Property Relationships. *J. Chem. Educ.* **1987**, *64* (7), 575. https://doi.org/10.1021/ed064p575.

(4) Thalladi, V. R.; Nüsse, M.; Boese, R. The Melting Point Alternation in α , ω - Alkanedicarboxylic Acids †. *J. Am. Chem. Soc.* **2000**, *122* (38), 9227–9236. https://doi.org/10.1021/ja0011459.

(5) Ritonavir: An Extraordinary Example of Conformational Polymorphism | SpringerLink https://link.springer.com/article/10.1023%2FA%3A1011052932607 (accessed Mar 10, 2020).

(6) Bauer, J.; Spanton, S.; Henry, R.; Quick, J.; Dziki, W.; Porter, W.; Morris, J. Ritonavir: An Extraordinary Example of Conformational Polymorphism. 8.

(7) Maat, L. Classics in Total Synthesis K.C. Nicolaou, E.J. Sorensen VCH, Weinheim 1996 ca. 700 Pp Hardcover DM 128.00/Softcover DM 78.00 ISBN 3-527-29284-5 / 3-527-29231-4. *Recueil des Travaux Chimiques des Pays-Bas* **1996**, *115* (11–12), 552–552. https://doi.org/10.1002/recl.19961151121.

(8) Supramolecular Chemistry and Heterocycles | Elsevier Enhanced Reader https://reader.elsevier.com/reader/sd/pii/B9780124095472053968?token=0B34F9B07D3C335EE87BF7B32D36850C6603E7D602A0F48FC0596F85B06D80DAC10397E3FE2D0E93FA72E9D9A6AC7586 (accessed Jan 7, 2020).

(9) Thalladi, V. R.; Goud, B. S.; Hoy, V. J.; Allen, F. H.; Howard, J. A. K.; Desiraju, G. R. Supramolecular Synthons in Crystal Engineering. Structure Simplification, Synthon Robustness and Supramolecular Retrosynthesis. *Chem. Commun.* **1996**, No. 3, 401–402. https://doi.org/10.1039/CC9960000401.

(10) Supramolecular Synthons in Crystal Engineering—A New Organic Synthesis - Desiraju - 1995 - Angewandte Chemie International Edition in English - Wiley Online Library https://onlinelibrary.wiley.com/doi/10.1002/anie.199523111 (accessed Mar 10, 2020).

(11) Thalladi, V. R.; Goud, B. S.; Hoy, V. J.; Allen, F. H.; Howard, J. A. K.; Desiraju, G. R. Supramolecular Synthons in Crystal Engineering. Structure Simplification, Synthon Robustness and Supramolecular Retrosynthesis. *Chem. Commun.* **1996**, No. 3, 401–402. https://doi.org/10.1039/CC9960000401.

(12) Mukherjee, A.; Desiraju, G. R. Combinatorial Exploration of the Structural Landscape of Acid–Pyridine Cocrystals. *Crystal Growth & Design* **2014**, *14* (3), 1375–1385. https://doi.org/10.1021/cg401851z.

(13) Friščić, T.; Trask, A. V.; Motherwell, W. D. S.; Jones, W. Guest-Directed Assembly of Caffeine and Succinic Acid into Topologically Different Heteromolecular Host Networks upon Grinding. *Crystal Growth & Design* **2008**, *8* (5), 1605–1609. https://doi.org/10.1021/cg700929e.

(14) Aakeröy, C. Is There Any Point in Making Co-Crystals? *Acta Crystallogr B Struct Sci Cryst Eng Mater* **2015**, *71* (4), 387–391. https://doi.org/10.1107/S2052520615010872.

(15) Dunitz, J. D. Crystal and Co-Crystal: A Second Opinion. *CrystEngComm* **2003**, *5* (91), 506–506. https://doi.org/10.1039/B315687G.

(16) Aakeröy, C. B.; Salmon, D. J. Building Co-Crystals with Molecular Sense and Supramolecular Sensibility. *CrystEngComm* **2005**, *7* (72), 439–448. https://doi.org/10.1039/B505883J.

(17) Wenger, M.; Bernstein, J. An Alternate Crystal Form of Gabapentin: A Cocrystal with Oxalic Acid. *Crystal Growth & Design* **2008**, *8* (5), 1595–1598. https://doi.org/10.1021/cg7008732.

(18) Basavoju, S.; Boström, D.; Velaga, S. P. Indomethacin–Saccharin Cocrystal: Design, Synthesis and Preliminary Pharmaceutical Characterization. *Pharm Res* **2008**, *25* (3), 530–541. https://doi.org/10.1007/s11095-007-9394-1.

(19) Preparation and Characterization of Theophylline−Nicotinamide Cocrystal | Organic Process Research & Development https://pubs.acs.org/doi/abs/10.1021/op900047r (accessed Mar 10, 2020).

(20) Jayasankar, A.; Somwangthanaroj, A.; Shao, Z. J.; Rodríguez-Hornedo, N. Cocrystal Formation during Cogrinding and Storage Is Mediated by Amorphous Phase. *Pharm Res* **2006**, *23* (10), 2381–2392. https://doi.org/10.1007/s11095-006-9110-6.

(21) Chakrabarty, R.; Mukherjee, P. S.; Stang, P. J. Supramolecular Coordination: Self-Assembly of Finite Two- and Three-Dimensional Ensembles. *Chem. Rev.* **2011**, *111* (11), 6810–6918. https://doi.org/10.1021/cr200077m.

(22) Aakeröy, C. B.; Chopade, P. D.; Desper, J. Avoiding "Synthon Crossover" in Crystal Engineering with Halogen Bonds and Hydrogen Bonds. *Crystal Growth & Design* **2011**, *11* (12), 5333–5336. https://doi.org/10.1021/cg2009013.

(23) Buckingham, A. D.; Del Bene, J. E.; McDowell, S. A. C. The Hydrogen Bond. *Chemical Physics Letters* **2008**, *463* (1–3), 1–10. https://doi.org/10.1016/j.cplett.2008.06.060.

(24) Lehn, J.-M. Toward Self-Organization and Complex Matter. *Science* **2002**, *295* (5564), 2400–2403. https://doi.org/10.1126/science.1071063.

(25) Arunan, E.; Desiraju, G. R.; Klein, R. A.; Sadlej, J.; Scheiner, S.; Alkorta, I.; Clary, D. C.; Crabtree, R. H.; Dannenberg, J. J.; Hobza, P.; Kjaergaard, H. G.; Legon, A. C.; Mennucci, B.; Nesbitt, D. J. Defining the Hydrogen Bond: An Account (IUPAC Technical Report). *Pure and Applied Chemistry* **2011**, *83* (8), 1619–1636. https://doi.org/10.1351/PAC-REP-10-01-01.

(26) Weyna, D. R.; Shattock, T.; Vishweshwar, P.; Zaworotko, M. J. Synthesis and Structural Characterization of Cocrystals and Pharmaceutical Cocrystals: Mechanochemistry vs Slow Evaporation from Solution. *Crystal Growth & Design* **2009**, *9* (2), 1106–1123. https://doi.org/10.1021/cg800936d.

(27) Halogen-Bonded Cocrystals of 4-(N,N-Dimethylamino)pyridine with Fluorinated Iodobenzenes | Crystal Growth & Design https://pubs.acs.org/doi/abs/10.1021/cg900823d (accessed Mar 11, 2020).

(28) Robertson, C. C.; Wright, J. S.; Carrington, E. J.; Perutz, R. N.; Hunter, C. A.; Brammer, L. Hydrogen Bonding vs. Halogen Bonding: The Solvent Decides. *Chem. Sci.* **2017**, *8* (8), 5392–5398. https://doi.org/10.1039/C7SC01801K.

(29) Desiraju, G. R.; Ho, P. S.; Kloo, L.; Legon, A. C.; Marquardt, R.; Metrangolo, P.; Politzer, P.; Resnati, G.; Rissanen, K. Definition of the Halogen Bond (IUPAC Recommendations

2013). *Pure Appl. Chem.* **2013**, *85* (8), 1711–1713. https://doi.org/10.1351/PAC-REC-12-05-10.

(30) Cavallo, G.; Metrangolo, P.; Milani, R.; Pilati, T.; Priimagi, A.; Resnati, G.; Terraneo, G. The Halogen Bond. *Chem. Rev.* **2016**, *116* (4), 2478–2601. https://doi.org/10.1021/acs.chemrev.5b00484.

(31) Kretz, W. J. A Computational Investigation of Halogen Bonding with Halomethanes and Their Group 14 Analogues; 2015.

(32) Aakeröy, C. B.; Baldrighi, M.; Desper, J.; Metrangolo, P.; Resnati, G. Supramolecular Hierarchy among Halogen-Bond Donors. *Chemistry – A European Journal* **2013**, *19* (48), 16240–16247. https://doi.org/10.1002/chem.201302162.

(33) Cavallo, G.; Metrangolo, P.; Milani, R.; Pilati, T.; Priimagi, A.; Resnati, G.; Terraneo, G. The Halogen Bond. *Chem. Rev.* **2016**, *116* (4), 2478–2601. https://doi.org/10.1021/acs.chemrev.5b00484.

(34) Wang; Ruimin; Hartnick; Daniel; Englert; Ulli. CCDC 1824725: Experimental Crystal Structure Determination, 2018. https://doi.org/10.5517/ccdc.csd.cc1z7s33.

(35) Shan, N.; Zaworotko, M. J. The Role of Cocrystals in Pharmaceutical Science. *Drug Discovery Today* **2008**, *13* (9), 440–446. https://doi.org/10.1016/j.drudis.2008.03.004.

(36) Cocrystal Engineering of a Prototype Energetic Material: Supramolecular Chemistry of 2,4,6-Trinitrotoluene | Crystal Growth & Design https://pubs.acs.org/doi/abs/10.1021/cg101300n (accessed Mar 10, 2020).

(37) Sandhu, B.; Sinha, A. S.; Desper, J.; Aakeröy, C. B. Modulating the Physical Properties of Solid Forms of Urea Using Co-Crystallization Technology. *Chem. Commun.* **2018**, *54* (37), 4657–4660. https://doi.org/10.1039/C8CC01144C.

(38) Sinha, A. S.; Maguire, A. R.; Lawrence, S. E. Cocrystallization of Nutraceuticals. *Crystal Growth & Design* **2015**, *15* (2), 984–1009. https://doi.org/10.1021/cg501009c.

(39) Sokolov, A. N.; Friščić, T.; Blais, S.; Ripmeester, J. A.; MacGillivray, L. R. Persistent One-Dimensional Face-to-Face π-Stacks within Organic Cocrystals. *Crystal Growth & Design* **2006**, *6* (11), 2427–2428. https://doi.org/10.1021/cg0605133.

(40) 朱伟钢甄永刚; Zhu Weigang, Z. Y. 有机共晶光电功能材料与器件. 化学进展 **2014**, *26* (08), 1292–1306. https://doi.org/10.7536/PC140339.

(41) Horiuchi, S.; Tokura, Y. Organic Ferroelectrics. *Nat Mater* **2008**, *7* (5), 357–366. https://doi.org/10.1038/nmat2137.

(42) Tayi, A. S.; Shveyd, A. K.; Sue, A. C.-H.; Szarko, J. M.; Rolczynski, B. S.; Cao, D.; Kennedy, T. J.; Sarjeant, A. A.; Stern, C. L.; Paxton, W. F.; Wu, W.; Dey, S. K.; Fahrenbach, A. C.; Guest, J. R.; Mohseni, H.; Chen, L. X.; Wang, K. L.; Stoddart, J. F.; Stupp, S. I. Room-Temperature Ferroelectricity in Supramolecular Networks of Charge-Transfer Complexes. *Nature* **2012**, *488* (7412), 485–489. https://doi.org/10.1038/nature11395.

(43) Zhu, W.; Zheng, R.; Zhen, Y.; Yu, Z.; Dong, H.; Fu, H.; Shi, Q.; Hu, W. Rational Design of Charge-Transfer Interactions in Halogen-Bonded Co-Crystals toward Versatile Solid-State Optoelectronics. *J. Am. Chem. Soc.* **2015**, *137* (34), 11038–11046. https://doi.org/10.1021/jacs.5b05586.

(44) Marder, S. R.; Perry, J. W.; Schaefer, W. P. Synthesis of Organic Salts with Large Second-Order Optical Nonlinearities. *Science* **1989**, *245* (4918), 626–628. https://doi.org/10.1126/science.245.4918.626.

(45) A Novel and Perfectly Aligned Highly Electro−Optic Organic Cocrystal of a Merocyanine Dye and 2,4-Dihydroxybenzaldehyde | Journal of the American Chemical Society https://pubs.acs.org/doi/10.1021/ja961087k (accessed Mar 11, 2020).

(46) Nguyen, H. L.; Horton, P. N.; Hursthouse, M. B.; Legon, A. C.; Bruce, D. W. Halogen Bonding: A New Interaction for Liquid Crystal Formation. *J. Am. Chem. Soc.* **2004**, *126* (1), 16–17. https://doi.org/10.1021/ja036994l.

(47) Hutchins, K. M.; Sumrak, J. C.; MacGillivray, L. R. Resorcinol-Templated Head-to-Head Photodimerization of a Thiophene in the Solid State and Unusual Edge-to-Face Stacking in a Discrete Hydrogen-Bonded Assembly. *Org. Lett.* **2014**, *16* (4), 1052–1055. https://doi.org/10.1021/ol4035403.

(48) Co-Crystallization as a Separation Technology: Controlling Product Concentrations by Co-Crystals | Crystal Growth & Design https://pubs.acs.org/doi/abs/10.1021/cg9010778 (accessed Mar 11, 2020).

(49) Springuel, G.; Leyssens, T. Innovative Chiral Resolution Using Enantiospecific Co-Crystallization in Solution. *Crystal Growth & Design* **2012**, *12* (7), 3374–3378. https://doi.org/10.1021/cg300307z.

(50) Golovanov, D. G.; Lyssenko, K. A.; Antipin, M. Yu.; Vygodskii, Y. S.; Lozinskaya, E. I.; Shaplov, A. S. Cocrystal of an Ionic Liquid with Organic Molecules as a Mimic of Ionic Liquid Solution. *Crystal Growth & Design* **2005**, *5* (1), 337–340. https://doi.org/10.1021/cg030086i.

(51) Berger, J.; Dunn, J. D.; Johnson, M. M.; Karst, K. R.; Shear, W. C. How Drug Life-Cycle Management Patent Strategies May Impact Formulary Management. *Am J Manag Care* **2016**, *22* (16 Suppl), S487–S495.

(52) Bedeković, N.; Stilinović, V.; Piteša, T. Aromatic versus Aliphatic Carboxyl Group as a Hydrogen Bond Donor in Salts and Cocrystals of an Asymmetric Diacid and Pyridine Derivatives. *Crystal Growth & Design* **2017**, *17* (11), 5732–5743. https://doi.org/10.1021/acs.cgd.7b00746.

(53) Drug Solubility: Importance and Enhancement Techniques https://www.hindawi.com/journals/isrn/2012/195727/ (accessed Mar 11, 2020).

(54) Kumar, S.; N, A.; a. Pharmaceutical Cocrystals: An Overview. *Indian Journal of Pharmaceutical Sciences* **2018**, *79* (6), 858–871. https://doi.org/10.4172/pharmaceutical-sciences.1000302.

(55) Zhou, Z.; Li, W.; Sun, W.-J.; Lu, T.; Tong, H. H. Y.; Sun, C. C.; Zheng, Y. Resveratrol Cocrystals with Enhanced Solubility and Tabletability. *Int J Pharm* **2016**, *509* (1–2), 391–399. https://doi.org/10.1016/j.ijpharm.2016.06.006.

(56) Krishna, G. R.; Shi, L.; Bag, P. P.; Sun, C. C.; Reddy, C. M. Correlation Among Crystal Structure, Mechanical Behavior, and Tabletability in the Co-Crystals of Vanillin Isomers. *Crystal Growth & Design* **2015**, *15* (4), 1827–1832. https://doi.org/10.1021/cg5018642.

(57) Chow, S. F.; Shi, L.; Ng, W. W.; Leung, K. H. Y.; Nagapudi, K.; Sun, C. C.; Chow, A. H. L. Kinetic Entrapment of a Hidden Curcumin Cocrystal with Phloroglucinol. *Crystal Growth & Design* **2014**, *14* (10), 5079–5089. https://doi.org/10.1021/cg5007007.

(58) Sanphui, P.; Goud, N. R.; Khandavilli, U. B. R.; Nangia, A. Fast Dissolving Curcumin Cocrystals. *Crystal Growth & Design* **2011**, *11* (9), 4135–4145. https://doi.org/10.1021/cg200704s.

(59) Bethune, S. J.; Schultheiss, N.; Henck, J.-O. Improving the Poor Aqueous Solubility of Nutraceutical Compound Pterostilbene through Cocrystal Formation. *Crystal Growth & Design* **2011**, *11* (7), 2817–2823. https://doi.org/10.1021/cg1016092.

(60) Kumar, S.; N, A.; a. Pharmaceutical Cocrystals: An Overview. *Indian Journal of Pharmaceutical Sciences* **2018**, *79* (6), 858–871. https://doi.org/10.4172/pharmaceutical-sciences.1000302.

(61) Fucke, K.; Myz, S. A.; Shakhtshneider, T. P.; Boldyreva, E. V.; Griesser, U. J. How Good Are the Crystallisation Methods for Co-Crystals? A Comparative Study of Piroxicam. *New J. Chem.* **2012**, *36* (10), 1969–1977. https://doi.org/10.1039/C2NJ40093F.

(62) Musumeci, D.; Hunter, C. A.; Prohens, R.; Scuderi, S.; McCabe, J. F. Virtual Cocrystal Screening. *Chem. Sci.* **2011**, *2* (5), 883. https://doi.org/10.1039/c0sc00555j.

(63) Hunter, C. A. Quantifying Intermolecular Interactions: Guidelines for the Molecular Recognition Toolbox. *Angewandte Chemie International Edition* **2004**, *43* (40), 5310–5324. https://doi.org/10.1002/anie.200301739.

(64) Sandhu, B.; McLean, A.; Sinha, A. S.; Desper, J.; Sarjeant, A. A.; Vyas, S.; Reutzel-Edens, S. M.; Aakeröy, C. B. Evaluating Competing Intermolecular Interactions through Molecular Electrostatic Potentials and Hydrogen-Bond Propensities. *Crystal Growth & Design* **2018**, *18* (1), 466–478. https://doi.org/10.1021/acs.cgd.7b01458.

(65) Blagden, N.; de Matas, M.; Gavan, P. T.; York, P. Crystal Engineering of Active Pharmaceutical Ingredients to Improve Solubility and Dissolution Rates. *Advanced Drug Delivery Reviews* **2007**, *59* (7), 617–630. https://doi.org/10.1016/j.addr.2007.05.011.

(66) Cruz-Cabeza, A. J. Acid–Base Crystalline Complexes and the PKa Rule. *CrystEngComm* **2012**, *14* (20), 6362–6365. https://doi.org/10.1039/C2CE26055G.

(67) Mohammad, M. A.; Alhalaweh, A.; Velaga, S. P. Hansen Solubility Parameter as a Tool to Predict Cocrystal Formation. *International Journal of Pharmaceutics* **2011**, *407* (1), 63–71. https://doi.org/10.1016/j.ijpharm.2011.01.030.

(68) Issa, N.; Karamertzanis, P. G.; Welch, G. W. A.; Price, S. L. Can the Formation of Pharmaceutical Cocrystals Be Computationally Predicted? I. Comparison of Lattice Energies. *Crystal Growth & Design* **2009**, *9* (1), 442–453. https://doi.org/10.1021/cg800685z.

(69) Musumeci, D.; Hunter, C. A.; Prohens, R.; Scuderi, S.; McCabe, J. F. Virtual Cocrystal Screening. *Chem. Sci.* **2011**, *2* (5), 883–890. https://doi.org/10.1039/C0SC00555J.

(70) Wood, P. A.; Feeder, N.; Furlow, M.; Galek, P. T. A.; Groom, C. R.; Pidcock, E. Knowledge-Based Approaches to Co-Crystal Design. *CrystEngComm* **2014**, *16* (26), 5839–5848. https://doi.org/10.1039/C4CE00316K.

(71) Galek, P. T. A.; Allen, F. H.; Fábián, L.; Feeder, N. Knowledge-Based H-Bond Prediction to Aid Experimental Polymorph Screening. *CrystEngComm* **2009**, *11* (12), 2634–2639. https://doi.org/10.1039/B910882C.

(72) Macrae, C. F.; Bruno, I. J.; Chisholm, J. A.; Edgington, P. R.; McCabe, P.; Pidcock, E.; Rodriguez-Monge, L.; Taylor, R.; Streek, J. van de; Wood, P. A. Mercury CSD 2.0 – New Features for the Visualization and Investigation of Crystal Structures. *J Appl Cryst* **2008**, *41* (2), 466–470. https://doi.org/10.1107/S0021889807067908.

(73) Fábián, L. Cambridge Structural Database Analysis of Molecular Complementarity in Cocrystals. *Crystal Growth & Design* **2009**, *9* (3), 1436–1443. https://doi.org/10.1021/cg800861m.

(74) The Design of Molecular Hosts, Guests, and Their Complexes (Nobel Lecture) - Cram - 2018 - Angewandte Chemie International Edition - Wiley Online Library https://onlinelibrary.wiley.com/doi/abs/10.1002/anie.198810093@10.1002/(ISSN)1521-3773.NobelLectures (accessed Mar 11, 2020).

(75) Supramolecular Chemistry - Fundamentals and Applications - Advanced Textbook | Katsuhiko Ariga | Springer https://www.springer.com/gp/book/9783540012986 (accessed Mar 11, 2020).

(76) Reinhoudt, D. N. Supramolecular Chemistry and Heterocycles. In *Reference Module in Chemistry, Molecular Sciences and Chemical Engineering*; Elsevier, 2013. https://doi.org/10.1016/B978-0-12-409547-2.05396-8.

(77) Strutt, N. L.; Zhang, H.; Schneebeli, S. T.; Stoddart, J. F. Functionalizing Pillar[n]Arenes. *Acc. Chem. Res.* **2014**, *47* (8), 2631–2642. https://doi.org/10.1021/ar500177d.

(78) Rational Strategies for the Selective Functionalization of Calixarenes - Lavendomme - 2015 - Asian Journal of Organic Chemistry - Wiley Online Library https://onlinelibrary.wiley.com/doi/10.1002/ajoc.201500178 (accessed Mar 11, 2020).

(79) Mezo, A. R.; Sherman, J. C. Water-Soluble Cavitands: Synthesis of Methylene-Bridged Resorcin[4]Arenes Containing Hydroxyls and Phosphates at Their Feet and Bromomethyls

and Thiomethyls at Their Rims. *J. Org. Chem.* **1998**, *63* (20), 6824–6829. https://doi.org/10.1021/jo980305k.

(80) Pinalli, R.; Dalcanale, E. Supramolecular Sensing with Phosphonate Cavitands. *Acc. Chem. Res.* **2013**, *46* (2), 399–411. https://doi.org/10.1021/ar300178m.

(81) Numanoğlu, U.; Şen, T.; Tarimci, N.; Kartal, M.; Koo, O. M. Y.; Önyüksel, H. Use of Cyclodextrins as a Cosmetic Delivery System for Fragrance Materials: Linalool and Benzyl Acetate. *AAPS PharmSciTech* **2007**, *8* (4), 34–42. https://doi.org/10.1208/pt0804085.

(82) Florea, M.; Nau, W. M. Strong Binding of Hydrocarbons to Cucurbituril Probed by Fluorescent Dye Displacement: A Supramolecular Gas-Sensing Ensemble. *Angew. Chem. Int. Ed. Engl.* **2011**, *50* (40), 9338–9342. https://doi.org/10.1002/anie.201104119.

(83) Turunen, L.; Pan, F.; Beyeh, N. K.; Trant, J. F.; Ras, R. H. A.; Rissanen, K. Bamboo-like Chained Cavities and Other Halogen-Bonded Complexes from Tetrahaloethynyl Cavitands with Simple Ditopic Halogen Bond Acceptors. *Crystal Growth & Design* **2018**, *18* (1), 513–520. https://doi.org/10.1021/acs.cgd.7b01517.

(84) Schultheiss, N.; Newman, A. Pharmaceutical Cocrystals and Their Physicochemical Properties. *Crystal Growth & Design* **2009**, *9* (6), 2950–2967. https://doi.org/10.1021/cg900129f.

(85) Thakuria, R.; Delori, A.; Jones, W.; Lipert, M. P.; Roy, L.; Rodríguez-Hornedo, N. Pharmaceutical Cocrystals and Poorly Soluble Drugs. *International Journal of Pharmaceutics* **2013**, *453* (1), 101–125. https://doi.org/10.1016/j.ijpharm.2012.10.043.

(86) Surov, A. O.; Voronin, A. P.; Manin, A. N.; Manin, N. G.; Kuzmina, L. G.; Churakov, A. V.; Perlovich, G. L. Pharmaceutical Cocrystals of Diflunisal and Diclofenac with Theophylline. *Mol. Pharmaceutics* **2014**, *11* (10), 3707–3715. https://doi.org/10.1021/mp5004652.

(87) Qiao, N.; Li, M.; Schlindwein, W.; Malek, N.; Davies, A.; Trappitt, G. Pharmaceutical Cocrystals: An Overview. *International Journal of Pharmaceutics* **2011**, *419* (1), 1–11. https://doi.org/10.1016/j.ijpharm.2011.07.037.

(88) K. Duggirala, N.; L. Perry, M.; Almarsson, Ö.; J. Zaworotko, M. Pharmaceutical Cocrystals: Along the Path to Improved Medicines. *Chemical Communications* **2016**, *52* (4), 640–655. https://doi.org/10.1039/C5CC08216A.

(89) Shaikh, R.; Singh, R.; Walker, G. M.; Croker, D. M. Pharmaceutical Cocrystal Drug Products: An Outlook on Product Development. *Trends in Pharmacological Sciences* **2018**, *39* (12), 1033–1048. https://doi.org/10.1016/j.tips.2018.10.006.

(90) Gadade, D. D.; Pekamwar, S. S. Pharmaceutical Cocrystals: Regulatory and Strategic Aspects, Design and Development. *Adv Pharm Bull* **2016**, *6* (4), 479–494. https://doi.org/10.15171/apb.2016.062.

(91) Shan, N.; Zaworotko, M. J. The Role of Cocrystals in Pharmaceutical Science. *Drug Discovery Today* **2008**, *13* (9), 440–446. https://doi.org/10.1016/j.drudis.2008.03.004.

(92) FDA/CDER/"Stewart, F. Regulatory Classification of Pharmaceutical Co-Crystals Guidance for Industry. 7.

Chapter 2 - Systematic Investigation of Hydrogen-Bond Propensity as a Tool for Predicting Co-crystal Screening Experiments

2.1. Introduction

Co-crystals and co-crystallization-based approaches[1,2,3] have been used to access new solid forms with improved properties[4,5,6,7,8,9,10,11,12,13] in pharmaceutics, agrochemicals, energetics, *etc*. In particular, pharmaceutical co-crystals[14,15] have gained considerable attention as solubility and stability are important defining factors in determining drug dosage, delivery, and storage. Other applications include agrochemicals[16], where co-crystallization has decreased the water solubility and hygroscopicity[17] of the targets. Co-crystallization of energetics[18] has altered the impact sensitivity and stability, resulting in safer handling and transportation of explosives.

The co-crystallization technique involves combination of a target and a potential partner (co-former) in the same crystalline lattice held together by intermolecular interactions. The formation of a co-crystal is highly dependent on which intermolecular interactions will prevail between the target•••target (homomeric), co-former•••co-former (homomeric), and target•••co-former (heteromeric). A co-crystal is likely to be formed if the heteromeric interactions are stronger than the homomeric interactions; consequently, if homomeric is more dominant the outcome is a recrystallization. Although co-crystallization and recrystallization is a competition between heteromeric and homomeric interactions, the probability of formation of a co-crystal is small. Hence, understanding of intermolecular interactions is essential for designing successful co-crystal screening experiments.

The most commonly used intermolecular interaction in co-crystallization is hydrogen bonding[19,20,21,22,23,24,25,26,27], due to its directionality and strength. The first step to co-crystallization is to select potential partners or co-formers. The selection of the ideal co-formers is generally based on a combinatorial and extensive experimental screening, which is relatively time consuming and expensive. Therefore, to make co-crystallization technology faster and cheaper, we need methods for predicting the outcome of an attempted co-crystallization.

Hunter and co-workers developed approaches based on molecular electrostatic potential surfaces (MEPS) and hydrogen-bond energies[28,29,30] for predicting the dominant interactions in the solid and solution phase. Lattice energy comparison of the co-crystal and pure compound was carried out by Price and co-workers to predict co-crystallization[31]. Valega considered Hansen solubility[32]

parameters, and Aakeröy *et al*. implemented pKa[33,34] values as a basis for predicting co-crystallization.

Several knowledge-based tools based on structural informatics of more than a million small molecule structures available in the Cambridge Structural Database (CSD) have been developed in Mercury[30,35,36,37]. Galek *et al*. introduced hydrogen-bond propensity[35,37] as a predictive tool, and Fábián[38,39] used molecular shape and polarity to predict co-crystallization. However, it still remains a challenge to accurately predict which specific hydrogen-bond(s) will likely dominate in the presence of numerous competing intermolecular forces and within widely different structural environments.

In order to examine the versatility and possible limitations of structure-based methods for predicting co-crystal formation, we carried out a systematic comparison of hydrogen-bond propensity-based predictions with experimental data on small multi-functional organic compounds for 150 co-crystal experiments. The hydrogen-bond propensity (HBP) tool, developed by the Cambridge Crystallographic Data Centre (CCDC)[38,40,41,42] and available within the Mercury software, was used to predict whether a co-crystal would form when a particular target molecule was combined with a potential co-former.

The hydrogen-bond propensity is the probability of forming a specific motif, which is dependent on the relative occurrence of the interaction in the given fitting data. When two different molecules are combined, we need to consider both homomeric and heteromeric interactions and use HBP to establish which possible outcome is likely to prevail, Figure 2.1.

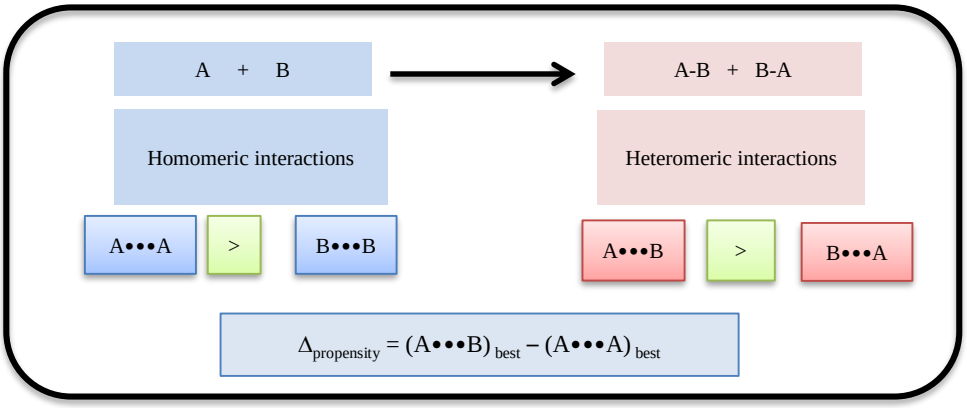

Figure 2.1. Hydrogen-bond propensity approach for co-crystal screening.

Six different molecules were selected as target compounds. The target compounds consist of pyrazole rings, amide and nitrile groups all of which are present in many pharmaceutically active compounds[43,44,45]. The targets **T1-T4** have two hydrogen-bond donors and two acceptor sites, and the presence of multiple donor-acceptor sites which means that co-crystallization can be driven through different paths. The targets **T5-T6** were deliberately selected in such a way that they are more likely to form co-crystals with suitable partners since both of them present two hydrogen-bond acceptor sites and no hydrogen-bond donor sites. The pairs **T1&T3**, **T2&T4**, and **T5&T6** are structural isomers, and **T1&T3** and **T2&T4** differ by the presence of methyl groups, Scheme 2.1. Each target was screened against 25 potential co-formers ranging from aliphatic diacids with increasing size of alkyl chains (Group 1), aromatic acids with varying electron withdrawing and electron donating groups (Group 2), hydrogen-bond acceptors with a pyridine back bone (Group 3), and mixed hydrogen-bond donor-acceptors with amino pyridine as a back bone (Group 4), Scheme 2.1.

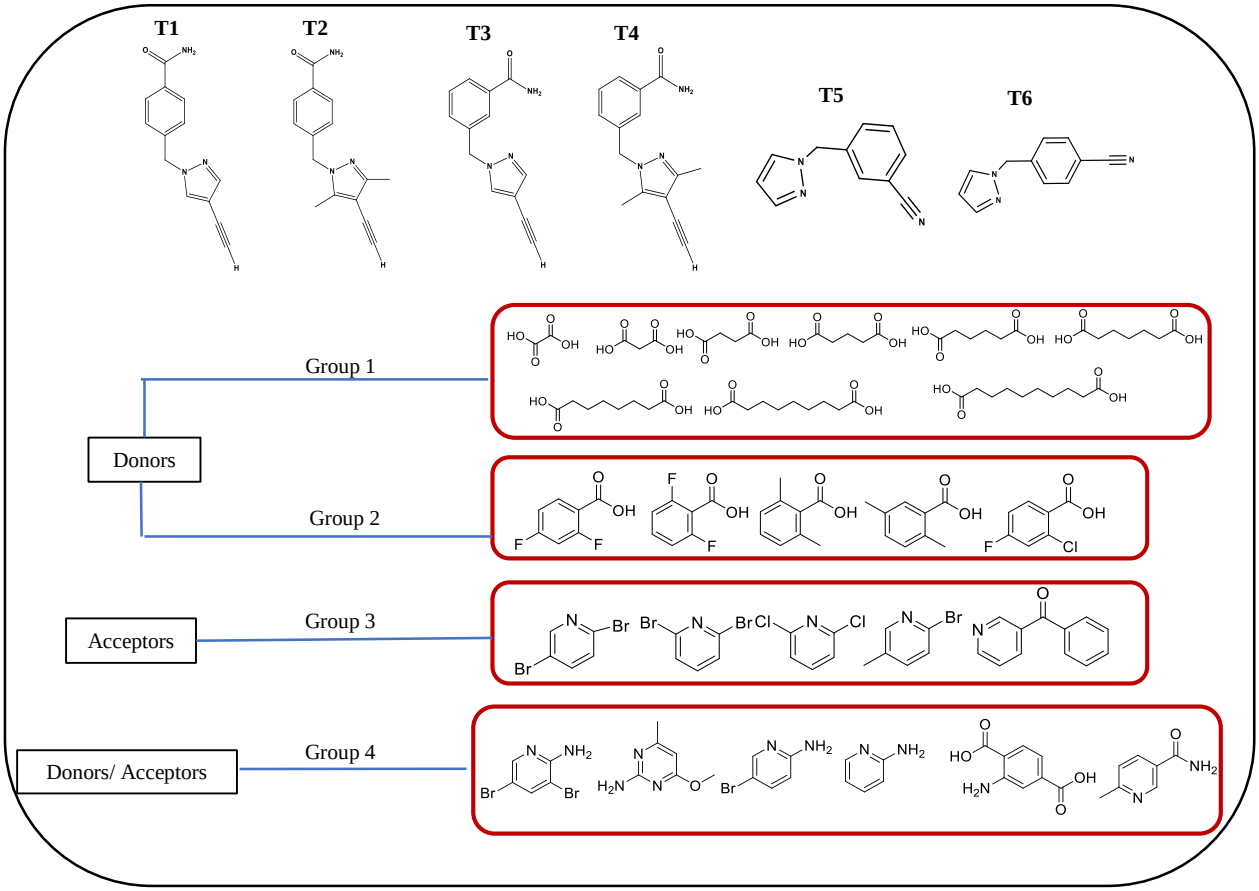

Scheme 2.1. Target molecules (top) and potential co-formers (bottom).

The study is done to answer the following questions:

1. Will targets **T1-T4** replace the self-complementary homomeric with heteromeric interactions to form co-crystals?
2. Will targets **T5-T6** co-crystallize with a higher supramolecular yield than **T1-T4**?
3. How accurate is HBP based co-crystal prediction?

2.2. Experimental

4-bromo-1H-pyrazole, 3-bromo-1H-pyrazole, 4-(bromomethyl)benzonitrile, 3-(bromomethyl) benzonitrile, THF were purchased from Alfa Aesar and were utilized without further purification. All 25 co-formers were purchased from commercial sources and used as received. Melting points were measured using a Fisher-Johns melting point apparatus. Solution ^{1}H NMR data were collected in $CDCl_3$ on a Varian Unity plus 400 MHz NMR spectrometer. IR spectra of the solids resulting from the co-crystal screening experiments were recorded with a Nicolet 380 FT-IR spectrometer (ATR) and a ZnSe crystal.

2.2.1. Synthesis of target compounds

*2.2.1.1. Synthesis of 4-((4-bromo-1H-pyrazol-1-yl)methyl)benzonitrile (**T5**)*

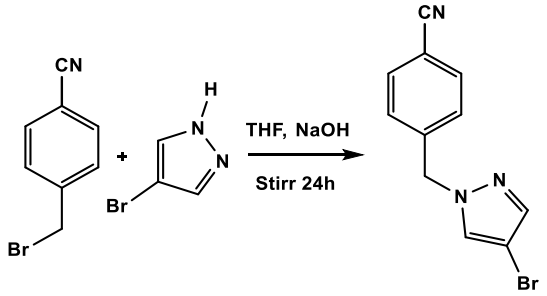

To a round bottom flask, 4-bromo-1H-pyrazole (1.50g, 9.32 mmol) and THF (80,0 mL) were added. To this solution, NaOH pellets (4.10g, 103 mmol) were added and the reaction was stirred at room temperature for 2 hours. On completion of the stir, 4-(bromomethyl)benzonitrile (2.00 g, 10.2 mmol) in THF (80.0mL) was added and the reaction mixture stirred at room temperature overnight. On completion, water was added to dissolve any excess NaOH, the organic layer was separated, dried over $MgSO_4$ and the solvent removed under vacuum to yield a white solid (2.00

g, 96%). M.P.: 55-57 ºC. 1H NMR (400MHz, $CDCl_3$): 8.10 (1H, s), 7.83 (2H, d), 7.58 (1H, s), 7.28 (2H, d), 5.37 (2H, s). IR υ: 2223, 1665, 1609, 1509, 1441, 1391, 1334 cm^{-1}.

2.2.1.2. Synthesis of 4-((3-bromocyclopenta-2,4-dien-1-yl)methyl)benzamide

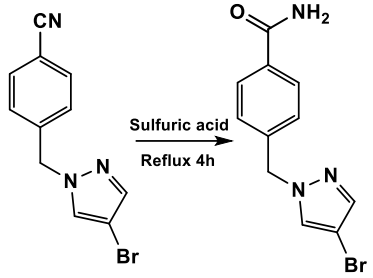

To a round bottom flask, 4-((4-bromo-1H-pyrazol-1-yl)methyl)benzonitrile (2.00g, 8.81 mmol) and 85% H_2SO_4 (10.0mL) were added. The mixture was heated to 80^0C and stirred for 4 hours. On completion, the solution was poured slowly over ice and the resulting brown solution was adjusted to basic pH using 5M NaOH. The aqueous solution was washed with $CHCl_3$ and the organic extracts were separated, dried over $MgSO_4$ and reduced to yield a white solid (1.90g, 88%). M.P.: 135-137 ºC. 1H NMR (400MHz, DMSO-d_6): 7.81 (1H, s), 7.83 (1H, s), 7.80 (1H, d), 7.55 (1H, d), 7.36 (1H,d), 7.24 (1H,d), 5.37 (2H, s). IR υ: 3365, 3210, 1665, 1480, 1301, 1334 cm^{-1}.

2.2.1.3. Synthesis of 4-((4-((trimethylsilyl)ethynyl)-1H-pyrazol-1-yl)methyl)benzamide

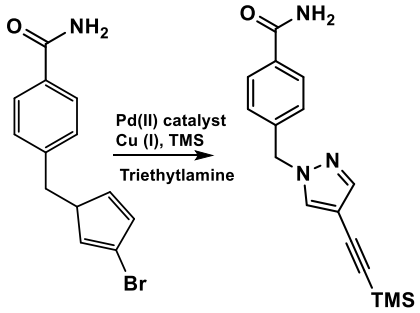

A stirred solution of 4-((3-bromocyclopenta-2,4-dien-1-yl)methyl)benzamide (1.50 g, 6.12 mmol), CuI (83.0 mg, 0.46 mmol), and Pd $(PPh_3)_2Cl_2$ (163 mg, 0.23 mmol) in 80.0 mL of trimethylamine was degassed with N_2 for 20 minutes. A solution of trimethylsilylacetylene 0.80 g (8.00 mmol) was added to the stirred solution. The mixture was refluxed overnight under N_2. Upon completion of the reaction, the solvent was evaporated by rotavap. The residue was dissolved in ethyl acetate and washed three times with water followed by a saturated NaCl solution. The organic layer was dried with $MgSO_4$ and the solvent was evaporated by rotavap. The residue was chromatographed on a silica column with hexanes as the eluent to obtain the pure the product. Yield: 1.80 g (85%).

M.P.: 150-157 ºC. 1H NMR (400MHz, $CDCl_3$): 7.77 (2H, d), 7.64 (2H, d), 7.44 (1H, s), 5.21 (2H, s), 0.02 (m).

*2.2.1.4. Synthesis of 4-((4-ethynyl-1H-pyrazol-1-yl)methyl)benzamide (**T1**)*

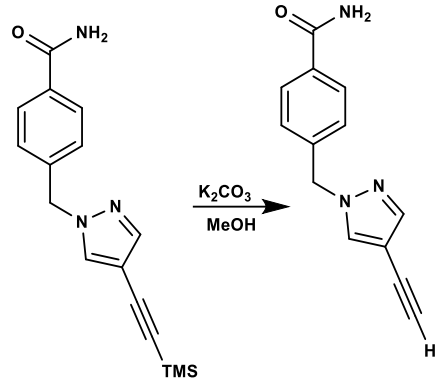

4-((4-((Trimethylsilyl)ethynyl)-1H-pyrazol-1-yl)methyl)benzamide (1.00 g, 2.89 mmol) and potassium carbonate (0.60g, 4.24 mmol) were dissolved in 50.0 mL of methanol. The reaction mixture was stirred for 24 hrs. and after completion of the reaction, the solvent was evaporated under vacuum. The solid mixture was dissolved in ethyl acetate and washed with brine. The organic layer was dried over magnesium sulfate and the solvent was evaporated to get a white powder as the product **T1**. Yield 0.70 g, (89%). M.P.: 130-135ºC, 1H NMR (400MHz, DMSO-d_6): 8.20 (1H, s), 8.06(1H, s), 7.84(1H, d), 7.67(1H, d), 7.6(1H, d), 7.27(1H, d), 5.4 (2H, s), 4.01 (1H, s).

*2.2.1.5. Synthesis of 3-((4-bromo-1H-pyrazol-1-yl)methyl)benzonitrile (**T6**)*

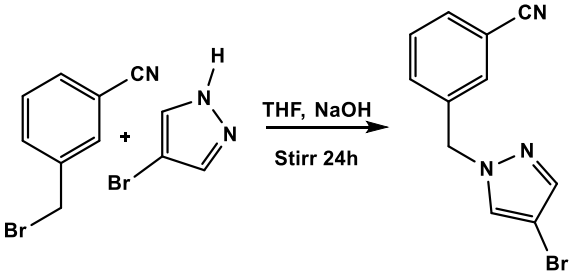

To a round bottom flask, 4-bromo-1H-pyrazole (1.50g, 9.32 mmol) and THF (80.0mL) were added. To this solution, NaOH pellets (4.10g, 103 mmol) were added and the reaction was stirred at room temperature for 2 hours. On completion of the stir, 3-(bromomethyl)benzonitrile (2.00 g, 10.2 mmol) in THF (80.0mL) was added and the reaction mixture stirred at room temperature overnight. On completion, water was added to dissolve any excess NaOH, the organic layer was separated off, dried over $MgSO_4$ and the solvent removed under vacuum to yield a white solid

(1.78 g, 84%). M.P.: 55-57 ºC, 1H NMR (400 MHz, DMSO-d_6): 7.93 (1H, s), 7.81 (1H, d), 7.34 (1H, t), 7.17 (1H, d), 7.15 (2H, s), 5.32 (2H, s) IR υ: 2223, 1666, 1609, 1509, 1441, 1391, 1334 cm^{-1}.

2.2.1.6. Synthesis of 3-((3-bromocyclopenta-2,4-dien-1-yl)methyl)benzamide

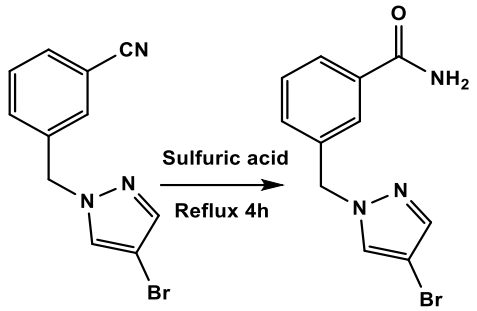

To a round bottom flask, 3-((4-bromo-1H-pyrazol-1-yl)methyl)benzonitrile (2.00g, 8.81 mmol) and 85% H_2SO_4 (10.0mL) were added. The mixture was heated to 80^0C and stirred for 4 hours. On completion, the solution was poured slowly over ice and the resulting brown solution was adjusted to basic pH using 5M NaOH. The aqueous solution was washed with $CHCl_3$ and the organic extracts were separated, dried over $MgSO_4$ and reduced to yield a white solid (1.98g, 92%). M.P.: 155-157 ºC, 1H NMR (400 MHz, DMSO-d_6): 8.04 (1H, s), 7.97 (1H, d), 7.77 (1H, t), 7.54 (1H, d), 7.38 (2H, s), 5.35 (2H, s).

2.2.1.7. Synthesis of 3-((3-((trimethylsilyl)ethynyl)cyclopenta-2,4-dien-1-yl)methyl)benzamide

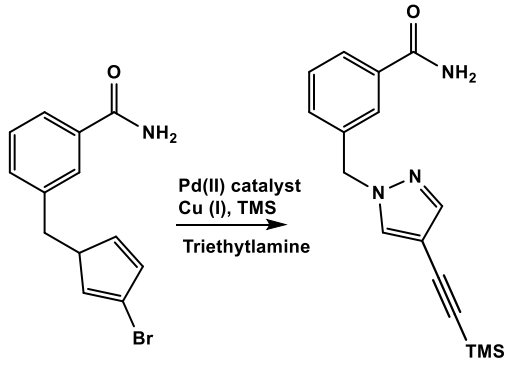

A stirred solution of 3-((3-bromocyclopenta-2,4-dien-1-yl)methyl)benzamide (1.50 g, 6.12 mmol), CuI (83.0 mg, 0.46 mmol), and Pd $(PPh_3)_2Cl_2$ (163 mg, 0.23 mmol) in 80 mL of trimethylamine was degassed with N_2 for 20 minutes. A solution of trimethylsilylacetylene (0.80 g, 8.00 mmol) was added to the stirred solution. The mixture was refluxed overnight under N_2. Upon completion of the reaction, the solvent was evaporated by rotavap. The residue was dissolved in ethyl acetate and washed three times with water followed by a saturated NaCl solution. The organic layer was dried with $MgSO_4$ and the solvent was evaporated by rotavap. The residue was chromatographed

on a silica column with hexanes as the eluent to obtain the pure product. Yield: 1.91 g (91%). M.P.: 160-163 ºC, 1H NMR (400 MHz, $CDCl_3$): 7.67 (1H, s), 7.59 (2H, d), 7.47 (1H, t), 7.47 (2H, s), 5.32 (2H, s) 0.02 (m).

*2.2.1.8. Synthesis of 3-((3-ethynylcyclopenta-2,4-dien-1-yl)methyl)benzamide (**T2**)*

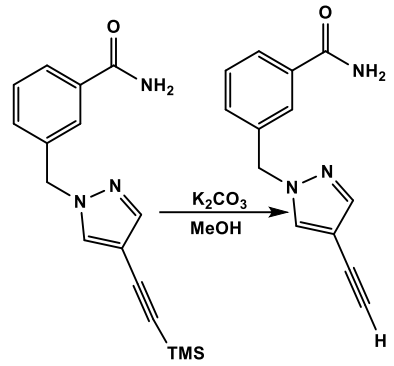

To 3-((3-((trimethylsilyl)ethynyl)cyclopenta-2,4-dien-1-yl)methyl)benzamide (1.00 g, 2.89 mmol) and potassium carbonate (0.60g, 4.24 mmol) were dissolved in 50.0mL of methanol. The reaction mixture was stirred for 24 hrs. and after completion of the reaction, the solvent was evaporated under vacuum. The solid mixture was dissolved in ethyl acetate and washed with brine. The organic layer was dried over magnesium sulfate and the solvent was evaporated to get a white powder as the product **T2**. Yield 0.69 g, (88%). M.P.: 132-140ºC, 1H NMR (400MHz, DMSO-d_6): 8.20 (1H, s), 7.95(1H, s), 7.82(1H, d), 7.60(1H, t), 7.37(1H, s), 7.26(1H, d), 5.40 (2H, s), 4.01 (1H, s).

2.2.1.9. Synthesis of 4-((4-bromo-1H-pyrazol-1-yl)methyl)benzonitrile

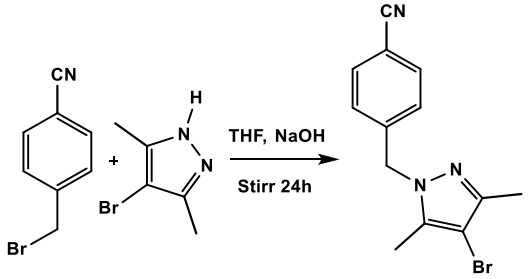

To a round bottom flask, 4-bromo-3,5-dimethyl-1H-pyrazole (1.50g, 7.85 mmol) and THF (80.0mL) were added. To this solution, NaOH pellets (4.10g, 103 mmol) were added and the reaction was stirred at room temperature for 2 hours. On completion of the stir, 4-

(bromomethyl)benzonitrile (2.00 g, 10.2 mmol) in THF (80.0mL) was added and the reaction mixture stirred at room temperature overnight. On completion, water was added to dissolve any excess NaOH, the organic layer was separated off, dried over $MgSO_4$ and the solvent removed under vacuum to yield a white solid (1.98 g, 98%). MP: 72-75 ºC. 1H NMR (400MHz, DMSO-d_6): 7.92 (1H, d), 7.79 (1H, d), 7.34 (1H, d), 7.13 (1H, d), 5.33 (2H, s), 2.17 (3H, s), 2.09 (3H, s).

2.2.1.10. Synthesis of 4-((3-bromocyclopenta-2,4-dien-1-yl)methyl)benzamide

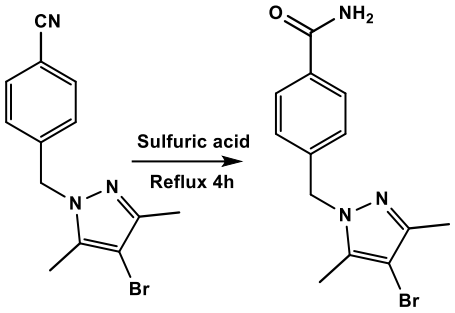

To a round bottom flask, 4-((4-bromo-1H-pyrazol-1-yl)methyl)benzonitrile (2.00g, 7.78 mmol) and 85% H_2SO_4 (10.0mL) were added. The mixture was heated to 80^0C and stirred for 4 hours. On completion, the solution was poured slowly over ice and the resulting brown solution was adjusted to basic pH using 5M NaOH. The aqueous solution was washed with $CHCl_3$ and the organic extracts were separated, dried over $MgSO_4$ and reduced to yield a white solid (1.72g, 80%). M.P.: 195-198 ºC, 1H NMR (400 MHz, DMSO-d_6): 7.97 (2H, s), 7.75 (1H, d), 7.66 (1H, d), 7.41 (1H, d), 7.23 (1H, d), 5.32 (2H, s), 2.18 (3H, s), 2.09 (3H, s).

2.2.1.11. Synthesis of 4-((3,5-dimethyl-4-((trimethylsilyl)ethynyl)-1H-pyrazol-1-yl)methyl)benzamide

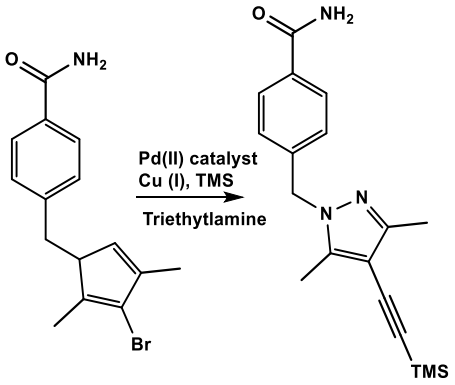

A stirred solution of 4-((3-bromocyclopenta-2,4-dien-1-yl)methyl)benzamide (1.50 g, 5.45 mmol), CuI (83.0 mg, 0.46 mmol), and Pd $(PPh_3)_2Cl_2$ (163 mg, 0.23 mmol) in 80.0mL of trimethylamine was degassed with N_2 for 20 minutes. A solution of 0.80 g (8.00 mmol) of trimethylsilylacetylene was added to the stirred solution. The mixture was refluxed overnight under N_2. Upon completion of the reaction, the solvent was evaporated by rotavap. The residue was dissolved in ethyl acetate and washed three times with water followed by a saturated NaCl solution. The organic layer was dried with $MgSO_4$ and the solvent was evaporated by rotavap. The residue was chromatographed on a silica column with hexanes as the eluent to obtain the pure product. Yield: 1.76 g (87%). MP: 210-213 ºC. 1H NMR (400MHz, DMSO-d_6): 7.99 (2H, s), 7.75 (2H, d), 7.67 (2H, d), 7.38 (1H, s), 7.25 (1H, s), 5.32 (2H, s), 2.51 (3H, s), 2.31 (3H, s), 0.02 (m).

*2.2.1.12. Synthesis of 4-((3-ethynyl-2,4-dimethylcyclopenta-2,4-dien-1-yl)methyl)benzamide (**T3**)*

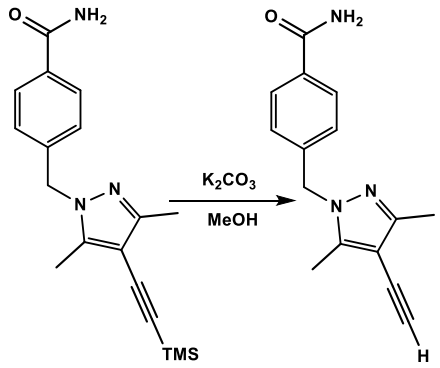

To 4-((3,5-dimethyl-4-((trimethylsilyl)ethynyl)-1H-pyrazol-1-yl)methyl)benzamide (1.00 g, 2.69 mmol) and potassium carbonate (0.60g, 4.24 mmol) were dissolved in 50ml of methanol. The reaction mixture was stirred for 24 hrs. and after completion of the reaction, the solvent was evaporated under vacuum. The solid mixture was dissolved in ethyl acetate and washed with brine. The organic layer was dried over magnesium sulfate and the solvent was evaporated to get a white powder as the product **T3**. Yield 0.63 g, (78%). M.P.: 200-205 ºC, 1H NMR (400MHz, DMSO-d_6): 7.93 (1H, d), 7.80 (1H, d), 7.16(1H, d), 7.19(1H, d), 5.40 (2H, s), 4.36 (1H, s), 2.19 (3H, s), 2.1 (3H, s).

2.2.1.13. Synthesis of 3-((4-bromo-3,5-dimethyl-1H-pyrazol-1-yl)methyl)benzonitrile

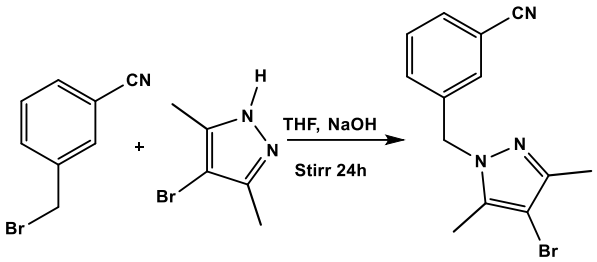

To a round bottom flask, 4-bromo-3,5-dimethyl-1H-pyrazole (1.50g, 7.85 mmol) and THF (80.0mL) were added. To this solution, NaOH pellets (4.10g, 103 mmol) were added and the reaction was stirred at room temperature for 2 hours. On completion of the stir, 3-(bromomethyl)benzonitrile (2.00 g, 10.2 mmol) in THF (80.0mL) was added and the reaction mixture stirred at room temperature overnight. On completion, water was added to dissolve any excess NaOH, the organic layer was separated off, dried over $MgSO_4$ and the solvent removed under vacuum to yield a white solid (1.95 g, 97%). M.P.: 61-63ºC, 1H NMR (400MHz, DMSO-d_6): 7.97 (1H, s), 7.75 (1H, d), 7.38 (1H, t), 7.22 (1H, d), 5.32 (2H, s), 2.20 (3H, s), 2.08 (3H, s).

2.2.1.14. Synthesis of 3-((3-bromo-2,4-dimethylcyclopenta-2,4-dien-1-yl)methyl)benzamide

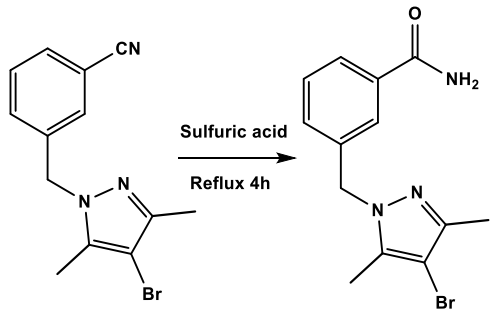

To a round bottom flask, 3-((4-bromo-3,5-dimethyl-1H-pyrazol-1-yl)methyl)benzonitrile (2.00g, 7.78 mmol) and 85% H_2SO_4 (10.0mL) were added. The mixture was heated to 80^0C and stirred for 4 hours. On completion, the solution was poured slowly over ice and the resulting brown solution was adjusted to basic pH using 5M NaOH. The aqueous solution was washed with $CHCl_3$ and the organic extracts were separated, dried over $MgSO_4$ and reduced to yield a white solid (1.85g, 86%).

M.P.: 132-140ºC, 1H NMR (400MHz, $CDCl_3$): 8.54 (2H, s), 7.99 (1H, t), 7.93 (1H, d), 7.79 (1H, d), 7.41 (1H, d), 5.25 (2H, s), 3.92 (1H, s), 2.25 (3H, s), 2.15 (3H, s).

2.2.1.15. Synthesis of 3-((3,5-dimethyl-4-((trimethylsilyl)ethynyl)-1H-pyrazol-1-yl)methyl)benzamide

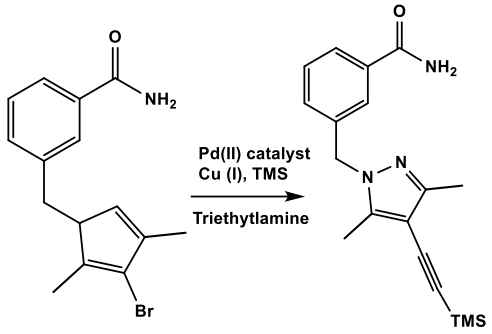

A stirred solution of 3-((3-bromo-2,4-dimethylcyclopenta-2,4-dien-1-yl)methyl)benzamide (1.50 g, 5.45 mmol), CuI (83.0 mg, 0.46 mmol), and Pd $(PPh_3)_2Cl_2$ (163 mg, 0.23 mmol) in 80.0mL of trimethylamine was degassed with N_2 for 20 minutes. A solution of 0.80g (8.00 mmol) of trimethylsilylacetylene was added to the stirred solution. The mixture was refluxed overnight under N_2. Upon completion of the reaction, the solvent was evaporated by rotavap. The residue was dissolved in ethyl acetate and washed three times with water followed by a saturated NaCl solution. The organic layer was dried with $MgSO_4$ and the solvent was evaporated by rotavap. The residue was chromatographed on a silica column with hexanes as the eluent to obtain the pure product. Yield: 1.77 g (87%). M.P.: 175-178ºC, 1H NMR (400MHz, $CDCl_3$): 7.79 (1H, t), 7.64 (1H, t), 7.54 (1H, d), 7.44 (1H, s), 5.31 (2H, s), 2.04 (6H, m).

*2.2.1.16. Synthesis of 3-((3-ethynyl-2,4-dimethylcyclopenta-2,4-dien-1-yl)methyl)benzamide (**T4**)*

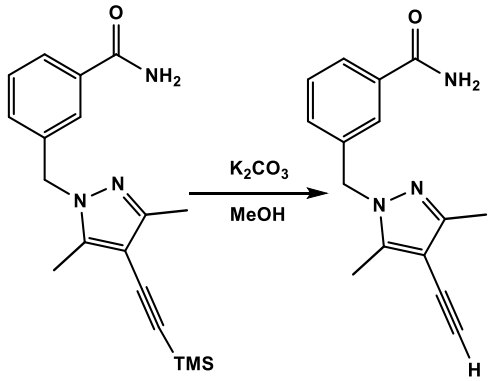

To 3-((3,5-dimethyl-4-((trimethylsilyl)ethynyl)-1H-pyrazol-1-yl)methyl)benzamide (1.00g, 2.69 mmol) and potassium carbonate (0.60g, 4.24 mmol) were dissolved in 50.0mL of methanol. The reaction mixture was stirred for 24 hrs. and after completion of the reaction, the solvent was

evaporated under vacuum. The solid mixture was dissolved in ethyl acetate and washed with brine. The organic layer was dried over magnesium sulfate and the solvent was evaporated to get a white powder as the product **T4**. Yield 0.68 g, (84%). M.P.: 203-205ºC, 1H NMR (400MHz, $CDCl_3$): 7.59 (1H, s), 7.57 (1H, d), 7.45 (1H, t), 7.3 (1H, d), 5.25 (2H, s), 3,92 (1H, s), 2.25 (3H, s), 2.15 (3H, s).

2.2.2. Experimental co-crystallization

T1-T6 were subjected to co-crystallization with the 25 co-formers. Each target and co-former were combined in a 1:1 stoichiometric ratio and ground together with a drop of methanol. The mixture was grinded for 30-40 seconds or until the solvent dried to yield a solid or glue-like paste. The resulting solid was analyzed using IR spectroscopy, to determine whether a co-crystal had formed or if the resulting solid was just a physical mixture of the two reactants. This procedure was performed for all the 150 combinations. In each reaction, 5-10 mg of the target was used with respective stoichiometric co-former. After IR spectroscopy was employed, the mixtures were dissolved in a minimum amount of solvent in a 2-dram borosilicate vial for slow evaporation in order to obtain single crystals for X-ray diffraction. In cases were slow evaporation failed, vapor diffusion, and anti-solvent crystallization techniques were employed.

2.2.3. Predicting co-crystallization using HBP

HBP calculations were employed to identify the most likely interactions between the target•••target and co-former•••co-former (homomeric interactions) and target•••co-former (heteromeric interactions). Each pair of targets and co-formers were sketched and auto edited. The first step in the process was to define the functional groups of both the target and co-former pair. Scheme 2.2 represents the defined functional groups of the targets. Step2 was to autogenerate the structures, in this step *Mercury* automatically searches through all the structures in the database with the functional groups as defined in step1. In step3 the fitting data, which is the number of structures (generated from step2) which will be used in the calculations, were selected. The final step was to define a model with seven given descriptors step4, Scheme 2.2. Each descriptor has a significance depending on the targets used in the study. However, for co-crystal screening all the seven descriptors were used in the calculations to keep the parameters constant.

The propensity values were calculated using a logistic regression model with Receiver Operator Curve (ROC) curve greater than 0.80. All the calculations were performed with the CSD[38,46,47,48] database 5.40, 2019 (updated on May 2019).

If $\Delta_{propensity} \geq 0$ it was assumed to indicate a "YES" to co-crystallization which means that a heteromeric interaction is more likely to occur than either of the two prevalent homomeric possibilities. Conversely, for $\Delta_{propensity} < 0$ the outcome was assumed to be equivalent to a "NO" to co-crystallization since homomeric interactions are more likely than heteromeric interactions.

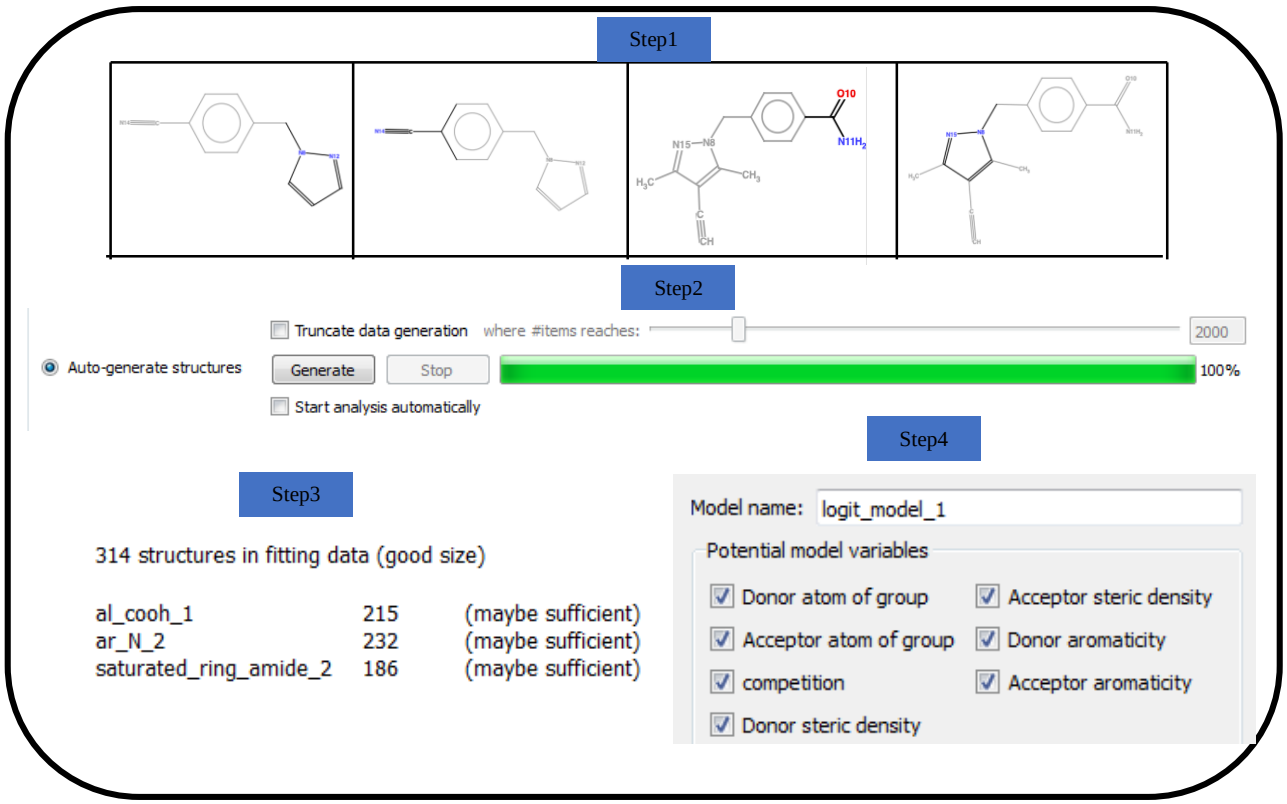

Scheme 2.2. Steps involved in predicting co-crystallization using HBP.

2.2.4. Single crystal x-ray crystallography

All datasets were collected on a Bruker Kappa APEX II system using MoKα radiation. Data were collected using APEX2 software[49]. Initial cell constants were found by small widely separated "matrix" runs. Data collection strategies were determined using COSMO[50]. Scan speed and scan widths were chosen based on scattering power and peak rocking curves. Datasets were collected at 23 °C using an Oxford Cryostream low-temperature device.

The unit cell constants and orientation matrix were improved by least-squares refinement of reflections thresholded from the entire dataset. Integration was performed with SAINT[51], using this improved unit cell as a starting point. Precise unit cell constants were calculated in SAINT from the final merged dataset. Lorenz and polarization corrections were applied. Multi-scan absorption corrections were performed with SADABS[52].

The data were reduced with SHELXTL[53]. The structure was solved with the XT[54] structure solution program using Intrinsic Phasing and refined with the XL[55] refinement package using Least Squares minimization. Also, the structures were finalized using OLEX2 1.2 suite of program[56,57]. Except as noted, hydrogen atoms were located in idealized positions and were treated with a riding model. All non-hydrogen atoms were assigned anisotropic thermal parameters. Refinements continued to convergence, using the recommended weighting schemes.

T1 – Coordinates of the amide protons H16A and H16B were allowed to refine.

T5 – Coordinates of the acid proton H19 was allowed to refine.

2.3. Results

2.3.1. Experimental co-crystallization

The solvent assisted grinding experiments were analyzed using IR spectroscopy. The IR analysis were focused on the positions of O=C targets, N-H co-formers, and O=C of acid co-formers as they have readily identifiable vibrational modes. In addition, these functional groups form the characteristic homomeric interactions that are subsequently broken when a co-crystal is formed, with new heteromeric interactions. The most likely homomeric and heteromeric interactions of the targets and co-formers are illustrated in Figure 2.2.

<table>
<tr><td>Homomeric interactions</td><td> 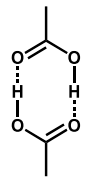
Synthon III
Group 1&2</td><td>No conventional hydrogen-bonds

Group 3</td><td> 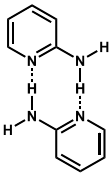
Synthon IV
Group 4</td></tr>
<tr><td></td><td colspan="3">Heteromeric interactions</td></tr>
<tr><td> 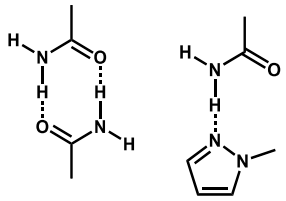
Synthon I Synthon II
T1-T4</td><td> 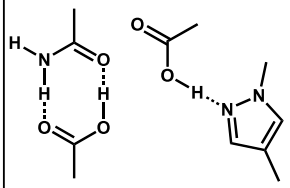
Synthon V Synthon VI
Group 1&2</td><td> 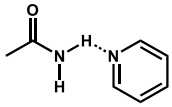
Synthon VII
Group 3</td><td> 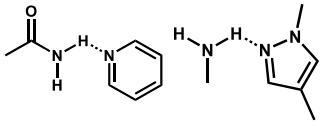
Synthon VIII Synthon IX
Group 4</td></tr>
<tr><td>No conventional hydrogen-bonds

T5-T6</td><td> 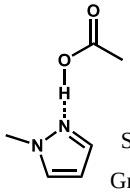
Synthon X
Group 1&2</td><td>Group 3
No conventional hydrogen-bonds</td><td> 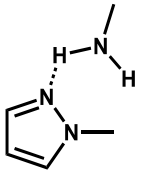
Synthon XI
Group 4</td></tr>
</table>

Figure 2.2. The possible homomeric and heteromeric interactions.

Instances where co-crystals were formed, we observed a shift in wavenumber by more than 3 cm^{-1} for the characteristic functional groups mentioned above, Table 2.1. In cases where co-crystals were not formed the peaks remained consistent.

Table 2.1. The IR data for experimentally observed positive co-crystallization outcomes in cm^{-1}.

	T1	**T2**	**T3**	**T4**	**T5**	**T6**
Co-former	C≡C 2359 C=O 1711	C≡C 2338 C=O 1665	C≡C 2335 C=O 1665	C≡C 2349 C=O 1666	C≡N 2227 C=C 1609	C≡N 2229 C=C 1605
2-Amino-3,5-dibromopyridine	Ground Mixture					
N-H 3463, 3270 C=C 1623	N-H 3350, 3166 C≡C 2359 C=O 1716	N-H 3369, 3166 C≡C 2338 C=O 1667	N-H 3362, 3167 C≡C 2333 C=O 1666	N-H 3352, 3143 C≡C 2350 C=O 1666	-	-
2-Amino-4-methoxy-6-methylpyrimidine	Ground Mixture					
N-H 3366, 3184 C=C 1632	N-H 3341, 3164 C≡C 2357 C=O 1712	N-H 3357, 3181 C≡C 2338 C=O 1668	N-H 3351, 3169 C≡C 2336 C=O 1664	N-H 3346, 3159 C≡C 2350 C=O 1664	N-H 3362, 3180 C≡N 2222 C=C 1633	N-H 3360, 3164 C≡N 2229 C=C 1633
2-Amino-5-bromopyridine	Ground Mixture					

N-H 3443, 3290 C=C 1621	N-H 3352, 3166 C≡C 2355 C=O 1712	N-H 3377, 3170 C≡C 2101 C=O 1665	N-H 3367, 3189 C≡C 2335 C=O 1670	N-H 3360, 3148 C≡C 2348 C=O 1665	-	-
2-Aminopyridine	Ground Mixture					
N-H 3437, 3284 C=C 1623	N-H 3351, 3169 C≡C 2356 C=O 1715	N-H 3367, 3180 C≡C 2100 C=O 1670	N-H 3370, 3187 C≡C 2336 C=O 1659	N-H 3352, 3153 C≡C 2349 C=O 1664	-	-
2-Aminoterephthalic acid	Ground Mixture					
N-H 3455, 3076 C=C 1681	N-H 3353, 3171 C≡C 2357 C=O 1706	N-H 3364, 3144 C≡C 2102 C=O 1668	N-H 3373, 3178 C≡C 2336 C=O 1664	N-H 3362, 3189 C≡C 2349 C=O 1665	N-H 3341,3148 C≡N 2226 C=C 1684	N-H 3354, 3180 C≡N 2229 C=C 1636
2-Chloro-4-fluorobenzoic acid	Ground Mixture					
C=O 1673	-	-	-	-	C≡N 2229 C=O 1663	C≡N 2229 C=O 1672
2,4-Difluorobenzoic acid	Ground Mixture					
C=O 1646	-	-	-	-	C≡N 2230 C=O 1669	C≡N 2231 C=O 1687
2,5-Dimethylbenzoic acid	Ground Mixture					
C=O 1668	-	-	-	-	C≡N 2222 C=O 1678	C≡N 2228 C=O 1679
2,6-Difluorobenzoic acid	Ground Mixture					
C=O 1679	-	-	-	-	C≡N 2224 C=O 1686	C≡N 2226 C=O 1689
2,6-Dimethylbenzoic acid	Ground Mixture					
C=O 1684	-	-	-	-	C≡N 2230 C=O 1667	C≡N 2225 C=O 1671
Adipic acid	Ground Mixture					
C=O 1683	-	-	-	-	C≡N 2227 C=O 1686	C≡N 2226 C=O 1678
Azelaic acid	Ground Mixture					
C=O 1683	-	-	-	-	C≡N 2225 C=O 1691	C≡N 2224 C=O 1689
Glutaric acid	Ground Mixture					
C=O 1682	-	-	-	-	C≡N 2228 C=O 1709	C≡N 2227 C=O 1710
Malonic acid	Ground Mixture					
C=O 1690	-	-	-	-	C≡N 2225 C=O 1712	C≡N 2227 C=O 1714
Oxalic acid	Ground Mixture					
C=O 1677	-	-	-	-	C≡N 2224 C=O 1687	C≡N 2227 C=O 1686
Pimelic acid	Ground Mixture					
C=O 1680	-	-	-	-	C≡N 2228 C=O 1701	C≡N 2229 C=O 1684
Sebacic acid	Ground Mixture					
C=O 1684	-	-	-	-	C≡N 2224 C=O 1689	C≡N 2230 C=O 1680
Suberic acid	Ground Mixture					
C=O 1686	-	-	-	-	C≡N 2230 C=O 1706	C≡N 2229 C=O 1702
Succinic acid	Ground Mixture					
C=O 1679	-	-	-	-	C≡N 2227 C=O 1686	C≡N 2226 C=O 1713
Supramolecular yield	20%	20%	20%	20%	64%	64%

T1- T4 experimentally co-crystallizes with 20% supramolecular yield and **T5-T6** co-crystallizes with 64% supramolecular yield. Specific trends were observed across the groups where; Groups 1-2 does not co-crystallize with **T1-T4** and co-crystallizes with **T5-T6**. Group3 with pyridine back-bone does not co-crystallize with any of the targets. And finally, Group4 with mixed donors and acceptors was found not to have any specific trend, this group of co-formers provided mixed results for formation of co-crystal.

2.3.2. HBP calculations

Based on Scheme 2.3. the homomeric, heteromeric and $\Delta_{propensity}$ values were calculated and summarized in Table 2.2. for the 150 combinations of targets and co-formers. (HBP for a few target•••co-former pair could not be calculated since the pair had zero donor, labeled as N/A).

Table 2.2. HBP calculations of attempted co-crystals on **T1-T6**.

Co-formers	**T1**	**T2**	**T3**	**T4**	**T5**	**T6**
2-Amino-3,5-dibromopyridine	0.08	0.08	0.08	0.08	-0. 07	-0.08
2-Amino-4-methoxy-6-methylpyridine	0.07	0.07	0.07	0.07	-0.05	-0.07
2-Amino-5-bromopyridine	0.01	0.01	0.01	0.01	-0.06	-0.09
2-Aminopyridine	0.08	0.08	0.08	0.08	-0.03	-0.07
2-Aminoterephthalic acid	-0.03	-0.03	-0.03	-0.03	0.07	0.06
2-Bromo-5-methylpyridine	-0.31	-0.31	-0.31	-0.31	N/A	N/A
2-Chloro-4-fluorobenzoic acid	-0.2	-0.2	-0.2	-0.2	0.3	0.29
2,4-Difluorobenzoic acid	-0.13	-0.13	-0.13	-0.13	0.3	0.3
2,5-Dibromopyridine	-0.27	-0.27	-0.27	-0.27	N/A	N/A
2,5-Dimethylbenzoic acid	-0.15	-0.15	-0.15	-0.15	0.34	0.31
2,6-Dibromopyridine	-0.2	-0.2	-0.2	-0.2	N/A	N/A
2,6-Dichloropyridine	-0.07	-0.07	-0.07	-0.07	N/A	N/A
2,6-Difluorobenzoic acid	-0.13	-0.13	-0.13	-0.13	0.3	0.34
2,6-Dimethylbenzoic acid	-0.18	-0.18	-0.18	-0.18	0.34	0.41
3-Benzoylpyridine	-0.15	-0.15	-0.15	-0.15	N/A	N/A
6-Methylnicotinamide	0	0	0	0	-0.1	-0.09
Adipic acid	-0.13	-0.13	-0.13	-0.13	0.32	0.33
Azelaic acid	-0.14	-0.14	-0.14	-0.14	0.32	0.33
Glutaric acid	-0.13	-0.13	-0.13	-0.13	0.32	0.32
Malonic acid	-0.12	-0.12	-0.12	-0.12	0.27	0.28
Oxalic acid	-0.15	-0.15	-0.15	-0.15	0.2	0.19
Pimelic acid	-0.13	-0.13	-0.13	-0.13	0.33	0.33
Sebacic acid	-0.13	-0.13	-0.13	-0.13	0.32	0.32
Suberic acid	-0.23	-0.23	-0.23	-0.23	0.32	0.32
Succinic acid	-0.13	-0.13	-0.13	-0.13	0.3	0.3

2.3.3. Single crystal x-ray crystallography

We were able to get crystal data for only three structures for which the crystallographic parameters are summarized in Table 2.3.

Table 2.3. Crystallographic parameters of single crystal X-ray diffraction.

Code	**T1**	**T5**	**$(T5)_2$:oxa**
Formula moiety	$C_{11}H_{10}N_3OI$	$C_{11}H_8N_3I$	$(C_{13}H_{13}N_3)$ $(C_2H_2O_4)_{0.5}$
Empirical formula	$C_{11}H_{10}N_3OI$	$C_{11}H_8N_3I$	$C_{14}H_{14}N_3O_2$
Molecular weight	327.12	309.10	256.28
Color, Habit	Colorless, Blocks	Colorless, Needles	Colorless, Plates
Crystal system	Monoclinic	Orthorhombic	Monoclinic
Space group, *Z*	$P2_1/c$, 4	$P2_12_12_1$, 4	$P2_1/c$, 4
a, Å	26.035(8)	4.4460(14)	10.478(3)
b, Å	4.7746(16)	13.030(4)	10.115(3)
c, Å	9.927(4)	19.520(7)	13.052(4)
α, º	90	90	90
β, º	99.80(2)	90	106.830(12)
γ, º	90	90	90
Volume, $Å^3$	1216.0(7)	1130.8(7)	1324.0(7)
Density, g/cm^3	1.787	1.816	1.286
T, ºK	296.(2)	296.(2)	296.(2)
Crystal size, min x mid x max	0.084 x 0.114 x 0.242	0.078 x 0.102 x 0.282	0.138 x 0.264 x 0.459
X-ray wavelength, Å	0.71073	0.71073	0.71073
μ, mm^{-1}	2.617	2.802	0.089
Trans min / max	0.57 / 0.81	0.51 / 0.81	0.67 / 0.75
θ_{min}, º	0.79	2.61	2.031
θ_{max}, º	25.34	25.91	25.468
Reflections			
collected	26370	11996	13912
independent	2204	2154	2426
observed	1378	1183	1429
R_{int}	0.0612	0.1091	0.0605
Threshold expression	> 2σ(*I*)	> 2σ(*I*)	> 2σ(*I*)
No. parameters	153	137	179
No. restraints	1	0	1
R_1 (observed)	0.0463	0.0539	0.0489
wR_2 (all)	0.1792	0.1061	0.1422
Goodness of fit (all)	1.081	0.972	1.017
ρ_{max}, ρ_{min}, e $Å^{-3}$	0.505, -1.043	0.439, -0.407	0.148, -0.174
Completeness to 2θ limit	0.995	0.974	0.989

2.4. Discussions

2.4.1. Experimental co-crystal screening

The supramolecular yield for **T1-T4** was 20% which indicates that the homomeric interactions between the target•••target and co-former•••co-former was more dominant than the heteromeric

interactions. There are two possible homomeric interactions in **T1-T4**, synthon I (amide•••amide) and synthon II (amide•••pyrazole) where either one or both the interactions can exist, Scheme 2.3. HBP values indicated that synthon I (0.71) was more likely to form in comparison to synthon II (0.67).

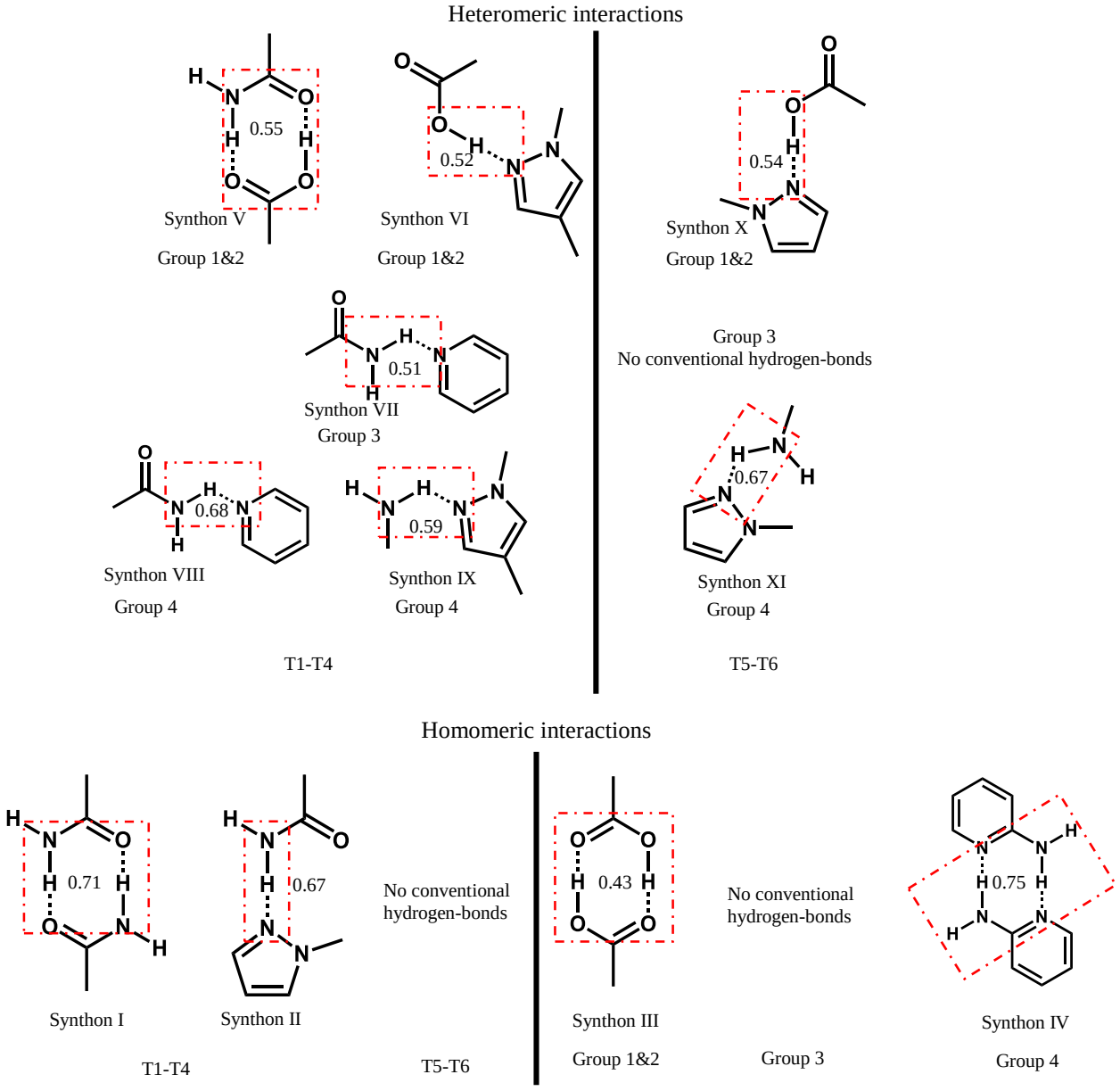

Scheme 2.3. Postulated homomeric (top) and heteromeric (bottom) synthons and hydrogen-bond propensities in targets and co-formers.

Although we were unable to obtain crystal structures with either of **T1-T4**, we did obtain a crystal structure of the iodo analogue of **T1**, Figure 2.3.

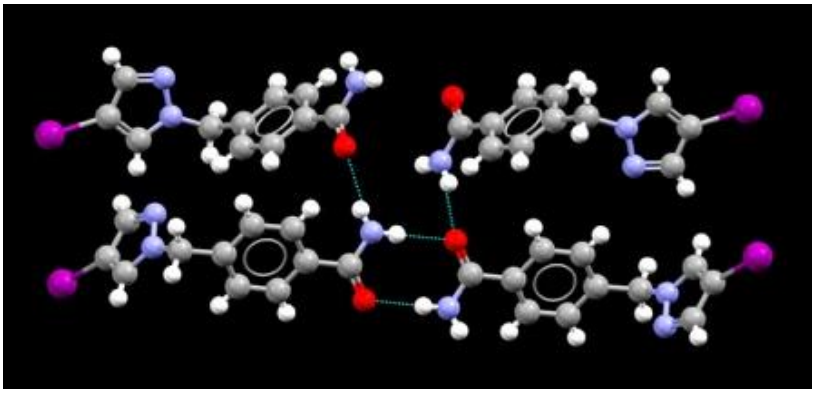

Figure 2.3. Crystal structure of iodo analogue of **T1**.

The crystal structure shows the formation of only synthon I and no synthon II (amide•••pyrazole). Such interactions are well-known from the literature and a CSD survey of comparable compounds shows exactly similar interactions in the crystal packing where only synthon I is formed[58, 59, 60, 61]. In all the attempted co-crystallization reactions in **T1-T4** with groups 1&2, the heteromeric synthons were not competitive enough to break the homomeric interactions. For groups 1&2 co-formers the homomeric interactions is self-complementary acid•••acid interactions, Scheme 2.3. Co-formers in group 3 have no conventional homomeric hydrogen-bonds. Since, the dominant amide•••amide interaction exists, and there was no potential competition, co-formers in this group do not co-crystallize with **T1-T4**, Scheme 2.3. Co-formers in group 4 can either form homomeric synthon IV (synthon III in case of 2-aminoterephtahlic acid and synthon I in case of 6- methyl nicotinamide) or heteromeric synthons VIII or IX. For a heteromeric interaction to exist in these pairs of co-formers and targets, it was not absolutely necessary to break homomeric synthon I. A heteromeric synthon VIII can co-exist with synthon I. Consequently, this group of co-formers had a higher probability to co-crystallize with **T1-T4**, which matches with our experimental outcomes. In order to break the strong homomeric interactions of the amide group (synthon I) and to shift the balance from homomeric to heteromeric interactions. We replaced the amide group with a nitrile functional group that cannot engage in any conventional self-complementary hydrogen-bonds, Scheme 2.4.

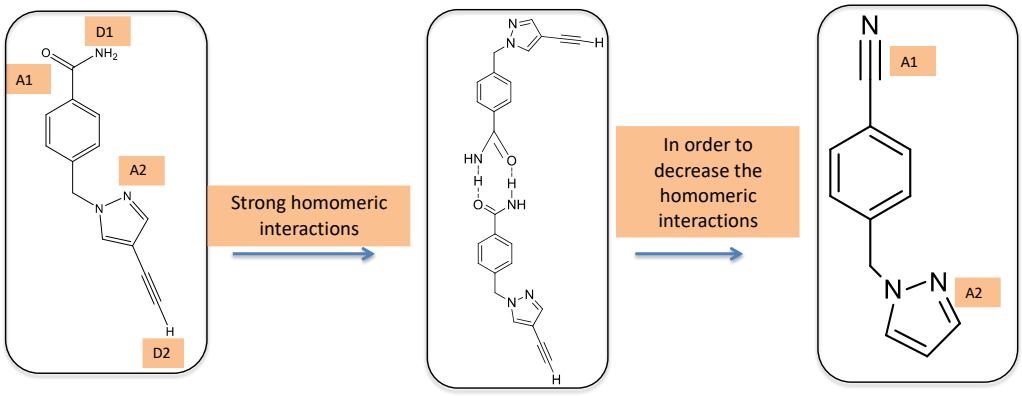

Scheme 2.4. Manipulating the structure to shift balance from homomeric to heteromeric interactions (A denotes hydrogen-bond acceptor and D corresponds to hydrogen-bond donor).

We did obtain a crystal structure of the iodo analogue of **T6**. As expected, there were no conventional hydrogen-bonds in the crystal structure, Figure 2.4.

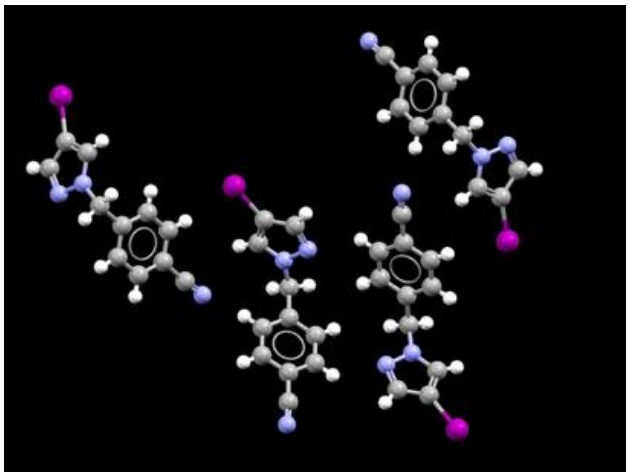

Figure 2.4. Crystal structure of iodo analogue of **T6**.

For targets **T5-T6** to co-crystallize with co-formers in group 1&2, the homomeric synthon III needs to be broken and subsequently replaced by heteromeric synthon X. Experimentally, we were able to get one crystal structure of **T6** with oxalic acid, Figure 2.5.

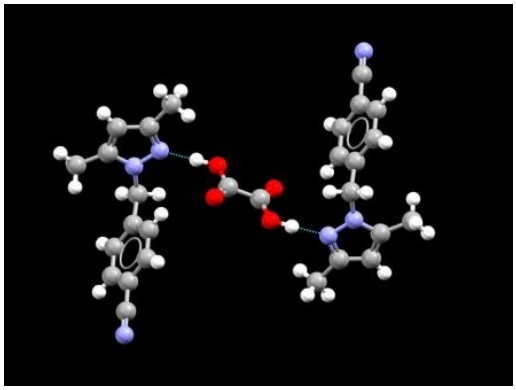

Figure 2.5. Crystal structure of (**T5**)$_2$:oxa.

T1-4 did not deliver similar interactions (acid•••pyrazole) with groups 1&2 co-formers. Further analysis gave an insight on why there was a difference in interactions between the targets. The preference of synthon X over synthon VI could be explained on the basis of short contacts which exist between CH_2•••pyrazole in **T1-T4** with bond distance of 3.643 Å and bond angle of 157.95°. These interactions are commonly known as non-conventional hydrogen-bonds consisting of chains built from CH•••N interactions[62, 63, 64]. These short contacts inhibit the formation of synthon II, VI, VII and IX. Whereas, in **T5-T6** these short contacts were absent which facilitated the formation of synthon X resulting in co-crystallization. Group3 co-formers contain only acceptors and no potential conventional donor•••acceptor interactions were possible and hence no co-crystals were obtained. In case of group4 co-formers similar to **T1-T4**, either synthon XI or both synthon XI and IV can exist together to form co-crystals which can lead to formation of co-crystals. Experimentally, we observed an increase in the supramolecular yield from 20% for **T1-T4** to 64% for **T5-T6**.

2.4.2. Experimental co-crystal screening results vs predictions

HBP calculations were used to predict co-crystallization of the 150 experiments. The training dataset step3, Scheme 2.3 was kept between 300-500 structures. When the calculations were repeated using a larger dataset than 500, we found that the structures included in the calculations were very different from the defined functional group step1, Scheme 2.3. We faced problems where the calculations were non-reproduceable and therefore, it was important to define a range for the fitting data. After testing the fitting dataset with a different range of structures, the dataset of 300-500 structures was found to be most reproducible.

A confusion matrix[35] was employed to analyze the true positives; HBP and experiment agree on formation of co-crystals, true negatives; HBP and experiment agree on formation of no co-crystals, false positives; HBP and experiment do not agree on formation of co-crystals and false negatives; HBP and experiment do not agree on formation of no co-crystals, Figure 2.6.

a)

		Predicted Outcomes	
		Co-crystal	No co-crystal
Experiment	Co-crystal	True Positive	False Negative
	No co-crystal	False Positive	True Negative

b)

$D_{propensity} \geq 0.0$		Predicted Outcomes	
		Co-crystal	No co-crystal
Experiment	Co-crystal	16	4
	No co-crystal	4	76

c)

$D_{propensity} \geq 0.0$		Predicted Outcomes	
		Co-crystal	No co-crystal
Experiment	Co-crystal	38	0
	No co-crystal	2	0

Figure 2.6. Confusion matrices from HBP results. a) explanation of matrix b) confusion matrix for **T1-T4** c) confusion matrix for **T5-T6**.

In addition, a success rate was calculated, which is the number of predictions that match with the experimental outcome divided by the total number of experiments, Figure 2.7. The match between prediction and experiment was excellent across the six compounds examined in this study.

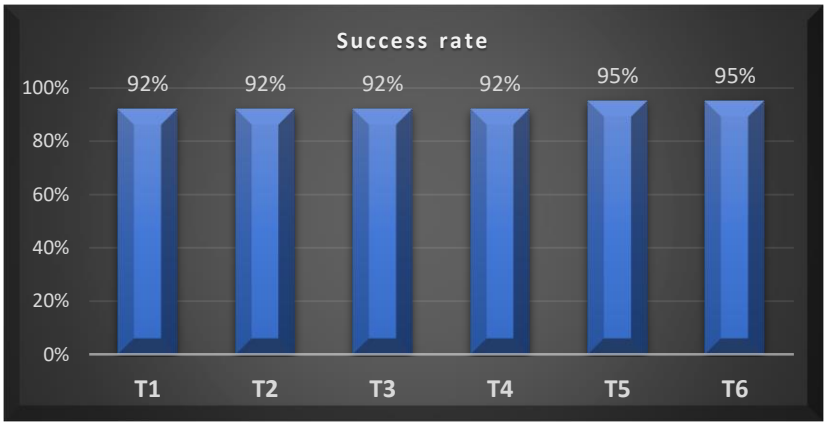

Figure 2.7. Comparison between HBP calculations and experimental co-crystal formation.

The consistency for the in-house compounds was reassuring since the members of this series maintain similar functional groups with different molecular geometry. Notably, both the results where a co-crystal was formed and not formed experimentally, matched the HBP predictions equally well. An important factor to be considered here is that this approach takes into account only enthalpic characteristics and does not include entropy terms[65]. Obviously, the crystal structure itself does not provide any information about the kinetics of seed formation. However, the structural preference might reflect thermodynamic and kinetic bias towards a crystal packing.
Although it is possible that the relatively limited structural diversity among **T1-T6** produces a very high prediction accuracy, there is no reason to believe that co-crystallizations with much larger and more flexible molecules with similar functional groups cannot also be predicted with high reliability. The next phase of this effort will be to examine compounds with more diverse functional groups (e.g. pyridines, pyrimidines, sulphonamides, methoxy *etc.*), rotatable bonds (*>3)* and molecular weight (*>250 g/mol*) to expand HBP as a tool to predict co-crystallization with high efficiency. The results presented herein underscore that systematic structure-informatics methods can provide important guidelines for defining the experimental space that needs to be explored in the efficient pursuit of new solid forms of high-value chemicals.[36,35]

2.5. Conclusions

1. The strong amide•••amide interactions (synthon I) in targets **T1-T4** dominates 80% of the co-crystallization experiments. **T1-4** co-crystallizes only with aminopyridine co-formers.
2. Altering the balance between homomeric and heteromeric interactions displayed very different supramolecular yield of 64% for **T5-T6**.
3. HBP produces an accuracy of 92-95% for the 150 combinations examined in this study.

HBP is a simple technique which is much less time consuming and labor intensive than actual experiments. The ability for HBP to predict co-crystallization with such high accuracy can be of considerable use in areas and applications that require new solid crystalline forms with improved bulk properties[36,35,37,5]. Therefore, the success of the cheminformatics in predicting co-crystallization will help narrow down the potential experimental search space which will save both time and cost.

2.6. References

(1) Williams, H. D.; Trevaskis, N. L.; Charman, S. A.; Shanker, R. M.; Charman, W. N.; Pouton, C. W.; Porter, C. J. H. Strategies to Address Low Drug Solubility in Discovery and Development. *Pharmacol Rev* **2013**, *65* (1), 315–499. https://doi.org/10.1124/pr.112.005660.

(2) Shan, N.; Zaworotko, M. J. The Role of Cocrystals in Pharmaceutical Science. *Drug Discovery Today* **2008**, *13* (9), 440–446. https://doi.org/10.1016/j.drudis.2008.03.004.

(3) B. Aakeröy, C.; R. Champness, N.; Janiak, C. Recent Advances in Crystal Engineering. *CrystEngComm* **2010**, *12* (1), 22–43. https://doi.org/10.1039/B919819A.

(4) Aakeröy, C. B.; Grommet, A. B.; Desper, J. Co-Crystal Screening of Diclofenac. *Pharmaceutics* **2011**, *3* (3), 601–614. https://doi.org/10.3390/pharmaceutics3030601.

(5) Gadade, D. D.; Pekamwar, S. S. Pharmaceutical Cocrystals: Regulatory and Strategic Aspects, Design and Development. *Adv Pharm Bull* **2016**, *6* (4), 479–494. https://doi.org/10.15171/apb.2016.062.

(6) Surov, A. O.; Voronin, A. P.; Manin, A. N.; Manin, N. G.; Kuzmina, L. G.; Churakov, A. V.; Perlovich, G. L. Pharmaceutical Cocrystals of Diflunisal and Diclofenac with Theophylline. *Mol. Pharmaceutics* **2014**, *11* (10), 3707–3715. https://doi.org/10.1021/mp5004652.

(7) Desiraju, G. R. Crystal Engineering: From Molecule to Crystal. *J. Am. Chem. Soc.* **2013**, *135* (27), 9952–9967. https://doi.org/10.1021/ja403264c.

(8) Babu, N. J.; Nangia, A. Solubility Advantage of Amorphous Drugs and Pharmaceutical Cocrystals. *Crystal Growth & Design* **2011**, *11* (7), 2662–2679. https://doi.org/10.1021/cg200492w.

(9) Jones, W.; Motherwell, W. D. S.; Trask, A. V. Pharmaceutical Cocrystals: An Emerging Approach to Physical Property Enhancement. *MRS Bulletin* **2006**, *31* (11), 875–879. https://doi.org/10.1557/mrs2006.206.

(10) Mir, N. A.; Dubey, R.; Desiraju, G. R. Strategy and Methodology in the Synthesis of Multicomponent Molecular Solids: The Quest for Higher Cocrystals. *Acc. Chem. Res.* **2019**. https://doi.org/10.1021/acs.accounts.9b00211.

(11) Friščić, T.; Jones, W. Recent Advances in Understanding the Mechanism of Cocrystal Formation via Grinding. *Crystal Growth & Design* **2009**, *9* (3), 1621–1637. https://doi.org/10.1021/cg800764n.

(12) Cherukuvada, S.; Kaur, R.; Row, T. N. G. Co-Crystallization and Small Molecule Crystal Form Diversity: From Pharmaceutical to Materials Applications. *CrystEngComm* **2016**, *18* (44), 8528–8555. https://doi.org/10.1039/C6CE01835A.

(13) Basavoju, S.; Boström, D.; Velaga, S. P. Indomethacin–Saccharin Cocrystal: Design, Synthesis and Preliminary Pharmaceutical Characterization. *Pharm Res* **2008**, *25* (3), 530–541. https://doi.org/10.1007/s11095-007-9394-1.

(14) Aakeröy, C. Is There Any Point in Making Co-Crystals? *Acta Cryst B* **2015**, *71* (4), 387–391. https://doi.org/10.1107/S2052520615010872.

(15) K. Duggirala, N.; L. Perry, M.; Almarsson, Ö.; J. Zaworotko, M. Pharmaceutical Cocrystals: Along the Path to Improved Medicines. *Chemical Communications* **2016**, *52* (4), 640–655. https://doi.org/10.1039/C5CC08216A.

(16) Bedeković, N.; Stilinović, V.; Piteša, T. Aromatic versus Aliphatic Carboxyl Group as a Hydrogen Bond Donor in Salts and Cocrystals of an Asymmetric Diacid and Pyridine Derivatives. *Crystal Growth & Design* **2017**, *17* (11), 5732–5743. https://doi.org/10.1021/acs.cgd.7b00746.

(17) Sandhu, B.; Sinha, A. S.; Desper, J.; Aakeröy, C. B. Modulating the Physical Properties of Solid Forms of Urea Using Co-Crystallization Technology. *Chem. Commun.* **2018**, *54* (37), 4657–4660. https://doi.org/10.1039/C8CC01144C.

(18) B. Aakeröy, C.; K. Wijethunga, T.; Benton, J.; Desper, J. Stabilizing Volatile Liquid Chemicals Using Co-Crystallization. *Chemical Communications* **2015**, *51* (12), 2425–2428. https://doi.org/10.1039/C4CC09650A.

(19) Chakrabarty, R.; Mukherjee, P. S.; Stang, P. J. Supramolecular Coordination: Self-Assembly of Finite Two- and Three-Dimensional Ensembles. *Chem. Rev.* **2011**, *111* (11), 6810–6918. https://doi.org/10.1021/cr200077m.

(20) Aakeröy, C. B.; Chopade, P. D.; Desper, J. Avoiding "Synthon Crossover" in Crystal Engineering with Halogen Bonds and Hydrogen Bonds. *Crystal Growth & Design* **2011**, *11* (12), 5333–5336. https://doi.org/10.1021/cg2009013.

(21) Arunan, E.; Desiraju, G. R.; Klein, R. A.; Sadlej, J.; Scheiner, S.; Alkorta, I.; Clary, D. C.; Crabtree, R. H.; Dannenberg, J. J.; Hobza, P.; et al. Defining the Hydrogen Bond: An Account (IUPAC Technical Report). *Pure Appl. Chem.* **2011**, *83* (8), 1619–1636. https://doi.org/10.1351/PAC-REP-10-01-01.

(22) Buckingham, A. D.; Del Bene, J. E.; McDowell, S. A. C. The Hydrogen Bond. *Chemical Physics Letters* **2008**, *463* (1), 1–10. https://doi.org/10.1016/j.cplett.2008.06.060.

(23) Lehn, J.-M. Toward Self-Organization and Complex Matter. *Science* **2002**, *295* (5564), 2400–2403. https://doi.org/10.1126/science.1071063.

(24) Moulton, B.; Zaworotko, M. J. From Molecules to Crystal Engineering: Supramolecular Isomerism and Polymorphism in Network Solids. *Chem. Rev.* **2001**, *101* (6), 1629–1658. https://doi.org/10.1021/cr9900432.

(25) Bosch, E. Chain-Link Hydrogen-Bonded Capsules. *CrystEngComm* **2007**, *9* (3), 191–198. https://doi.org/10.1039/B615899D.

(26) Aakeröy, C. B.; Salmon, D. J.; Smith, M. M.; Desper, J. Cyanophenyloximes: Reliable and Versatile Tools for Hydrogen-Bond Directed Supramolecular Synthesis of Cocrystals. *Crystal Growth and Design* **2006**, *6* (4), 1033–1042. https://doi.org/10.1021/cg0600492.

(27) Aakeröy, C. B.; Desper, J.; Leonard, B.; Urbina, J. F. Toward High-Yielding Supramolecular Synthesis: Directed Assembly of Ditopic Imidazoles/Benzimidazoles and Dicarboxylic Acids into Cocrystals via Selective O−H···N Hydrogen Bonds. *Crystal Growth & Design* **2005**, *5* (3), 865–873. https://doi.org/10.1021/cg049682i.

(28) Hunter, C. A. Quantifying Intermolecular Interactions: Guidelines for the Molecular Recognition Toolbox. *Angew. Chem. Int. Ed. Engl.* **2004**, *43* (40), 5310–5324. https://doi.org/10.1002/anie.200301739.

(29) McKenzie, J.; Feeder, N.; Hunter, C. A. H-Bond Competition Experiments in Solution and the Solid State. *CrystEngComm* **2016**, *18* (3), 394–397. https://doi.org/10.1039/C5CE02223A.

(30) Musumeci, D.; Hunter, C. A.; Prohens, R.; Scuderi, S.; McCabe, J. F. Virtual Cocrystal Screening. *Chem. Sci.* **2011**, *2* (5), 883–890. https://doi.org/10.1039/C0SC00555J.

(31) Issa, N.; Karamertzanis, P. G.; Welch, G. W. A.; Price, S. L. Can the Formation of Pharmaceutical Cocrystals Be Computationally Predicted? I. Comparison of Lattice Energies. *Crystal Growth & Design* **2009**, *9* (1), 442–453. https://doi.org/10.1021/cg800685z.

(32) Mohammad, M. A.; Alhalaweh, A.; Velaga, S. P. Hansen Solubility Parameter as a Tool to Predict Cocrystal Formation. *International Journal of Pharmaceutics* **2011**, *407* (1), 63–71. https://doi.org/10.1016/j.ijpharm.2011.01.030.

(33) Aakeröy, C. B.; Beatty, A. M.; Helfrich, B. A. “Total Synthesis” Supramolecular Style: Design and Hydrogen-Bond-Directed Assembly of Ternary Supermolecules. *Angewandte Chemie International Edition* **2001**, *40* (17), 3240–3242. https://doi.org/10.1002/1521-3773(20010903)40:17<3240::AID-ANIE3240>3.0.CO;2-X.

(34) Cruz-Cabeza, A. J. Acid–Base Crystalline Complexes and the PKa Rule. *CrystEngComm* **2012**, *14* (20), 6362–6365. https://doi.org/10.1039/C2CE26055G.

(35) Wood, P. A.; Feeder, N.; Furlow, M.; Galek, P. T. A.; Groom, C. R.; Pidcock, E. Knowledge-Based Approaches to Co-Crystal Design. *CrystEngComm* **2014**, *16* (26), 5839–5848. https://doi.org/10.1039/C4CE00316K.

(36) Sandhu, B.; McLean, A.; Sinha, A. S.; Desper, J.; Sarjeant, A. A.; Vyas, S.; Reutzel-Edens, S. M.; Aakeröy, C. B. Evaluating Competing Intermolecular Interactions through Molecular Electrostatic Potentials and Hydrogen-Bond Propensities. *Crystal Growth & Design* **2018**, *18* (1), 466–478. https://doi.org/10.1021/acs.cgd.7b01458.

(37) Galek, P. T. A.; Allen, F. H.; Fábián, L.; Feeder, N. Knowledge-Based H-Bond Prediction to Aid Experimental Polymorph Screening. *CrystEngComm* **2009**, *11* (12), 2634–2639. https://doi.org/10.1039/B910882C.

(38) Macrae, C. F.; Bruno, I. J.; Chisholm, J. A.; Edgington, P. R.; McCabe, P.; Pidcock, E.; Rodriguez-Monge, L.; Taylor, R.; Streek, J. van de; Wood, P. A. Mercury CSD 2.0 – New Features for the Visualization and Investigation of Crystal Structures. *J Appl Cryst* **2008**, *41* (2), 466–470. https://doi.org/10.1107/S0021889807067908.

(39) Fábián, L. Cambridge Structural Database Analysis of Molecular Complementarity in Cocrystals. *Crystal Growth & Design* **2009**, *9* (3), 1436–1443. https://doi.org/10.1021/cg800861m.

(40) Allen, F. H. The Cambridge Structural Database: A Quarter of a Million Crystal Structures and Rising. *Acta Crystallogr., B* **2002**, *58* (Pt 3 Pt 1), 380–388.

(41) Mapp, L. K.; Coles, S. J.; Aitipamula, S. Design of Cocrystals for Molecules with Limited Hydrogen Bonding Functionalities: Propyphenazone as a Model System. *Crystal Growth & Design* **2017**, *17* (1), 163–174. https://doi.org/10.1021/acs.cgd.6b01399.

(42) Vologzhanina, A. V.; Sokolov, A. V.; Purygin, P. P.; Zolotarev, P. N.; Blatov, V. A. Knowledge-Based Approaches to H-Bonding Patterns in Heterocycle-1-

Carbohydrazoneamides. *Crystal Growth & Design* **2016**, *16* (11), 6354–6362. https://doi.org/10.1021/acs.cgd.6b00990.

(43) Xu, Z.; Gao, C.; Ren, Q.-C.; Song, X.-F.; Feng, L.-S.; Lv, Z.-S. Recent Advances of Pyrazole-Containing Derivatives as Anti-Tubercular Agents. *European Journal of Medicinal Chemistry* **2017**, *139*, 429–440. https://doi.org/10.1016/j.ejmech.2017.07.059.

(44) Ong, C. K. S.; Lirk, P.; Tan, C. H.; Seymour, R. A. An Evidence-Based Update on Nonsteroidal Anti-Inflammatory Drugs. *Clinical Medicine & Research* **2007**, *5* (1), 19–34. https://doi.org/10.3121/cmr.2007.698.

(45) Fleming, F. F.; Yao, L.; Ravikumar, P. C.; Funk, L.; Shook, B. C. Nitrile-Containing Pharmaceuticals: Efficacious Roles of the Nitrile Pharmacophore. *J. Med. Chem.* **2010**, *53* (22), 7902–7917. https://doi.org/10.1021/jm100762r.

(46) Taylor, R.; Macrae, C. F. Rules Governing the Crystal Packing of Mono- and Dialcohols. *Acta Cryst B* **2001**, *57* (6), 815–827. https://doi.org/10.1107/S010876810101360X.

(47) Bruno, I. J.; Cole, J. C.; Edgington, P. R.; Kessler, M.; Macrae, C. F.; McCabe, P.; Pearson, J.; Taylor, R. New Software for Searching the Cambridge Structural Database and Visualizing Crystal Structures. *Acta Cryst B* **2002**, *58* (3), 389–397. https://doi.org/10.1107/S0108768102003324.

(48) Macrae, C. F.; Edgington, P. R.; McCabe, P.; Pidcock, E.; Shields, G. P.; Taylor, R.; Towler, M.; Streek, J. van de. Mercury: Visualization and Analysis of Crystal Structures. *J Appl Cryst* **2006**, *39* (3), 453–457. https://doi.org/10.1107/S002188980600731X.

(49) APEX2 V2013.10-0, © 2013, Bruker Analytical X-Ray Systems, Madison, WI.

(50) COSMO v1.61, © 1999 - 2009, Bruker Analytical X-Ray Systems, Madison, WI.

(51) SAINT v8.34a, © 1997 - 2013, Bruker Analytical X-Ray Systems, Madison, WI.

(52) SADABS V2012/1, © 2012, Bruker Analytical X-Ray Systems, Madison, WI.

(53) SHELXTL V2008/4, © 2008, Bruker Analytical X-Ray Systems, Madison, WI.

(54) Sheldrick, G. M., Acta Cryst., 2015, A71, 3-8.

(55) Sheldrick, G. M., Acta Cryst., 2008, A64, 112-122.

(56) Olex2 1.2 - Compiled 2018.04.26 Svn.R3504 for OlexSys, GUI Svn.R5492.

(57) Dolomanov, O. V.; Bourhis, L. J.; Gildea, R. J.; Howard, J. A. K.; Puschmann, H. *OLEX2* : A Complete Structure Solution, Refinement and Analysis Program. *J Appl Crystallogr* **2009**, *42* (2), 339–341. https://doi.org/10.1107/S0021889808042726.

(58) Thamotharan, S.; Parthasarathi, V.; Sanyal, R.; Badami Bharati, V.; Linden, A. Dimethyl 1-(3-Chloro-4-Methylphenyl)Pyrazole-3,4-Dicarboxylate. *Acta Crystallogr E Struct Rep Online* **2003**, *59* (1), o44–o45. https://doi.org/10.1107/S1600536802020718.

(59) Tang, Z.; Ding, X.-L.; Xie, Y.-S.; Zhao, B.-X. 1-(4- *Tert* -Butylbenzyl)-3-Phenyl-1 *H* -Pyrazole-5-Carboxylic Acid. *Acta Crystallogr E Struct Rep Online* **2009**, *65* (6), o1273–o1273. https://doi.org/10.1107/S1600536809017000.

(60) Fun, H.-K.; Quah, C. K.; Chandrakantha, B.; Isloor, A. M.; Shetty, P. 1-Cyclohexyl-5-(4-Methoxyphenyl)-1 *H* -Pyrazole-4-Carboxylic Acid. *Acta Crystallogr E Struct Rep Online* **2011**, *67* (12), o3513–o3513. https://doi.org/10.1107/S1600536811050872.

(61) Zhang, X.-Y.; Liu, W.; Tang, W.; Lai, Y.-B. 3-Phenyl-1 *H* -Pyrazole-5-Carboxylic Acid. *Acta Crystallogr E Struct Rep Online* **2007**, *63* (9), o3764–o3764. https://doi.org/10.1107/S1600536807038809.

(62) Dubey, R.; Lim, D. ChemInform Abstract: Weak Interactions: A Versatile Role in Aromatic Compounds. *ChemInform* **2011**, *42* (45), no-no. https://doi.org/10.1002/chin.201145260.

(63) Oruganti, M.; Khade, P.; Kumar Das, U.; R. Trivedi, D. The Hierarchies of Hydrogen Bonds in Salts/Cocrystals of Isoniazid and Its Schiff Base – a Case Study. *RSC Advances* **2016**, *6* (19), 15868–15876. https://doi.org/10.1039/C5RA14951G.

(64) Koch, U.; Popelier, P. L. A. Characterization of C-H-O Hydrogen Bonds on the Basis of the Charge Density. *J. Phys. Chem.* **1995**, *99* (24), 9747–9754. https://doi.org/10.1021/j100024a016.

(65) Perlovich, G. L. Two-Component Molecular Crystals: Relationship between the Entropy Term and the Molecular Volume of Co-Crystal Formation. *CrystEngComm* **2018**, *20* (26), 3634–3637. https://doi.org/10.1039/C8CE00592C.

Chapter 3 – The Role of Molecular Electrostatic Potentials in Crystal Engineering

3.1. Introduction

Crystal engineering involves intermolecular interactions as the primary tool for building supramolecular architectures[1,2]. Therefore, understanding the behavior of these interactions is essential in order to design supramolecular frameworks. Chapter 2 explores the importance of hydrogen-bonding, the most commonly used intermolecular interactions in the design and development of these frameworks. Halogen-bonding[3] is another emerging non-covalent interaction that has similar fundamental characteristics in terms of strength and directionality as that of hydrogen-bond[4]. However, halogen-bonds are intrinsically lipophilic and hydrophobic, which makes them well suited in biomedical applications such as drug delivery and transport. It is, therefore, imperative to compare the structural outcomes of halogen and hydrogen bonds when they are confronted with similar chemical environments to identify the synthons that can mimic each other to form the desired motif.

In a system with several structural outcomes, an established set of guidelines is required to design supramolecular architecture in a rational and predictable manner. In such a context, Etter[5] proposed that the best hydrogen-bond donor preferentially interacts with the best hydrogen-bond acceptor. With respect to co-crystallization, if the best donor-acceptor pair corresponds to heteromeric interaction (target•••co-former), it is called co-crystallization. If the best donor-acceptor pair forms homomeric interactions (target•••target or co-former•••co-former) it is likely to be recrystallization[6,7]. The major challenge is to determine what is "best". In Chapter 2 we used hydrogen-bond propensity (HBP) to define the best donor-acceptor pair. Although HBP was highly reliable, it has not been developed for halogen-bond driven co-crystals. It is therefore necessary to recognize a convenient method for predicting the co-crystallization screening experiments driven by halogen bonds. A more general approach to define "best" utilizes molecular electrostatic potential surfaces (MEPS), where the highest positive potential represents the best donor and the highest negative potential corresponds to the best acceptor. Although MEPS was conventionally designed for hydrogen-bonded systems, considering the fundamental similarity of hydrogen and halogen bond, MEPS can potentially be utilized in the same manner.

Hydrogen and iodine are far apart in the periodic table with a dramatic difference in the chemical and electronic properties, Table 3.1. However, in a given chemical environment, hydrogen and iodine possess similar [8,9,10] MEPS values, Figure 3.1.

Table 3.1. Comparison between hydrogen and iodine.

	Hydrogen	Iodine
Atomic weight (amu)	1.0079	126.90
Atomic radius (Å)	0.25	1.40
Atomic volume $(Å)^3$	0.065	11.49
Electronic configuration	$1s^2$	[Kr] $4d^{10}$ $5s^2$ $5p^5$
1^{st} Ionization energy (KJ/mol)	1312	1008

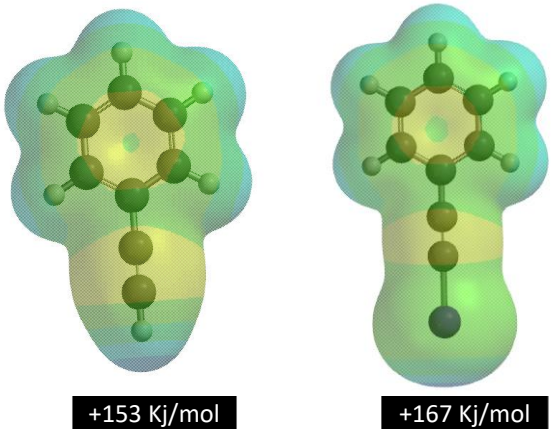

Figure 3.1. MEPS of structurally similar hydrogen-bond (left) and halogen-bond (right) compound (calculated using DFT and 6-311++G** basis set in vacuum).

There are various examples in the solid-state where hydrogen-bond and halogen-bond[11] structurally imitate each other. For example, 4,4'-bipyridine interacts with hydrogen-bond donor hydroquinone in the same fashion as halogen-bond donor, 1,4-diiodotetrafluorobenzene, Figure 3.2[12].

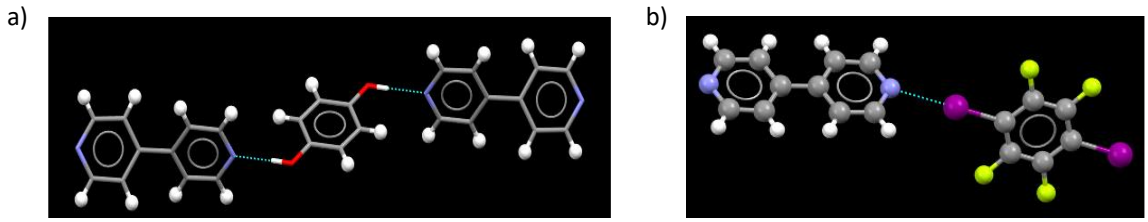

Figure 3.2. a) Hydrogen-bond interaction between 4,4'-bipyridine and hydroquinone, b) Halogen-bond interaction between 4,4'-bipyridine and 1,4-diiodotetrafluorobenzene[12].

Furthermore, a few studies report[13] that when hydrogen-bond and halogen-bond are present together in the same compound, there is a competition between the interactions. For example, equimolar amounts of 1,2-bis(4-pyridyl)-ethane, 1,4- diiodotetrafluorobenzene and hydroquinone yielded a dominating hydrogen-bond[14,15]. However, in an equimolar mixture of N,N,N',N'-tetramethylethylenediamine, 1,2- diiodo-tetrafluoroethane and ethylene glycol, the halogen-bond was more dominant, Figure 3.3.

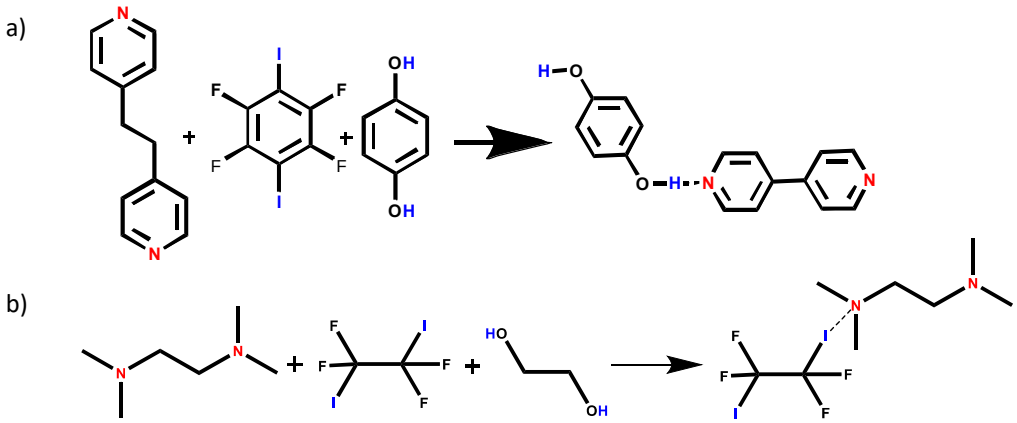

Figure 3.3. a) Hydrogen-bond as a dominant outcome b) Halogen-bond as a dominant outcome

There is a scarcity of reports where synthon mimicry is examined when a hydrogen-bond donor is replaced with a halogen-bond donor in the same molecular backbone. In order to explore this idea, we designed four iodo-analogous of **T1-T4** which were investigated in Chapter 2, Scheme 3.1. The potential co-formers used in this study were also kept same as in Chapter 2, Scheme 3.1.

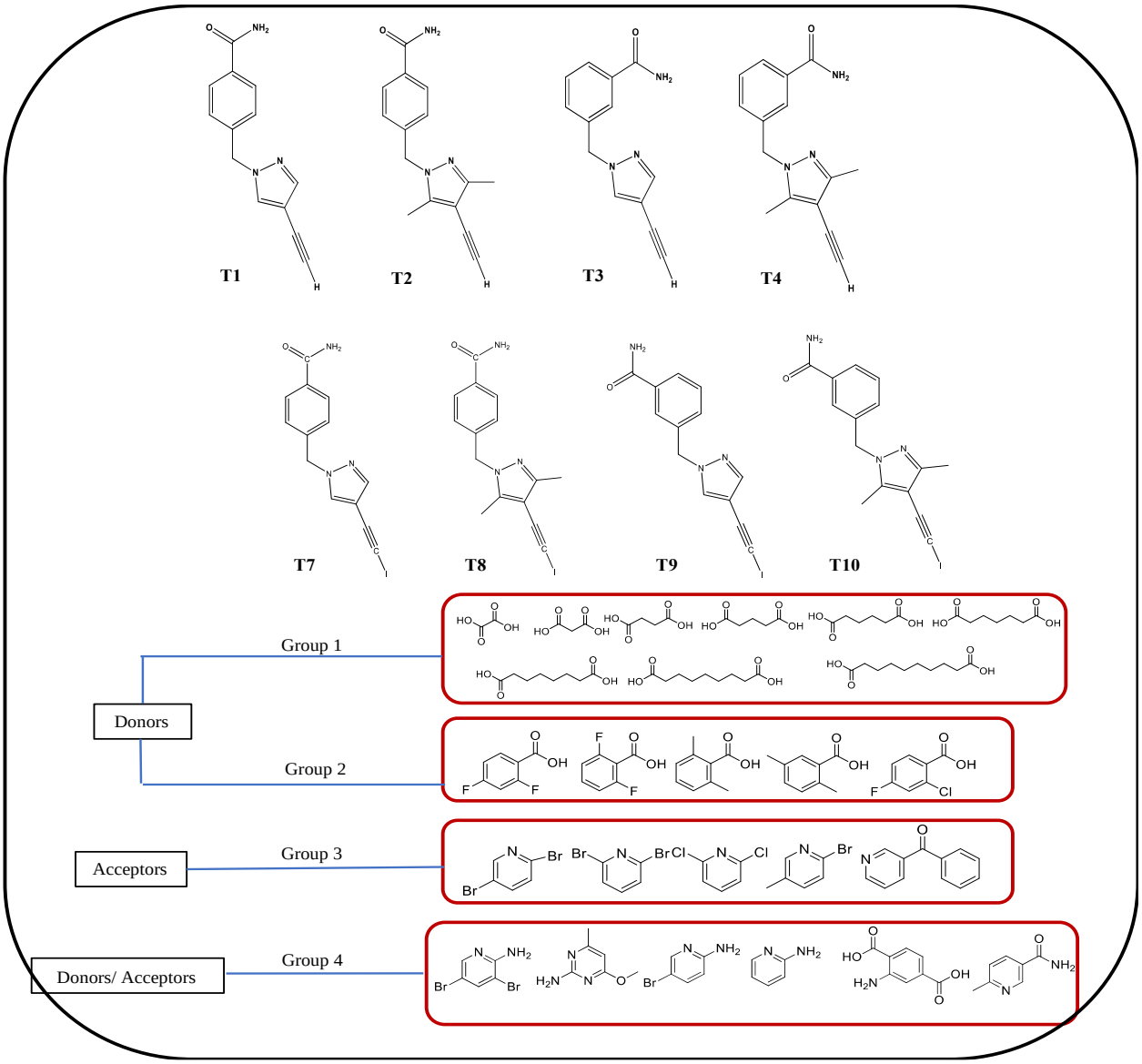

Scheme 3.1. Target compounds and co-formers of choice.

Each of these targets carries multiple binding sites. All the targets have two acceptor sites pyrazole-N and carbonyl (C=O) and one donor site amide-NH_2. **T1-T4** have additional hydrogen-bond ethynyl donor, and **T7-T10** have iodo-ethynyl as a halogen-bond donor. There are various homomeric and heteromeric interactions possible between the targets and co-formers. Scheme 3.2. summarizes all the potential interactions.

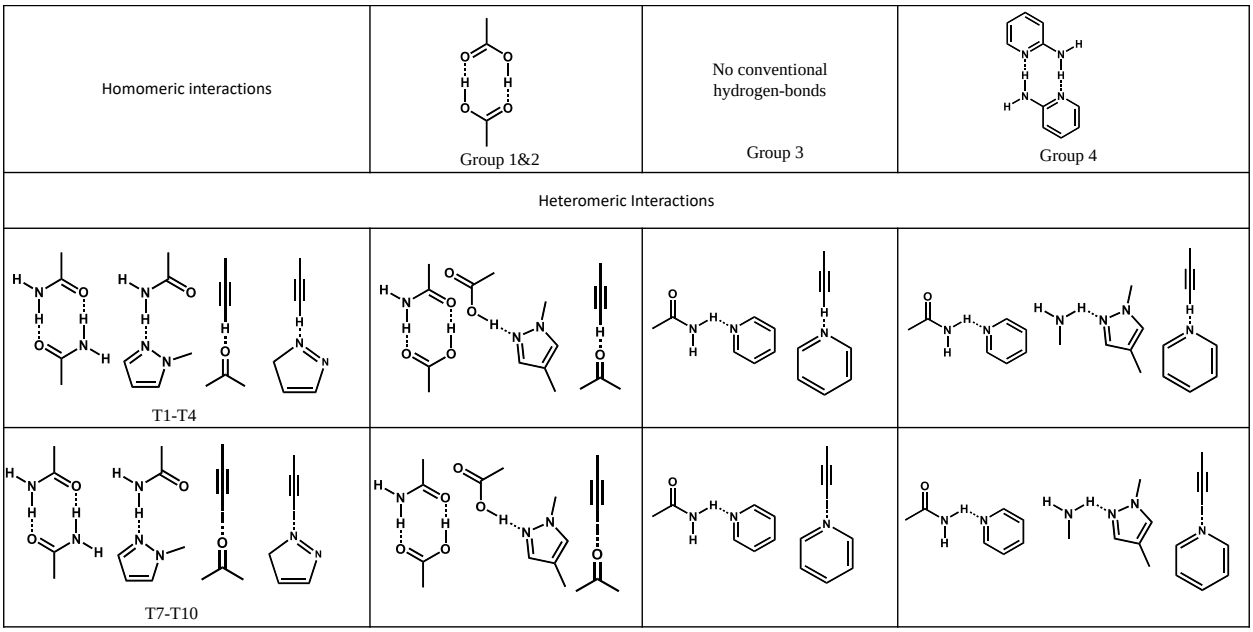

Scheme 3.2. Potential homomeric and heteromeric interactions.

In this chapter we will investigate if **T7-T10** will form similar homomeric and heteromeric interactions as that of **T1-T4** in combination with 25 co-formers. We will use MEPS to define the best donor-acceptor pair to predict the most likely synthon formation. The predicted interactions will be compared to the experimentally observed synthons to examine the role of electrostatics in crystal engineering.

This research is carried out to answer the following questions:

1. Can electrostatics determine the potential homomeric and heteromeric interactions observed between a target and co-former?
2. Will **T7-T10** produce similar homomeric and heteromeric synthons as that of **T1-T4**?

3.2. Experimental

The synthesis and characterization of **T1-T4** are described in Chapter 2. 4-bromo-1H-pyrazole, 3-bromo-1H-pyrazole, 4-(bromomethyl)benzonitrile, 3-(bromomethyl)benzonitrile, THF were purchased from Alfa Aesar and were utilized without further purification. All 25 co-formers were purchased from commercial sources and used as received. Melting points were measured using a Fisher-Johns melting point apparatus. Solution ^{1}H NMR data were collected in $CDCl_3$ and DMSO

on a Varian Unity plus 400 MHz NMR spectrometer. IR spectra of the solids resulting from the co-crystal screening experiments were recorded with a Nicolet 380 FT-IR spectrometer (ATR) and a ZnSe crystal.

3.2.1. Syntheses

*3.2.1.1. Synthesis of 4-((4-(iodoethynyl)-1H-pyrazol-1-yl)methyl)benzamide (**T7**)*

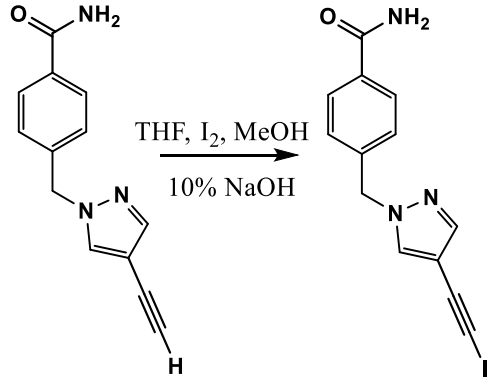

T7 was synthesized by dissolving **T1** (0.50g, 1.85 mmol) in THF (50 mL). Simultaneously adding dropwise, a concentrated solution of iodine in methanol (1.40g, 5.50 mmol) and a 10% sodium hydroxide solution over 30 min, with vigorous stirring. The solution was stirred overnight and quenched with 100 mL water upon which light yellow color precipitate formed. The filtered solid was washed with sodium bisulfite solution to deliver yellow powder of **T7** (0.67g, 91%). M.P.: 132-140ºC, 1H NMR (400MHz, DMSO-d_6): 8.07(2H, d), 7.79(2H, d), 7.57(1H, s), 7.33(1H, s), 5.44 (2H, s).

*3.2.1.2. Synthesis of 3-((4-(iodoethynyl)-1H-pyrazol-1-yl)methyl)benzamide (**T8**)*

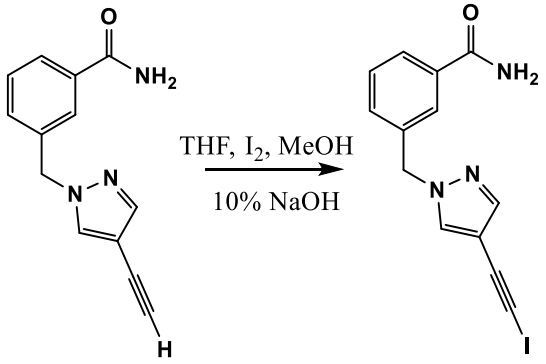

T2 (0.50g, 1.85 mmol) was dissolved in THF (50 mL). Then simultaneously adding dropwise, a concentrated solution of iodine in methanol (1.40g, 5.50 mmol) and a 10% sodium hydroxide solution over 30 min, with vigorous stirring. The solution was stirred overnight and quenched with 100 mL water upon which light yellow color precipitate formed. The filtered solid was washed with sodium bisulfite solution to deliver pale powder of **T8** (0.64g, 87%). M.P.: 133-135ºC, 1H NMR (400 MHz, $CDCl_3$): 8.10(1H, s), 7.92(1H, d), 7.83(1H, t), 7.56(1H, d), 7.33(2H, s), 5.33 (2H, s).

*3.2.1.3. Synthesis of 4-((4-(iodoethynyl)-3,5-dimethyl-1H-pyrazol-1-yl)methyl)benzamide (**T9**)*

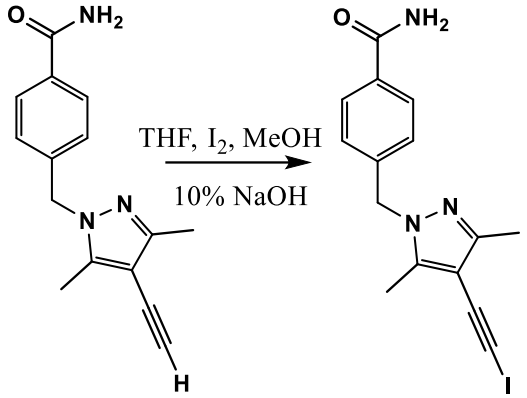

T3 (0.50g, 1.67 mmol) was dissolved in THF (50 mL). Simultaneously adding dropwise, a concentrated solution of iodine in methanol (1.40g, 5.50 mmol) and a 10% sodium hydroxide solution over 30 min, with vigorous stirring. The solution was stirred overnight and quenched with 100 mL water upon which light yellow color precipitate formed. The filtered solid was washed with sodium bisulfite solution to deliver pale powder of **T9** (0.57g, 80%). M.P.: 132-137ºC, 1H NMR (400 MHz, $CDCl_3$): 9.40(2H, s), 7.78(2H, d), 7.12(2H, d), 5.31 (2H, s), 2.26(3H, s), 2.13(3H, s).

*3.2.1.4. Synthesis of 3-((4-(iodoethynyl)-3,5-dimethyl-1H-pyrazol-1-yl)methyl)benzamide (**T10**)*

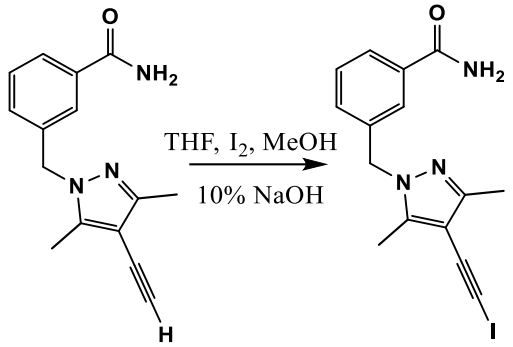

T4 (0.50g, 1.67 mmol) was dissolved in THF (50 mL). Simultaneously adding dropwise, a concentrated solution of iodine in methanol (1.40g, 5.50 mmol) and a 10% sodium hydroxide solution over 30 min, with vigorous stirring. The solution was stirred overnight and quenched with 100 mL water upon which light yellow color precipitate formed. The filtered solid was washed with sodium bisulfite solution to deliver pale powder of **T10** (0.54g, 76%). M.P.: 131-134ºC, 1H NMR (400MHz, $CDCl_3$): 7.77 (1H, s), 7.66 (1H, d), 7.46 (1H, d), 7.13 (1H, t), 5.25 (2H, s), 2.25 (3H, s), 2.15 (3H, s).

3.2.2. Calculation of molecular electrostatic potential surfaces

MEPS were calculated for **T1-T4** and **T7-T10** and 25 co-formers implementing density functional theory using B3LYP and 6-311++G** basis set in vacuum. All calculations were executed with the Spartan'14 software. The compounds were sketched, and the geometries were optimized so that the calculation could be set up on the most stable geometry of the compound. A positive point in the vacuum is used as a probe against the surface of the molecules. The numbers are represented in kJ/ mol, which is the interaction energy between the positive probe and the surface of the molecule. The numbers indicate electrostatic potentials, where a negative number corresponds to an acceptor and positive number to a donor.

3.2.3. Co-crystallization experiments

The co-crystal screening of **T1-T4** is described in section 2.2.3. **T7-T10** targets were subjected to co-crystallization screening experiments with the 25 co-formers. See section 2.2.3 for detailed description on co-crystallization experiments.

3.3. Results

3.3.1. Molecular electrostatic potential surface (MEPS) calculations

The targets examined in this study **T1-T4** and **T7-T10** contain two acceptor sites carbonyl C=O & pyrazole-N, and two donor sites amide-NH & ethynyl-H/ iodo-ethynyl. The MEPS calculations for the targets are summarized in Figure 3.4.

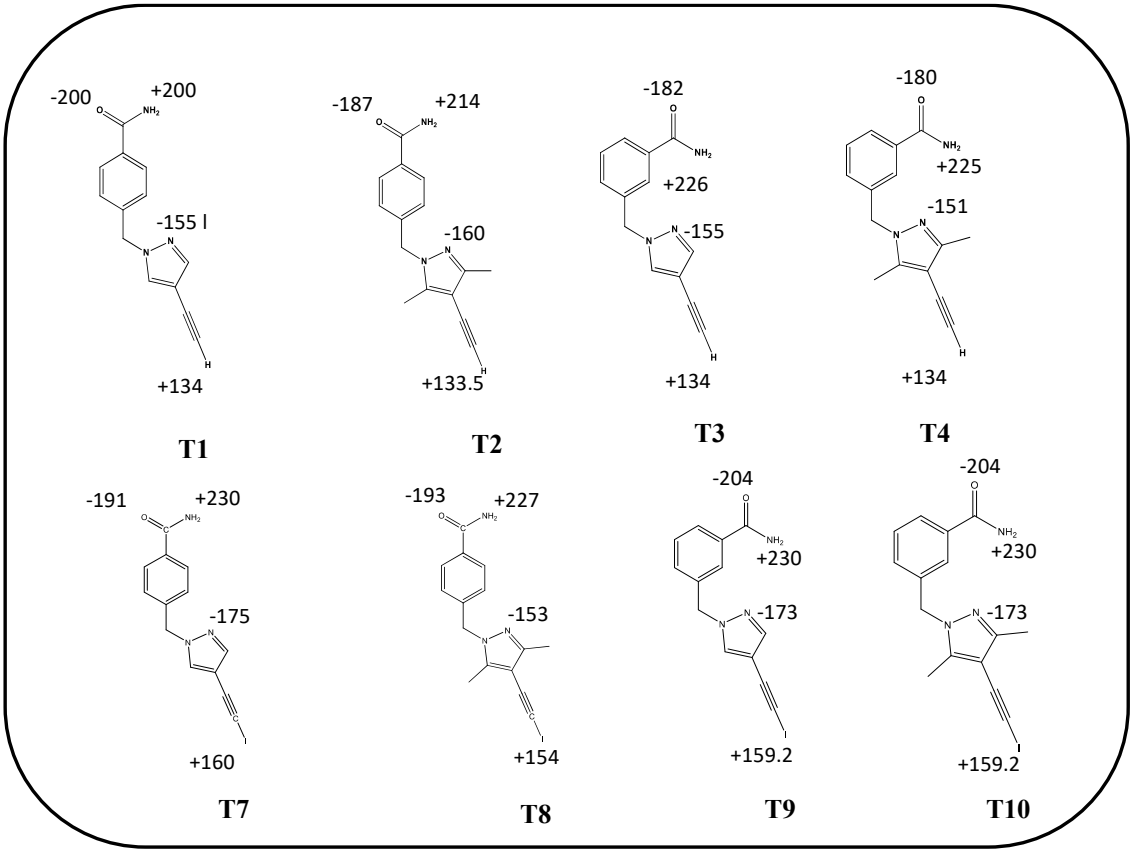

Figure 3.4. Calculated MEPS values for the targets (kJ/ mol).

We ranked the acceptor and donor sites according to MEPS, where a higher positive potential indicates the best donor and the highest negative potential indicates the best acceptor. The MEPS data indicated carbonyl C=O as the best acceptor and amide N-H as the best donor which was consistent for all the targets. Hence MEPS predicted amide•••amide as the most likely homomeric interaction for all the targets, Figure 3.5.

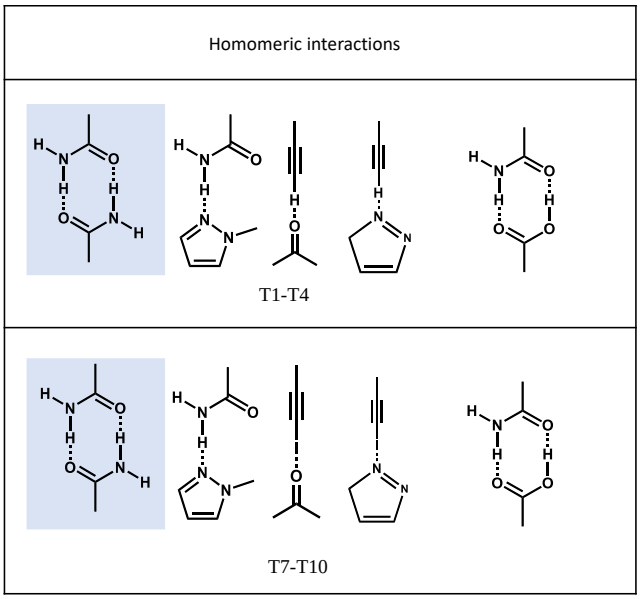

Figure 3.5. The homomeric interactions predicted by MEPS (highlighted in blue).

Similar MEPS calculations were carried out for the 25 co-formers to analyze the best donor and acceptor for the homomeric interaction in the co-former. Table 3.2 summarizes the electrostatic potentials of the best donor-acceptor for the co-formers (rounded to the nearest whole number).

Table 3.2. Best donor-acceptor for the co-formers ranked using the MEPS data.

Co-formers	Best donor (kJ/ mol)	Best acceptor (kJ/ mol)	MEPS predicted Interaction
2-Chloro-4-fluorobenzoic acid	154	-184	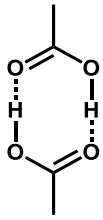 Groups 1&2
2,4-Difluorobenzoic acid	201	-191	
2,6-Difluorobenzoic acid	191	-193	
2,6-Dimethylbenzoic acid	267	-187	
6-Methylnicotinamide	222	-184	
2,5-Dimethylbenzoic acid	253	-194	
Adipic acid	287	-189	
Azealic acid	284	-193	
Glutaric acid	296	-190	
Malonic acid	318	-171	
Oxalic acid	307	-147	
Pimelic acid	285	-192	
Sebacic acid	288	-194	
Suberic acid	288	-191	

Succinic acid	314	-211	
2-Bromo-5-methylpyridine	N/A	-178	No conventional hydrogen-bonds Group 3
2,5-Dibromopyridine	N/A	-152	
2,6-Dibromopyridine	N/A	-157	
2,6-Dichloropyridine	N/A	-157	
3-Benzoylpyridine	N/A	-165	
2-Amino-3,5-dibromopyridine	169	-206	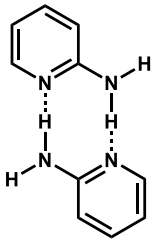 Group 4
2-Amino-4-methoxy-6-methylpyridine	140	-255	
2-Amino-5-bromopyridine	173	-223	
2-Aminopyridine	155	-246	
2-Aminoterephthalic acid	275	-151	

3.3.2. Experimental co-crystal screening

Formation of a co-crystal was established by carefully comparing the IR spectrum of the ground solid mixture with the IR spectra of the pure donor and the acceptor. The C=O, N-H, and C≡C bond stretch of the targets and co-formers were analyzed which if a new interaction is formed was directly affected. A shift greater than 3cm^{-1} corresponds to a successful co-crystal event. Table 3.3. summarizes the IR stretching frequencies of successful co-crystallization experiments. The IR stretching frequencies remained unchanged for the instances where the co-crystallization experiments failed.

Table 3.3. IR stretching frequencies (cm^{-1}) of the successful co-crystals experiment.

	T1	**T2**	**T3**	**T4**	**T7**	**T8**	**T9**	**T10**
Co-former	C≡C 2359 C=O 1711	C≡C 2338 C=O 1665	C≡C 2335 C=O 1665	C≡C 2349 C=O 1666	C≡C 2222 C=O 1648	C≡C 2229 C=O 1672	C≡C 2226 C=O 1654	C≡C 2229 C=O 1673
2-Amino-3,5-dibromopyridine	Ground Mixture							
N-H 3463, 3270 C=C 1623	N-H 3350, 3166 C≡C 2359 C=O 1716	N-H 3369, 3166 C≡C 2338 C=O 1667	N-H 3362, 3167 C≡C 2333 C=O 1666	N-H 3352, 3143 C≡C 2350 C=O 1666	N-H 3406, 3262 C≡C 2223 C=O 1650	N-H 3452, 3213 C≡C 2223 C=O 1670	N-H 3457, 3367 C≡C 2223 C=O 1654	N-H 3320, 3168 C≡C 2223 C=O 1669
2-Amino-4-methoxy-6-methylpyrimidine	Ground Mixture							
N-H 3366, 3184 C=C 1632	N-H 3341, 3164 C≡C 2357 C=O 1712	N-H 3357, 3181 C≡C 2338 C=O 1668	N-H 3351, 3169 C≡C 2336 C=O 1664	N-H 3346, 3159 C≡C 2350 C=O 1664	N-H 3483, 3396 C≡C 2223 C=O 1650	N-H 3362, 3180 C≡C 2222 C=O 1673	N-H 3374 3182 C≡C 2229 C=O 1658	N-H 3483, 3396 C≡C 2223 C=O 1671
2-Amino-5-bromopyridine	Ground Mixture							

N-H 3443, 3290 C=C 1621	N-H 3352, 3166 C≡C 2355 C=O 1712	N-H 3377, 3170 C≡C 2101 C=O 1665	N-H 3367, 3189 C≡C 2335 C=O 1670	N-H 3360, 3148 C≡C 2348 C=O 1665	N-H 3388, 3374 C≡C 2223 C=O 1647	N-H 3345, 3155 C≡C 2223 C=O 1669	N-H 3412, 3216 C≡C 2223 C=O 1659	N-H 3483, 3345 C≡C 2223 C=O 1672
2-Aminopyridine	Ground Mixture							
N-H 3437, 3284 C=C 1623	N-H 3351, 3169 C≡C 2356 C=O 1715	N-H 3367, 3180 C≡C 2100 C=O 1670	N-H 3370, 3187 C≡C 2336 C=O 1659	N-H 3352, 3153 C≡C 2349 C=O 1664	N-H 3485, 3216 C≡C 2223 C=O 1645	N-H 3330, 3171 C≡C 2223 C=O 1670	N-H 3369, 3250 C≡C 2223 C=O 1659	N-H 3336, 3246 C≡C 2223 C=O 1671
2-Aminoterephthalic acid	Ground Mixture							
N-H 3455, 3076 C=C 1681	N-H 3353, 3171 C≡C 2357 C=O 1706	N-H 3364, 3144 C≡C 2102 C=O 1668	N-H 3373, 3178 C≡C 2336 C=O 1664	N-H 3362, 3189 C≡C 2349 C=O 1665	N-H 3440, 3398 C≡C 2223 C=O 1644	N-H 3341,3148 C≡C 2226 C=O 1674	N-H 3339, 3165 C≡C 2223 C=O 1654	N-H 3475, 3298 C≡C 2223 C=O 1669

3.4. Discussions

3.4.1. Using MEPS calculations for co-crystal screening

Implementing MEPS to select the best donor-acceptor pair for the homomeric interaction for all the targets resulted in N-H as the best donor and O=C as the best acceptor. MEPS predicted similar homomeric interactions for all the targets. Although we were unable to obtain crystal structures either of **T1-T4**, we did obtain a crystal structure of **T7**, Figure 3.6. The observed homomeric synthon of the target matches the MEPS predicted amide•••amide interaction.

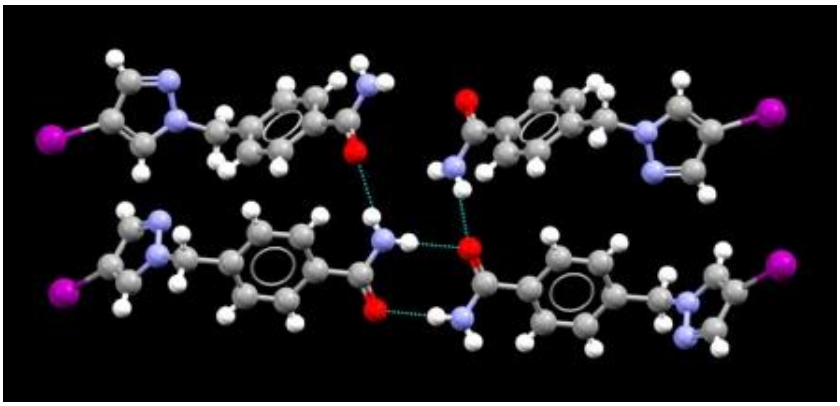

Figure 3.6. Crystal structure of **T7**.

There was only one combination for the most optimal homomeric interactions of co-formers which were correctly predicted by MEPS, Figure 3.7.

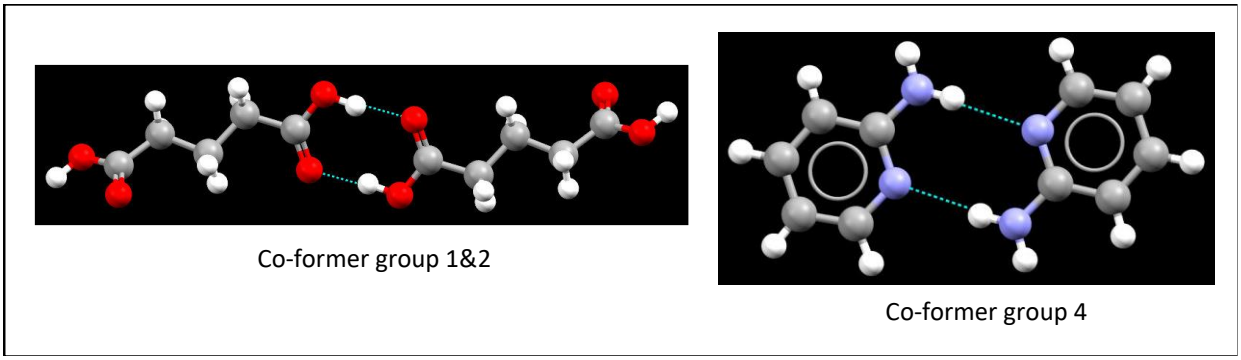

Figure 3.7. Crystal structure of glutaric acid (left), and aminopyridine (right)[16,17].

The targets in combination with co-formers of groups 1and 2, indicated OH of the acid as the best donor (highest positive potential), and comparable negative potential between acid C=O or target C=O. In instances where the target C=O was the best acceptor it corresponded to a heteromeric interaction, whereas in cases where the acid C=O was the best acceptor it was a homomeric interaction leading to recrystallization. Experimentally the C=O stretch in IR remain consistent for both acids and the targets demonstrating that no new interaction was formed. In addition, the C≡C stretch for both **T1-T4** and **T7-T10** remained consistent indicating C≡C does not participate in the assembly. The targets did not form co-crystals with either group1 or 2 co-formers, Scheme 3.3.

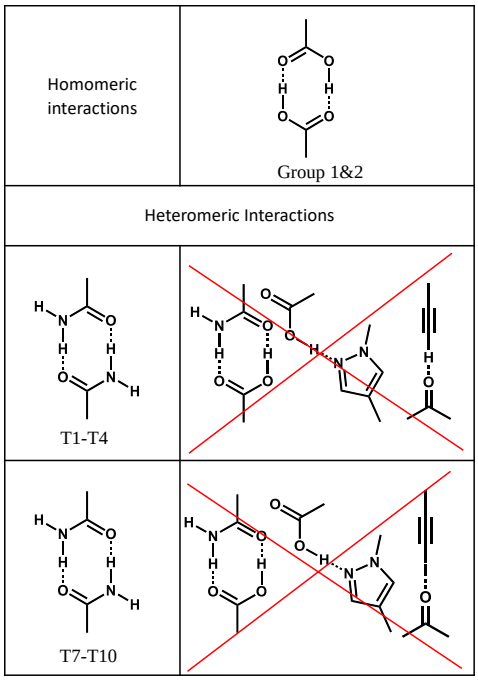

Scheme 3.3. The observed homomeric and heteromeric interactions in targets with group1 and 2 co-formers.

With group 3 co-formers, MEPS indicate amide N-H as the best donor. The choice of the best acceptor was either carbonyl C=O (-200 kJ/mol) of the target or pyridine-N (-157 kJ/mol). The best donor-acceptor pair according to MEPS was the amide•••amide interaction, Scheme 3.4. Experimentally we don't see any change in the C=O or N-H stretch which suggests that no new interactions were formed. The heteromeric interactions in the majority of the reactions for co-formers in groups 1-3 were not competitive enough to break the expected self-complementary interactions. Again, the C≡C stretch remained consistent indicating neither the ethynyl-H nor iodo-ethynyl formed any new interaction.

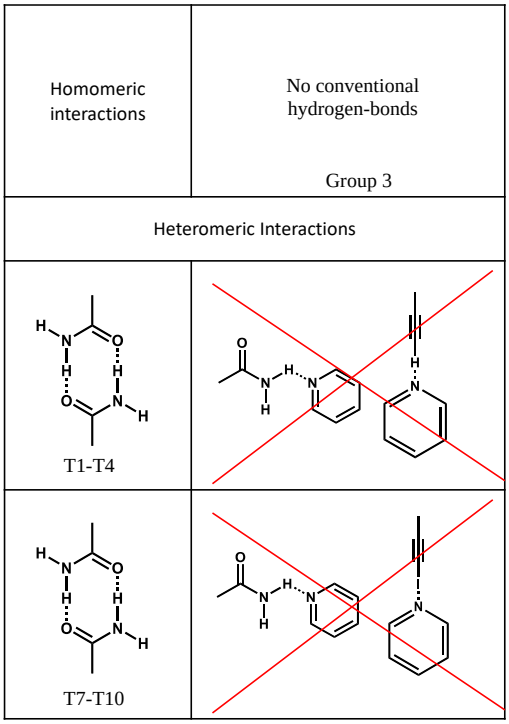

Scheme 3.4. The observed homomeric and heteromeric interactions in targets with group3 co-formers.

The combination of targets with the co-formers of group 4, followed the same trend where the amide N-H (except 2-aminoterephthalic acid) was the best donor. However, with this group of co-formers the pyridine-N was found to be the best acceptor resulting in a "YES" to co-crystallization. Experimentally we did not observe any difference in the C=O stretches of the targets which in turn suggests that the amide•••amide interaction was still present. We observed a huge shift in the N-H amine stretch of the co-former which, suggest that the N-H•••pyridine-N interaction is broken to form a new interaction with N-H•••pyrazole leading to co-crystallization, Scheme 3.5. Although

MEPS could not predict the synthons that drive the co-crystallization, it predicted the outcomes correctly.

Homomeric interactions	Group 4 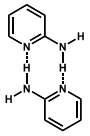	
	Heteromeric Interactions	
	Predicted synthons	Observed synthons
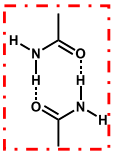 T1-T4	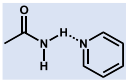	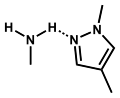
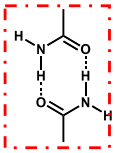 T7-T10	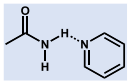	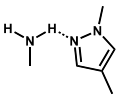

Scheme 3.5. The observed homomeric and heteromeric interactions in targets with group 4 co-formers.

Overall the amide N-H was the best donor according to MEPS in all the cases in combination with 25 co-formers. Experimentally, the amide•••amide self-complementarity interaction was strong and could not be replaced with any new interaction. The IR spectra associated with the C≡C remained consistent in all the cases, which also proves that C≡C did not participate in these reactions. The MEPS for -C≡C-H and -C≡C-I show that both the positive potentials were comparable, where C≡C-H ranged from +134-135 kJ/ mol and C≡C-I were +154-160 kJ/ mol. Although the MEPS of C≡C-I was slightly higher than C≡C-H, overall, in the presence of other functional groups, it did not participate in any co-crystallization experiments. The results indicate that both hydrogen-bond and halogen-bond targets provide consistent interactions with all the different groups of co-formers.

3.5. Conclusions

1. The preferred homomeric interactions were amide N-H•••O=C interactions in both iodo-ethynyl and ethynyl-H targets. The targets formed co-crystals only with group 4 co-formers, where in addition to strong amide•••amide interaction a new heteromeric interaction was observed between amine N-H•••pyrazole-N. This study also points out that, although the hydrogen and iodine is far apart in the periodic table, if used in the same chemical environment that can mimic each other. This structural similarity could be significant in biomedical areas as halogen bonds are hydrophobic and lipophilic when compared to hydrogen bonds.

2. MEPS could guide the structural preference for all homomeric interactions and failed co-crystallization experiments. However, MEPS could not recognize the best donor-acceptor synthon pair for heteromeric interactions of the targets with group 4 co-formers.

3.6. References

(1) Lehn, J.-M. From Supramolecular Chemistry towards Constitutional Dynamic Chemistry and Adaptive Chemistry. *Chem. Soc. Rev.* **2007**, *36* (2), 151–160. https://doi.org/10.1039/B616752G.

(2) Benedict, J. B. *Recent Advances in Crystallography*; 2012. https://doi.org/10.5772/2711.

(3) Meyer, F.; Dubois, P. Halogen Bonding at Work: Recent Applications in Synthetic Chemistry and Materials Science. *CrystEngComm* **2013**, *15* (16), 3058–3071. https://doi.org/10.1039/C2CE26150B.

(4) Cinčić, D.; Friščić, T.; Jones, W. Isostructural Materials Achieved by Using Structurally Equivalent Donors and Acceptors in Halogen-Bonded Cocrystals. *Chemistry – A European Journal* **2008**, *14* (2), 747–753. https://doi.org/10.1002/chem.200701184.

(5) Etter, M. C. Encoding and Decoding Hydrogen-Bond Patterns of Organic Compounds. *Acc. Chem. Res.* **1990**, *23* (4), 120–126. https://doi.org/10.1021/ar00172a005.

(6) Musumeci, D.; Hunter, C. A.; Prohens, R.; Scuderi, S.; McCabe, J. F. Virtual Cocrystal Screening. *Chem. Sci.* **2011**, *2* (5), 883–890. https://doi.org/10.1039/C0SC00555J.

(7) Etter, M. C. Encoding and Decoding Hydrogen-Bond Patterns of Organic Compounds. *Acc. Chem. Res.* **1990**, *23* (4), 120–126. https://doi.org/10.1021/ar00172a005.

(8) Saha, B. K. Ethynyl Group as a Supramolecular Halogen and C≡C−H···C≡C Trimer Synthon in 2,4,6-Tris(4-Ethynylphenoxy)-1,3,5-Triazine. 9.

(9) Aakeröy, C. B.; Welideniya, D.; Desper, J. Ethynyl Hydrogen Bonds and Iodoethynyl Halogen Bonds: A Case of Synthon Mimicry. *CrystEngComm* **2016**, *19* (1), 11–13. https://doi.org/10.1039/C6CE02201D.

(10) Dubey, R.; Lim, D. Weak Interactions: A Versatile Role in Aromatic Compounds. *COC* **2011**, *15* (12), 2072–2081. https://doi.org/10.2174/138527211795703667.

(11) Robinson, J. M. A.; Philp, D.; Harris, K. D. M.; Kariuki, B. M. Weak Interactions in Crystal Engineering—Understanding the Recognition Properties of the Nitro Group. *New J. Chem.* **2000**, *24* (10), 799–806. https://doi.org/10.1039/B004086J.

(12) Walsh, R. B.; Padgett, C. W.; Metrangolo, P.; Resnati, G.; Hanks, T. W.; Pennington, W. T. Crystal Engineering through Halogen Bonding: Complexes of Nitrogen Heterocycles with Organic Iodides. *Crystal Growth & Design* **2001**, *1* (2), 165–175. https://doi.org/10.1021/cg005540m.

(13) Gamekkanda, J. C.; Sinha, A. S.; Desper, J.; Đaković, M.; Aakeröy, C. B. Competition between Hydrogen Bonds and Halogen Bonds: A Structural Study. *New J. Chem.* **2018**, *42* (13), 10539–10547. https://doi.org/10.1039/C8NJ00537K.

(14) Corradi, E.; Meille, S. V.; Messina, M. T.; Metrangolo, P.; Resnati, G. Halogen Bonding versus Hydrogen Bonding in Driving Self-Assembly Processes. *Angewandte Chemie International Edition* **2000**, *39* (10), 1782–1786. https://doi.org/10.1002/(SICI)1521-3773(20000515)39:10<1782::AID-ANIE1782>3.0.CO;2-5.

(15) Aakeröy, C. B.; Wijethunga, T. K.; Desper, J. Molecular Electrostatic Potential Dependent Selectivity of Hydrogen Bonding. *New J. Chem.* **2015**, *39* (2), 822–828. https://doi.org/10.1039/C4NJ01324G.

(16) Morrison, J. D.; Robertson, J. M. 212. The Crystal and Molecular Structure of Certain Dicarboxylic Acids. Part VII. β-Glutaric Acid. *J. Chem. Soc.* **1949**, No. 0, 1001–1008. https://doi.org/10.1039/JR9490001001.

(17) Chao, M.; Schemp, E.; Rosenstein, R. D. 2-Aminopyridine. *Acta Cryst B* **1975**, *31* (12), 2922–2924. https://doi.org/10.1107/S0567740875009272.

Chapter 4 - Evaluating Hydrogen-Bond Propensity, Hydrogen-Bond Coordination and Hydrogen-Bond Energy as Tools for Predicting the Outcome of Attempted Co-crystallizations

4.1. Introduction

With the prevalence of co-crystals in pharmaceutics[1,2,3,4,5,6,7,8,9,10,11,12] co-crystal prediction methodologies that could complement the experimental screening processes are becoming highly relevant [13,14,15,16,17,18,19,20,21,22,23,24,25,26]. Despite reports of some predictive approaches[27,28] there is a scarcity[15] of systematic in-depth comparisons between different methods for co-crystal prediction. Therefore, in this study, we aim to remedy this problem in two ways. The first goal is to evaluate three predictive methodologies by comparing their outcomes with experimental co-crystal screening results. The second goal is to predict which hydrogen-bond interactions are most likely to drive the synthesis of co-crystals, for cases where crystallographic data are available. We will examine two structure informatics models; hydrogen-bond propensity (HBP) and hydrogen-bond coordination (HBC), and one approach based on calculated hydrogen-bond energies (HBE). In Chapter 2, we explored hydrogen-bond propensity as a predictive tool for 150 combinations of targets/ co-formers, which gave an accuracy of 92-95%. Other studies reported by Delori et al.[29,30] employed HBP on Pyrimethamine, an antimalarial drug against seven potential co-formers producing a minimum of 78% accuracy. Given the high reliability of HBP, it was selected as Methodology 1 in this study.

The second method examined in this study is hydrogen-bond coordination (HBC)[24]. HBC is the probability of observing a 0,1,2 or 3 coordination number (CN) between a hydrogen-bond donor and an acceptor; contrary to HBP, which is the probability of formation of only one bond. Since, the chances of forming a co-crystal, are highly dependent on the presence of key hydrogen-bond donors and acceptors greater understanding of such interactions is essential for selecting co-formers.

Electrostatics play an integral part in hydrogen-bonding,[31] and therefore, an electrostatic based method was used to obtain hydrogen-bond energy (HBE), as the third methodology. The maxima and minima of the molecular electrostatic potential surfaces (MEPS) were combined with Hunter's parameters[32,14] to determine HBE[13,15] of key hydrogen-bond interactions.

The three methodologies were tested on Nevirapine and Diclofenac, two known drugs used as non-nucleoside reverse transcriptase inhibitors, and nonsteroidal anti-inflammatory formulations, respectively[33, 34]. These active pharmaceutical ingredients (APIs) were selected because they are; (i) relatively small and, (ii) have limited conformational flexibility, Figure 4.1. We utilized previously published experimental data from systematic co-crystal screens of Nevirapine[33] against fourteen co-formers and of Diclofenac[34] against sixteen co-formers, Figure 4.1.

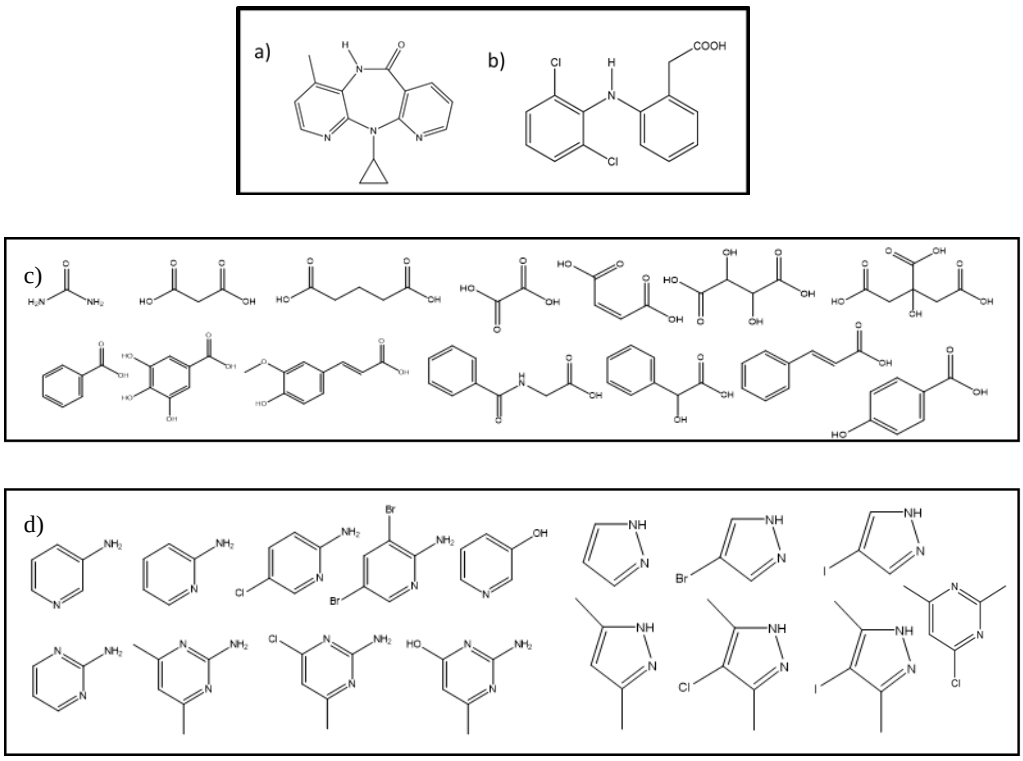

Figure 4.1. (a) Nevirapine; (b) Diclofenac;
c) co-formers screened against Nevirapine; and d) co-formers screened against Diclofenac.

We used HBP, HBC, and HBE approaches to predict the co-crystallization outcomes followed by predicting which homomeric or heteromeric interactions will most likely prevail for Nevirapine and Diclofenac in combinations with 14 and 16 co-formers respectively. The predicted outcomes were compared with the experimental results to determine if one method is better than the other. Figure 4.2. summarizes the outline of this study.

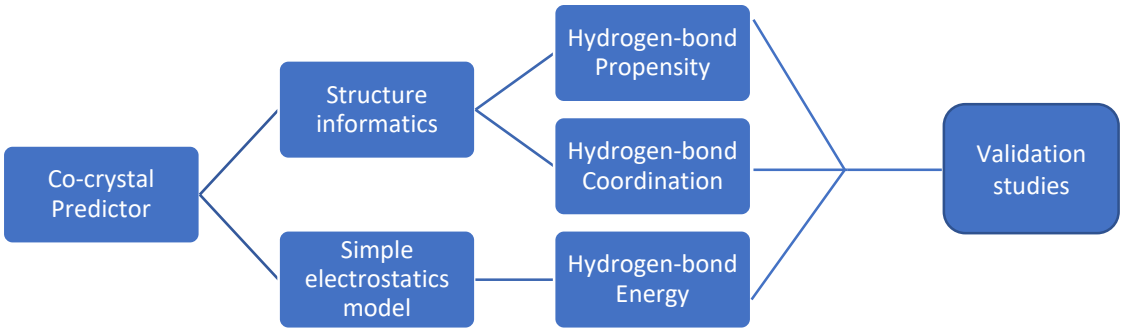

Figure 4.2. Outline of this study.

This study will address the following questions:

1. Which method provides a better accuracy in predicting co-crystallization outcomes?
2. Can the methods predict the primary hydrogen-bond interactions that drive the co-crystal synthesis correctly?

4.2. Prediction studies

4.2.1. Hydrogen-bond propensity (HBP)

The CSD contains a large amount of structural information which can be used in a statistical model to provide valuable insights about existing hydrogen-bond interactions. The hydrogen-bond propensity (HBP) is the probability of formation of an interaction based on defined functional groups and fitting data[35,22,36,37,30,29].

Figure 4.3 lists the defined functional groups of Nevirapine, and Diclofenac. All the calculations were done in Mercury 5.40, 2019 (updated on May 2019) [35,38,39,40].

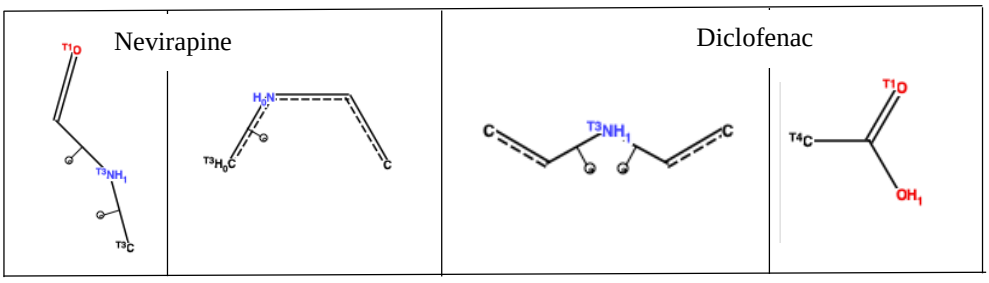

Figure 4.3. Functional groups defined for Nevirapine (left) and Diclofenac (right).

When the API and co-former are combined in a solution there will be a balance between homomeric interactions (intermolecular interactions between API•••API and co-former•••co-former) and heteromeric interaction (API•••co-former). Using HBP, we calculated a $\Delta_{propensity}$ to establish which interactions prevail. $\Delta_{propensity} \geq 0$ was deemed as a "YES" to co-crystallization (i.e. heteromeric hydrogen-bonds dominate); $\Delta_{propensity} < 0$ deemed as a "NO" to co-crystallization with homomeric hydrogen-bonds being more likely, Scheme 4.1.

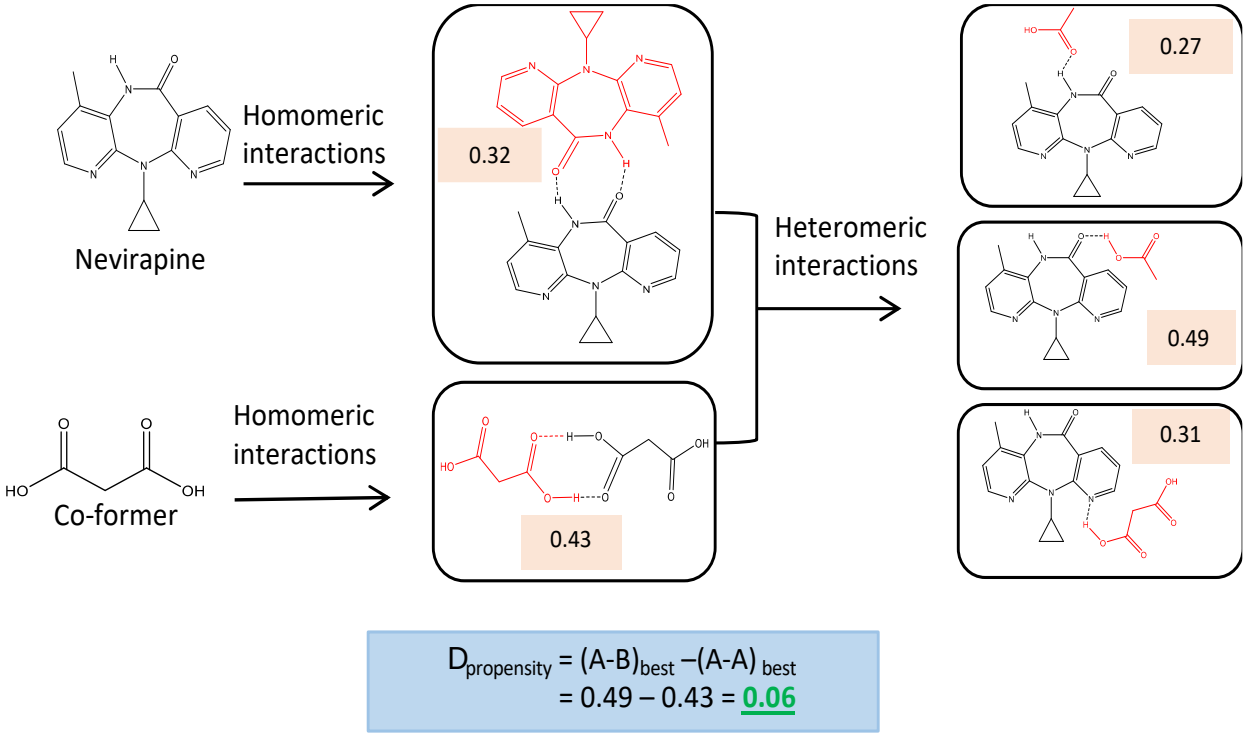

Scheme 4.1. Approach for calculating HBP for Nevirapine and malonic acid.

4.2.2. Hydrogen-bond coordination (HBC)

Hydrogen-bond coordination (HBC) is the probability of observing a coordination number for any given hydrogen-bond donor and acceptor atom. The coordination number (CN) is defined as the number of interatomic hydrogen-bonds formed between a donor and an acceptor[24]. Contrary to HBP, which is the probability of formation of one bond, HBC gives the probability of formation of 0,1,2 and 3 CNs by a given donor/ acceptor. The CN with the highest probability corresponds to the most optimal hydrogen-bond interaction.

HBC was calculated for each combination of an API and a co-former. The highest donor CN was matched with the highest acceptor CN between the similar molecules (API•••API and co-former•••co-former) to select the most optimal homomeric interaction, Scheme 4.2 (highlighted in green). Using HBC to predict if a co-crystal was formed, the highest CN of a donor was paired with the highest CN of an acceptor between API and co-former, Scheme 4.2 (highlighted in red). If this donor-acceptor pair was heteromeric, it was assigned "YES" to co-crystallization, and if it was homomeric, then it was assigned as "NO" to co-crystallization.

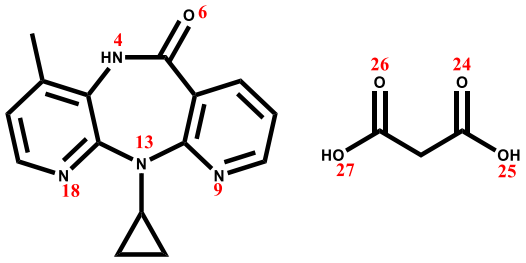

Homomeric interactions (API•••API)				
Atom (D/A)	=0	=1	=2	=3
N4 (D)	0.30	0.69	0.00	0.00
N18 (A)	0.87	0.11	0.01	0.00
N9 (A)	0.88	0.11	0.01	0.00
O6 (A)	0.28	**0.68**	0.04	0.00
Homomeric interactions (co-former•••co-former)				
O25 (D)	0.00	**0.95**	0.05	0.00
O27 (D)	0.00	0.95	0.05	0.00
O24 (A)	0.49	0.47	0.03	0.00
O25 (A)	0.91	0.09	0.00	0.00
O26 (A)	0.49	0.47	0.03	0.00
O27 (A)	0.91	0.09	0.00	0.00

Scheme 4.2. Approach for calculating HBC for Nevirapine and malonic acid**.**

(D: hydrogen-bond donor, A: hydrogen-bond acceptor; green: homomeric interactions, red: heteromeric interaction)

In Scheme 4.2, HBC predicted the most likely hydrogen-bond coordination between acceptor (O=C) of Nevirapine and donor (O-H) of malonic acid; therefore, it was assigned "YES" to co-crystallization.

4.2.3. Hydrogen-bond energy (HBE)

HBE was calculated using molecular electrostatic potentials (MEPs) combined with Hunter's parameters. MEPs were calculated using density functional theory (B3LYP 6-311++G** in vacuum) as implemented in Spartan'14 Version 1.1.0[41]. The maxima of the MEPs[13] were used to calculate α (hydrogen-bond donor) following eq.4.1; similarly, eq.4.2 was applied to calculate β (hydrogen-bond acceptor) using the minima in the MEPs. We calculated the interaction energy between the donor (highest α) and acceptor (highest β) implementing eq.4.3. Only conventional hydrogen-bonds donors (N-H, O-H) and acceptors (O=C, pyridine/pyrimidine/ pyrazole-N) were included.

$$\alpha = 0.0000162\mathrm{MEP}_{max}{}^{2} + 0.00962\mathrm{MEP}_{max} \qquad \textbf{Equation 4.1}$$

$$\beta = 0.000146\mathrm{MEP}_{min}{}^{2} - 0.00930\mathrm{MEP}_{min} \qquad \textbf{Equation 4.2.}$$

$$\boldsymbol{E = -\sum_{ij} \alpha_i \beta_j} \qquad \textbf{Equation 4.3.}$$

The ΔE was calculated by subtracting the homomeric interactions (API•••API and co-former•••co-former) from the heteromeric interactions (API•••co-former). ΔE ≥ 0 was assigned a "YES" to co-crystallization (dominant heteromeric interactions); ΔE <0 assigned a "NO" to co-crystallization (favoring homomeric interactions), Scheme 4.3.

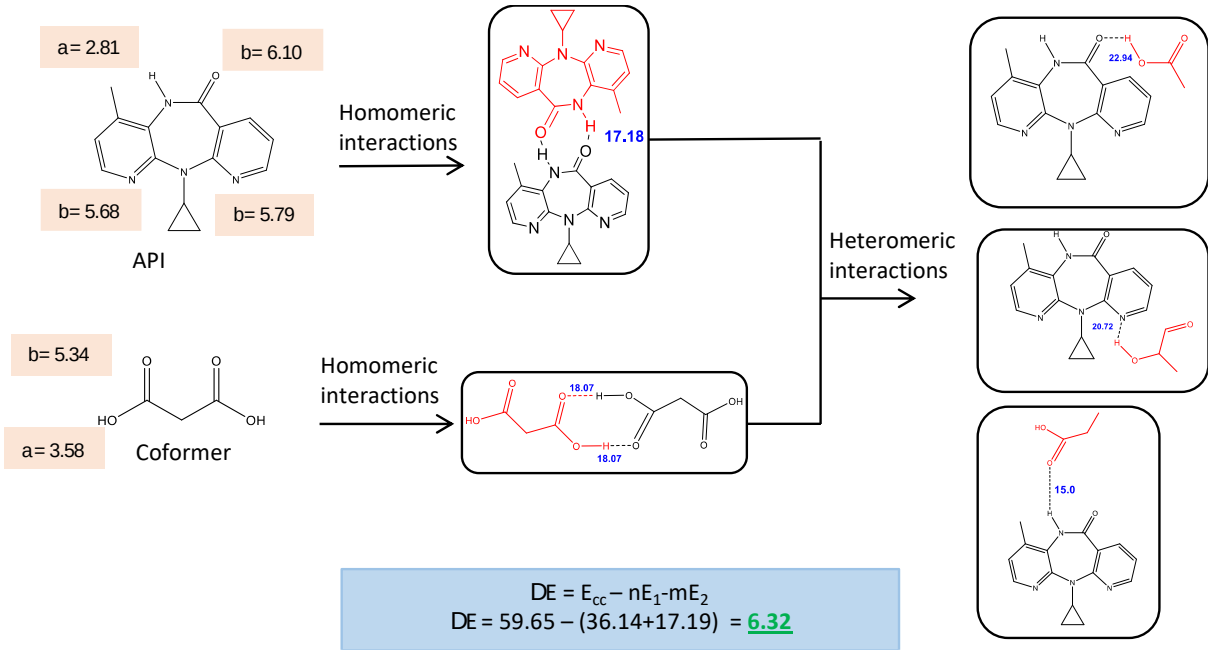

Scheme 4.3. Approach for calculating HBE methodology for Nevirapine and malonic acid.

(ΔE and E in kJ/mol)

4.3. Results

4.3.1. Predictive outcomes of HBP, HBC, and HBE for Nevirapine

Based on Scheme 4.1. the HBP values of homomeric, heteromeric and $\Delta_{propensity}$ values were calculated and summarized in Table 4.1. for Nevirapine and 14 co-formers.

Table 4.1. Hydrogen-bond propensity (HBP) calculations of Nevirapine in combination with 14 co-formers.

Co-formers	Homomeric interactions	Heteromeric interactions	Δ= |Hetero-Homo|
4-Hydroxybenzoic acid	0.28	0.43	0.15
Benzoic acid	0.29	0.39	0.1
Cinnamic acid	0.33	0.4	0.07
Citric acid	0.32	0.44	0.12
Ferulic acid	0.34	0.42	0.08
Gallic acid	0.27	0.44	0.17
Glutaric acid	0.37	0.48	0.11
Hippuric acid	0.34	0.39	0.05
Maleic acid	0.37	0.43	0.06
Malonic acid	0.43	0.49	0.06
Mandelic acid	0.29	0.4	0.11

Oxalic acid	0.25	0.28	0.03
Tartaric acid	0.37	0.44	0.07
Urea	0.98	0.93	-0.05

The HBC calculation is dependent on conventional hydrogen-bond donors and acceptors. Therefore, we divided the co-formers into two groups aliphatic and aromatics acids. Based on Scheme 4.2. the HBC values were calculated for Nevirapine and 14 co-formers.

Table 4.2. Hydrogen-bond coordination (HBC) calculations of Nevirapine in combination with 14 co-formers.

Aromatic acids

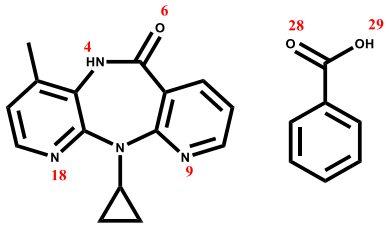

Homomeric interactions (API•••API)				
Atom (D/A)	=0	=1	=2	=3
N4 (D)	0.51	0.49	0.00	0.00
N18 (A)	0.90	0.09	0.01	0.00
N9 (A)	0.90	0.09	0.01	0.00
O6 (A)	0.29	**0.67**	0.04	0.00
Homomeric interactions (co-former•••co-former)				
O29 (D)	0.01	**0.95**	0.04	0.00
O28 (A)	0.45	0.51	0.03	0.00
O29 (A)	0.93	0.07	0.00	0.00

Aliphatic acids

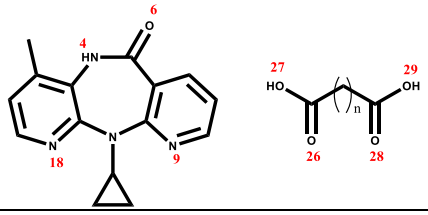

Homomeric interactions (API•••API)				
Atom (D/A)	=0	=1	=2	=3
N4 (D)	0.51	0.49	0.00	0.00
N18 (A)	0.91	0.08	0.01	0.00
N9 (A)	0.91	0.08	0.01	0.00
O6 (A)	0.32	**0.64**	0.03	0.00
Homomeric interactions (co-former•••co-former)				

O27 (D)	0.00	**0.95**	0.04	0.00
O29 (D)	0.00	0.95	0.04	0.00
O26 (A)	0.50	0.47	0.03	0.00
O27 (A)	0.93	0.07	0.00	0.00
O28 (A)	0.49	0.47	0.03	0.00
O29 (A)	0.91	0.07	0.03	0.00

Highlighted in green are the most optimal homomeric interactions predicted by HBC, in red are the most optimal heteromeric interactions. In both aliphatic and aromatic acids in combination with Nevirapine, donor (OH) of acid and acceptor (O=C) of Nevirapine was the most optimal interaction, which was deemed as a "YES" to co-crystallization.

Table 4.3. summarizes the homomeric, heteromeric and ΔE values of Nevirapine and 14 co-formers.

Table 4.3. Hydrogen-bond energy (HBE) calculations of Nevirapine in combination with 14 co-formers.

Co-formers	Homomeric interactions	Heteromeric interactions	Δ=Hetero-Homo (kJ/ mol)
4-Hydroxybenzoic acid	28.29	28.64	0.35
Benzoic acid	16.56	16.90	0.36
Cinnamic acid	17.95	17.93	-0.02
Citric acid	28.00	35.05	7.05
Ferulic acid	21.97	27.00	5.03
Gallic acid	28.07	38.60	10.53
Glutaric acid	24.41	27.31	2.91
Hippuric acid	30.91	33.09	2.18
Maleic acid	18.69	21.56	2.87
Malonic acid	24.23	29.19	4.96
Mandelic acid	20.56	24.50	3.94
Oxalic acid	19.63	30.98	11.35
Tartaric acid	21.34	39.4	18.06
Urea	32.51	48.47	15.96

4.3.2. Predictive outcomes of HBP, HBC, and HBE for Diclofenac

The HBP values of homomeric, heteromeric and $\Delta_{propensity}$ was calculated and summarized in Table 4.4. for Diclofenac and 16 co-formers.

Table 4.4. Hydrogen-bond propensity (HBP) calculations of Diclofenac in combination with 16 co-formers.

Co-formers	Homomeric interactions	Heteromeric interactions	Δ=Hetero-Homo
2-Amino-3,5-dibromopyridine	0.73	0.82	0.09
2-Amino-4-chloro-6-methylpyrimidine	0.82	0.82	0
2-Amino-4-hydroxy-6-methylpyrimidine	0.81	0.83	0.02
2-Amino-4,6-dimethylpyrimidine	0.76	0.81	0.05
2-Amino-5-chloropyridine	0.69	0.81	0.12
2-Aminopyridine	0.69	0.82	0.13
2-Aminopyrimidine	0.82	0.71	-0.11
2-Chloropyrimidine	0.51	0.55	0.04
3-Aminopyridine	0.87	0.64	-0.23
3-Hydroxypyridine	0.73	0.75	0.02
3,5-Dimethyl-4-chloropyrazole	0.37	0.32	-0.05
3,5-Dimethylpyrazole	0.36	0.3	-0.06
4-Bromopyraole	0.52	0.45	-0.07
4-Chloro-2,6-diaminopyrimidine	0.81	0.78	-0.03
4-Iodo-3,5-dimethylpyrazole	0.41	0.32	-0.09
4-Iodopyrazole	0.69	0.64	-0.05
Pyrazole	0.56	0.53	-0.03

Based on Scheme 4.2. the HBC values of Diclofenac were calculated. The co-formers for Diclofenac can be divided into three categories pyridine, pyrimidine and pyrazole.

Table 4.5. Hydrogen-bond coordination (HBC) calculations of Diclofenac in combination with 16 co-formers.

Pyridine group of co-formers

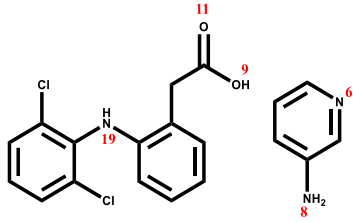

Homomeric interactions (API•••API)				
Atom (D/A)	=0	=1	=2	=3
N19 (D)	0.43	0.56	0.00	0.00
O9 (D)	0.10	**0.87**	0.03	0.00
N19 (A)	1.0	0.00	0.00	0.00
O11 (A)	0.01	0.52	0.45	0.02
O9 (A)	0.93	0.07	0.00	0.00
Homomeric interactions (co-former—co-former)				
N8 (D)	0.02	**0.30**	0.60	0.08

N6 (A)	0.03	0.81	0.16	0.00
N8 (A)	0.98	0.02	0.00	0.00

Pyrimidine group of co-formers

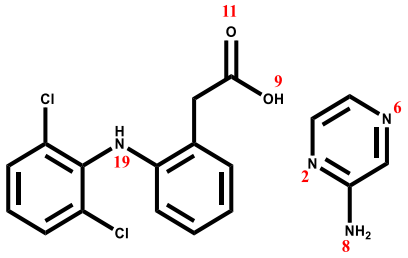

Homomeric interactions (API•••API)				
Atom (D/A)	=0	=1	=2	=3
N20 (D)	0.38	0.61	0.01	0.00
O9 (D)	0.04	**0.93**	0.03	0.00
N19 (A)	1.0	0.00	0.00	0.00
O11 (A)	0.95	0.05	0.00	0.02
O9 (A)	0.08	0.73	0.18	0.01
Homomeric interactions (co-former—co-former)				
N9 (D)	0.01	**0.19**	0.73	0.07
N6 (A)	0.17	0.79	0.03	0.00
N9 (A)	0.98	0.02	0.03	0.00
N2 (A)	0.16	0.80	0.03	0.00

Pyrazole group of co-formers

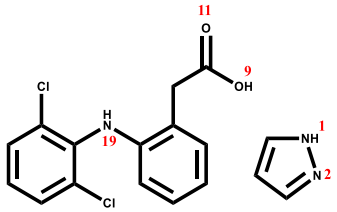

Homomeric interactions (API•••API)				
Atom (D/A)	=0	=1	=2	=3
N19 (D)	0.41	0.58	0.01	0.00
O9 (D)	0.09	**0.88**	0.03	0.00
N19 (A)	1.0	0.00	0.00	0.00
O11 (A)	0.01	0.56	0.41	0.02
O9 (A)	0.93	0.07	0.00	0.00
Homomeric interactions (co-former—co-former)				
N1 (D)	0.01	**0.82**	0.16	0.00
N2 (A)	0.09	0.91	0.00	0.00

Highlighted in green are the most optimal homomeric interactions predicted by HBC, in red are the most optimal heteromeric interactions. In all instances, donor (OH) of Diclofenac and the

acceptor (pyridine/ pyrimidine/ pyrazole-N) of co-former was the most optimal interaction. Hence, HBC predicted Diclofenac to co-crystallize with all the 16 co-formers.

Using Scheme 4.3. we calculated HBE values for Diclofenac, summarized in Table 4.6.

Table 4.6. Hydrogen-bond energy (HBE) calculations of Diclofenac in combination with 16 co-formers.

Co-formers	Homomeric interactions	Heteromeric interactions	∆=Hetero-Homo KJ/ mol
2-Amino-3,5-dibromopyridine	12.15	12.74	0.59
2-Amino-4-chloro-6-methylpyrimidine	17.60	17.60	0.00
2-Amino-4-hydroxy-6-methylpyrimidine	19.95	19.97	0.027
2-Amino-4,6-dimethylpyrimidine	18.35	18.37	0.02
2-Amino-5-chloropyridine	14.50	15.20	0.70
2-Aminopyridine	16.18	17.57	1.39
2-Aminopyrimidine	18.29	18.28	-0.01
2-Chloropyrimidine	14.50	15.20	0.70
3-Aminopyridine	19.73	22.07	2.34
3-Hydroxypyridine	21.41	21.10	-0.31
3,5-Dimethyl-4-chloropyrazole	20.67	21.83	1.17
3,5-Dimethylpyrazole	20.67	21.83	1.17
4-Bromopyraole	19.75	20.12	0.37
4-Chloro-2,6-diaminopyrimidine	20.13	19.40	-0.72
4-Iodo-3,5-dimethylpyrazole	20.67	21.83	1.17
4-Iodopyrazole	19.75	20.12	0.37
Pyrazole	19.75	20.12	0.37

4.4. Discussions

4.4.1. Experimental co-crystal screening results vs. prediction outcomes

Table 4.7. summarizes the results of the experimental co-crystal screen as well as the results from the three different methods that were employed in order to predict whether a co-crystal would form when Nevirapine[33] was combined with fourteen co-formers.

Table 4.7. Experimental and HBP, HBC, and HBE data for attempted co-crystallizations targeting Nevirapine.

Nevirapine	Exp.	HBP	HBC	HBE
4-Hydroxybenzoic acid	Yes	Yes	Yes	Yes
Benzoic acid	Yes	Yes	Yes	Yes
Cinnamic acid	Yes	Yes	Yes	No
Citric acid	Yes	Yes	Yes	Yes
Ferulic acid	Yes	Yes	Yes	Yes
Gallic acid	Yes	Yes	Yes	Yes
Glutaric acid	Yes	Yes	Yes	Yes
Hippuric acid	Yes	Yes	Yes	Yes
Maleic acid	Yes	Yes	Yes	Yes
Malonic aid	Yes	Yes	Yes	Yes
Mandelic acid	Yes	Yes	Yes	Yes
Oxalic acid	Yes	Yes	Yes	Yes
Tartaric acid	Yes	Yes	Yes	Yes
Urea	Yes	No	No	Yes
Prediction match		13/14	13/14	13/14

Nevirapine delivered 14/14 positive co-crystallization results. The success rate for predicting co-crystallization in the case of Nevirapine with HBP, HBC, and HBE was 93%. This indicates that all three methods have high accuracy for predicting co-crystallization outcomes.

Diclofenac, on the other hand, co-crystallized with 8/16 co-formers, 2/16 formed salts, and the rest, 6/16 did not react. A salt is formed when a proton migrates from an acidic -COOH to basic pyridine acceptor. Whereas in a co-crystal, the proton forms non-covalent interactions with the acceptor pyridine. However, in both cases, new, heteromeric interactions were formed. For the two salts observed in Diclofenac, we carried out the calculations with both neutral and charged species. Both the calculations yielded the same results, and therefore, a similar cut-off for salt and co-crystal were employed[29].

Table 4.8 summarizes the results of the experimental co-crystal screen and the results from the three different methods that were employed in order to predict whether a co-crystal would form when Diclofenac[34] was combined with sixteen co-formers.

Table 4.8. Experimental and HBP, HBC, and HBE data for attempted co-crystallizations targeting Diclofenac.

Diclofenac	Exp.	HBP	HBC	HBE
2-Amino-3,5-dibromopyridine	Yes	Yes	Yes	Yes
2-Amino-4-chloro-6-methylpyrimidine	Yes	Yes	Yes	No
2-Amino-4-hydroxy-6-methylpyrimidine	Yes	Yes	No	Yes
2-Amino-4,6-dimethylpyrimidine	Yes	Yes	Yes	Yes
2-Amino-5-chloropyridine	Yes	Yes	Yes	Yes
2-Aminopyridine	salt	Yes	Yes	Yes
2-Aminopyrimidine	Yes	No	Yes	Yes
3-Aminopyridine	salt	No	Yes	Yes
3-Hydroxypyridine	Yes	Yes	Yes	No
3,5-Dimethyl-4-chloropyrazole	No	No	Yes	No
3,5-Dimethylpyrazole	No	No	Yes	Yes
4-Bromopyrazole	No	No	Yes	Yes
4-Chloro-2,6-diaminopyrimidine	Yes	No	Yes	No
4-Iodo-3,5-dimethylprazole	No	No	Yes	Yes
4-Iodopyrazole	No	No	Yes	Yes
Pyrazole	No	No	Yes	Yes
Prediction match		13/16= 81%	7/16= 44%	8/16= 50%

Undoubtedly, HBP produced better predictive accuracies for Diclofenac in comparison to HBC and HBE. Although HBP predicted Nevirapine (93%) with higher accuracy than Diclofenac (81%). The prediction differences can be attributed to the fact that the CSD database consists of only positive co-crystallization results; hence, it was not surprising that the structure informatics methodologies have a lower success rate for instances where co-crystal was not formed. Calculating an overall success rate for both Nevirapine and Diclofenac yielded a success rate of 87% (26/30) with HBP compared to 67% (20/30) for HBC and 70% (21/30) for the HBE. Clearly, among the three methodologies, HBP shows a higher accuracy for predicting co-crystallization, Figure 4.4.

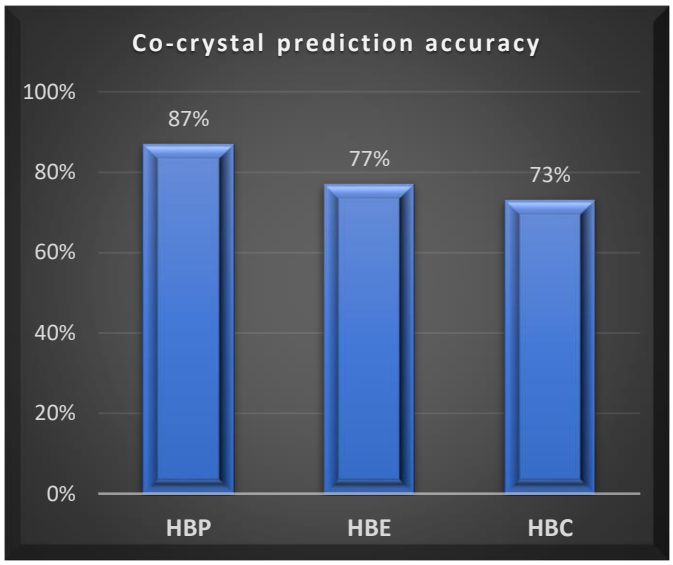

Figure 4.4. Co-crystal prediction accuracy.

4.4.2. Observed interactions in the crystal structures vs. prediction results

We also analyzed the abilities of these methods to predict which specific hydrogen-bond interaction was likely to be present in the experimentally determined crystal structures (targets and co-crystals thereof). Nevirapine has two possible homomeric interactions, synthons I and II wherein only one of these interactions can exist at a time, Scheme 4.4. HBP calculations showed that there was a higher probability that synthon I will form. The co-formers examined in the case of Nevirapine were carboxylic acids (urea being the exception), and the most likely homomeric interaction was synthon III.

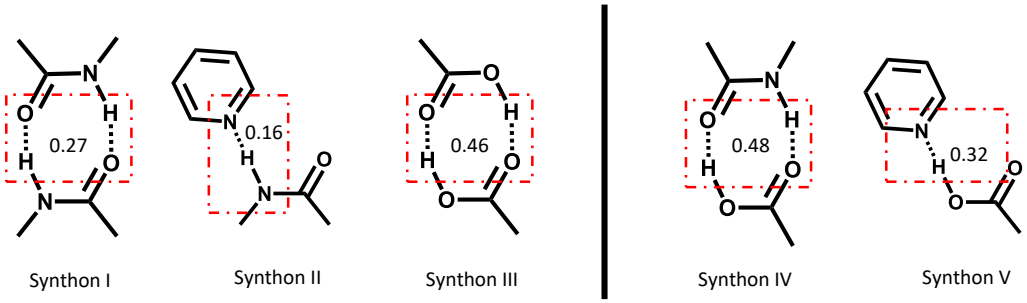

Scheme 4.4. Postulated synthons of homomeric (left) and heteromeric (right) interactions and HBPs in Nevirapine and co-formers.

In the crystal structure of Nevirapine synthon I was observed; and synthon III for co-formers, which match the predicted homomeric interactions by HBP, Figure 4.5[42].

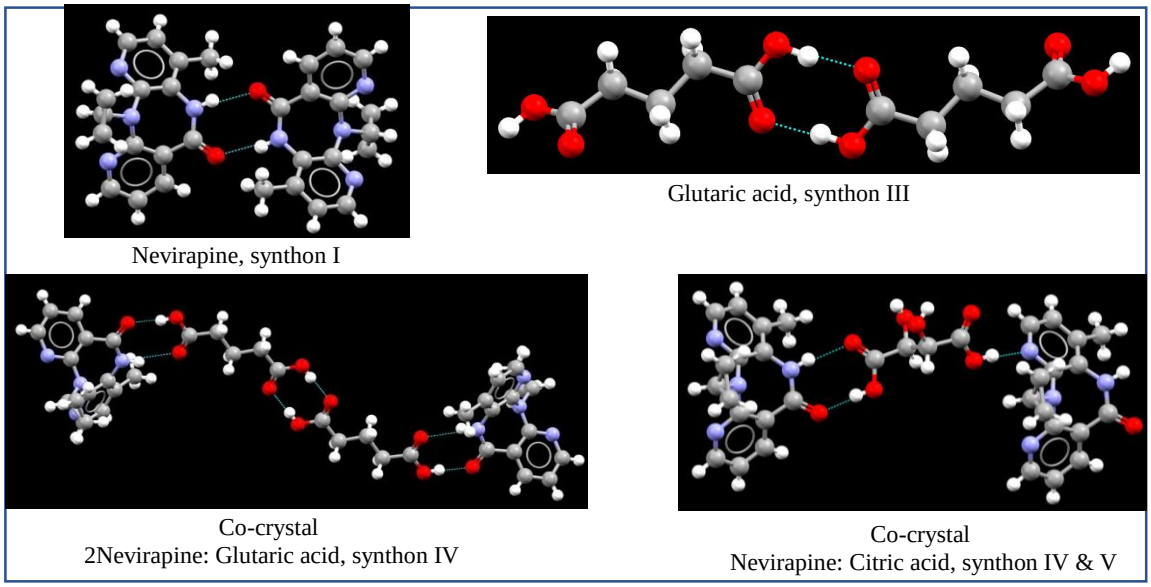

Figure 4.5. Crystal structure of nevirapine, glutaric acid (top) and co-crystals (bottom)[42,43,44].

To achieve co-crystals, either or both synthon(s) IV and V needs to be formed, Scheme 4.4. HBP predicts the formation of synthon IV (0.48) with a higher probability than synthon V (0.32). However, to satisfy the pyridine acceptor, either synthon II or V might form in addition to that of synthon IV. Between synthon II and V, HBP predicts the formation of synthon V.

There were five reported co-crystal structures of Nevirapine. In four of these structures, both synthon IV and V were observed. The co-crystal structure of glutaric acid and Nevirapine was found to have only synthon IV[44]. The HBP predicted heteromeric (synthons IV and V, with a higher probability for synthon IV) and homomeric interaction (synthons I and III) match the experimentally observed interactions. HBP correctly predicts the synthons in 5/5 reported cases for Nevirapine. HBP fails to predict Nevirapine and urea accurately, where the homomeric interactions of urea were favored over heteromeric interactions. However, experimentally, a co-crystal was formed.

Implementing the HBC protocol, for predicting the most optimal homomeric interactions resulted in synthon I for Nevirapine and synthon III for the co-formers. The predicted heteromeric interactions correspond to synthon IV. HBC predicted interactions were consistent with the experimental observations, Figure 4.5. However, unlike HBP, HBC could not predict the presence

of synthon V in addition to that of synthon IV. HBC also fails to determine the correct outcome for urea.

In the case of HBE, the predicted homomeric interactions for both Nevirapine and co-formers agree with the experimental outcomes. The predicted heteromeric interactions were synthons II, IV, and V; however, experimentally, we only see synthons IV and V in the crystal structures.

Diclofenac has two possible homomeric interactions, synthon VII displaying a higher HBP than VI, Scheme 4.5.

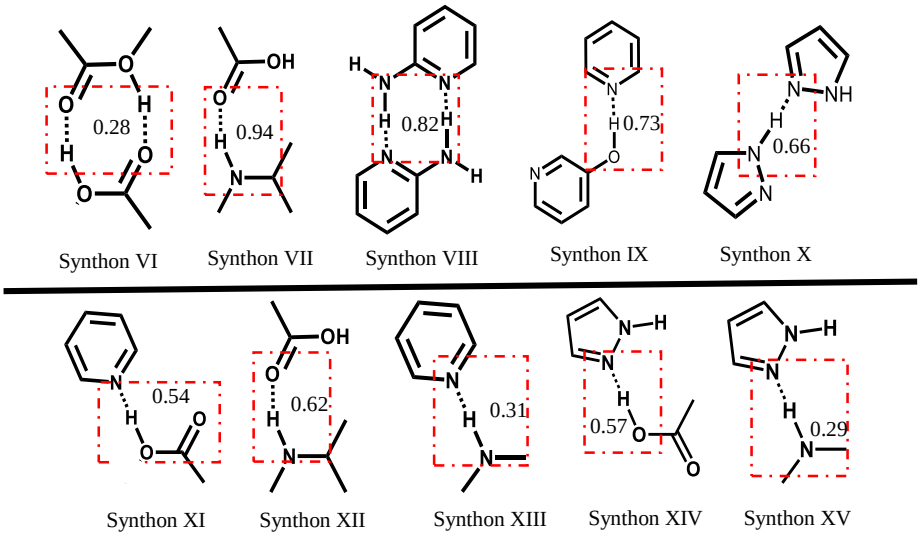

Scheme 4.5. Postulated synthons of homomeric (top) and heteromeric (bottom) interactions and HBPs in diclofenac and co-formers.

The crystal structure of Diclofenac was found to have both synthon VI and VII, where the latter is an intramolecular interaction, Figure 4.6. The list of co-formers for Diclofenac can be divided into two groups pyridines and pyrimidines, and pyrazoles. The co-formers from the pyridine and pyrimidine groups experimentally formed co-crystal with Diclofenac. Synthon VIII (synthon IX in case of 3-hydroxy pyridine) depicts the homomeric interactions for this group of co-formers which, match the experimentally observed interaction.

For a heteromeric interaction to occur with pyridines and pyrimidines, there were three possibilities, synthon XI, XII and XIII. HBP predicts the formation of synthon XII with a lower probability (0.31) when compared with the other synthons. We found only one reported co-crystal structure, wherein synthons XI and XIII were observed[34], Figure 4.6.

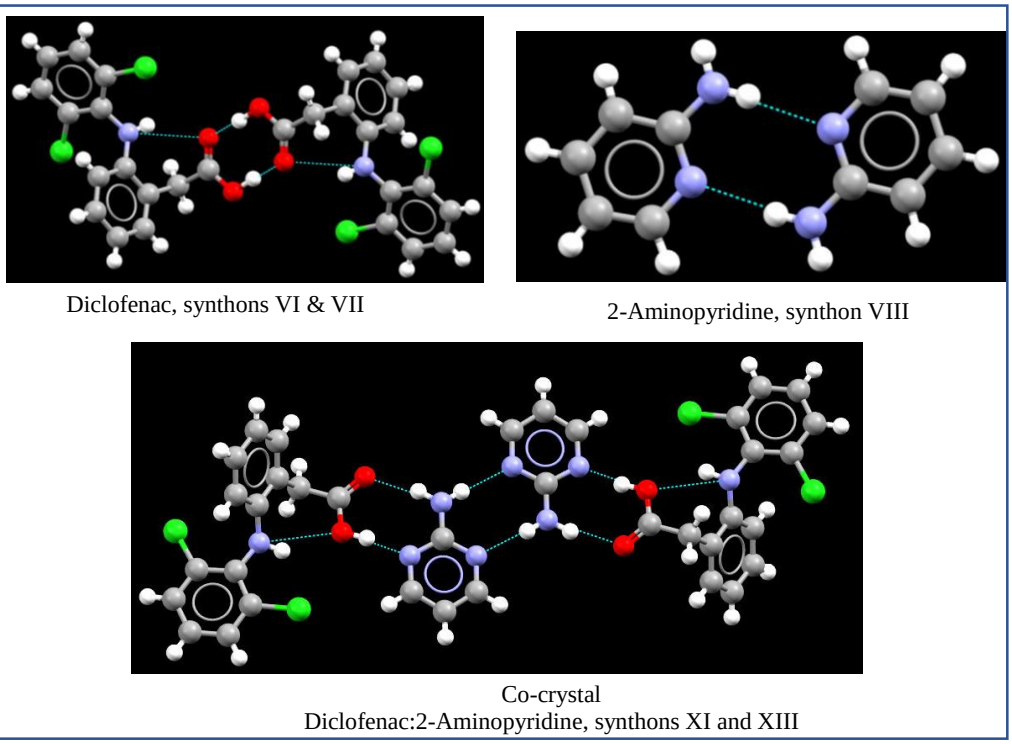

Figure 4.6. Crystal structure of diclofenac, 2-aminopyridine (top) and co-crystal (bottom)[45,46,47].

The predicted homomeric interaction by HBP with the pyrazole group of co-formers was synthon X (0.66), and either synthon XIV (0.57) or XV (0.29) as the heteromeric interactions. Homomeric interactions were predicted to be more dominant than heteromeric interactions, which was consistent with the experimental observation of no reaction.

In the case of HBC, homomeric interactions were correctly predicted for Diclofenac and pyridine & pyrimidine co-formers. The most optimal heteromeric interaction predicted with this group of co-formers was synthon XI. In the reported crystal structure, synthon XI was observed; however, unlike HBP, it fails to predict the presence of synthon XIII. For the pyrazole containing co-formers, synthon XV was found to be the most optimal interaction; although experimentally, it does not form a co-crystal. HBC fails to predict the correct interactions with the pyrazole groups of co-formers.

HBE could correctly predict the homomeric and heteromeric interactions for the co-formers containing pyridines and pyrimidines. However, for the group of co-formers containing pyrazoles,

HBE predicts to form synthon XV over X, which was not consistent with the experimentally observed outcomes.

A comparison of the predicted interactions with the experimentally observed results is summarized in Table 4.9.

Table 4.9. Predicted vs experimentally observed synthons (green: homomeric interactions, red: heteromeric interaction).

	Co-crystal	Experimental	HBP	HBC	HBE
Nevirapine	Yes	IV and V	IV and V	IV	II, IV and V
Diclofenac (Pyridines/Pyrimidines)	Yes	**VII**, XI and XII	**VII**, XI and XII	XI	**VII**, XI and XII
Diclofenac (Pyrazoles)	No	**X**	**X**	XV	XV

HBP predicted interactions were consistent with the five reported crystal structures for Nevirapine and one reported structure for Diclofenac. HBC could not predict any of the combinations correctly, and finally, HBE could correctly predict the interactions only for Diclofenac.

The HBP protocol was in good agreement with the co-crystallization screening outcomes, as well as the homomeric and heteromeric interactions involved during co-crystallization. Overall, HBP performs better than HBC and HBE protocols for Nevirapine and Diclofenac.

The information provided by HBP can be essential in narrowing the co-formers and reducing the number of experiments. However, it is worth noting that HBP is only limited to reactions where direct interactions between hydrogen-bond donors and acceptors are involved.

Although most studies reported to date employing HBP as a predictive methodology, examine targets/ APIs that are rigid and have molecular weight <300 g/mol. We believe that it would be of great interest to expand HBP tests on more flexible (rotatable bonds >3) and larger (molecular weight >300 g/mol) compounds that resemble most drug molecules closely.

4.5. Conclusions

1. Out of the three methodologies considered in this study for Nevirapine HBP, HBC and HBE all produced a 93% success rate. However, for Diclofenac HBP results outperformed HBC and HBE. The results from the three methodologies and their success rates are summarized in Table

4.10.

Table 4.10. Success rates for predicting the co-crystal formation of Nevirapine and Diclofenac.

Compounds	Methodology	Success rate
Nevirapine	HBP	13/14= 93%
	HBC	13/14= 93%
	HBE	13/14= 93%
Diclofenac	HBP	13/16= 81%
	HBC	9/16= 56%
	HBE	10/16= 63%

2. The homomeric and heteromeric interactions predicted by HBP matched the experimental interactions in all the 6 cases; HBC could not correctly predict in any of the instances and HBE prediction matched in only one case.

The success of HBP in predicting co-crystallization and the most likely synthon formation outperforms the results obtained from HBC and HBE. The reliability of HBP is significant and critical in drug design as it requires minimum time and resources to complement the experimental trials[3,23].

4.6. References

(1) Wnek, G. E. Structure–Property Relationships of Small Organic Molecules as a Prelude to the Teaching of Polymer Science. *J. Chem. Educ.* **2017**, *94* (11), 1647–1654. https://doi.org/10.1021/acs.jchemed.6b00747.

(2) Li, S.; Yu, T.; Tian, Y.; McCoy, C. P.; Jones, D. S.; Andrews, G. P. Mechanochemical Synthesis of Pharmaceutical Cocrystal Suspensions via Hot Melt Extrusion: Feasibility Studies and Physicochemical Characterization. *Mol. Pharmaceutics* **2016**, *13* (9), 3054–3068. https://doi.org/10.1021/acs.molpharmaceut.6b00134.

(3) Gadade, D. D.; Pekamwar, S. S. Pharmaceutical Cocrystals: Regulatory and Strategic Aspects, Design and Development. *Adv Pharm Bull* **2016**, *6* (4), 479–494. https://doi.org/10.15171/apb.2016.062.

(4) Friščić, T.; Jones, W. Recent Advances in Understanding the Mechanism of Cocrystal Formation via Grinding. *Crystal Growth & Design* **2009**, *9* (3), 1621–1637. https://doi.org/10.1021/cg800764n.

(5) Cherukuvada, S.; Kaur, R.; Row, T. N. G. Co-Crystallization and Small Molecule Crystal Form Diversity: From Pharmaceutical to Materials Applications. *CrystEngComm* **2016**, *18* (44), 8528–8555. https://doi.org/10.1039/C6CE01835A.

(6) Basavoju, S.; Boström, D.; Velaga, S. P. Indomethacin–Saccharin Cocrystal: Design, Synthesis and Preliminary Pharmaceutical Characterization. *Pharm Res* **2008**, *25* (3), 530–541. https://doi.org/10.1007/s11095-007-9394-1.

(7) Surov, A. O.; Voronin, A. P.; Manin, A. N.; Manin, N. G.; Kuzmina, L. G.; Churakov, A. V.; Perlovich, G. L. Pharmaceutical Cocrystals of Diflunisal and Diclofenac with Theophylline. *Mol. Pharmaceutics* **2014**, *11* (10), 3707–3715. https://doi.org/10.1021/mp5004652.

(8) Jones, W.; Motherwell, W. D. S.; Trask, A. V. Pharmaceutical Cocrystals: An Emerging Approach to Physical Property Enhancement. *MRS Bulletin* **2006**, *31* (11), 875–879. https://doi.org/10.1557/mrs2006.206.

(9) Vishweshwar, P.; McMahon, J. A.; Bis, J. A.; Zaworotko, M. J. Pharmaceutical Co-Crystals. *Journal of Pharmaceutical Sciences* **2006**, *95* (3), 499–516. https://doi.org/10.1002/jps.20578.

(10) The role of cocrystals in pharmaceutical science - ScienceDirect https://www.sciencedirect.com/science/article/pii/S1359644608000779?via%3Dihub (accessed May 12, 2019).

(11) Berger, J.; Dunn, J. D.; Johnson, M. M.; Karst, K. R.; Shear, W. C. How Drug Life-Cycle Management Patent Strategies May Impact Formulary Management. *Am J Manag Care* **2016**, *22* (16 Suppl), S487–S495.

(12) Aakeröy, C. Is There Any Point in Making Co-Crystals? *Acta Cryst B* **2015**, *71* (4), 387–391. https://doi.org/10.1107/S2052520615010872.

(13) Musumeci, D.; Hunter, C. A.; Prohens, R.; Scuderi, S.; McCabe, J. F. Virtual Cocrystal Screening. *Chem. Sci.* **2011**, *2* (5), 883. https://doi.org/10.1039/c0sc00555j.

(14) Hunter, C. A. Quantifying Intermolecular Interactions: Guidelines for the Molecular Recognition Toolbox. *Angewandte Chemie International Edition* **2004**, *43* (40), 5310–5324. https://doi.org/10.1002/anie.200301739.

(15) Sandhu, B.; McLean, A.; Sinha, A. S.; Desper, J.; Sarjeant, A. A.; Vyas, S.; Reutzel-Edens, S. M.; Aakeröy, C. B. Evaluating Competing Intermolecular Interactions through Molecular

Electrostatic Potentials and Hydrogen-Bond Propensities. *Crystal Growth & Design* **2018**, *18* (1), 466–478. https://doi.org/10.1021/acs.cgd.7b01458.

(16) Blagden, N.; de Matas, M.; Gavan, P. T.; York, P. Crystal Engineering of Active Pharmaceutical Ingredients to Improve Solubility and Dissolution Rates. *Advanced Drug Delivery Reviews* **2007**, *59* (7), 617–630. https://doi.org/10.1016/j.addr.2007.05.011.

(17) Cruz-Cabeza, A. J. Acid–Base Crystalline Complexes and the PKa Rule. *CrystEngComm* **2012**, *14* (20), 6362–6365. https://doi.org/10.1039/C2CE26055G.

(18) Mohammad, M. A.; Alhalaweh, A.; Velaga, S. P. Hansen Solubility Parameter as a Tool to Predict Cocrystal Formation. *International Journal of Pharmaceutics* **2011**, *407* (1), 63–71. https://doi.org/10.1016/j.ijpharm.2011.01.030.

(19) Macrae, C. F.; Bruno, I. J.; Chisholm, J. A.; Edgington, P. R.; McCabe, P.; Pidcock, E.; Rodriguez-Monge, L.; Taylor, R.; Streek, J. van de; Wood, P. A. Mercury CSD 2.0 – New Features for the Visualization and Investigation of Crystal Structures. *J Appl Cryst* **2008**, *41* (2), 466–470. https://doi.org/10.1107/S0021889807067908.

(20) Chakrabarty, R.; Mukherjee, P. S.; Stang, P. J. Supramolecular Coordination: Self-Assembly of Finite Two- and Three-Dimensional Ensembles. *Chem. Rev.* **2011**, *111* (11), 6810–6918. https://doi.org/10.1021/cr200077m.

(21) Aakeröy, C. B.; Chopade, P. D.; Desper, J. Avoiding "Synthon Crossover" in Crystal Engineering with Halogen Bonds and Hydrogen Bonds. *Crystal Growth & Design* **2011**, *11* (12), 5333–5336. https://doi.org/10.1021/cg2009013.

(22) Wood, P. A.; Feeder, N.; Furlow, M.; Galek, P. T. A.; Groom, C. R.; Pidcock, E. Knowledge-Based Approaches to Co-Crystal Design. *CrystEngComm* **2014**, *16* (26), 5839. https://doi.org/10.1039/c4ce00316k.

(23) Galek, P. T. A.; Allen, F. H.; Fábián, L.; Feeder, N. Knowledge-Based H-Bond Prediction to Aid Experimental Polymorph Screening. *CrystEngComm* **2009**, *11* (12), 2634. https://doi.org/10.1039/b910882c.

(24) Galek, P. T. A.; Chisholm, J. A.; Pidcock, E.; Wood, P. A. Hydrogen-Bond Coordination in Organic Crystal Structures: Statistics, Predictions and Applications. *Acta Crystallogr B Struct Sci Cryst Eng Mater* **2014**, *70* (1), 91–105. https://doi.org/10.1107/S2052520613033003.

(25) Sarkar, N.; Sinha, A. S.; Aakeröy, C. B. Systematic Investigation of Hydrogen-Bond Propensities for Informing Co-Crystal Design and Assembly. *CrystEngComm* **2019**. https://doi.org/10.1039/C9CE01196J.

(26) Issa, N.; Karamertzanis, P. G.; Welch, G. W. A.; Price, S. L. Can the Formation of Pharmaceutical Cocrystals Be Computationally Predicted? I. Comparison of Lattice Energies. *Crystal Growth & Design* **2009**, *9* (1), 442–453. https://doi.org/10.1021/cg800685z.

(27) Bučar, D.-K.; Lancaster, R. W.; Bernstein, J. Disappearing Polymorphs Revisited. *Angewandte Chemie International Edition* **2015**, *54* (24), 6972–6993. https://doi.org/10.1002/anie.201410356.

(28) Corpinot, M. K.; Stratford, S. A.; Arhangelskis, M.; Anka-Lufford, J.; Halasz, I.; Judaš, N.; Jones, W.; Bučar, D.-K. On the Predictability of Supramolecular Interactions in Molecular Cocrystals – the View from the Bench. *CrystEngComm* **2016**, *18* (29), 5434–5439. https://doi.org/10.1039/C6CE00293E.

(29) Delori, A.; Galek, P. T. A.; Pidcock, E.; Jones, W. Quantifying Homo- and Heteromolecular Hydrogen Bonds as a Guide for Adduct Formation. *Chemistry – A European Journal* **2012**, *18* (22), 6835–6846. https://doi.org/10.1002/chem.201103129.

(30) Delori, A.; Galek, P. T. A.; Pidcock, E.; Patni, M.; Jones, W. Knowledge-Based Hydrogen Bond Prediction and the Synthesis of Salts and Cocrystals of the Anti-Malarial Drug Pyrimethamine with Various Drug and GRAS Molecules. *CrystEngComm* **2013**, *15* (15), 2916. https://doi.org/10.1039/c3ce26765b.

(31) Arunan, E.; Desiraju, G. R.; Klein, R. A.; Sadlej, J.; Scheiner, S.; Alkorta, I.; Clary, D. C.; Crabtree, R. H.; Dannenberg, J. J.; Hobza, P.; et al. Defining the Hydrogen Bond: An Account (IUPAC Technical Report). *Pure Appl. Chem.* **2011**, *83* (8), 1619–1636. https://doi.org/10.1351/PAC-REP-10-01-01.

(32) McKenzie, J.; Feeder, N.; Hunter, C. A. H-Bond Competition Experiments in Solution and the Solid State. *CrystEngComm* **2016**, *18* (3), 394–397. https://doi.org/10.1039/C5CE02223A.

(33) Nalte, Y. K. Solubility Enhancement of Nevirapine by Cocrystallisation Technique. *Journal of Pharmacy Research* **2015**, No. 8, 6.

(34) Aakeröy, C. B.; Grommet, A. B.; Desper, J. Co-Crystal Screening of Diclofenac. *Pharmaceutics* **2011**, *3* (3), 601–614. https://doi.org/10.3390/pharmaceutics3030601.

(35) Macrae, C. F.; Bruno, I. J.; Chisholm, J. A.; Edgington, P. R.; McCabe, P.; Pidcock, E.; Rodriguez-Monge, L.; Taylor, R.; Streek, J. van de; Wood, P. A. Mercury CSD 2.0 – New Features for the Visualization and Investigation of Crystal Structures. *J Appl Cryst* **2008**, *41* (2), 466–470. https://doi.org/10.1107/S0021889807067908.

(36) Mapp, L. K.; Coles, S. J.; Aitipamula, S. Design of Cocrystals for Molecules with Limited Hydrogen Bonding Functionalities: Propyphenazone as a Model System. *Crystal Growth & Design* **2017**, *17* (1), 163–174. https://doi.org/10.1021/acs.cgd.6b01399.

(37) Vologzhanina, A. V.; Sokolov, A. V.; Purygin, P. P.; Zolotarev, P. N.; Blatov, V. A. Knowledge-Based Approaches to H-Bonding Patterns in Heterocycle-1-Carbohydrazoneamides. *Crystal Growth & Design* **2016**, *16* (11), 6354–6362. https://doi.org/10.1021/acs.cgd.6b00990.

(38) Taylor, R.; Macrae, C. F. Rules Governing the Crystal Packing of Mono- and Dialcohols. *Acta Cryst B* **2001**, *57* (6), 815–827. https://doi.org/10.1107/S010876810101360X.

(39) Bruno, I. J.; Cole, J. C.; Edgington, P. R.; Kessler, M.; Macrae, C. F.; McCabe, P.; Pearson, J.; Taylor, R. New Software for Searching the Cambridge Structural Database and Visualizing Crystal Structures. *Acta Cryst B* **2002**, *58* (3), 389–397. https://doi.org/10.1107/S0108768102003324.

(40) Macrae, C. F.; Edgington, P. R.; McCabe, P.; Pidcock, E.; Shields, G. P.; Taylor, R.; Towler, M.; Streek, J. van de. Mercury: Visualization and Analysis of Crystal Structures. *J Appl Cryst* **2006**, *39* (3), 453–457. https://doi.org/10.1107/S002188980600731X.

(41) Aakeröy, C. B.; Wijethunga, T. K.; Desper, J. Molecular Electrostatic Potential Dependent Selectivity of Hydrogen Bonding. *New J. Chem.* **2015**, *39* (2), 822–828. https://doi.org/10.1039/C4NJ01324G.

(42) Mui, P. W.; Jacober, S. P.; Hargrave, K. D.; Adams, J. Crystal Structure of Nevirapine, a Non-Nucleoside Inhibitor of HIV-1 Reverse Transcriptase, and Computational Alignment with a Structurally Diverse Inhibitor. *J. Med. Chem.* **1992**, *35* (1), 201–202. https://doi.org/10.1021/jm00079a029.

(43) Morrison, J. D.; Robertson, J. M. 212. The Crystal and Molecular Structure of Certain Dicarboxylic Acids. Part VII. β-Glutaric Acid. *J. Chem. Soc.* **1949**, No. 0, 1001–1008. https://doi.org/10.1039/JR9490001001.

(44) Caira, M. R.; Bourne, S. A.; Samsodien, H.; Engel, E.; Liebenberg, W.; Stieger, N.; Aucamp, M. Co-Crystals of the Antiretroviral Nevirapine: Crystal Structures, Thermal Analysis and Dissolution Behaviour. *CrystEngComm* **2012**, *14* (7), 2541–2551. https://doi.org/10.1039/C2CE06507J.

(45) Aakeröy, C. B.; Grommet, A. B.; Desper, J. Co-Crystal Screening of Diclofenac. *Pharmaceutics* **2011**, *3* (3), 601–614. https://doi.org/10.3390/pharmaceutics3030601.

(46) Moser, P.; Sallmann, A.; Wiesenberg, I. Synthesis and Quantitative Structure-Activity Relationships of Diclofenac Analogs. *J. Med. Chem.* **1990**, *33* (9), 2358–2368. https://doi.org/10.1021/jm00171a008.

(47) Chao, M.; Schemp, E.; Rosenstein, R. D. 2-Aminopyridine. *Acta Cryst B* **1975**, *31* (12), 2922–2924. https://doi.org/10.1107/S0567740875009272.

Chapter 5 – Evaluating the Predictive Abilities of Hydrogen-Bond Propensity, Molecular Complementarity, and Hydrogen-Bond Energy for Co-crystal Screening

5.1. Introduction

A cocrystal is composed of two (or more) different molecular entities, in the same crystal lattice which are held together by weak non-covalent interactions[1,2,3]. The design and synthesis of co-crystals can be used as a modular approach to develop new materials with desirable properties in various fields[4,5,6,7,8,9,10,11,12,13]. Pharmaceutical co-crystals[14,15] are of particular importance wherein the target compound, the active pharmaceutical ingredient (API), is combined with a 'co-former' that is intended to impart optimal physical properties without loss of biological activity. Although various promising strategies have been developed to synthesize co-crystals, many challenges still remain. The rational design of co-crystals have usually been based on supramolecular synthons[16,17,18,19]. Substantial experimental and theoretical studies have been conducted for relatively strong interactions, such as hydrogen bonding. However, recent studies by Kaźmierczak and Katrusiak[20,21], found that there are ~450 organic structures in the CSD that contain no intermolecular contact (shorter than the sum of vdw radii) so-called "loose" crystals.

The question of what determines the packing of the molecules in a specific way in crystal structures is therefore of great research interest in co-crystallization. The "principle of close packing" pioneered by Kitaigorodsky[22], recognizes that molecules are packed in such a way that there is minimum void between them where the "projections" of one molecule get into the "hollows" of adjacent molecules in a dovetail fashion, Figure 5.1.

Figure 5.1. Close packing principle.

Applying Kitaigorodsky's principle on a binary system to form a homogenous phase, both the components should have comparable size, shape, and charge distribution which would result in a dense structure with minimum volume. These characteristics were later referred to as molecular and crystal isostructurality.

Hence the goal of this study is to evaluate Molecular Complementarity[23] (MC) a shape and size dependent approach for predicting co-crystallization. Secondly, to bring forward MC in comparison[24,25] to other approaches (based on hydrogen bonding) to identify the most reliable tool for predicting co-crystallization screening outcomes.

MC is dependent on three shape descriptors and two polarity-based descriptors[26]. It is based on a box model of crystal packing, with three unequal dimensions where $l > m > s$ in the model, Figure 5.2[27].

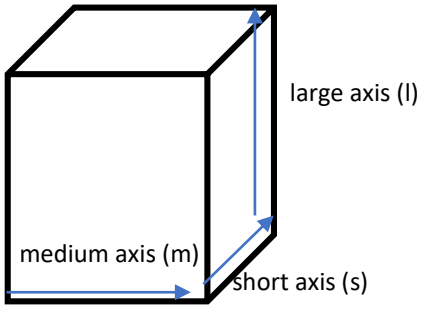

Figure 5.2. Box model with three unequal dimensions.

In Chapter 3, we examined prediction accuracies of hydrogen-bond propensity (HBP), hydrogen-bond coordination (HBC), and hydrogen-bond energy (HBE) for the co-crystal synthesis on small (molecular weight 180-300 g/mol) and rigid compounds. The results from the study ranked their predictive capabilities as HBP> HBE> HBC[28,29,30,31]. Therefore, in this study, we used HBP and HBE approaches in combination with MC.

The three predictive methodologies were employed on seven APIs in combination with 42 co-formers on the GRAS (generally regarded as safe)[32] list, Table 5.1. The targets used in this study have a higher molecular weight (400-600 g/mol) and are more flexible (rotatable bonds greater than 3), compared to those that were examined in Chapters 2-4. Since the average molecular weight of organic structures reported in CSD is ~400 g/mol[33] it will be interesting to investigate HBP and

MC on compounds with a higher molecular weight. The APIs and are labeled T11- T17, Figure 5.3.

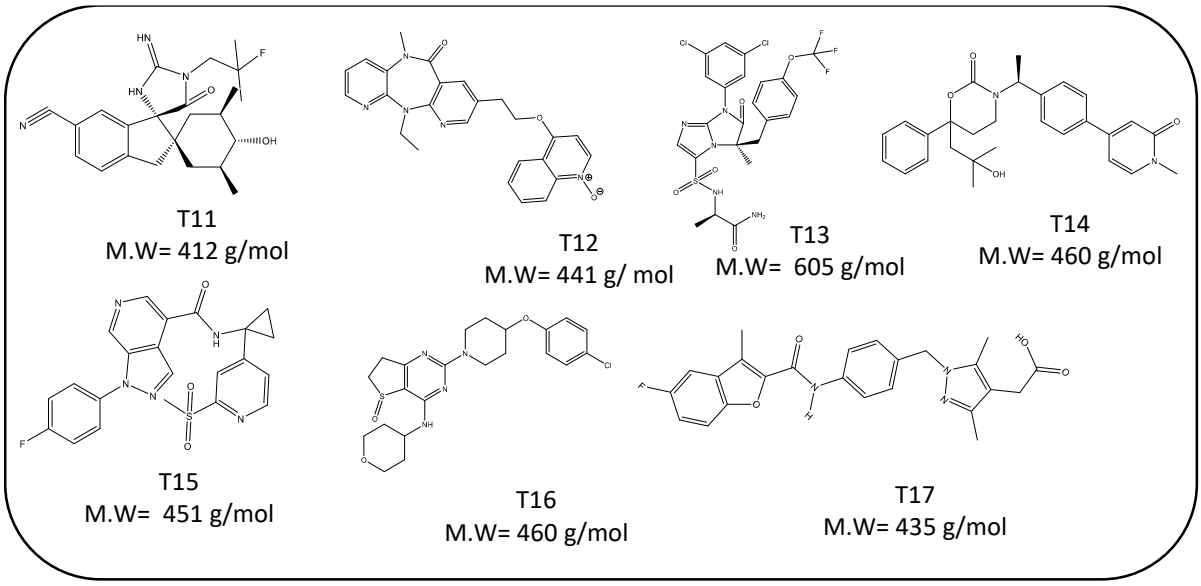

Figure 5.3. APIs of interest.

Table 5.1.. Selected GRAS list co-formers.

3-Hydroxy-2-naphthoic acid	EDTA	L-Proline	Pamoic acid
4-Hydroxybenzoic acid	Folic acid	L-Serine	Phosphoric acid
Adipic acid	Fumaric acid	L-Tartaric acid	Piperazine
Apigenin	Glutaric acid	Maleic acid	Riboflavin
Benzenesulfonic acid	Glycine	Malic acid	Saccharin
Benzoic acid	Glycolic acid	Malonic acid	Salicylic acid
Caffeine	Hydrocinnamic acid	Maltitol	Sorbic acid
Cholic acid	Isonicotinamide	Mannitol	Succinic acid
Citric acid	L-Glutamic acid	Nicotinamide	Theophylline
D-glucuronic acid	L-Mandelic acid	Oxalic acid	Urea
			Xanthine

Figure 5.4 shows a road map of this study. The predictions were compared with the experimental data to determine the relative accuracies of the different models.

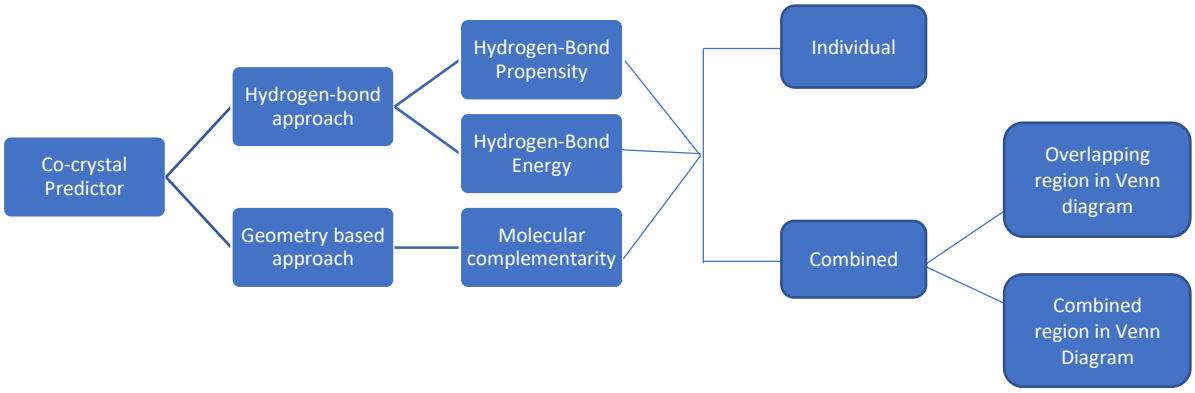

Figure 5.4. Road map of this study.

This study is carried out to answer the following questions:

1. Can HBP and HBE predict co-crystallization outcomes?
2. Can MC predict co-crystallization outcomes?
3. Will the individual or combination of the methodologies provide a better accuracy?

5.2. Co-crystal screening

GRAS list co-formers were purchased from Aldrich, Fischer, and Oakwood and was used as received. To measure the melting points, the Fischer-Johns melting point apparatus was used. FT-IR spectra of the API, co-former, and potential co-crystals were analyzed using Nicolet 380 FT-IR spectrometer applying an attenuated total reflection (ATR) technique and ZnSe as the crystal.

5.2.1. Experimental co-crystal screening

Liquid assisted grinding experiments were done with the APIs in combination with 42 GRAS list co-formers (294 co-crystal experiments). The target and co-former were added in a 1:1 molar ratio to a spotting plate with a few drops of methanol. The mixture was ground for 30-40 seconds or until the solvent was completely evaporated, which resulted in a solid or a glue-like material. Eventually, IR spectroscopy was carried out to determine if the ground mixture consists of peaks from both the starting materials and consequently if there was any shift in the stretches. A shift greater than 3 cm^{-1} in the IR peaks was labeled as "YES" to co-crystallization, and consistent peaks were labeled as "NO" to co-crystallization[34].

5.2.2. Predicting co-crystallization using hydrogen-bond propensity (HBP)

When HBP is applied to an API and a co-former of interest,[35,36,37,38,39] there are two possible outcomes; higher HBP value for a hydrogen-bond motif between a) API•••co-former, or b) API•••API and co-former•••co-former. To determine which motif will prevail, we calculated a Δ_{HBP} ($HBP_{API\cdots co\text{-}former} - HBP_{API\cdots API/\ co\text{-}former\cdots co\text{-}former}$). If $\Delta_{HBP} \geq 0$, it was assigned as a "YES" to co-crystallization, and if $\Delta_{HBP} < 0$, it was assigned as a "NO" to co-crystallization.
See section 2.2.3. for detailed description of hydrogen-bond propensity calculations.

5.2.3. Predicting co-crystallization using hydrogen-bond energy (HBE)

The same approach as HBP was applied, where we calculated a ΔE ($HBE_{API\cdots co\text{-}former} - HBE_{API\cdots API/\ co\text{-}former\cdots co\text{-}former}$). If $\Delta E \geq 0$, it was assigned as a "YES" to co-crystallization and, if $\Delta E < 0$, it was a "NO" to co-crystallization[40]. See section 4.2.3. for detailed description on hydrogen-bond energy calculations.

5.2.4. Predicting co-crystallization using molecular complementarity (MC)

MC is a knowledge-based predictive tool available in Mercury. In the default settings, MC is based on three shape descriptors (S-axis, S/L axis, and M/L axis) and two polarity descriptors (fraction of nitrogen and oxygen, and dipole moment)[23]. Each descriptor has a criterion to afford a "PASS/ FAIL." A "PASS" corresponds to the formation of a co-crystal and "FAIL" means no reaction[26,41,42]. Overall it predicts the formation of a co-crystal if and only if all five descriptors exhibit a "PASS." MC in default settings offered a reliability of 27-70%.
Since the accuracy produced by default MC was very low, we investigated the descriptor relationships and their significance. Figure 5.5 shows the correlation coefficients of the descriptors, where a positive sign indicates a higher significance.[26] Fábián[23], proposed that although *Fraction of polar volume* (FPV) has a higher positive correlation coefficient than *Fraction of nitrogen and oxygen* (FNO), FPV could be replaced by FNO in the calculations as an easier alternative.

Descriptor (molecule 1)	Descriptor (molecule 2)	ρ	r
FPV	*FPV*	0.41	0.37
S/L	*S/L*	0.40	0.38
Dipole	*Dipole*	0.39	0.28
S/M	*S/M*	0.38	0.38
M/L	*M/L*	0.38	0.41
PV	*FPV*	0.35	0.27
APV	*FPV*	-0.34	-0.32
ASAN	*Dplu*	-0.32	-0.29
PV	*APV*	-0.31	-0.28
ASAN	*Davg*	-0.31	-0.27
FNO	*FNO*	0.31	0.30
ASAN	*ASAP_P*	-0.31	-0.29
ASAN	*FASAP_P*	-0.31	-0.28
ASAN	*qHmax*	-0.30	-0.33
ASAN	*HBD2*	-0.30	-0.27
PV	*PV*	0.30	0.22
ASAN	*Aavg+Davg*	-0.30	-0.28
ASAN	*HBD1*	-0.30	-0.29

Figure 5.5. Molecular descriptors and their significance[26].

In order to investigate if the replacement of FPV with FNO affects the MC success rate, we included FPV in the calculations. Moreover, *Polar Volume* (PV) also displayed a positive correlation and was therefore, included as a descriptor in the updated/modified calculations.

To calculate the "polar volume" and "fraction polar volume," two different sources were used for the volume of the elements labeled as 'source **1**'[43] and 'source **2**'[44], respectively, Table 5.2. Both FPV and PV were calculated for 42 co-formers and seven APIs. The difference between source 1 and 2 is that source 1 neglects hydrogen atoms, whereas, in source 2, the volume of the elements is dependent on the number of neighboring hydrogen atoms.

Table 5.2. Numerical values of volumes of elements used in calculations from two different sources.

Source 1	Atomic volume
Volume of N	17.3 cm^3 / mol
Volume of O	14.0 cm^3 / mol
Volume of S	15.5 cm^3 / mol
Volume of C	4.58 cm^3 / mol
Volume of F	17.1 cm^3 / mol

Source 2

O (2,1)	**O (1,0)**	**O(2,0)**	**N(3,0)**	**N(3,1)**	**N(2,0)**	**N(3,2)**	
15.764 $Å^3$	13.935$Å^3$	12.512$Å^3$	9.944$Å^3$	18.148$Å^3$	13.324$Å^3$	24.643$Å^3$	
C (3,0)	**C (4,1)**	**C(4,3)**	**C(4,2)**	**C(3,1)**	**C(4,0)**	**S(4,0)**	**P(4,0)**
12.119$Å^3$	18.13$Å^3$	33.468$Å^3$	24.409$Å^3$	21.02$Å^3$	10.286$Å^3$	17.531$Å^3$	22.161$Å^3$

By carefully modifying the MC settings from five descriptors to seven descriptors, the accuracy range increased to 50-64% across the seven APIs, Table 5.3. The results from the modified settings were more consistent than the default for the APIs examined in this study. A total of 1050,000 data points was analyzed to introduce an updated and modified MC settings. A detailed instruction on how to implement the seven-descriptor settings for MC is provided in Appendix A.

Table 5.3. Default vs. modified combinations of descriptor settings for MC calculations.

Default Settings						
M/L axis ratio	S/L axis ratio	S-axis	Dipole Moment Magnitude	FNO		
Modified Settings						
M/L axis ratio	S/L axis ratio	S-axis	Dipole Moment Magnitude	FNO	PV	FPV

5.3. Results

5.3.1. Experimental co-crystallization

The solvent assisted grinding experiments were analyzed using IR spectroscopy. See section 2.3.1 for detailed description. Table 5.4. summarizes the experimental screening results.

Table 5.4. Experimental grinding results for seven targets against 42 potential co-formers.

	T11	T12	T13	T14	T15	T16	T17
IR data	2228,1774, 1717, 1660	1626, 1569, 1452, 1434	1771, 1680, 1580, 1560	1648, 1582, 1482, 1441	1665, 1588, 1505, 1463	1566, 1513, 1480, 1422	1702, 1685, 1603, 1532
Co-former	Ground Mixture	Ground Mixture	Ground Mixture	Ground Mixture	Ground Mixture	Ground Mixture	Ground Mixture
3-Hydroxy-2-naphthoic acid 1655, 1626, 1597, 1513	2228, 1763, 1696, 1540 Yes	1646, 1619, 1580, 1437 Yes	1770, 1679, 1579, 1559 No	1658, 1581, 1513, 1483 Yes	1666, 1589, 1507, 1464 No	1573, 1514, 1481, 1420 Yes	1701, 1685, 1603, 1532 No
4-Hydroxybenzoic acid 1667, 1605, 1592, 1509	2228, 1775, 1714, 1591 No	1668, 1630, 1570, 1433 No	1760, 1679, 1579, 1557 Yes	1650, 1581, 1483, 1445 No	1666, 1588, 1507, 1469 No	1565, 1513, 1480, 1422 No	1700, 1684, 1624, 1596 No
Adipic acid 1683, 1461, 1426, 1407	2228, 1785, 1689, 1521 Yes	1701, 1641, 1599, 1574 Yes	1763, 1680, 1579, 1556 Yes	1645, 1565, 1484, 1433 Yes	1667, 1588, 1505, 1423 No	1579, 1553, 1482, 1422 Yes	1700, 1684, 1624, 1596 No
Apigenin 1649, 1604, 1586, 1554	2228, 1775, 1714, 1591 No	1648, 1602, 1555, 1491 No	1645, 1600, 1573, 1553 Yes	1649, 1604, 1575, 1554 No	1649, 1611, 1589, 1577 No	1648, 1601, 1553, 1498 Yes	1708, 1687, 1650, 1605 Yes
Benzenesulfonic acid 1663, 1445, 1092, 1031	2222, 1776, 1696, 1539 Yes	1640, 1577, 1455, 1435 Yes	1786, 1637, 1577, 1557 Yes	1658, 1566, 1483, 1436 Yes	1666, 1588, 1507, 1463 Yes	1619, 1566, 1485, 1457 Yes	1710, 1660, 1630, 1550 Yes
Benzoic acid 1677, 1602, 1581, 1452	1774, 1716, 1623, 1601 No	1770, 1602, 1596, 1450 No	1761, 1686, 1578, 1502 Yes	1648, 1568, 1484, 1445 No	1666, 1588, 1504, 1426 No	1565, 1543, 1515, 1482 No	1684, 1599, 1532, 1467 Yes
Caffeine 1694, 1639, 1545, 1454	2227, 1775, 1694, 1649 No	1694, 1648, 1599, 1546 No	1693, 1651, 1636, 1546 Yes	1692, 1659, 1644, 1544 No	1698, 1675, 1587, 1505 Yes	1697, 1652, 1566, 1512 Yes	1696, 1655, 1597, 1532 No
Cholic acid 1712, 1247, 1090, 1077	2228, 1774, 1717, 1578 No	1716, 1630, 1599, 1574 No	1770, 1683, 1578, 1498 No	1648, 1583, 1287, 1176 No	1666, 1587, 1506, 1464 No	1562, 1511, 1481, 1425 No	1701, 1685, 1603, 1532 No
Citric acid 1741, 1691, 1425, 1391	2228, 1691, 1539, 1392 Yes	1726, 1641, 1623, 1600 Yes	1711, 1654, 1579, 1559 Yes	1721, 1643, 1558, 1485 Yes	1666, 1588, 1505, 1463 No	1563, 1512, 1480, 1421 No	1702, 1684, 1602, 1531 Yes
D-Glucuronic acid 1703, 1456, 1362, 1347	1702, 1458, 1346, 1254 No	1701, 1458, 1363, 1346 No	1702, 1579, 1489, 1460 No	1704, 1584, 1446, 1341 No	1713, 1660, 1587, 1507 Yes	1712, 1566, 1513, 1481 Yes	1702, 1685, 1603, 1532 No
EDTA 1690, 1412, 1386, 1309	1687, 1411, 1388, 1341 No	1687, 1629, 1440, 1407 No	1690, 1413, 1385, 1310 No	1650, 1585, 1440, 1412 No	1669, 1505, 1410, 1310 Yes	1700, 1558, 1513, 1480 Yes	1690, 1603, 1533, 1468 No
Folic acid 1688, 1602, 1481, 1451	2228, 1706, 1604, 1508 Yes	1668, 1629, 1651, 1631 Yes	1681, 1606, 1577, 1498 Yes	1678, 1649, 1601, 1569 Yes	1666, 1590, 1507, 1406 Yes	1694, 1565, 1514, 1482 Yes	1701, 1686, 1602, 1533 No
Fumaric acid 1653, 1406, 1315, 1270	2228, 164, 1559, 1420 No	1630, 1570, 1460, 1435 No	1770, 1682, 1579, 1502 No	1650, 1405, 1272, 1230 No	1666, 1589, 1506, 1466 No	1695, 1584, 1563, 1523 Yes	1701, 1685, 1624, 1604 No
Gentisic acid 1662, 1620, 1592, 1437	2230, 1775, 1697, 1612 Yes	1637, 1616, 1603, 1575 Yes	1763, 1672, 1579, 1500 Yes	1658, 1564, 1482, 1438 Yes	1666, 1587, 1573, 1506 No	1565, 1511, 1482, 1418 No	1702, 1685, 1602, 1532 No
Glutaric acid 1682, 1466, 1430, 1406	2228, 1695, 1540, 1392 Yes	1706, 1642, 1575, 1456 Yes	1762, 1700, 1682, 1578 Yes	1706, 1644, 1561, 1485 Yes	1694, 1667, 1587, 1507 No	1561, 1514, 1478, 1421 No	1685, 1603, 1532, 1466 No
Glycine 1607, 1577, 1500, 1441	1577, 1502, 1405, 1330 No	1610, 1572, 1502, 1405 No	1579, 1497, 1404, 1330 No	1577, 1580, 1498, 1404 No	1682, 1667, 1588, 1572 No	1563, 1510, 1481, 1420 No	1702, 1686, 1603, 1532 No
Glycolic acid 1701, 1428, 1226, 1081	2230, 1695, 1538, 1488 Yes	1727, 1625, 1577, 1434 Yes	1759, 1676, 1578, 1560 No	1728, 1647, 1565, 1484 Yes	1731, 1885, 1587, 1505 Yes	1734, 1625, 1565, 1512 Yes	1702, 1685, 1603, 1532 No
Hydrocinnamic acid 1692, 1426, 1406, 1299	2228, 1772, 1694, 1532 No	1693, 1639, 1599, 1572 No	1766, 1703, 1663, 1579 Yes	1649, 1583, 1484, 1432 No	1666, 1588, 1506, 1462 No	1707, 1565, 1513, 1480 Yes	1701, 1684, 1623, 1596 No
Isonicotinamide 1653, 1621, 1594, 1546	2228, 1778, 1704, 1675	1679, 1635, 1596, 1570	1763, 1676, 1620, 1578	1639, 1585, 1553, 1403	1665, 1588, 1506, 1462	1563, 1513, 1480, 1421	1704, 1684, 1623, 1600

	Yes	Yes	Yes	Yes	No	No	No
L-Glutamic acid 1641, 1499, 1407, 1350	2228, 1775, 1718, 1638 Yes	1640, 1572, 1511, 1476 Yes	1643, 1500, 1495, 1420 No	1650, 1581, 1512, 1484 Yes	1666, 1506, 1294, 1215 No	1574, 1562, 1545, 1510 Yes	1703, 1685, 1623, 1602 No
L-Mandelic acid 1708, 1491, 1455, 1241	1696, 1540, 1361, 1286 Yes	1644, 1569, 1552, 1494 Yes	1760, 1719, 1679, 1577 Yes	1728, 1648, 1565, 1484 Yes	1649, 1602, 1578, 1555 No	1560, 1509, 1480, 1425 No	1701, 1684, 1602, 1531 No
L-Proline 1608, 1565, 1541, 1473	2227, 1700, 1602, 1544 Yes	1620, 1557, 1449, 1435 Yes	1753, 1672, 1578, 1497 Yes	1653, 1565, 1435, 1409 Yes	1666, 1653, 1589, 1506 No	1566, 1512, 1480, 1421 Yes	1702, 1685, 1623, 1603 No
L-Serine 1582, 1466, 1408, 1382	2229, 1785, 1718, 1590 Yes	1629, 1587, 1466, 1410 Yes	1758, 1681, 1578, 1557 Yes	1609, 1579, 1468, 1410 Yes	1666, 1589, 1506, 1467 Yes	1569, 1514, 1480, 1421 Yes	1701, 1685, 1626, 1595 No
L-Tartaric acid 1732, 1706, 1442, 1251	1732, 1706, 1442, 1251 No	1732, 1706, 1442, 1251 No	1650, 1589, 1490, 1420 Yes	1732, 1706, 1442, 1251 No	1666, 1588, 1506, 1464 No	1666, 1588, 1506, 1464 No	1701, 1686, 1596, 1588 No
Maleic acid 1703, 1558, 1458, 1428	2228, 1754, 1694, 1618 Yes	1646, 1554, 1449, 1420 Yes	1764, 1677, 1579, 1501 Yes	1708, 1646, 1561, 1484 Yes	1667, 1588, 1505, 1451 No	1569, 1543, 1481, 1455 No	1702, 1685, 1623, 1597 No
Malic acid 1737, 1682, 1438, 1407	2228, 1695, 1539, 1392 Yes	1718, 1635, 1599, 1575 Yes	1713, 1579, 1558, 1509 Yes	1719, 1643, 1558, 1485 Yes	1666, 1590, 1506, 1293 Yes	1564, 1515, 1482, 1437 Yes	1700, 1685, 1623, 1597 No
Malonic acid 1691, 1432, 1387, 1301	2229, 1691, 1538, 1375 Yes	1719, 1640, 1619, 1575 Yes	1708, 1661, 1578, 1505 Yes	1719, 1642, 1560, 1484 Yes	1729, 1666, 1641, 1588 Yes	1561, 1510, 1480, 1435 No	1700, 1685, 1602, 1532 No
Mannitol 1712, 1538, 1455, 1415	2229, 1702, 1645, 1593 Yes	1700, 1416, 1299, 1279 Yes	1691, 1577, 1554, 1503 Yes	1656, 1646, 1504, 1423 Yes	1667, 1588, 1506, 1464 Yes	1565, 1516, 1482, 1421 No	1702, 1685, 1603, 1532 Yes
Methylparaben 1676, 1605, 1584, 1559	2229, 1774, 1676, 1606 No	1677, 1630, 1605, 1572 No	1761, 1681, 1606, 1579 Yes	1649, 1605, 1585, 1560 No	1666, 1588, 1507, 1292 No	1568, 1556, 1481, 1419 Yes	1677, 1604, 1583, 1532 Yes
Nicotinamide 1673, 1617, 1595, 1484	2228, 1774, 1716, 1523 No	1670, 1626, 1572, 1455 No	1665, 1628, 1617, 1576 Yes	1650, 1582, 1552, 1484 No	1666, 1588, 1506, 1464 No	1564, 1512, 1479, 1437 No	1564, 1512, 1479, 1437 No
Oxalic acid 1677, 1161, 1128, 826	2229, 1691, 1539, 1455 Yes	1723, 1633, 1576, 1434 Yes	1757, 1660, 1579, 1554 Yes	1720, 1644, 1484, 1442 Yes	1666, 1588, 1507, 1465 No	1566, 1513, 1481, 1420 No	1744, 1699, 1682, 1622 Yes
Pamoic acid 1649, 1452, 1428, 1308	1646, 1450, 1428, 1289 No	1649, 1452, 1427, 1308 No	1646, 1500, 1452, 1427 No	1648, 1452, 1430, 1291 No	1653, 1507, 1453, 1427 No	1649, 1566, 1482, 1452 Yes	1685, 1649, 1624, 1602 Yes
Phosphoric acid N/A	1695, 1635, 1122, 963 Yes	1695, 1635, 1122, 963 Yes	1646, 1582, 1241, 1118 Yes	1642, 1589, 1147, 1062 Yes	1666, 1590, 1507, 1412 No	1646, 1567, 1120, 956 Yes	1564, 1512, 1479, 1437 No
Piperazine 1648, 1456, 1322, 1270	2225, 1727, 1665, 1600 Yes	1629, 1567, 1449, 1430 Yes	1698, 1659, 1558, 1493 Yes	1668, 1577, 1400, 1316 Yes	1666, 1590, 1507, 1412 No	1562, 1512, 1479, 1421 No	1564, 1512, 1479, 1437 No
Riboflavin 1730, 1645, 1578, 1536	1730,1644, 1620, 1577 No	1730, 1643, 1620, 1577 No	1729, 1646, 1578, 1537 No	1730, 1645, 1577, 1535 No	1730, 1645, 1577, 1537 No	1731, 1645, 1578, 1543 No	1725, 1713, 1685, 1647 Yes
Saccharin 1714, 1591, 1458, 1332	2228, 1764, 1697, 1617 Yes	1731, 1639, 1600, 1576 Yes	1714, 1679, 1578, 1556 No	1731, 1649, 1578, 1484 Yes	1667, 1588, 1506, 1464 No	1567, 1513, 1481, 1422 No	1701, 1685, 1604, 1533 No
Salicylic acid 1652, 1608, 1480, 1440	2229, 1774, 1657, 1659 No	1630, 1570, 1456, 1436 No	1762, 1669, 1578, 1561 Yes	1665, 1654, 1442, 1404 No	1666, 1588, 1506, 1465 No	1565, 1512, 1480, 1419 No	1699, 1684, 1656, 1603 No
Sorbic acid 1672, 1634, 1608, 1411	2227, 1763, 1683, 1609 Yes	1664, 1623, 1585, 1485 Yes	1759, 1685, 1616, 1577 Yes	1645, 1577, 1483, 1432 Yes	1670, 1508, 1493, 1459 No	1566, 1514, 1480, 1423 No	1685, 1623, 1604, 1532 Yes
Succinic acid 1679, 1411, 1307, 1197	2229, 1774, 1715, 1701 No	1679, 1630, 1600, 1574 No	1759, 1678, 1578, 1557 Yes	1679, 1646, 1566, 1484 No	1663, 1588, 1507, 1461 No	1565, 1524, 1483, 1457 Yes	1685, 1603, 1532, 1410 No
Theophylline 1700, 1659, 1555, 1481	1715, 1656, 1560, 1523	1708, 1694, 1647, 1564	1702, 1659, 1557, 1482	1706, 1661, 1559, 1486	1664, 1587, 1503, 1465	1711, 1666, 1562, 1513	1702, 1685, 1603, 1532

	Yes	Yes	No	Yes	No	Yes	No
Urea 1674, 1590, 1550, 1454	2228, 1775, 1716, 1600 No	1630, 1571, 1451, 1428 No	1684, 1578, 1554, 1550 Yes	1650, 1577, 1483, 1431 No	1666, 1588, 1506, 1463 No	1560, 1513, 1480, 1421 No	1685, 1623, 1596, 1523 No
Xanthine 1692, 1650, 1564, 1454	1697,1656, 1565, 1458 No	1690, 1654, 1569, 1457 No	1656, 1569, 1508, 1460 No	1695, 1648, 1566, 1435 No	1697, 1666, 1572, 1507 Yes	1705, 1654, 1565, 1544 Yes	1685, 1624, 1604, 1531 No
Experimental supramolecular yield	55%	55%	69%	55%	24%	50%	24%

5.3.2. HBP calculations

The homomeric, heteromeric and $\Delta_{propensity}$ values were calculated and summarized in Table 5.5. for the 294 combinations of targets and co-formers.

Table 5.5. HBP outcomes for seven targets against 42 potential co-formers.

Co-former	**T11**	**T12**	**T13**	**T14**	**T15**	**T16**	**T17**
3-hydroxy-2naphthoic acid	-0.1	0.48	-0.09	0.15	0.06	0.22	0.01
4-hydroxybenzoic acid	-0.05	0.47	-0.06	0.17	0.07	0.24	0.03
Adipic acid	-0.01	0.52	0.03	0.11	0.23	0.31	-0.08
Apigenin	-0.03	0.57	0.02	0.09	0.06	0.37	-0.05
Benzenesulfonic acid	0.1	0.46	-0.02	0	0.24	0.26	0.03
Benzoic acid	-0.12	0.45	-0.07	0.14	0.17	0.26	0.04
Caffeine	0.05	0.41	0.03	0.26	0.3	-0.11	0.41
Cholic acid	0.09	0.49	-0.01	0.08	0.06	0.24	-0.17
Citric acid	-0.1	0.05	0.08	0.07	0.11	0.32	0.05
D- Glucuronic acid	-0.14	0.54	0.01	0.12	0.07	0.26	0.06
EDTA	-0.01	0.3	0.02	0.12	0.23	0.3	-0.09
Folic acid	0.05	0.42	0.1	0.1	0.1	0.29	-0.26
Fumaric acid	-0.06	0.49	-0.03	0.08	0.17	0.26	-0.01
Gentisic acid	-0.11	0.53	-0.07	0.09	0.19	0.27	0.05
Glutaric acid	-0.02	0.1	0.03	0.1	0.24	0.31	-0.07
Glycine	-0.07	0.38	0.04	0.01	0.33	0.05	-0.1
Glycolic acid	0.03	0.61	-0.01	0.06	0.17	0.27	-0.04
Hydrocinnamic acid	-0.07	0.3	0.01	0.24	0.23	0.34	-0.01
Isonicotinamide	-0.02	0.38	0.02	-0.05	-0.07	0.33	-0.12
L-glutamic acid	0.07	0.6	0.08	0.12	0.36	0.13	-0.07
L-Mandelic acid	-0.02	0.29	0.03	0.31	0.24	0.48	0.03
L-prolin	0.02	0.11	0.02	0	0.12	0.25	-0.07
L-Serine	0.02	0.51	0.03	0.07	0.12	0.24	-0.07
L-tartaric acid	0	0.43	0.05	0.21	0.2	0.36	-0.02
Maleic acid	-0.1	0.49	0	0.08	0.17	0.27	-0.05
Malic acid	0.01	0.47	0.06	0.2	0.2	0.37	-0.03
Malonic acid	0	0.15	0.04	0.1	0.25	0.24	-0.07
Mannitol	-0.06	0.43	-0.02	-0.04	0.02	0.33	0.03
Methylparaben	0.11	0.66	-0.1	0.06	0.33	0.33	-0.02
Nicotinamide	-0.03	0.3	0.02	0.26	-0.07	0.31	-0.1
Oxalic acid	-0.03	0.54	-0.17	-0.04	0.02	0.09	-0.01

Pamoic acid	-0.11	0.5	-0.09	-0.03	0.22	0.19	0.02
Phosphoric acid	-0.22	-0.02	-0.19	0.15	-0.31	0	-0.16
Piperazine	-0.02	0.29	0	0.12	0.03	0.33	-0.11
Riboflavin	0.07	0.15	-0.02	0.01	-0.07	0.02	-0.01
Saccharin	0.06	0.4	-0.01	-0.22	0.22	0.24	0.04
Salicylic acid	-0.1	0.49	-0.07	0.12	0.25	0.25	0.05
Sorbic acid	-0.1	0.44	-0.03	0.09	0.16	0.28	-0.01
Succinic acid	-0.01	0.52	0.04	0.09	0.24	0.29	-0.07
Theophylline	0.1	0.47	-0.1	0.11	-0.03	0.08	0.08
Urea	-0.09	0.02	-0.02	-0.05	-0.04	0.03	-0.05
Xanthine	0.05	0.33	0.05	-0.02	-0.13	0.26	0.01
Predicted supramolecular yield	38%	98%	55%	83%	83%	97%	36%

5.3.3. HBE calculations

The homomeric, heteromeric and ΔE values were calculated and summarized in Table 5.6. for the 294 combinations of targets and co-formers.

Table 5.6. HBE outcomes for seven targets against 42 potential co-formers.

Co-former	**T11**	**T12**	**T13**	**T14**	**T15**	**T16**	**T17**
3-hydroxy-2naphthoic acid	4.17	13.8	1.82	6.32	3.73	11.58	5.17
4-hydroxybenzoic acid	3.23	10	1.74	6.22	3.65	7.705	5.09
Adipic acid	1.19	8.3	-0.4	7.68	4.14	5.947	4.81
Apigenin	0.21	7.5	-1.4	8.18	3.22	5.058	3.9
Benzenesulfonic acid	3.91	11	2.4	7.41	4.51	8.62	5.98
Benzoic acid	2.14	9.5	0	2.97	1.3	7.578	2.65
Caffeine	-0.8	6.3	0.31	-5.88	-3.1	2.722	-3.2
Cholic acid	2.14	10.8	0	2.97	1.3	9.846	2.66
Citric acid	3.11	8.4	1.41	9.64	6.3	8.24	6.4
D- Glucuronic acid	0.41	9.7	-1.6	0.1	-0.8	6.786	0.5
EDTA	1.18	0.25	-0.7	12.4	4.7	6.838	5.49
Folic acid	-7.2	10.4	-5.1	3.13	-4.1	-2.217	-3.4
Fumaric acid	3.12	14.2	0.88	4.59	2.48	8.317	3.87
Gentisic acid	3.46	10.1	1.18	5.15	2.88	11.58	4.29
Glutaric acid	2.7	9.8	0.5	3.9	1.97	8.124	3.35
Glycine	2.58	14.1	0.39	3.69	1.82	7.76	3.2
Glycolic acid	4.5	9.5	2.11	6.86	4.12	11.85	5.58
Hydrocinnamic acid	1.53	6	-0.5	1.96	0.57	7.642	1.9
Isonicotinamide	0.29	11.1	-1.7	-0.1	-0.9	4.363	0.36
L-glutamic acid	3.21	11.1	0.95	4.73	2.57	9.028	3.98
L-Mandelic acid	4.18	8.8	2.17	6.97	4.2	8.806	5.66
L-prolin	1.53	10.7	-0.5	1.96	0.57	6.99	1.9
L-Serine	3.78	15.6	1.47	5.68	3.26	8.495	4.69
L-tartaric acid	6.66	10.5	4.04	10.4	6.7	12.94	8.25

Maleic acid	3.14	13.9	0.9	4.62	2.5	8.403	3.9
Malic acid	5.5	12.1	3	8.51	5.31	11.4	6.81
Malonic acid	3.65	3.7	1.35	5.47	3.11	9.93	4.53
Mannitol	-2.9	8.7	-2.1	5.89	3.03	6.6	4.45
Methylparaben	2.36	9	0.88	5.36	3.57	6.817	5.01
Nicotinamide	0.43	5.5	-1.3	6.11	-0.5	3.816	0.79
Oxalic acid	6.47	14.6	4.54	0.48	7.36	11.93	8.94
Pamoic acid	2.53	9.2	1.06	11.4	3.57	6.99	5.01
Phosphoric acid	0	7.6	-1.7	6.11	3.13	5.044	3.84
Piperazine	-1.1	3	0	9.18	-3.4	0.553	-3.5
Riboflavin	-6	0.69	-3	-7.94	-3.3	-1.563	-2.6
Saccharin	2.7	12.4	0.5	3.31	1.97	10.39	3.35
Salicylic acid	3.4	14.1	1.12	3.9	2.8	11.49	4.21
Sorbic acid	1.38	7	-0.4	5.04	0.79	5.11	2.13
Succinic acid	1.29	8.4	-0.3	2.26	4.25	6.058	4.92
Theophylline	1.97	8.5	0.52	7.74	3.26	6.35	4.69
Urea	-0.2	1.6	2.59	5.68	1.16	0	-0.2
Xanthine	2.45	9.4	0.92	-0.29	4.2	13.03	5.66
Predicted supramolecular yield	88%	100%	69%	90%	83%	95%	88%

5.3.4. MC calculations

The MC values were calculated using the updated seven descriptors for the 294 combinations of targets and co-formers and are summarized in Table 5.7.

Table 5.7. MC outcomes for seven targets against 42 potential co-formers.

Co-former	**T11**	**T12**	**T13**	**T14**	**T15**	**T16**	**T17**
3-hydroxy-2naphthoic acid	0	30	10	50	45	85	50
4-hydroxybenzoic acid	0	0	0	100	0	20	0
Adipic acid	0	0	0	100	0	96	16
Apigenin	0	0	0	100	0	20	0
Benzenesulfonic acid	0	0	0	100	0	60	0
Benzoic acid	0	0	0	100	0	20	0
Caffeine	0	0	0	0	0	80	0
Cholic acid	0	0	0	100	0	80	0
Citric acid	0	0	32	0	0	0	0
D- Glucuronic acid	0	52	8	0	60	0	0
EDTA	0	100	84	0	12	64	20
Folic acid	72	0	72	20	96	100	92
Fumaric acid	0	0	0	0	0	52	0
Gentisic acid	0	0	0	33	0	80	0
Glutaric acid	0	0	0	60	0	96	16
Glycine	0	0	0	0	0	0	0
Glycolic acid	0	40	0	0	0	0	0
Hydrocinnamic acid	0	0	12	40	60	96	68

Isonicotinamide	0	16	0	100	0	20	0
L-glutamic acid	0	40	4	0	16	100	48
L-Mandelic acid	4	0	12	0	52	100	72
L-prolin	0	0	20	0	0	0	0
L-Serine	0	0	0	0	0	0	0
L-tartaric acid	0	24	0	0	0	0	0
Maleic acid	0	0	0	0	36	20	36
Malic acid	0	0	0	0	0	0	0
Malonic acid	0	40	0	0	0	0	0
Mannitol	92	56	96	0	68	100	96
Methylparaben	0	0	0	0	0	80	0
Nicotinamide	0	0	0	100	0	20	0
Oxalic acid	0	0	0	100	0	0	0
Pamoic acid	100	100	100	0	44	100	48
Phosphoric acid	0	0	0	20	0	0	0
Piperazine	0	0	0	0	0	20	0
Riboflavin	84	8	84	0	0	80	**0**
Saccharin	0	0	0	20	0	80	0
Salicylic acid	0	10	10	0	0	55	0
Sorbic acid	0	0	0	25	0	80	0
Succinic acid	0	0	0	100	0	96	16
Theophylline	0	0	0	0	0	80	0
Urea	0	0	0	0	0	0	0
Xanthine	0	0	0	0	0	0	0
Predicted supramolecular yield	64%	45%	71%	40%	43%	29%	50%

5.4. Discussions

5.4.1. Individual prediction outcomes vs. experimental results

The accuracy of the methodologies was calculated by comparing the individual prediction results with the experimental co-crystallization outcomes. In order to ease the process of comparison, we calculated a success rate which is the number of predictions that match the experimental outcome divided by the total number of combinations (294). The success rates of the seven APIs are summarized in Table 5.8.

Table 5.8. Success rates of HBP, HBE, and MC (* TP: true positive and TN: true negative).

	HBP			**HBE**			**MC**		
	TP	TN	Overall	TP	TN	Overall	TP	TN	Overall
T11	11/23=49%	14/19=74%	60%	21/23=91%	3/19=16%	57%	16/23=70%	8/19=42%	57%
T12	22/23=96%	0/19=0%	52%	21/23=91%	0/19=0%	50%	10/23=43%	10/19=43%	50%
T13	17/29=57%	8/13=62%	60%	19/29=66%	3/13=23%	52%	23/29=79%	5/13=38%	64%

T14	20/23=87%	4/19=21%	57%	21/23=91%	2/19=11%	55%	9/23=39%	11/19=58%	50%
T15	9/10=90%	9/32=28%	43%	7/10=70%	4/32=13%	26%	6/10=60%	21/32=66%	64%
T16	20/21=95%	1/21=5%	50%	20/21=95%	1/21=5%	50%	5/21=24%	14/21=67%	52%
T17	4/10=40%	22/32=69%	62%	8/10=80%	4/32=13%	29%	8/10=80%	19/32=59%	64%
Overall	103/139 =74%	58/155 =37%	161/294 =55%	117/139 =84%	17/155 =11%	134/294 =46%	77/139 =55%	88/155 =55%	165/294 =56%

HBP across the seven compounds gave a success rate of 43%-62%. The true positives (TP, where the prediction matches the positive co-crystal experiment) and true negatives (TN, where the prediction matches the negative co-crystal experiments) were separately analyzed. An accuracy range of 40-96% was observed for TP and 0-74% for TN. The higher accuracy for TP than TN can be attributed to the fact that CSD only contains positive co-crystallization results. Therefore, it is not surprising that HBP was better at predicting TP than TN.

HBE delivered success rates of 26-57%, with TP 66-95% and TN 0-23%. HBE offered the lowest accuracy for TN and highest for TP across all the methods. Although HBE performed better for smaller compounds in Chapter 4, it failed for larger compounds studied here. The HBE calculations were entirely based on electrostatics and any shape or geometry factors were not included. Due to this HBE produced more false positives than true negatives leading to lower TN success rates. This raises the question whether we can extrapolate the accuracy of predictive approaches to larger compounds?

Finally, MC exhibited a prediction match of 50-64% for the seven compounds with TP 24-80% and TN and 38-67% success rates. Similar to any other methods, MC is built on a database of small molecules. Although, Fábián[23] mentioned that the short and the long axes appear to be more influential than other frequently used size descriptors, such as molecular weight. The cut-off values of "l, m and s" tested on small compounds might not translate to larger compounds.

We ranked the methodologies in decreasing order of their overall predictive accuracy for TP, which resulted in HBE (84%)> HBP (74%)> MC (55%); and for TN MC (55%)> HBP (37%)> HBE (11%). Additionally, if we combine TP and TN results, the predictive ability of MC (56%)> HBP (55%)> HBE (46%).

5.4.2. Using Venn diagram to interpret the predictive outcomes

Since the average molecular weight of organic structures reported in CSD is ~400 g/mol[33] therefore, individually the methods did not deliver a high accuracy, compared to 80-90% observed on small molecules in Chapter 4[31], Hence, we used Venn diagrams to apply a combination of the methods. The regions inside the circles of the Venn diagrams represent the outcomes that were correctly predicted by that particular methodology. For example, the co-formers which reside inside the HBP region of the Venn diagram was correctly predicted by HBP. Those co-formers that were present in the combined regions such as HBP&HBE; HBP&MC; HBE&MC denotes that both the methodologies correctly match the experimental results. Subsequently, the co-formers that were accurately predicted by all three methods occupy the region where all the methods overlap. Lastly, co-formers outside the Venn diagram (for example, xanthine, cholic acid, and methylparaben in case of **T11**) were not predicted correctly by any of the three methods. The co-formers who experimentally formed co-crystals were represented in "green," and those who did not form co-crystals in "red", Figure 5.6.

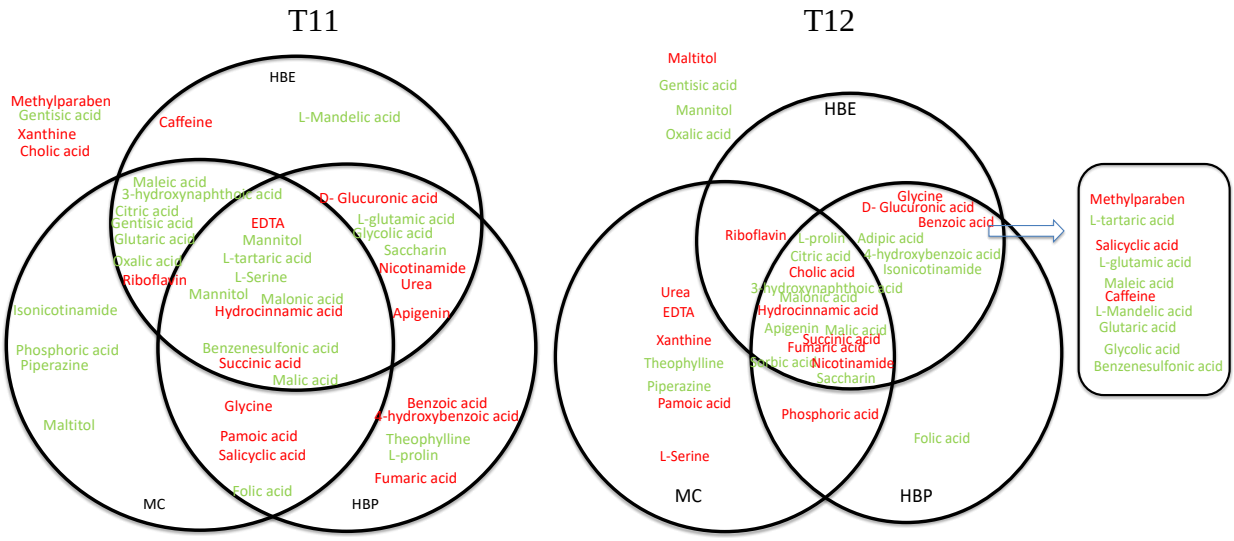

T13

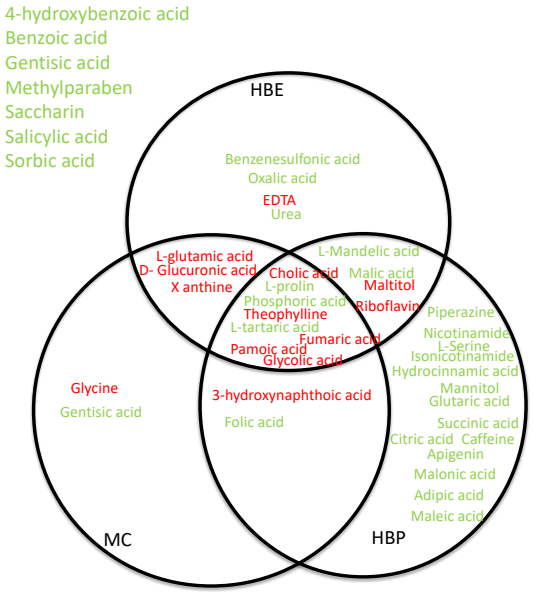

T14

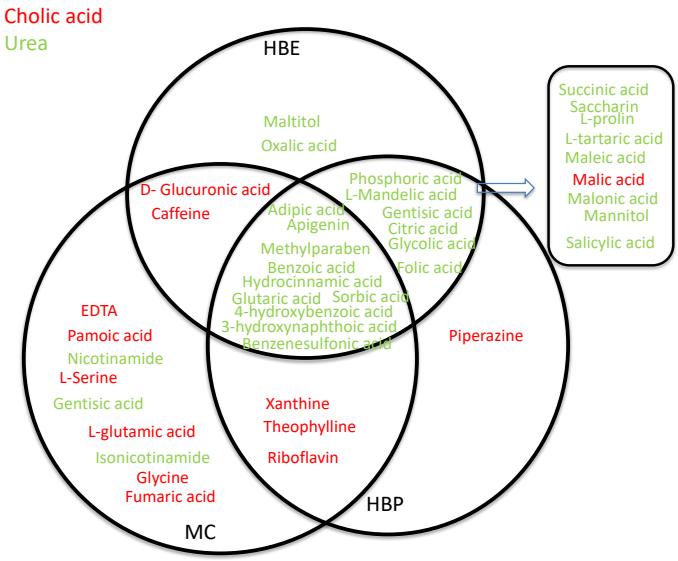

T15

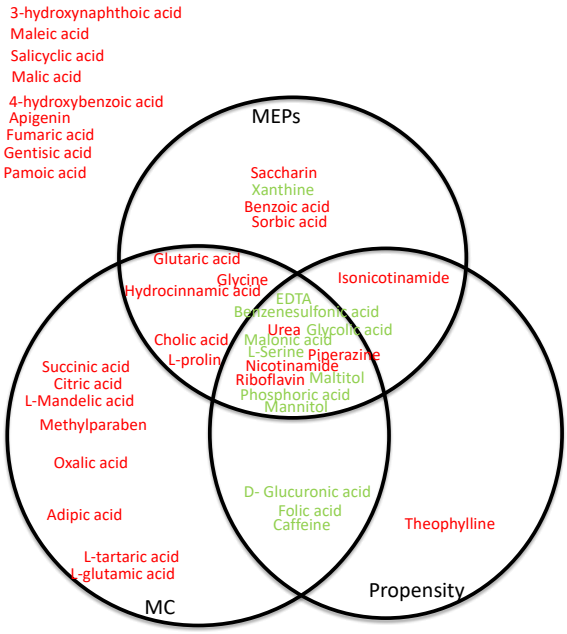

T16

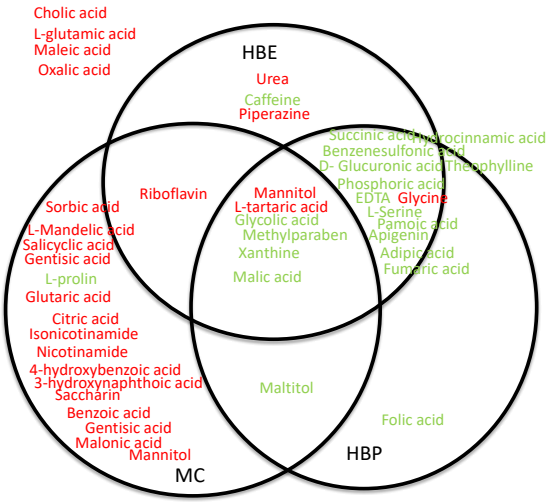

T17

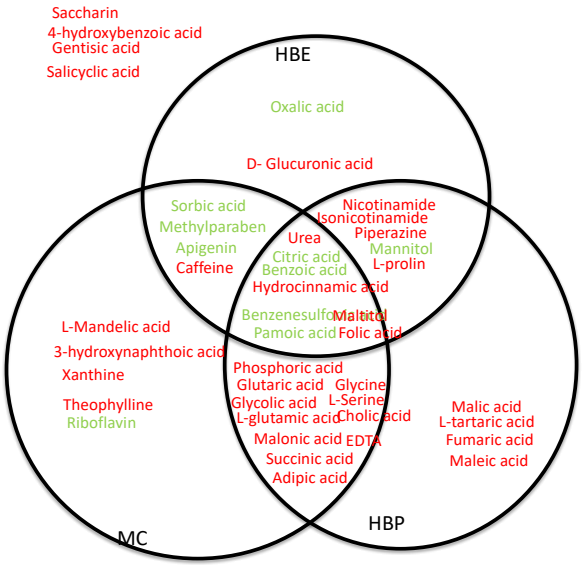

Figure 5.6. Venn diagram representation for combination of methods.

(*green & red represents experimentally obtained positive and negative co-crystals respectively)

Two different approaches were employed to analyze the Venn diagram, Figure 5.7. Approach1, is only employing a fraction of the correctly predicted results from a particular method and requires two or more methods to provide similar prediction for it to be present in the overlapping region. The success rates of the overlapping region (approach 1) from the Venn diagrams are listed in Table 5.9.

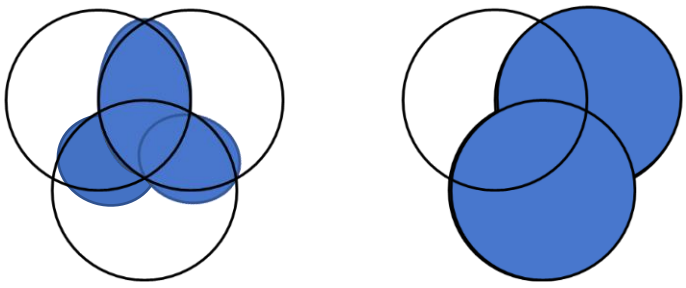

a) Overlapping region (Approach 1)

b) Combined region (Approach 2)

Figure 5.7. Approaches used to analyze the Venn diagrams.

Table 5.9. Success rates of the overlapping regions (* TP: true positive and TN: true negative).

	Overlapping regions		
	TP	TN	Overall
T11	20/23=87%	11/19=58%	31/42=74%
T12	22/23=96%	1/19=5%	23/42=55%
T13	20/29=69%	5/13=38%	25/42=60%
T14	20/23=87%	3/19=16%	23/42=55%
T15	10/10=100%	7/32=22%	17/42=40%
T16	20/21=95%	2/21=10%	22/42=52%
T17	8/10=80%	16/32=50%	24/42=57%
Overall	120/139=86%	45/155=29%	165/294=56%

Overall, the overlapping region displayed a 56% success rate, with a considerable imbalance between the TP and TN. The high accuracy for TP over TN corresponds to CSD consisting of only positive results. Hence, it is not surprising that the TN does not exhibit similar accuracy. Clearly, this approach would not be useful as a co-crystal prediction tool.

Consequently, we moved to approach 2 which includes the combined region of two methods at a time. There were three possible combinations, i.e., HBP & MC, HBP & HBE, and HBE & MC. The success rates from the combination methods are summarized in Table 5.10.

Table 5.10. Success rates of the combined region (* TP: true positive and TN: true negative).

	HBP & MC			**HBP&HBE**			**HBE&MC**		
	TP	TN	Overall	TP	TN	Overall	TP	TN	Overall
T11	12/23 =52%	13/19 =68%	25/42 =60%	13/23 =57%	6/19 =32%	29/42 =69%	15/23 =65%	7/19 =37%	22/42 =52%
T12	22/23 =96%	10/19 =53%	32/42 =76%	23/23 =100%	0/19 =0%	23/42 =55%	23/23 =100%	10/19 =53%	33/42 =79%
T13	27/29 =93%	11/13 =85%	38/42 =90%	26/29 =90%	10/13 =77%	36/42 =86%	25/29 =86%	8/13 =62%	33/42 =79%
T14	21/23 =91%	12/19 =63%	33/42 =79%	22/23 =96%	5/19 =26%	27/42 =64%	23/23 =100%	10/19 =53%	33/42 =79%
T15	10/10 =100%	22/32 =69%	32/42 =76%	10/10 =100%	7/32 =22%	17/42 =40%	10/10 =100%	22/32 =69%	32/42 =76%
T16	21/21 =100%	14/21 =67%	35/42 =83%	21/21 =100%	2/21 =10%	23/42 =55%	20/21 =95%	14/21 =67%	34/42 =81%
T17	9/10 =90%	27/32 =84%	36/43 =86%	9/10 =90%	23/32 =72%	32/42 =76%	10/10 =100%	20/32 63%	30/42 =71%
Overall	122/139 =88%	109/155 =70%	231/294 =79%	124/139 =89%	53/155 =33%	177/294 =60%	126/139 =91%	91/155 =59%	217/294 =74%

We would assume that the region corresponding to HBP&MC would provide better accuracy since it is combination of the probability of hydrogen-bond formation with close packing principle. For

the seven compounds it provides an accuracy range of 60-90%. TP exhibited an accuracy greater than 90% in all cases (except 52% for **T11**). For TN, we observed 53-85% success rates. Both HBP and MC are based on CSD which includes only positive results hence, as expected TP performs better than TN. The results are however significantly higher than any other approach could demonstrate at this point.

HBP&HBE region corresponds to hydrogen-bonding synthons hierarchy and does not include any geometric factors. This combination provided high false positive results comparable. Needless to say, this combination was not the best candidate.

Finally, a combination of HBE&MC, similar to HBP&MC includes both hydrogen-bonding and geometry factors. Hence, one would anticipate similar reliability. The TP accuracy ranges from 65-100% and TN 52-81%. As expected, the results were comparable to that of HBP&MC. Although if we include time as a factor, calculating HBP and MC is faster in comparison to HBE. Overall the combination of HBP&MC methods provided faster and reliable prediction for designing co-crystallization experiments.

5.5. Conclusions

1. HBP produces a success rate of 55% with 74% and 37% accuracies for TP and TN, respectively. HBE delivered the highest TP results (84%) and lowest TN accuracy (11%).
2. MC could predict the co-crystallization outcomes overall with 56% accuracy. In comparison to other methods, MC produces the lowest TP (55%) and highest TN accuracies (55%).
3. The combined region of HBP&MC in the Venn diagram produced the highest reliability of 79% (TP accuracy was 88%, and TN was 70%).

5.6. References

(1) Williams, H. D.; Trevaskis, N. L.; Charman, S. A.; Shanker, R. M.; Charman, W. N.; Pouton, C. W.; Porter, C. J. H. Strategies to Address Low Drug Solubility in Discovery and Development. *Pharmacol Rev* **2013**, *65* (1), 315–499. https://doi.org/10.1124/pr.112.005660.

(2) Shan, N.; Zaworotko, M. J. The Role of Cocrystals in Pharmaceutical Science. *Drug Discovery Today* **2008**, *13* (9), 440–446. https://doi.org/10.1016/j.drudis.2008.03.004.

(3) B. Aakeröy, C.; R. Champness, N.; Janiak, C. Recent Advances in Crystal Engineering. *CrystEngComm* **2010**, *12* (1), 22–43. https://doi.org/10.1039/B919819A.

(4) Aakeröy, C. B.; Grommet, A. B.; Desper, J. Co-Crystal Screening of Diclofenac. *Pharmaceutics* **2011**, *3* (3), 601–614. https://doi.org/10.3390/pharmaceutics3030601.

(5) Gadade, D. D.; Pekamwar, S. S. Pharmaceutical Cocrystals: Regulatory and Strategic Aspects, Design and Development. *Adv Pharm Bull* **2016**, *6* (4), 479–494. https://doi.org/10.15171/apb.2016.062.

(6) Surov, A. O.; Voronin, A. P.; Manin, A. N.; Manin, N. G.; Kuzmina, L. G.; Churakov, A. V.; Perlovich, G. L. Pharmaceutical Cocrystals of Diflunisal and Diclofenac with Theophylline. *Mol. Pharmaceutics* **2014**, *11* (10), 3707–3715. https://doi.org/10.1021/mp5004652.

(7) Desiraju, G. R. Crystal Engineering: From Molecule to Crystal. *J. Am. Chem. Soc.* **2013**, *135* (27), 9952–9967. https://doi.org/10.1021/ja403264c.

(8) Babu, N. J.; Nangia, A. Solubility Advantage of Amorphous Drugs and Pharmaceutical Cocrystals. *Crystal Growth & Design* **2011**, *11* (7), 2662–2679. https://doi.org/10.1021/cg200492w.

(9) Jones, W.; Motherwell, W. D. S.; Trask, A. V. Pharmaceutical Cocrystals: An Emerging Approach to Physical Property Enhancement. *MRS Bulletin* **2006**, *31* (11), 875–879. https://doi.org/10.1557/mrs2006.206.

(10) Mir, N. A.; Dubey, R.; Desiraju, G. R. Strategy and Methodology in the Synthesis of Multicomponent Molecular Solids: The Quest for Higher Cocrystals. *Acc. Chem. Res.* **2019**. https://doi.org/10.1021/acs.accounts.9b00211.

(11) Friščić, T.; Jones, W. Recent Advances in Understanding the Mechanism of Cocrystal Formation via Grinding. *Crystal Growth & Design* **2009**, *9* (3), 1621–1637. https://doi.org/10.1021/cg800764n.

(12) Cherukuvada, S.; Kaur, R.; Row, T. N. G. Co-Crystallization and Small Molecule Crystal Form Diversity: From Pharmaceutical to Materials Applications. *CrystEngComm* **2016**, *18* (44), 8528–8555. https://doi.org/10.1039/C6CE01835A.

(13) Basavoju, S.; Boström, D.; Velaga, S. P. Indomethacin–Saccharin Cocrystal: Design, Synthesis and Preliminary Pharmaceutical Characterization. *Pharm Res* **2008**, *25* (3), 530–541. https://doi.org/10.1007/s11095-007-9394-1.

(14) Aakeröy, C. Is There Any Point in Making Co-Crystals? *Acta Cryst B* **2015**, *71* (4), 387–391. https://doi.org/10.1107/S2052520615010872.

(15) K. Duggirala, N.; L. Perry, M.; Almarsson, Ö.; J. Zaworotko, M. Pharmaceutical Cocrystals: Along the Path to Improved Medicines. *Chemical Communications* **2016**, *52* (4), 640–655. https://doi.org/10.1039/C5CC08216A.

(16) Chakrabarty, R.; Mukherjee, P. S.; Stang, P. J. Supramolecular Coordination: Self-Assembly of Finite Two- and Three-Dimensional Ensembles. *Chem. Rev.* **2011**, *111* (11), 6810–6918. https://doi.org/10.1021/cr200077m.

(17) Aakeröy, C. B.; Chopade, P. D.; Desper, J. Avoiding "Synthon Crossover" in Crystal Engineering with Halogen Bonds and Hydrogen Bonds. *Crystal Growth & Design* **2011**, *11* (12), 5333–5336. https://doi.org/10.1021/cg2009013.

(18) Arunan, E.; Desiraju, G. R.; Klein, R. A.; Sadlej, J.; Scheiner, S.; Alkorta, I.; Clary, D. C.; Crabtree, R. H.; Dannenberg, J. J.; Hobza, P.; et al. Defining the Hydrogen Bond: An Account (IUPAC Technical Report). *Pure Appl. Chem.* **2011**, *83* (8), 1619–1636. https://doi.org/10.1351/PAC-REP-10-01-01.

(19) Buckingham, A. D.; Del Bene, J. E.; McDowell, S. A. C. The Hydrogen Bond. *Chemical Physics Letters* **2008**, *463* (1), 1–10. https://doi.org/10.1016/j.cplett.2008.06.060.

(20) Kaźmierczak, M.; Katrusiak, A. The Most Loose Crystals of Organic Compounds. *J. Phys. Chem. C* **2013**, *117* (3), 1441–1446. https://doi.org/10.1021/jp311403k.

(21) Kitaigorodskii, A. I. The Principle of Close Packing and the Condition of Thermodynamic Stability of Organic Crystals. *Acta Cryst* **1965**, *18* (4), 585–590. https://doi.org/10.1107/S0365110X65001391.

(22) Molecular crystals and Molecules - 1st Edition https://www.elsevier.com/books/molecular-crystals-and-molecules/kitaigorodsky/978-0-12-410550-8 (accessed Feb 12, 2020).

(23) Fábián, L. Cambridge Structural Database Analysis of Molecular Complementarity in Cocrystals. *Crystal Growth & Design* **2009**, *9* (3), 1436–1443. https://doi.org/10.1021/cg800861m.

(24) Siegler, M. A.; Fu, Y.; Simpson, G. H.; King, D. P.; Parkin, S.; Brock, C. P. An Unexpected Co-Crystal with a Variable Degree of Order: 1:1 *Rac* -1,2-Cyclohexanediol/Triphenylphosphine Oxide. *Acta Cryst Sect A Found Cryst* **2007**, *63* (6), 912–925. https://doi.org/10.1107/S0108768107054699.

(25) Schneider, H.-J. Quantification of Noncovalent Interactions – Promises and Problems. *New J. Chem.* **2019**, *43* (39), 15498–15512. https://doi.org/10.1039/C9NJ03325D.

(26) Fábián, L. Cambridge Structural Database Analysis of Molecular Complementarity in Cocrystals. *Crystal Growth & Design* **2009**, *9* (3), 1436–1443. https://doi.org/10.1021/cg800861m.

(27) Pidcock, E.; Motherwell, W. D. S. A New Model of Crystal PackingElectronic Supplementary Information (ESI) Available: Equation Used to Calculate Goodness of Fit, Mean Goodness of Fit Values Calculated for Z = 4 Datasets, Results of Pattern Assignment for Z = 2 and Z = 8 Structures, Examples of Unit Cell Dimension Calculations. See Http://Www.Rsc.Org/Suppdata/Cc/B3/B310873b/. *Chem. Commun.* **2003**, No. 24, 3028. https://doi.org/10.1039/b310873b.

(28) Delori, A.; Galek, P. T. A.; Pidcock, E.; Jones, W. Quantifying Homo- and Heteromolecular Hydrogen Bonds as a Guide for Adduct Formation. *Chemistry – A European Journal* **2012**, *18* (22), 6835–6846. https://doi.org/10.1002/chem.201103129.

(29) Musumeci, D.; Hunter, C. A.; Prohens, R.; Scuderi, S.; McCabe, J. F. Virtual Cocrystal Screening. *Chem. Sci.* **2011**, *2* (5), 883. https://doi.org/10.1039/c0sc00555j.

(30) Sarkar, N.; Aakeröy, C. B. Evaluating Hydrogen-Bond Propensity, Hydrogen-Bond Coordination and Hydrogen-Bond Energy as Tools for Predicting the Outcome of Attempted Co-Crystallisations. *Supramolecular Chemistry* **2019**, 1–10. https://doi.org/10.1080/10610278.2019.1693043.

(31) Sarkar, N.; Sinha, A. S.; Aakeröy, C. B. Systematic Investigation of Hydrogen-Bond Propensities for Informing Co-Crystal Design and Assembly. *CrystEngComm* **2019**. https://doi.org/10.1039/C9CE01196J.

(32) Shaikh, R.; Singh, R.; Walker, G. M.; Croker, D. M. Pharmaceutical Cocrystal Drug Products: An Outlook on Product Development. *Trends in Pharmacological Sciences* **2018**, *39* (12), 1033–1048. https://doi.org/10.1016/j.tips.2018.10.006.

(33) Groom, C. R.; Bruno, I. J.; Lightfoot, M. P.; Ward, S. C. The Cambridge Structural Database. *Acta Crystallographica Section B* **2016**, *72* (2), 171–179. https://doi.org/10.1107/S2052520616003954.

(34) Brittain, H. G. Vibrational Spectroscopic Studies of Cocrystals and Salts. 1. The Benzamide−Benzoic Acid System. *Crystal Growth & Design* **2009**, *9* (5), 2492–2499. https://doi.org/10.1021/cg801397t.

(35) Wood, P. A.; Feeder, N.; Furlow, M.; Galek, P. T. A.; Groom, C. R.; Pidcock, E. Knowledge-Based Approaches to Co-Crystal Design. *CrystEngComm* **2014**, *16* (26), 5839. https://doi.org/10.1039/c4ce00316k.

(36) Delori, A.; Galek, P. T. A.; Pidcock, E.; Jones, W. Quantifying Homo- and Heteromolecular Hydrogen Bonds as a Guide for Adduct Formation. *Chemistry – A European Journal* **2012**, *18* (22), 6835–6846. https://doi.org/10.1002/chem.201103129.

(37) Mapp, L. K.; Coles, S. J.; Aitipamula, S. Design of Cocrystals for Molecules with Limited Hydrogen Bonding Functionalities: Propyphenazone as a Model System. *Crystal Growth & Design* **2017**, *17* (1), 163–174. https://doi.org/10.1021/acs.cgd.6b01399.

(38) Galek, P. T. A.; Allen, F. H.; Fábián, L.; Feeder, N. Knowledge-Based H-Bond Prediction to Aid Experimental Polymorph Screening. *CrystEngComm* **2009**, *11* (12), 2634–2639. https://doi.org/10.1039/B910882C.

(39) Macrae, C. F.; Bruno, I. J.; Chisholm, J. A.; Edgington, P. R.; McCabe, P.; Pidcock, E.; Rodriguez-Monge, L.; Taylor, R.; Streek, J. van de; Wood, P. A. Mercury CSD 2.0 – New Features for the Visualization and Investigation of Crystal Structures. *J Appl Cryst* **2008**, *41* (2), 466–470. https://doi.org/10.1107/S0021889807067908.

(40) Sarkar, N.; Aakeröy, C. B. Evaluating Hydrogen-Bond Propensity, Hydrogen-Bond Coordination and Hydrogen-Bond Energy as Tools for Predicting the Outcome of Attempted Co-Crystallisations. *Supramolecular Chemistry* **2019**, 1–10. https://doi.org/10.1080/10610278.2019.1693043.

(41) Pallipurath, A. R.; Civati, F.; Eziashi, M.; Omar, E.; McArdle, P.; Erxleben, A. Tailoring Cocrystal and Salt Formation and Controlling the Crystal Habit of Diflunisal. *Crystal Growth & Design* **2016**, *16* (11), 6468–6478. https://doi.org/10.1021/acs.cgd.6b01154.

(42) Karki, S.; Friščić, T.; Fábián, L.; Jones, W. New Solid Forms of Artemisinin Obtained through Cocrystallisation. *CrystEngComm* **2010**, *12* (12), 4038. https://doi.org/10.1039/c0ce00428f.

(43) Periodic Table of the Elements http://hyperphysics.phy-astr.gsu.edu/hbase/pertab/pertab.html#c1 (accessed Aug 25, 2019).

(44) Beaucamp, S.; Mathieu, D.; Agafonov, V. Optimal Partitioning of Molecular Properties into Additive Contributions: The Case of Crystal Volumes. *Acta Crystallogr B Struct Sci* **2007**, *63* (2), 277–284. https://doi.org/10.1107/S0108768106052463.

Chapter 6 - CoForm: An Automatic Tool for Predicting Co-crystallization

6.1. Introduction

In the previous chapters, we investigated predictive tools based on hydrogen-bond propensity[1], hydrogen-bond coordination[2], molecular complementarity[3], and molecular electrostatic potential surface calculations[4] in order to predict co-crystallization screening outcomes. These approaches were complex and required in-depth knowledge of either theoretical, quantum-mechanical, or statistical data analysis. With the growing demand of co-crystallization and co-crystallization-based[5] approaches to access new solid forms in various fields[6,7,8] related to agrochemicals, energetics, and smart materials[9,10,11,12,13,14,15,16,17,18,19], it is imperative that we develop cheaper, faster, and more reliable methods for predicting when a pair of molecules will co-crystallize and when they will not. In order to address these issues, we have developed CoForm, an automatic tool for predicting co-crystallization. A comparison between existing predictive tools and CoForm is given in Figure 6.1.

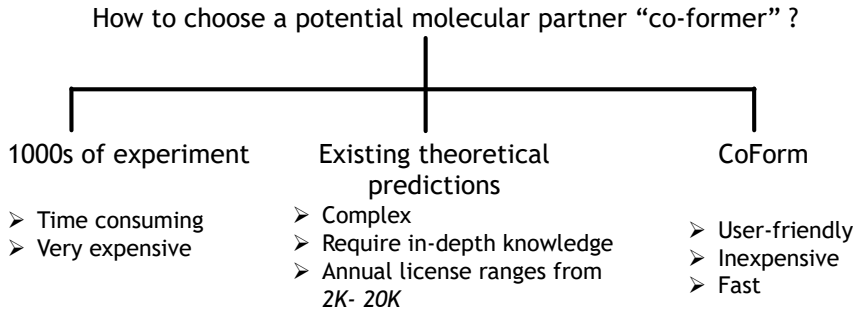

Figure 6.1. Comparison between existing co-crystallization techniques and CoForm.

CoForm is based on a mathematical model that compares the target of interest with a known set of targets. The known targets are associated with a list of co-formers that form co-crystals (positive partners), and a list of co-formers that do not form co-crystals (negative partners). The database for the known targets was created using approximately 2000 experimental data collected from past and present Aakeröy lab members over a period of 15 years. All experiments were done either by liquid assisted grinding (LAG) or melt co-crystallization. The experiments were analyzed using IR spectroscopy, where the fingerprint region was investigated for any potential shift in stretching

frequency. Further analysis using melting points, differential scanning calorimetry (DSC), thermogravimetric analysis (TGA), and single-crystal analysis were also carried out.

CoForm, utilizes 42 co-formers that are generally regarded as safe[20] (GRAS) for pharmaceutical co-crystals and an additional 50 co-formers, which are conventionally used as co-formers in co-crystallization experiments, Table 6.1.

Table 6.1. List of co-formers.

GRAS list co-formers	Non GRAS list co-formers
3-Hydroxy-2-naphthoic acid	1-Bromo-4- iodotetrafluorobenzene
4-Hydroxybenzoic acid	1,2-Bis(4-pyridyl)ethane
Adipic acid	1,2-Bis(4-pyridyl)ethylene
Apigenin	1,4-Dihydroxybenzene
Benzenesulfonic acid	1,4-Diiodobenzene
Benzoic acid	1,4-Diiodotetrafluorobenzene
Caffeine	2-Amino-3,5-dibromopyridine
Cholic acid	2-Amino-3-hydroxypyridine
Citric acid	2-Amino-4,6-dimethylpyrimidine
D-glucuronic acid	2-Amino-4-chloro-6-methylpyrimidine
EDTA	2-Amino-4-hydroxy-6-methylpyrimidine
Folic acid	2-Amino-4-methylpyrimidine
Fumaric acid	2-Amino-5-chloropyridine
Glutaric acid	2-Aminopyridine
Glycine	2-Aminopyrimidine
Glycolic acid	2-Chlorocyanoxime
Hydrocinnamic acid	2-Fluorocyanoxime
Isonicotinamide	2,4,6-Triaminopyrimidine
L-Glutamic acid	2,6-Diaminopyridine
L-Mandelic acid	2,6-Difluorobenzoic acid
L-Proline	3-Aminobenzoic acid
L-Serine	3-Aminopyridine
L-Tartaric acid	3-Benzoylpyridine
Maleic acid	3-Hydroxypyridine
Malic acid	3-Nitrobenzoic acid
Malonic acid	3,4-Dichlorobenzoic acid
Maltitol	3,5-Dinitrobenzoic acid
Mannitol	4,4’-Bipyridine
Nicotinamide	4-Aminobenzoic acid
Oxalic acid	4-Aminopyridine
Pamoic acid	4-Benzoylpyridine
Phosphoric acid	4-Bromocyanoxime
Piperazine	4-Bromotetrafluorobenzoic acid
Riboflavin	4-Chloro-2_6-diaminopyrimidine
Saccharin	4-Cyanobenzoic acid
Salicylic acid	4-Fluorocyanoxime
Sorbic acid	4-Hydroxybenzoic acid

Succinic acid	4-iodotetrafluorobenzoic acid
Theophylline	4-Nitrobenzoic acid
Urea	4-Phenylpyridine
Xanthine	4,4-Bisphenol
	4,4'-Dipyridyl
	4,4'-Trimethylenedipyridine
	Azelic acid
	Cyanoxime
	Dodecanedioic acid
	Pentafluorobenzoic acid
	Pimelic acid
	Sebacic acid
	Suberic acid

CoForm is a data-driven analysis of already existing targets, which is similar to hydrogen-bond propensity (HBP) and molecular complementarity (MC) studied in Chapters 2-5. A comparison between CoForm and HBP/ MC methods is summarized in Table 6.2.

Table 6.2. Comparison between HBP/ MC vs. CoForm.

HBP/ MC	**CoForm**
• Based on cheminformatics of crystal structures present in CSD. • Select a sampling dataset which is comparable to the defined functional groups of the target and co-former. • Understand the descriptors on which the calculations are based. • Each calculation takes 15-20 mins, further calculations to find $\Delta_{propensity}$ is needed.	• Based on cheminformatics of hydrogen-bond donors and hydrogen-bond acceptors. • Two inputs required: # of donors and # of acceptors. • It takes 10- 15 seconds to provide a list of co-formers which will likely or not likely to form co-crystal.

In order to examine the accuracy of CoForm and its potential limitations in predicting co-crystallization, we carried out a systematic study where we matched the predicted results with the experimental outcomes. Two known antihistamine drugs, loratadine, and desloratadine were used in this study to predict the co-crystal screening outcomes, Figure 6.2. These targets were chosen as they have similar molecular backbone but with different hydrogen-bond donor acceptor ratio.

Loratadine has zero hydrogen-bond donors and two acceptors. It does not have any conventional homomeric hydrogen-bond interaction. Whereas desloratadine has one donor and one acceptor.

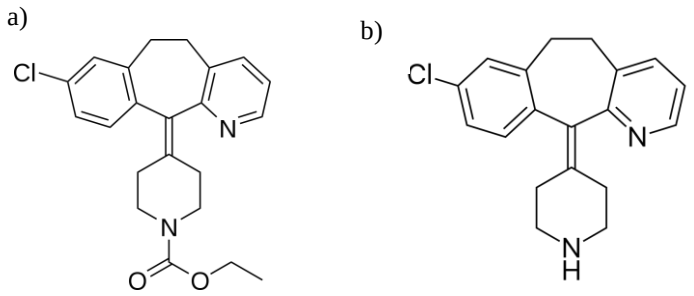

Figure 6.2. Targets used in this study, a) Loratadine and b) Desloratadine.

The study is carried out to answer the following questions:

1. Can CoForm predict the co-crystallization outcomes of loratadine and desloratadine?
2. Can CoForm perform better than commercial and established HBP/ MC methods?

6.2. Co-crystal screening

6.2.1. Experimental co-crystal screening

Loratadine and desloratadine were experimentally screened against 42 GRAS list co-formers. The co-former and target was combined in 1:1 stoichiometry with a drop of methanol in a spotting plate. The mixture was ground for 30-40 seconds or until the solvent evaporated. The mixture was then analyzed using IR spectroscopy. The IR spectra of the target, co-former and the mixtures were compared and shifts greater than 3 cm^{-1} in the C=O stretch was indicated as "YES" to co-crystallization. The consistent peaks were labeled as "NO" to co-crystallization.

6.2.2. Predicting co-crystal screening using CoForm

The CoForm database, consists of approximately 2000 data points including, both positive and negative co-crystallization results. The predictions from CoForm are dependent on the compounds present in the database. It is designed as a user-specific tool and can include co-formers and interactions that the user is specifically interested in.

CoForm is built using Groovy programming language. Groovy was chosen because it is platform-independent and, therefore, CoForm can be used on all three major operating systems, i.e., Windows, Linux, and Mac OSX. Moreover, Groovy is a scripting language that allows quick prototyping of software[21]. Consequently, we were quickly able to translate our prediction model into a prototype.

CoForm requires three inputs from the user:

1. Name of the target for which co-crystals need to be predicted.
2. Number of donors (donor: molecule or molecular fragment X-H in which X is an electronegative atom).
3. Number of acceptors (acceptor: an electronegative element usually N, O, F, occasionally S).

CoForm ranks the co-formers as highly likely, likely, and least likely to produce a co-crystal with a specific target. The output is in the form of tables that can be exported as *.csv* files, Figure 6.3. The most likely and least likely lists, as the name suggests corresponds to the co-formers with the highest and lowest probability to form a co-crystal, respectively. The likely lists consist of co-formers which were found to form co-crystals in some cases and did not form in certain instances. This list corresponds to maybes, and hence the co-formers fall between the highly likely and least likely lists. Since the co-crystallization outcomes are binary hence, we used the likely list of co-formers as a YES to co-crystallization. This will produce some false positives, which is a better alternative than false negatives.

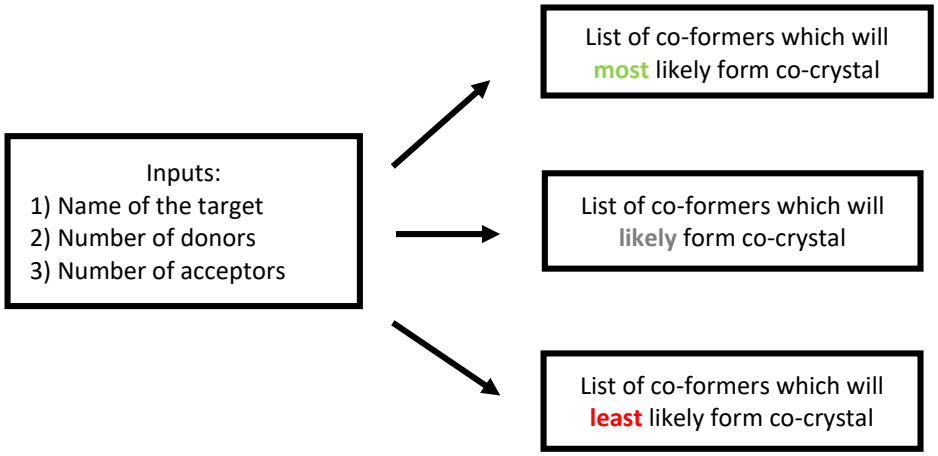

Figure 6.3. Implementing CoForm for predicting co-crystal outcomes.

6.2.3. Co-crystal screening using hydrogen-bond propensity (HBP)

The detailed description of HBP calculations[22,23,24,25,26] was illustrated in section 3.2.1. The functional groups used to determine the HBP values for loratadine and desloratadine are listed in Figure 6.4.

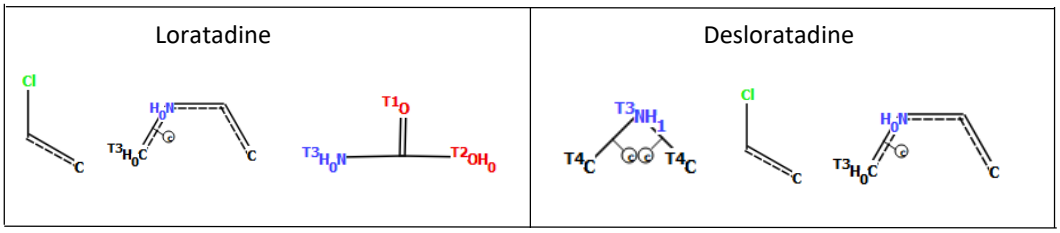

Figure 6.4. Functional groups used in the calculations.

6.2.4. Co-crystal screening using molecular complementarity (MC)

Five conformers of targets and co-formers were generated to conduct MC calculations. The detailed description of MC calculations[27,28,29] was illustrated in Appendix A.

6.3. Results

6.3.1. Experimental co-crystallization outcomes

Solvent assisted grinding experiments between loratadine and desloratadine and 42 co-formers were analyzed using IR spectroscopy, Table 6.3.

Table 6.3. Grinding results of loratadine and desloratadine.

IR data (cm^{-1})	**Loratadine**		**Desloratadine**	
	1699, 1472, 1432, 1381, 1354, 1320, 1273		1584, 1477, 1434, 1419, 1176, 1100, 1085	
Co-former	**Ground mixture**	**Results**	**Ground mixture**	**Results**
3-Hydroxy-2-naphthoic acid 1655, 1626, 1597, 1513, 1463, 1439	1683, 1632, 1591, 1474, 1422, 1394, 1322, 1276, 1227, 1172	Yes	1671, 1621, 1588, 1568, 1476, 1436, 1418, 1384, 1243, 1114	Yes
4-Hydroxybenzoic acid 1667, 1605, 1592, 1509, 1445, 1411	1676, 1600, 1582, 1452, 1420, 1322, 1278, 1232, 1177, 1124	Yes	1706, 1619, 1561, 1476, 1437, 1415, 1383, 1275, 1170, 1097	Yes
Adipic acid 1683, 1461, 1426, 1407, 1267, 1187	1689, 1477, 1418, 1384, 1326, 1301, 1277, 1220, 1175, 1112	Yes	1588, 1566, 1480, 1454, 1376, 1328, 1297, 1248, 1218, 1139	Yes
Apigenin 1649, 1604, 1586, 1554, 1491, 1442	1649, 1604, 1586, 1554, 1491, 1442, 1351, 1267, 1241	No	1706, 1582, 1567, 1476, 1424, 1336, 1159, 1116, 1106	Yes

Benzenesulfonic acid 1663, 1445, 1092, 1031, 1009, 986	1730, 1689, 1646, 1578, 1503, 1426, 1394, 1343, 1304, 1273	Yes	1731, 1646, 1578, 1540, 1497, 1455, 1394, 1343, 1246, 1225	Yes
Benzoic acid 1677, 1602, 1581, 1452, 1419, 1323	1700, 1471, 1430, 1226, 1218, 1151, 1111, 1066, 1015, 992	Yes	1425, 1328, 1147, 1100, 1091, 1075, 1049, 1009, 968, 958	Yes
Caffeine 1694, 1639, 1545, 1454, 1428, 1357	1691, 1648, 1562, 1418, 1332, 1220, 1205, 1152, 1112, 995	Yes	1696, 1646, 1564, 1463, 1436, 1416, 1332, 1258, 1202, 1150	Yes
Cholic acid 1712, 1247, 1090, 1077, 1043, 979	1691, 1643, 1425, 1276, 1222, 1112, 995	Yes	1621, 1590, 1542, 1507, 1475, 1437, 1420, 1365, 1341, 1325	Yes
Citric acid 1741, 1691, 1425, 1391, 1358, 1235	1700, 1698, 1470, 1432, 1360, 1349, 1278, 1259, 1221	Yes	1642, 1586, 1566, 1475, 1435, 1421, 1331, 1282, 1246, 1236	Yes
D-Glucuronic acid 1703, 1456, 1362, 1347, 1249, 1224	1700, 1430, 1382, 1280, 1227, 1177, 1112, 1077, 1017, 993	No	1426, 1280, 1259, 1075, 1018, 950, 877, 864	Yes
EDTA 1690, 1412, 1386, 1309, 1253, 1092	1678, 1655, 1639, 1617, 1572, 1559, 1476, 1445, 1429, 1399	Yes	1705, 1616, 1576, 1474, 1450, 1349, 1260, 1198, 1140, 1117	Yes
Folic acid 1688, 1602, 1481, 1451, 1410, 1336	1688, 1434, 1278, 1219, 1170, 1097, 1086, 1056, 994	No	1624, 1567, 1475, 1436, 1422, 1318, 1081, 1039, 999, 952	Yes
Fumaric acid 1653, 1406, 1315, 1270, 1226, 1172	1692, 1663, 1642, 1561, 1476, 1438, 1420, 1220, 1187, 1113	Yes	1707, 1661, 1560, 1528, 1481, 1436, 1311, 1282, 1239, 1223	Yes
Glutaric acid 1682, 1466, 1430, 1406, 1301, 1264	1693, 1559, 1470, 1431, 1321, 1273, 1219, 1170, 1114, 1081	Yes	1644, 1560, 1475, 1436, 1421, 1366, 1270, 1246, 1173, 1083	Yes
Glycine 1607, 1577, 1500, 1441, 1409, 1315	1678, 1473, 1433, 1384, 1324, 1277, 1227, 1170, 1094, 1022	No	1711, 1574, 1476, 1438, 1422, 1382, 1254, 1171, 1088	Yes
Glycolic acid 1701, 1428, 1226, 1081, 925, 683	1701, 1428, 1226, 1081, 925, 683, 884, 850	No	1655, 1627, 1608, 1578, 1514, 1476, 1468, 1437, 1382	Yes
Hydrocinnamic acid 1692, 1426, 1406, 1299, 1216, 927	1695, 1509, 1472, 1430, 1304, 1224, 1114, 995	Yes	1581, 1555, 1518, 1477, 1434, 1396, 1340, 1309, 1154, 1073	Yes
Isonicotinamide 1653, 1621, 1594, 1546, 1388, 1290	1690, 1635, 1602, 1480, 1417, 1330, 1275, 1225, 1191, 1177	Yes	1687, 1661, 1601, 1474, 1438, 1401, 1332, 1178	Yes
L-Glutamic acid 1641, 1499, 1407, 1350, 1302, 1251	1689, 1482, 1463, 1381, 1354, 1320, 1273	Yes	1716, 1645, 1589, 1579, 1473, 1421, 1359, 1340	Yes
L-Mandelic acid 1708, 1491, 1455, 1241, 1187, 1096	1693, 1684, 1638, 1473, 1429, 1374, 1321, 1272, 1227, 1201	Yes	1553, 1439, 1417, 1379, 1345, 1309, 1293, 1264, 1239, 1182	Yes
L-Proline 1608, 1565, 1541, 1473, 1447, 1374	1649, 1604, 1586, 1554, 1491, 1442, 1351, 1267, 1241	No	1554, 1476, 1436, 1421, 1394, 1332, 1076, 1001, 973, 944	Yes
L-Serine 1582, 1466, 1408, 1382, 1337, 1301	1696, 1620, 1590, 1540, 1523, 1508, 1413, 1394, 1383, 1333	Yes	1585, 1563, 1519, 1506, 1476, 1438, 1420, 1332, 1272	Yes
L-Tartaric acid 1732, 1706, 1442, 1251, 1211, 1181	1688, 1654, 1473, 1422, 1382, 1321, 1275, 1224, 1114, 1084	Yes	1707, 1561, 1551, 1477, 1439, 1385, 1231, 1150, 1116	Yes
Maleic acid 1703, 1558, 1458, 1428, 1257, 1216	1664, 1605, 1586, 1475, 1436, 1386, 1356, 1276, 1221, 1159	Yes	1583, 1556,1458, 1440, 1364, 1267, 1235, 1160	No
Malic acid 1737, 1682, 1438, 1407, 1355, 1279	1693, 1682, 1650, 1604, 1572, 1556, 1472, 1421, 1351, 1267	Yes	1646, 1603, 1571, 1549, 1515, 1472, 1430, 1359, 1296, 1270	Yes
Malonic acid 1691, 1432, 1387, 1301, 1214, 1163	1667, 1647, 1420, 1386, 1273, 1224, 1161, 1112, 1085, 995	Yes	1703, 1692, 1631, 1577, 1560, 1437, 1425, 1376, 1355, 1311	Yes
Maltitol 1149, 1047, 1016, 992, 968, 903	1695, 1472, 1432, 1381, 1354, 1320, 1273	No	1584, 1477, 1434, 1419, 1176, 1100, 1083, 1006, 993	No
Mannitol 1712, 1538, 1455, 1415, 1387, 1251	1701, 1667, 1466, 1446, 1429, 1375, 1360, 1222, 1203, 1156	Yes	1712, 1538, 1455, 1415, 1387, 1251	No
Nicotinamide 1673, 1617, 1595, 1484, 1421, 1391	1695, 1415, 1387, 1311, 1277, 1212, 1166, 1107, 968, 862	Yes	1882, 1645, 1633, 1579, 1564, 1440, 1415, 1401, 1379, 1308	Yes

Oxalic acid 1677, 1161, 1128, 826, 779	1690, 1619, 1586, 1544, 1424, 1386, 1320, 1276, 1218, 1170	Yes	1587, 1475, 1434, 1419, 1176, 1100, 1085	No
Pamoic acid 1649, 1452, 1428, 1308, 1290, 1204	1691, 1652, 1596, 1552, 1473, 1432, 1356, 1323, 1226	Yes	1697, 1647, 1546, 1479, 1428, 1357, 1284, 1237, 1087	Yes
Phosphoric acid N/A	1690, 1676, 1582, 1474, 1434, 1383, 1278, 1226, 1178, 1112	Yes	1581, 1473, 1439, 1422, 1394, 1369, 1356, 1310, 1272, 1185	Yes
Piperazine 1648, 1456, 1322, 1270, 1127, 1084	1698, 1645, 1456, 1426, 1383, 1326, 1277, 1221, 1169	No	1584, 1477, 1434, 1419, 1176, 1100, 1085	No
Riboflavin 1730, 1645, 1578, 1536, 1503, 1395	1730, 1645, 1578, 1536, 1503, 1395, 1343, 1241, 1178	No	1730, 1645, 1578, 1536, 1503, 1395, 1343, 1241, 1178	No
Saccharin 1714, 1591, 1458, 1332, 1295, 1255	1694, 1649, 1453, 1429, 1306, 1293, 1206, 1171, 1112, 1093	Yes	1650, 1639, 1625, 1608, 1579, 1558, 1508, 1444, 1432, 1384	Yes
Salicylic acid 1652, 1608, 1480, 1440, 1292, 1233	1674, 1625, 1587, 1463, 1425, 1384, 1324, 1276, 1219, 1171	Yes	1682, 1625, 1599, 1560, 1540, 1469, 1425, 1349, 1260, 1243	Yes
Sorbic acid 1672, 1634, 1608, 1411, 1374, 1314	1688, 1477, 1432, 1384, 1325, 1277, 1222, 1173, 1115, 1025	Yes	1730, 1707, 1654, 1576, 1555, 1538, 1519, 1505, 1441, 1417	Yes
Succinic acid 1679, 1411, 1307, 1197, 1156, 1131	1688, 1627, 1579, 1512, 1431, 1380, 1318, 1276, 1224, 1116	Yes	1648, 1561, 1512, 1456, 1437, 1399, 1366, 1314, 1271	Yes
Theophylline 1700, 1659, 1555, 1481, 1441, 1313	1679, 1624, 1600, 1554, 1475, 1434, 1275, 1223, 1160, 1112	Yes	1679, 1651, 1624, 1591, 1553, 1476, 1436, 1411, 1398, 1364	Yes
Urea 1674, 1590, 1550, 1454, 1148, 1118	1695, 1670, 1470, 1434, 1226, 1161, 1120, 1086	No	1645, 1609, 1591, 1569, 1516, 1478, 1443, 1388, 1213, 1162	Yes
Xanthine 1692, 1650, 1564, 1454, 1436, 1415	1695, 1433, 1280, 1225, 1196, 1168, 1115, 995	No	1694, 1669, 1615, 1570, 1559, 1528, 1438, 1422, 1408	No
Experimental supramolecular yield		64%		83%

6.3.2. CoForm prediction outcomes

CoForm was used to predict the co-crystal screening outcome for Loratadine and Desloratadine, Table 6.4.

Table 6.4. CoForm co-crystal screening outputs for loratadine and desloratadine.

Co-former	Loratadine	Desloratadine
3-Hydroxy-2-naphthoic acid	Yes	Yes
4-Hydroxybenzoic acid	Yes	Yes
Adipic acid	No	Yes
Apigenin	Yes	Yes
Benzenesulfonic acid	Yes	Yes
Benzoic acid	Yes	Yes
Caffeine	Yes	Yes
Cholic acid	Yes	Yes
Citric acid	Yes	Yes
D-glucuronic acid	No	Yes
EDTA	Yes	Yes
Folic acid	No	No
Fumaric acid	No	Yes

Glutaric acid	Yes	Yes
Glycine	Yes	Yes
Glycolic acid	No	No
Hydrocinnamic acid	Yes	Yes
Isonicotinamide	Yes	No
L-glutamic acid	Yes	Yes
L-mandelic acid	No	Yes
L-proline	No	Yes
L-serine	Yes	Yes
L-tartaric acid	Yes	Yes
Maleic acid	Yes	Yes
Malic acid	Yes	Yes
Malonic acid	No	Yes
Maltitol	No	Yes
Mannitol	Yes	Yes
Nicotinamide	Yes	Yes
Oxalic acid	No	Yes
Pamoic acid	Yes	Yes
Phosphoric acid	Yes	Yes
Piperazine	Yes	Yes
Riboflavin	No	Yes
Saccharin	Yes	Yes
Salicylic acid	Yes	Yes
Sorbic acid	Yes	No
Succinic acid	No	Yes
Theophylline	Yes	Yes
Urea	No	No
Xanthine	Yes	Yes

6.3.3. HBP prediction outcomes

HBP was used to predict the co-crystal screening outcomes, Table 6.5.

Table 6.5. Hydrogen-bond propensity (HBP) calculations for loratadine and desloratadine.

Co-former	**Homomeric interactions**	**Heteromeric interactions**	Δ=Hetero-Homo	**Homomeric interactions**	**Heteromeric interactions**	Δ=Hetero-Homo
3-Hydroxy-2-naphthoic acid	0.23	0.47	0.24	0.4	0.31	-0.09
4-Hydroxybenzoic acid	0.28	0.51	0.23	0.35	0.41	0.06
Adipic acid	0.42	0.66	0.24	0.45	0.45	0
Apigenin	0.31	0.41	0.1	0.4	0.4	0
Benzenesulfonic acid	0.47	0.59	0.12	0.47	0.47	0
Benzoic acid	0.27	0.43	0.16	0.35	0.35	0
Caffiene	-	-	N/A	0.25	0.8	0.55
Cholic acid	0.45	0.64	0.19	0.54	0.6	0.06
Citric acid	0.33	0.53	0.2	0.37	0.52	0.15
D-glucuronic acid	0.53	0.56	0.03	0.49	0.53	0.04

EDTA	0.4	0.67	0.27	0.42	0.45	0.03
Folic acid	0.56	0.7	0.14	0.54	0.45	-0.09
Fumaric acid	0.46	0.59	0.13	0.42	0.41	-0.01
Glutaric acid	0.43	0.67	0.24	0.45	0.44	-0.01
Glycine	0.64	0.72	0.08	0.67	0.53	-0.14
Glycolic acid	0.53	0.6	0.07	0.54	0.6	0.06
Hydrocinnamic acid	0.37	0.58	0.21	0.35	0.35	0
Isonicotinamide	0.56	0.47	-0.09	0.58	0.4	-0.18
L-glutamic acid	0.56	0.7	0.14	0.6	0.52	-0.08
L-mandelic acid	0.34	0.58	0.24	0.44	0.51	0.07
L-proline	0.49	0.59	0.1	0.45	0.47	0.02
L-serine	0.62	0.62	0	0.61	0.61	0
L-tartaric acid	0.42	0.61	0.19	0.45	0.54	0.09
Maleic acid	0.45	0.59	0.14	0.42	0.41	-0.01
Malic acid	0.45	0.62	0.17	0.48	0.55	0.07
Malonic acid	0.5	0.67	0.17	0.5	0.44	-0.06
Maltitol	0.74	0.68	-0.06	0.7	0.76	0.06
Mannitol	0.36	0.48	0.12	0.38	0.59	0.21
Nicotinamide	0.57	0.48	-0.09	0.58	0.4	-0.18
Oxalic acid	0.17	0.21	0.04	0.41	0.28	-0.13
Pamoic acid	0.22	0.48	0.26	0.43	0.33	-0.1
Phosphoric acid	0.87	0.53	-0.34	0.86	0.82	-0.04
Piperazine	0.62	0.58	-0.04	0.47	0.41	-0.06
Riboflavin	0.66	0.5	-0.16	0.66	0.55	-0.11
Saccharin	0.44	0.46	0.02	0.41	0.33	-0.08
Salicylic acid	0.25	0.5	0.25	0.41	0.34	-0.07
Sorbic acid	0.44	0.58	0.14	0.41	0.4	-0.01
Succinic acid	0.44	0.67	0.23	0.46	0.42	-0.04
Theophylline	0.26	0.32	0.06	0.33	0.49	0.16
Urea	0.97	0.93	-0.04	0.97	0.84	-0.13
Xanthine	0.67	0.5	-0.17	0.64	0.56	-0.08

6.3.4. MC prediction outcomes

MC was used to predict the co-crystal screening outcomes, Table 6.6.

Table 6.6. Molecular Complementarity (MC) calculations for loratadine and desloratadine.

Co-former	**Loratadine hit rate %**	**Desloratadine hit rate %**
3-Hydroxy-2-naphthoic acid	50	50
4-Hydroxybenzoic acid	0	0
Adipic acid	84	0
Apigenin	0	0
Benzenesulfonic acid	0	0
Benzoic acid	0	0
Caffiene	20	0
Cholic acid	60	0
Citric acid	0	0

D-glucuronic acid	0	0
EDTA	0	0
Folic acid	100	0
Fumaric acid	0	0
Glutaric acid	67	67
Glycine	0	0
Glycolic acid	0	0
Hydrocinnamic acid	0	0
Isonicotinamide	84	60
L-glutamic acid	0	0
L-mandelic acid	0	0
L-proline	100	100
L-serine	60	100
L-tartaric acid	0	0
Maleic acid	0	0
Malic acid	0	0
Malonic acid	0	0
Maltitol	0	0
Mannitol	0	0
Nicotinamide	20	0
Oxalic acid	0	0
Pamoic acid	0	0
Phosphoric acid	100	100
Piperazine	0	0
Riboflavin	100	100
Saccharin	64	90
Salicylic acid	60	25
Sorbic acid	50	50
Succinic acid	20	0
Theophylline	0	0
Urea	0	0
Xanthine	0	0
Supramolecular yield	31%	21%

6.4. Discussions

6.4.1. Current stage of CoForm

CoForm, HBP, and MC were used to predict the potential co-crystallizing partners for loratadine and desloratadine. The accuracy of the predicting approaches was determined by calculating a success rate, which is the number of predictions that match the experimental results over the total number of predictions. CoForm produced a prediction success rate of 80%, HBP predicted 76% of the co-crystallization outcomes correctly and, MC 39%. The true positives and true negatives were

analyzed separately. We displayed the results in a confusion matrix, Figure 6.5. Each cell in the figure is defined as follows:

True positive: Prediction and experiment agree on successful co-crystallization partners.

True negative: Prediction and experiment agree on failed co-crystallization partners.

False positive: Prediction and experiment do not agree on successful co-crystallization partners.

False negative: Prediction and experiment do not agree on failed co-crystallization partners.

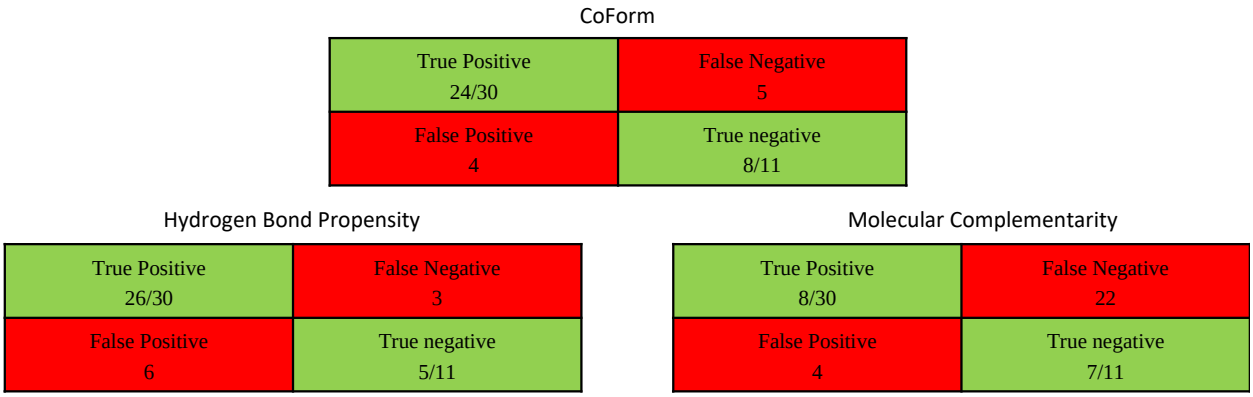

Figure 6.5. Correlation between the experimental and predicted outcomes for loratadine.

CoForm exhibits 80% accuracy for true positives and 72% for true negatives. HBP delivered 86% correctness for true positives and 45% for true negatives. The true positive results by HBP are comparable to that of CoForm however, with a very low accuracy for true negatives. MC delivered very low accuracies of 26% for true positives and 63% for true negatives. The prediction success rates of HBP and MC followed similar trends as we observed in Chapter 4. Individually both the methods were not very reliable for co-crystallization screening experiments.

Similar comparisons using confusion matrices were carried out for desloratadine, and the correlation between the prediction and experimental outcomes are listed in Figure 6.6.

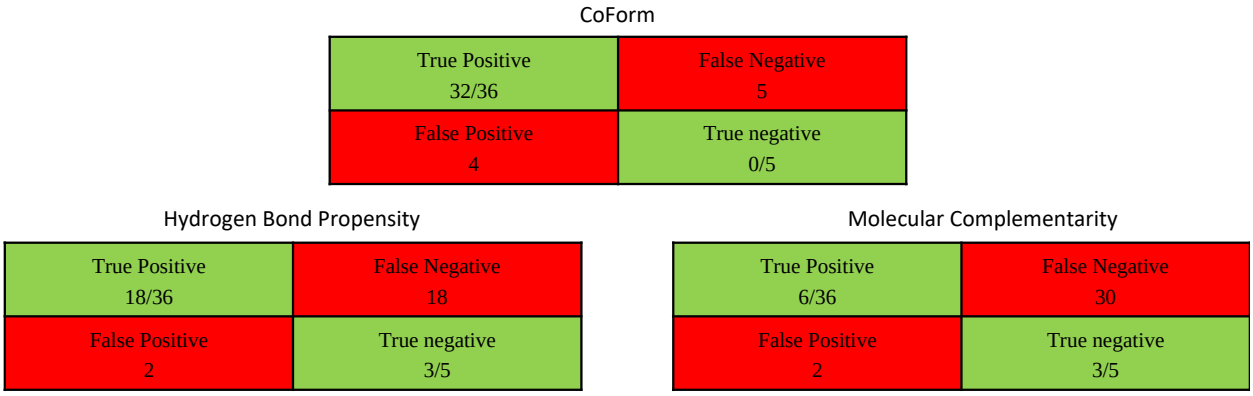

Figure 6.6. Correlation between the experimental and predicted outcomes for desloratadine.

CoForm displays 89% accuracy for true positives but could not predict any true negatives correctly. For HBP, the correctness for true positive was 50% and for true negative 60%. Finally, MC gave a 16% success for true positive and 60% for true negative.

Overall for both loratadine and desloratadine, CoForm produced higher success rates for true positives than true negatives. When we compared the ratio of true positives to true negatives in our database, we found that there is a total of 373 positive co-crystals and 119 negative co-crystals results. The positive partners accounts for 76% in comparison to 24% for the negative partners which accounts for the imbalance in the prediction outcomes. Unfortunately, at this point, we could not add more failed co-crystallization experiments in our database.

Table 6.7. summarizes the overall prediction abilities of the three methods in comparison to experimental results.

Table 6.7. Success rates for predicting the co-crystal formation.

Compounds	Method	Success rate
Loratadine	CoForm	33/41= 80%
	HBP	31/41= 76%
	MC	16/41= 39%
Desloratadine	CoForm	33/41= 80%
	HBP	22/41= 54%
	MC	9/41= 22%

6.4.2. Evolution of CoForm

The CoForm database currently consists of 2000 data for small molecules and approximately 500 data for co-formers from the GRAS list. For CoForm to deliver results with high accuracy, we need to add more co-crystallization results. Additionally, the database only consists of hydrogen-bond driven target and co-former pairs. In order to make CoForm more versatile, we have to ensure that other non-covalent interactions (such as halogen and chalcogen bonds) that drive the co-crystallization experiments are also added into the database. We also plan to incorporate machine learning approaches to further benefit the prediction abilities of CoForm.

Having said that, CoForm is designed as a user-specific tool and will produce the most reliable outcomes, if the unknown target is a close match (similar molecular weight, rotatable bonds, functional groups) to the known targets in the database. Therefore, having a user-specific database could increase the accuracy of CoForm. The user specificity of CoForm also extends its usability not only in pharmaceutics, agrochemicals, energetics, but any field where physical properties play an important role.

6.5. Conclusions

We attempted to develop a fast and user-friendly software application to facilitate co-crystallization screening experiments. We hope this tool will be widely adopted and used by both academic and industrial scientists interested in the crystalline solid-state, especially in the context of improving physical properties.

1. CoForm could predict the results with 80% accuracy for loratadine and 80% for desloratadine.
2. HBP produced a success rate of 76% and 54% for loratadine and desloratadine, respectively; whereas MC delivered a very low success of 39% and 22% each.

6.6. References

(1) Sarkar, N.; Sinha, A. S.; Aakeröy, C. B. Systematic Investigation of Hydrogen-Bond Propensities for Informing Co-Crystal Design and Assembly. *CrystEngComm* **2019**, *21* (40), 6048–6055. https://doi.org/10.1039/C9CE01196J.

(2) Sarkar, N.; Aakeröy, C. B. Evaluating Hydrogen-Bond Propensity, Hydrogen-Bond Coordination and Hydrogen-Bond Energy as Tools for Predicting the Outcome of Attempted Co-Crystallisations. *Supramolecular Chemistry* **2019**, 1–10. https://doi.org/10.1080/10610278.2019.1693043.

(3) Fábián, L. Cambridge Structural Database Analysis of Molecular Complementarity in Cocrystals. *Crystal Growth & Design* **2009**, *9* (3), 1436–1443. https://doi.org/10.1021/cg800861m.

(4) Musumeci, D.; Hunter, C. A.; Prohens, R.; Scuderi, S.; McCabe, J. F. Virtual Cocrystal Screening. *Chem. Sci.* **2011**, *2* (5), 883–890. https://doi.org/10.1039/C0SC00555J.

(5) Sandhu, B.; McLean, A.; Sinha, A. S.; Desper, J.; Sarjeant, A. A.; Vyas, S.; Reutzel-Edens, S. M.; Aakeröy, C. B. Evaluating Competing Intermolecular Interactions through Molecular Electrostatic Potentials and Hydrogen-Bond Propensities. *Crystal Growth & Design* **2018**, *18* (1), 466–478. https://doi.org/10.1021/acs.cgd.7b01458.

(6) Williams, H. D.; Trevaskis, N. L.; Charman, S. A.; Shanker, R. M.; Charman, W. N.; Pouton, C. W.; Porter, C. J. H. Strategies to Address Low Drug Solubility in Discovery and Development. *Pharmacol Rev* **2013**, *65* (1), 315–499. https://doi.org/10.1124/pr.112.005660.

(7) Shan, N.; Zaworotko, M. J. The Role of Cocrystals in Pharmaceutical Science. *Drug Discovery Today* **2008**, *13* (9), 440–446. https://doi.org/10.1016/j.drudis.2008.03.004.

(8) B. Aakeröy, C.; R. Champness, N.; Janiak, C. Recent Advances in Crystal Engineering. *CrystEngComm* **2010**, *12* (1), 22–43. https://doi.org/10.1039/B919819A.

(9) Aakeröy, C. B.; Grommet, A. B.; Desper, J. Co-Crystal Screening of Diclofenac. *Pharmaceutics* **2011**, *3* (3), 601–614. https://doi.org/10.3390/pharmaceutics3030601.

(10) Li, S.; Yu, T.; Tian, Y.; McCoy, C. P.; Jones, D. S.; Andrews, G. P. Mechanochemical Synthesis of Pharmaceutical Cocrystal Suspensions via Hot Melt Extrusion: Feasibility Studies and Physicochemical Characterization. *Mol. Pharmaceutics* **2016**, *13* (9), 3054–3068. https://doi.org/10.1021/acs.molpharmaceut.6b00134.

(11) Gadade, D. D.; Pekamwar, S. S. Pharmaceutical Cocrystals: Regulatory and Strategic Aspects, Design and Development. *Adv Pharm Bull* **2016**, *6* (4), 479–494. https://doi.org/10.15171/apb.2016.062.

(12) Surov, A. O.; Voronin, A. P.; Manin, A. N.; Manin, N. G.; Kuzmina, L. G.; Churakov, A. V.; Perlovich, G. L. Pharmaceutical Cocrystals of Diflunisal and Diclofenac with Theophylline. *Mol. Pharmaceutics* **2014**, *11* (10), 3707–3715. https://doi.org/10.1021/mp5004652.

(13) Desiraju, G. R. Crystal Engineering: From Molecule to Crystal. *J. Am. Chem. Soc.* **2013**, *135* (27), 9952–9967. https://doi.org/10.1021/ja403264c.

(14) Babu, N. J.; Nangia, A. Solubility Advantage of Amorphous Drugs and Pharmaceutical Cocrystals. *Crystal Growth & Design* **2011**, *11* (7), 2662–2679. https://doi.org/10.1021/cg200492w.

(15) Jones, W.; Motherwell, W. D. S.; Trask, A. V. Pharmaceutical Cocrystals: An Emerging Approach to Physical Property Enhancement. *MRS Bulletin* **2006**, *31* (11), 875–879. https://doi.org/10.1557/mrs2006.206.

(16) Mir, N. A.; Dubey, R.; Desiraju, G. R. Strategy and Methodology in the Synthesis of Multicomponent Molecular Solids: The Quest for Higher Cocrystals. *Acc. Chem. Res.* **2019**. https://doi.org/10.1021/acs.accounts.9b00211.

(17) Friščić, T.; Jones, W. Recent Advances in Understanding the Mechanism of Cocrystal Formation via Grinding. *Crystal Growth & Design* **2009**, *9* (3), 1621–1637. https://doi.org/10.1021/cg800764n.

(18) Cherukuvada, S.; Kaur, R.; Row, T. N. G. Co-Crystallization and Small Molecule Crystal Form Diversity: From Pharmaceutical to Materials Applications. *CrystEngComm* **2016**, *18* (44), 8528–8555. https://doi.org/10.1039/C6CE01835A.

(19) Basavoju, S.; Boström, D.; Velaga, S. P. Indomethacin–Saccharin Cocrystal: Design, Synthesis and Preliminary Pharmaceutical Characterization. *Pharm Res* **2008**, *25* (3), 530–541. https://doi.org/10.1007/s11095-007-9394-1.

(20) Kumar, A.; Kumar, S.; Nanda, A. A Review about Regulatory Status and Recent Patents of Pharmaceutical Co-Crystals. *Adv Pharm Bull* **2018**, *8* (3), 355–363. https://doi.org/10.15171/apb.2018.042.

(21) The Apache Groovy programming language http://groovy-lang.org/ (accessed Nov 7, 2019).

(22) Macrae, C. F.; Bruno, I. J.; Chisholm, J. A.; Edgington, P. R.; McCabe, P.; Pidcock, E.; Rodriguez-Monge, L.; Taylor, R.; Streek, J. van de; Wood, P. A. Mercury CSD 2.0 – New Features for the Visualization and Investigation of Crystal Structures. *J Appl Cryst* **2008**, *41* (2), 466–470. https://doi.org/10.1107/S0021889807067908.

(23) Allen, F. H. The Cambridge Structural Database: A Quarter of a Million Crystal Structures and Rising. *Acta Crystallogr., B* **2002**, *58* (Pt 3 Pt 1), 380–388.

(24) Mapp, L. K.; Coles, S. J.; Aitipamula, S. Design of Cocrystals for Molecules with Limited Hydrogen Bonding Functionalities: Propyphenazone as a Model System. *Crystal Growth & Design* **2017**, *17* (1), 163–174. https://doi.org/10.1021/acs.cgd.6b01399.

(25) Vologzhanina, A. V.; Sokolov, A. V.; Purygin, P. P.; Zolotarev, P. N.; Blatov, V. A. Knowledge-Based Approaches to H-Bonding Patterns in Heterocycle-1-Carbohydrazoneamides. *Crystal Growth & Design* **2016**, *16* (11), 6354–6362. https://doi.org/10.1021/acs.cgd.6b00990.

(26) Wood, P. A.; Feeder, N.; Furlow, M.; Galek, P. T. A.; Groom, C. R.; Pidcock, E. Knowledge-Based Approaches to Co-Crystal Design. *CrystEngComm* **2014**, *16* (26), 5839–5848. https://doi.org/10.1039/C4CE00316K.

(27) Fábián, L. Cambridge Structural Database Analysis of Molecular Complementarity in Cocrystals. *Crystal Growth & Design* **2009**, *9* (3), 1436–1443. https://doi.org/10.1021/cg800861m.

(28) Pallipurath, A. R.; Civati, F.; Eziashi, M.; Omar, E.; McArdle, P.; Erxleben, A. Tailoring Cocrystal and Salt Formation and Controlling the Crystal Habit of Diflunisal. *Crystal Growth & Design* **2016**, *16* (11), 6468–6478. https://doi.org/10.1021/acs.cgd.6b01154.

(29) Karki, S.; Friščić, T.; Fábián, L.; Jones, W. New Solid Forms of Artemisinin Obtained through Cocrystallisation. *CrystEngComm* **2010**, *12* (12), 4038. https://doi.org/10.1039/c0ce00428f.

Chapter 7 – Molecular Recognition by Cavitands via Cavity Inclusion

7.1. Introduction

Supramolecular chemistry deals with the assembly of multifunctional molecules to form complex architectures through reversible non-covalent interactions[1]. Inspiration often comes from nature's use of these interactions in molecular recognition for biological processes[2,3]. Supramolecular chemistry has advanced from small molecular building blocks to larger aggregates contributing in various fields such as nanotechnology, selective transport[4], sensors, drug delivery[5], selective separation[6], *etc*. In the previous chapters we explored different strategies to form solid-state architectures using hydrogen and halogen bonds on small molecules (molecular weight 250-600 g/mol). In this chapter we attempted to extend our understanding of such interactions on larger molecular hosts such as, cavitands (molecular weight 950-1150 g/mol).

Cavitands are bowl shaped macromolecules introduced by Cram in 1982[7,8]. Cram defined cavitands as "molecules that contained enforced cavities large enough to accommodate simple molecules or ions". Resorcinarene based cavitands can act as versatile molecular containers[9,10,11] since the defined space, volume and functional groups can be modulated. These containers can encapsulate guests like cations[12], anions, and solvents through a variety of intermolecular interactions. This has made cavitands useful receptors with particular attention in molecular catalysis[9], molecular sensing[13,14,15,16], stabilization of reaction intermediates[17,18], gas capsulation[19], and photosensitizers[20,21]. Furthermore, the "nanospace" with these cavitands have unique well-defined size, volume and chemical characteristics that are well suited for incorporating complementary guest molecules inside.

The structural framework of a cavitand can be divided into four different parts: feet, body, bridge and rim, Figure 7.1. The lower end of the cavitand, the "feet" mostly consists of carbon and hydrogen. Covalent modifications to the *feet* alter solubility[22,23]. The middle part of the cavitand, the *body*, which is electron rich,[24,25] can encapsulate electron deficient guest molecules. The *bridging group* determines the width of the cavity[26,27,28]. Finally, the *rim* is the top part of the cavitand. A cavitand bears four positions on the rim which on functionalization can offer four binding sites to complementary guest molecules per one host molecule.

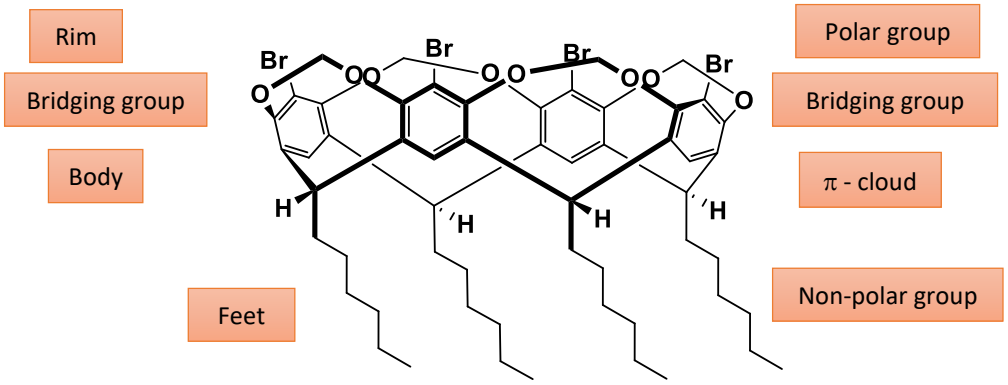

Figure 7.1. Structural framework of a cavitand.

Cavitands are known as versatile hosts since each structural feature of the cavitand can deliver characteristic host-guest interactions. In this study we focus our efforts on investigating the cavity of the cavitand. Figure 7.2 illustrates different ways cavitand can interact with a guest molecule at the cavity.

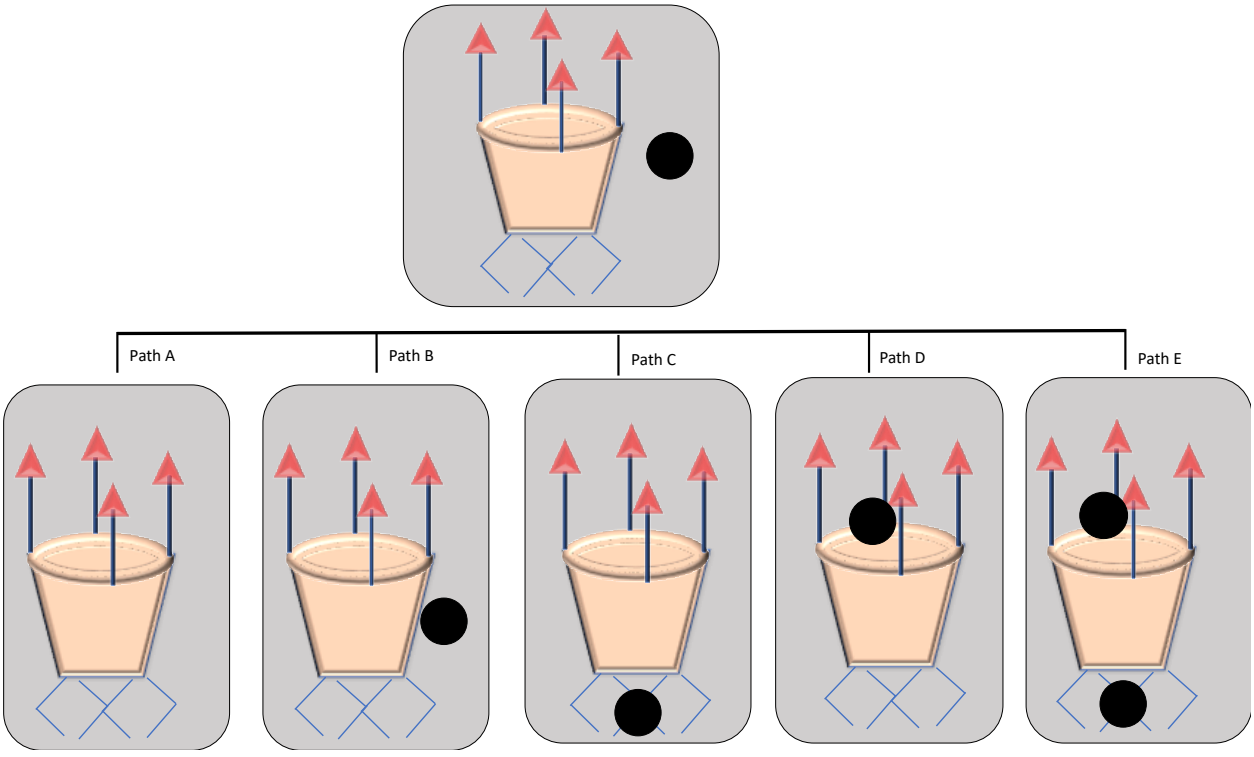

Figure 7.2. Cartoon representation of five possible guest binding modes to a cavitand.

In order to explore binding capabilities of the cavity without involving the rim, we specifically designed cavitands where the rim does not participate in any conventional hydrogen/ halogen

bonds. Therefore, for guest encapsulation to take place, complementarity between the host cavity and guest is crucial. The difference in the size, shape and dipole moment of the guest can possibly determine the selectivity.

We selected a series of isostructural cavitands where the upper rim of the target cavitand **T18** is bromo-functionalized and **T19** is iodo-functionalized Scheme 7.1. Target cavitands **T20**- **T23** are deeper cavitands[29] in comparison to **T18**-**T19** due to the presence of triple bonds on the rim.

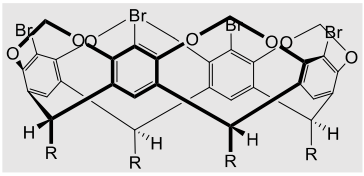

T18

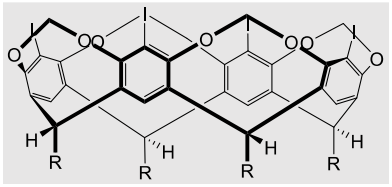

T19

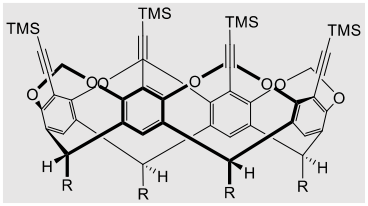

T20

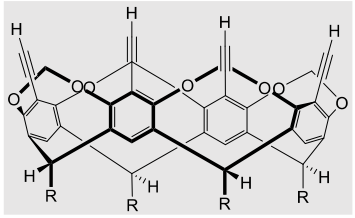

T21

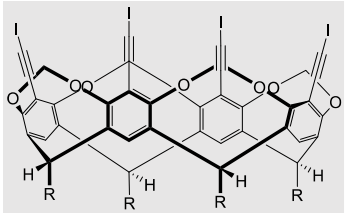

T22

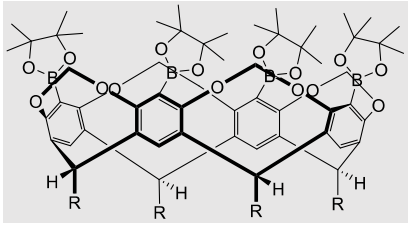

T23

Scheme 7.1. Target cavitands (R=hexyl).

A series of solvent molecules with varied dipole moment were selected as guests, in order to explore the binding ability of the cavitands., Table 7.1. We conducted selectivity studies to examine if the cavitands are particularly biased towards encapsulating any solvent.

Table 7.1. Solvents of choice.

Dipole moment	0.64	0.37	0.00	1.15	1.88	3.44	4.10
Debye	Xylenes 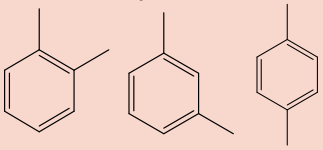			Dichloromethane 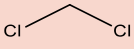	Ethyl acetate 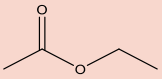	Acetonitrile 	Dimethyl sulfoxide 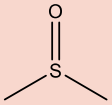

The study is done to answer the following questions:

1. Will the solvent encapsulation by isostructural hosts, **T18** and **T19** remain consistent?
2. Will the depth of the cavity effect where the solvent is encapsulated?
3. Will the dipole moment effect the location of the solvent in the cavitand?

7.2. Experimental

All chemicals were purchased from Aldrich, Fischer, TCI America, Oakwood and Alfa Aesar and used without further purification unless otherwise mentioned. Column chromatography was carried out using silica gel (150 Å pore size) from Analtech, Inc. ^{1}H and ^{13}C NMR spectra were recorded on Varian Unity plus 400 MHz spectrometer in $CDCl_3$ or DMSO. The NMR data is in parts per millions (ppm) with downfield shift from tetramethylsilane which is an internal reference. Nicolet 380 FT-IR was used for infrared spectroscopy and the data was analyzed using Omnic 8.0 Thermo Fischer Scientific Inc. software. DSC and TGA analysis were done using TA instruments Q20 and Q50, respectively.

7.2.1. Syntheses

*7.2.1.1. Synthesis of C-hexylcalix[4]resorcinarene, **1**[30]*

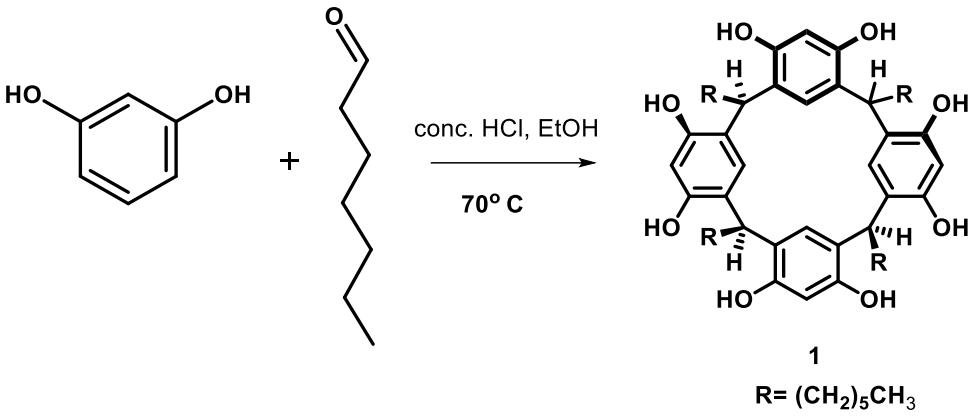

To a solution of resorcinol (50.0 g, 450 mmol) dissolved in ethanol (500 mL), heptanal (45.5 g, 450 mmol) was added. The mixture was cooled to 0 ^{o}C under dinitrogen atmosphere and conc. HCl (70 mL) was added dropwise over 15-20 mins. The mixture was refluxed at 70 ^{o}C for 16 - 24 hrs. The reaction was monitored using thin layer chromatography (TLC). Upon completion, the reaction mixture was allowed to cool to room temperature and diluted with water (500- 700 mL) to obtain a dark brown/ orange precipitate. The precipitate was filtered using Buchner funnel and washed with hot water until a neutral pH was obtained. The product was air dried overnight and further dried in an oven set at 100 ^{o}C further for 24 hrs to yield **1** (75 g, 87% yield).

M.P.: > 280 ^{o}C. ^{1}H NMR (400MHz, DMSO-d_6): 8.84 (s, 8H), 7.11 (s, 4H), 6.12 (s, 4H), 4.19 (t, J = 7.6Hz, 4H), 2.49 (m, 8H), 1.97-1.19 (m, 24H), 0.84 (t, 12 H, J=6.4Hz).

7.2.1.2. Synthesis of C-hexyltetrabromocalix[4]resorcinarene, ***2***[31]

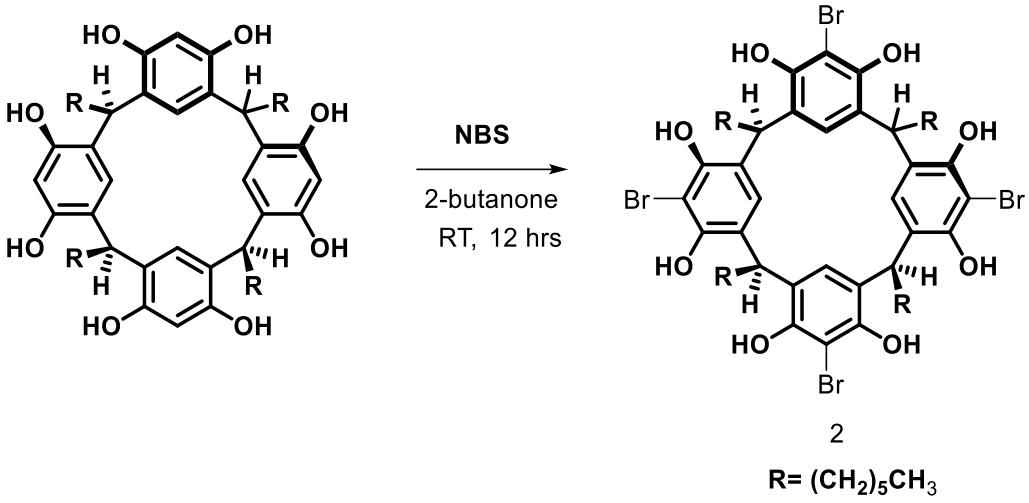

2

R= $(CH_2)_5CH_3$

C-hexylcalix[4]resocinarene, **1** (50.0 g, 65.0 mmol) was added to the flask containing 2-butanone (400 mL) cooled to 0 ^oC and covered with aluminum foil. The solution was stirred for 10-15 mins under dinitrogen atmosphere. Under dark conditions, N-bromosuccinamide (69 g, 390 mmol) was slowly added in small portions for a period of 30 mins. The condenser was attached, and the reaction was stirred at room temperature for 16- 24 hrs. The reaction was monitored using TLC. The precipitate formed in the reaction was filtered using Buchner filtration and washed with cold 2-butanone (3 X 50 mL), then with cold acetone (3 X 100 mL) to yield **2**. Product **2** was air dried and then dried in an oven at 100 ^oC to produce white solid (52 g, 78% yield).

M.P.: > 280 ^oC. ^1H NMR (400MHz, DMSO-d_6): 9.07 (s, 8H), 7.32 (s, 4H), 4.33 (t, J = 6.4Hz, 4H), 2.12 (m, 8H), 1.22 (m, 24H), 0.82 (t, J = 7.2Hz, 12H).

7.2.1.3. Synthesis of C-hexyltetrabromocavitand, ***T18***[32]

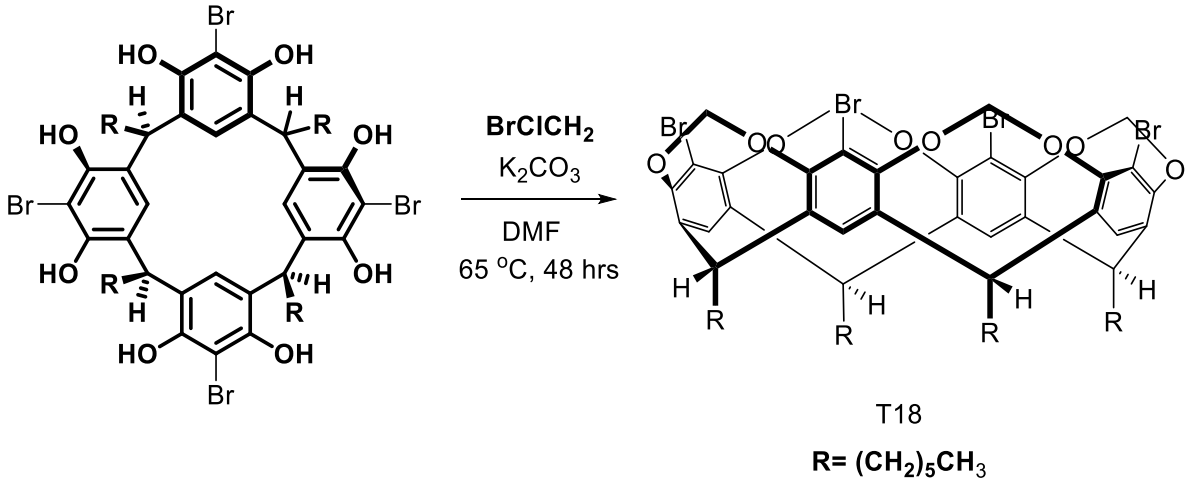

T18

R= $(CH_2)_5CH_3$

To a stirred solution of C-hexyltetrabromocalix[4]resorcinarene, **2** (40.0 g, 31.0 mmol) dissolved in DMF (500 mL), K_2CO_3 (60 g, 435 mmol) was added under dinitrogen atmosphere. Bromochloromethane (55 g, 415 mmol) was added to the reaction mixture after 20-30 mins. A condenser was added, and the solution was heated at 65 °C for 24 hrs. After 24 hrs an additional amount of bromochloromethane (7.00 g, 55.0 mmol) was added and the mixture was further stirred at 65 °C for 24 hrs. The reaction was monitored using TLC. After completion, the reaction was cooled to room temperature and poured slowly into an aqueous HCl solution (2%, 650 mL). The solid was filtered off and washed with water until neutral pH was obtained. Additionally, the water layer was extracted using dichloromethane and the solid obtained after rotavap was added to the solid filtrate. The combined solids were then purified using column chromatography using hexane: ethyl acetate 9:1 mixture as an eluent. The product **T18** was isolated as a white solid (24 g, 77% yield).

M.P.: > 280 °C. ^{1}H NMR (400MHz, $CDCl_3$): 7.03 (s, 4H), 5.95 (d, J = 7.4Hz, 4H), 4.85 (t, J = 7.6Hz, 4H), 4.38 (d, J = 7.2Hz, 4H), 2.21 (m, 8H), 1.29 (m, 24H), 0.90 (t, 12H).

*7.2.1.4. Synthesis of C-hexyltetraiodocavitand, **T19***

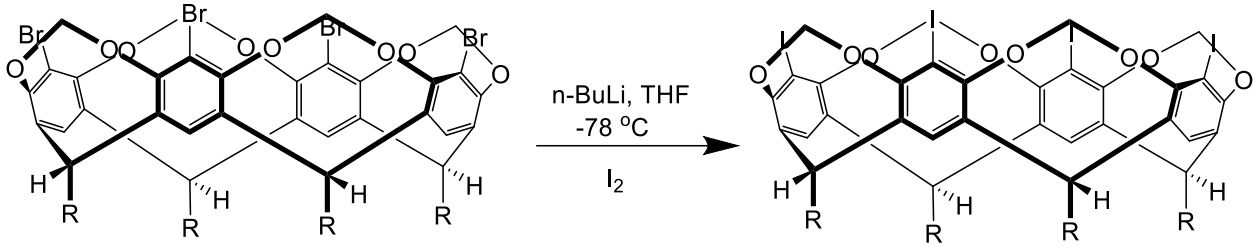

T19
R= $(CH_2)_5CH_3$

C-hexyltetrabromoresorcinarene, **T18** (10.0 g, 31.0 mmol) was dissolved in dry THF (10 mL) and the solution was evaporated and dried at 80 °C for 2 hrs under dinitrogen atmosphere using the Schlenk line. This procedure was repeated twice. The resulting solid was dissolved in dry THF (60 mL) and cooled to -78 °C (dry ice/ acetone bath) under dinitrogen atmosphere for 30 mins. To the solution n-BuLi (1.6 M in hexanes, 2.5 mL, 4.00 mmol) was added dropwise for 30 mins and additionally stirred for an hour. Iodine dissolved in methanol was added dropwise in excess to the solution until the solution turned light yellow. The solution was stirred additionally for 2 hours, and the dry ice/ acetone bath was removed for the reaction mixture to reach room temperature. Upon reaching room temperature, the reaction was quenched with saturated solution of sodium thiosulfate (100 mL). The mixture was extracted using dichloromethane three times which was filtered and brought to dryness using rotavap to yield white solid (9.50 g, 98% yield).

M.P.: > 280 °C. ^{1}H NMR (400MHz, $CDCl_3$): 7.06 (s, 4H), 5.96 (d, J = 7.4Hz, 4H), 4.85 (t, J = 7.6Hz, 4H), 4.33 (d, J = 7.2Hz, 4H), 2.19 (m, 8H), 1.34 (m, 24H), 0.91 (t, 12H).

7.2.1.5. Synthesis of C-hexyltetra((trimethylsilyl)ethynyl)cavitand, ***T20***[33]

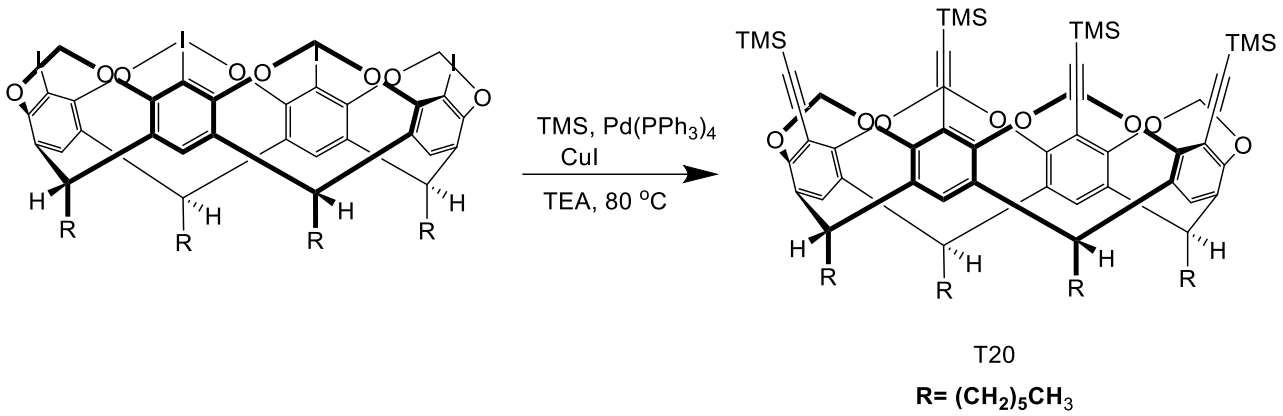

C-hexyltetraiodoresorcinarene, **T19** (4.00 g, 3.55 mmol) was dissolved in triethylamine (TEA) and degassed by bubbling dinitrogen through the reaction mixture for 20-30 mins. TMS-acetylene (1.74 g, 17.80 mmol), $PdCl_2(PPh_3)_2$ (0.20 g, 0.35 mmol) and CuI (0.13 g, 0.71 mmol) were added to the mixture. The resulting mixture was refluxed at 70- 80 ^oC overnight under dinitrogen atmosphere. The reaction was monitored using TLC. Upon completion the solvent was evaporated using rotavap and the residue was dissolved in diethyl ether and washed with brine solution (100-200 mL). The organic layer was extracted thrice and dried over anhydrous magnesium sulfate. The solvent was removed using rotavap and the residue was purified by column chromatography with hexane: ethyl acetate 9:1 mixture as eluant to obtain **T20** (3.00 g, 77% yield), a light yellow solid. M.P.: > 280 ^oC. ^1H NMR (400MHz, $CDCl_3$): 7.01 (s,4H), 5.94 (d, J= 7.2Hz, 4H), 4.83 (t, J = 7.6Hz, 4H), 4.38 (d, J = 8.4Hz, 4H), 2.17 (m, 8H), 1.89 (m, 24H), 0.86 (t, 12H), 0.16 (s, 36H).

*7.2.1.6. Synthesis of C-hexyltetra(ethynyl)cavitand, **T21**[34]*

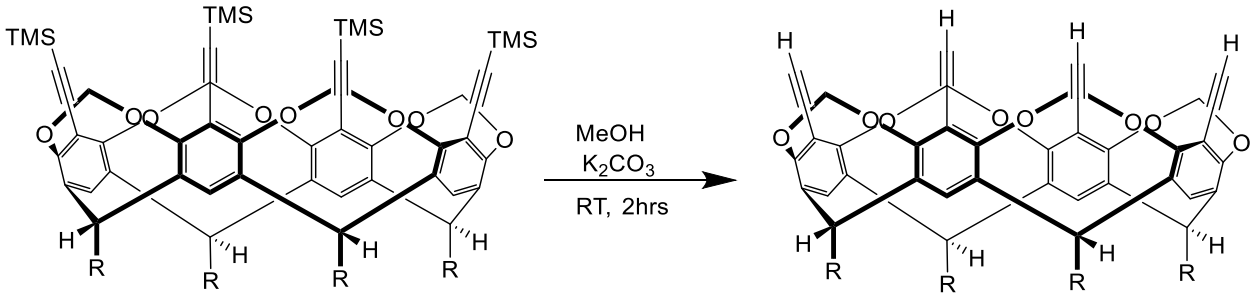

T21

R= $(CH_2)_5CH_3$

C-hexyltetra((trimethylsilyl)ethynyl) cavitand, **T20** (5.00 g, 4.45 mmol) and potassium carbonate (2.50 g, 18.00 mmol) were stirred in methanol at room temperature for 2- 4 hrs. Upon completion the solvent was removed by rotavap and the solid was dissolved in diethyl ether and washed with water. The organic layer was dried using anhydrous magnesium sulfate and the solvent was removed via rotavap to obtain the product **T21** (3.2 g, 79% yield), a light yellow solid.

M.P.: > 280 ºC. 1H NMR (400MHz, $CDCl_3$): 7.03 (s, 4H), 5.95 (d, J = 6.8Hz, 4H), 4.85 (t, J = 7.4Hz, 4H), 4.40 (d, J = 8.2Hz, 4H), 4.11 (s, 4H), 2.21 (m, 8H), 1.24 (m, 24H), 0.90 (t, 12H).

*7.2.1.7. Synthesis of C-hexyltetra(iodoethynyl)cavitand, **T22***

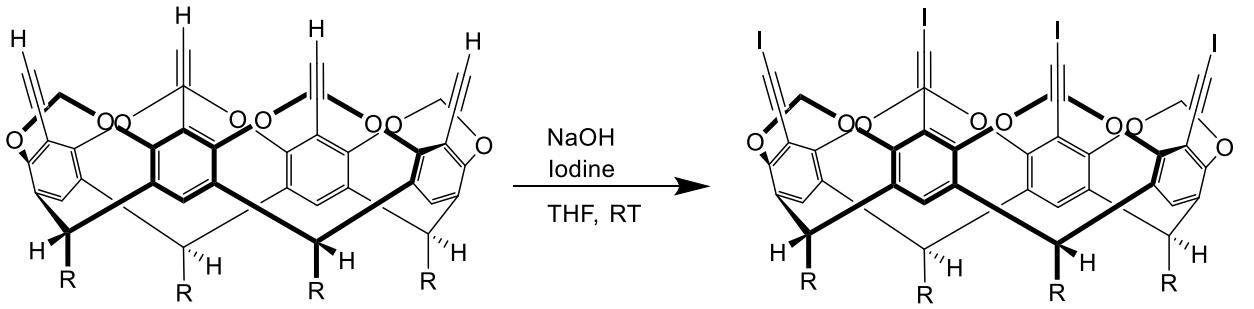

T22

R= $(CH_2)_5CH_3$

To a solution of C-hexyltetra(ethynyl) cavitand **T21** (1.00 g, 1.20 mmol) dissolved in methanol (50 mL), a concentrated solution of iodine in methanol (2.00 g, 7.87 mmol) was added dropwise; simultaneously followed by addition of 10% sodium hydroxide for 30 mins. The solution was

vigorously stirred and the NaOH was added until the final solution turned brown/ yellow. The solution was stirred overnight and quenched with 100 mL water upon which light yellow color precipitate was formed. The solid was filtered and washed with sodium bisulfite which afforded **T22** (0.80 g, 75% yield).

M.P.: > 280 ºC. ^{1}H NMR (400MHz, $CDCl_3$): 7.06 (s, 4H), 5.98 (d, J = 7.2Hz, 4H), 4.85 (t, J = 7.4Hz, 4H), 4.32 (d, J = 7.2Hz, 4H), 2.17 (m, 8H), 1.55 (m, 24H), 0.89 (t, 12H).

7.2.1.8. Synthesis of C- hexyltetraboronic acid dipinacolyl ester cavitand, ***T23***[35]

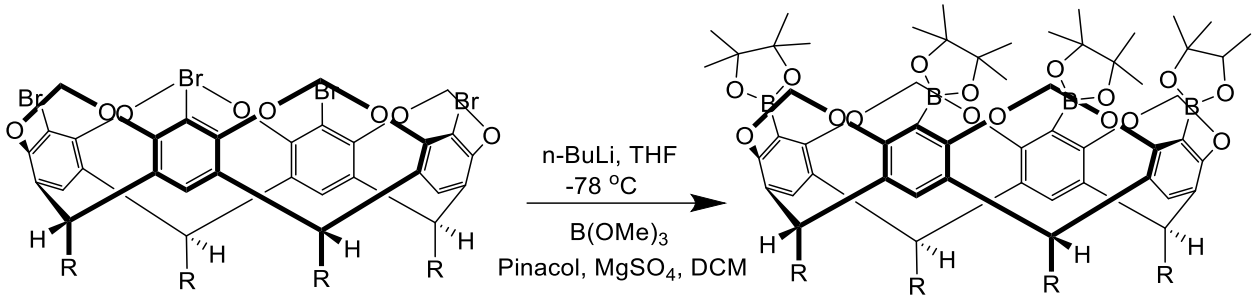

T23

R= $(CH_2)_5CH_3$

C-hexyltetrabromoresorcinarene, **T18** (1.00 g, 0.09 mmol) was dissolved in dry THF (10 mL), the solution was evaporated and dried at 80 ºC for 2 hrs under dinitrogen atmosphere using Schlenk line. This procedure was repeated twice. The resulting solid was dissolved in dry THF (60 mL) and cooled at -78 ºC (dry ice/ acetone bath) under dinitrogen atmosphere for 30 mins. To the solution n-BuLi (1.6 M in hexanes, 2.5 mL, 4.00 mmol) was added dropwise for 30 mins and additionally stirred for an hour. Trimethoxyborane (0.60 mL, 5.30 mmol) was added dropwise over 10 mins and the resulting solution was stirred at -78 ºC for an hour, after which the dry ice/ acetone bath was removed, and the solution was allowed to reach room temperature. Upon reaching the room temperature the mixture was quenched with 1M hydrochloric acid (HCl) and stirred for 30 mins. The mixture was extracted using dichloromethane (DCM) and the organic layer was dried over magnesium sulfate and the solvent removed using rotavap. The resulting residue was dissolved in DCM (100 mL), excess pinacol (750 mg, 6.30 mmol) and magnesium sulfate (3.00 g) was added and the mixture was stirred overnight. Upon completion the mixture was filtered, and the solvent was dried using rotavap. The resulting residue was dissolved in DCM

and added to a beaker of acetone to induce precipitation. The resulting solid was filtered resulting in pure **T23**, a white flaky solid (600 mg, 55% yield).

M.P.: > 280 ºC. ^{1}H NMR (400MHz, $CDCl_3$): 7.10 (s, 4H), 5.57 (d, J = 6.8 Hz, 4H), 4.74 (t, J = 7.2 Hz, 4H), 4.53 (d, J = 7.6 Hz, 4H), 2.17 (m, 8H), 1.56-1.31 (m, 72H), 0.86 (m, 12H).

7.2.2. Preparation of the host-guest complexes

The host-guest encapsulations studies were carried out by dissolving the host in guest solvents. After which we attempted to grow single crystals, by slow evaporation technique. The single crystal was then analyzed using thermogravimetric analysis (TGA) followed by single crystal X-ray diffraction, Scheme 7.2.

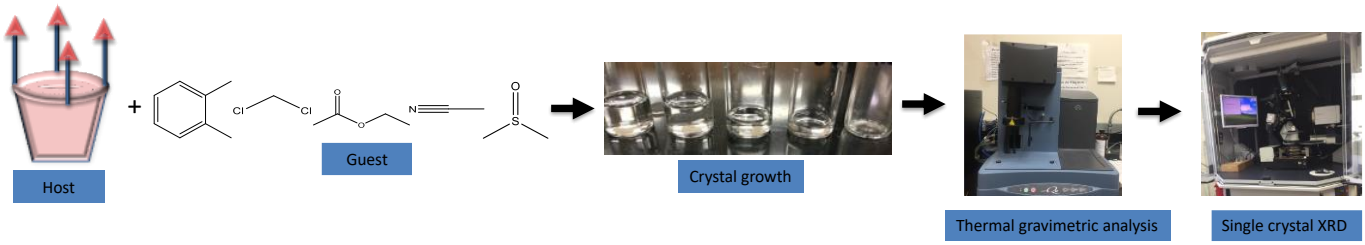

Scheme 7.2. Schematic representation of the steps involved.

7.2.3. Thermogravimetric analysis (TGA) of target cavitands recrystallized from the solvents

TGA analysis of the recrystallized hosts were performed to confirm the presence or absence of solvent in the crystal lattice. A mass of a sample was measured over time with gradual increase in the temperature. The weight loss observed was compared with the weight of the solvent molecules, to find the number of solvents present in the crystal lattice.

7.2.4. Single crystal X-ray crystallography

The target cavitand was dissolved in a minimum amount of guest solvent in a 2-dram borosilicate vial for slow evaporation in order to obtain single crystals for X-ray diffraction. In cases were slow evaporation failed, vapor diffusion, and anti-solvent crystallization techniques were employed.

The single crystal X-ray crystallographic data was collected for each instance. The detailed description is illustrated in section 2.2.4.

7.3. Results

7.3.1. Thermogravimetric analysis (TGA) of target cavitands recrystallized from the solvents

Figure 7.3. illustrates TGA analysis of the target cavitand **T18** recrystallized from ethyl acetate. The weight loss is 14% at around 300 ºC, which suggests that the solvents are not loosely bound to the cavitand. Loss of one ethyl acetate corresponds to 7.4% weight loss indicating that in this instance there was loss of two solvent molecules. Since the experiments were not done in dry conditions, water molecule weight% was always considered in these calculations.

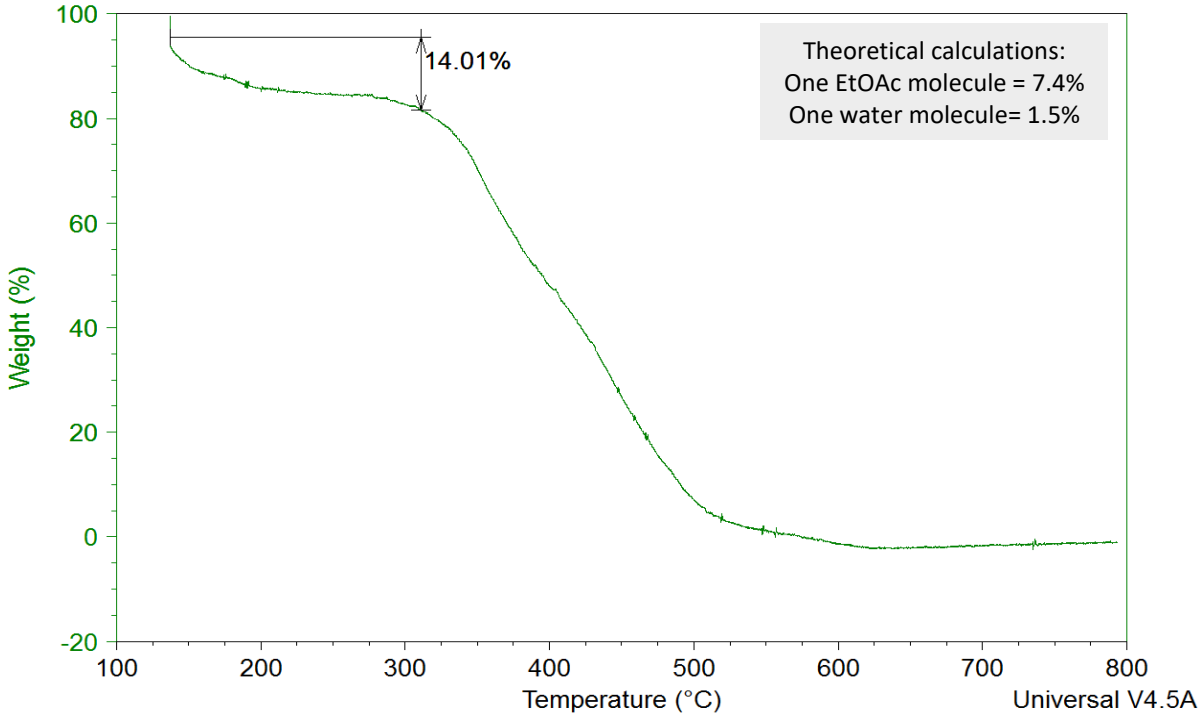

Figure 7.3. TGA of **T18** recrystallized from ethyl acetate.

Similar TGA analysis was done for all the target cavitands recrystallized from solvents. Table 7.2. summarizes the number of solvent molecules encapsulated by the cavitands w.r.t the weight loss shown in the TGA. See Appendix C for all the TGA data.

Table 7.2. TGA data analysis of the target cavitands recrystallized from solvents.

	Xylene	DCM	Ethyl acetate	ACN	DMSO	Mixture of solvents
T18	1	0	2	1	1	1 DMSO
T19	1	0	2	1	1	1 DMSO
T20	1	1	2	1	2	2 DMSO
T21	1	1	2	1	2	2 DMSO
T22	1	1	2	1	2	2 DMSO
T23	1	1	2	1	2	2 DMSO

7.3.2. Single crystal X-ray crystallography

We were able to get 13 crystal structures out of 30 combinations of cavitands and solvents. The crystallographic tables are listed in Appendix E. We got crystal structures of **T18** with all five solvents, Figure 7.4. In **T18**:xylene, xylene was not present in the cavity of the cavitand rather was present as a part of crystal packing, exocyclically. Recrystallizing **T18** in DCM, we did not observe the presence of any solvent molecules and the host were absolutely vacant. With **T18**:$(EtOAc)_2$ we observed 1:2 stoichiometry between the host and solvent. The solvent molecules were located at the rim as well as around the feet of the cavitand. In **T18**:ACN, the ACN was present around the feet of cavitand. Finally, with DMSO **T18** shows similar binding and stoichiometry as that of ACN.

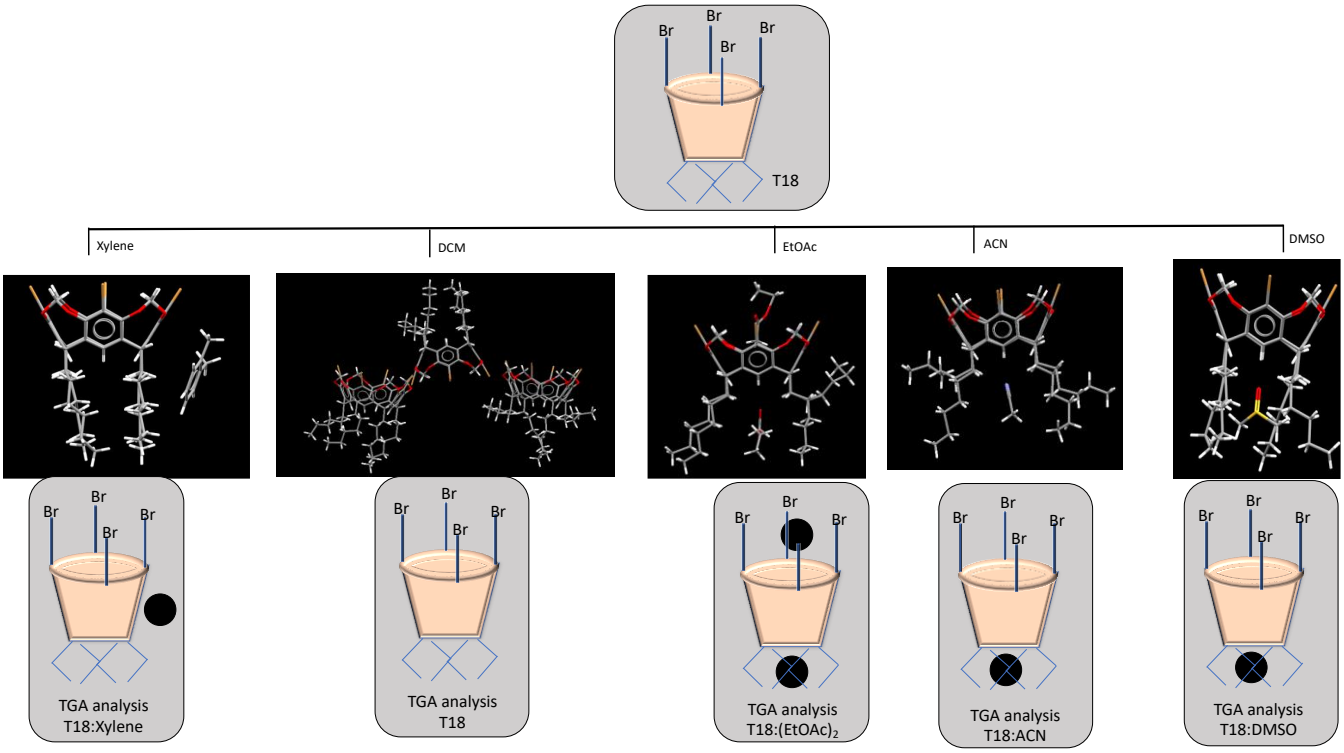

Figure 7.4. Crystal structures of **T18** recrystallized from different solvents (color codes: red-oxygen, mustard -bromine, violet-iodine, yellow-sulfur, grey-carbon, white-hydrogen).

With **T19** we were able to get three crystal structures. In **T19**:xylene, xylene was present around the feet of the cavitands. For **T19** recrystallized from DCM we only obtained **T19** by itself and no solvent in the cavity. For **T19**:DMSO, we observed 1:1 stoichiometry with DMSO located at the rim of the cavitand, Figure 7.5.

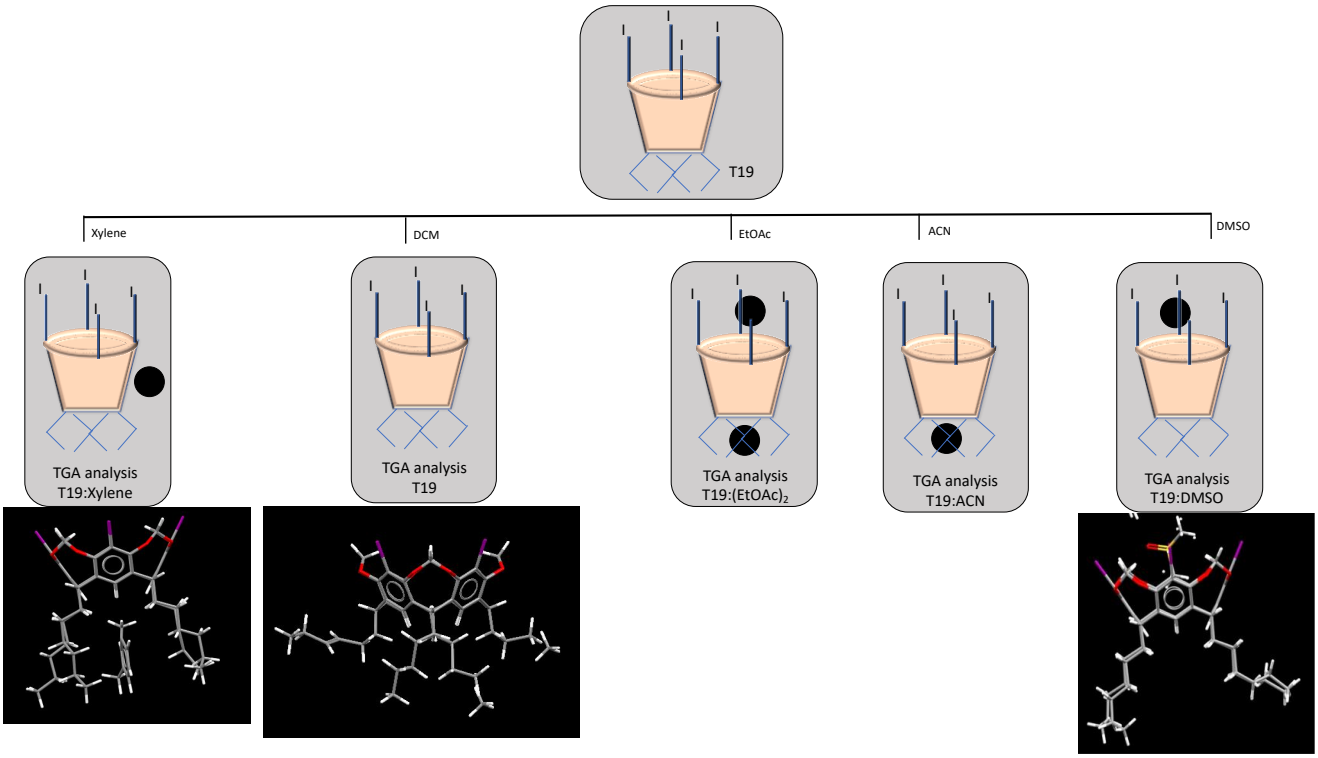

Figure 7.5. Crystal structures of **T19** recrystallized from different solvents (color codes: red-oxygen, mustard -bromine, violet-iodine, yellow-sulfur, grey-carbon, white-hydrogen).

The isostructural deeper cavitands **T20-T23**, demonstrated similar stoichiometries between host and solvents according to TGA analysis. We were able to get one crystal structure of **T21** with DMSO, where the solvent molecules were located both around the rim and feet, Figure 7.6.

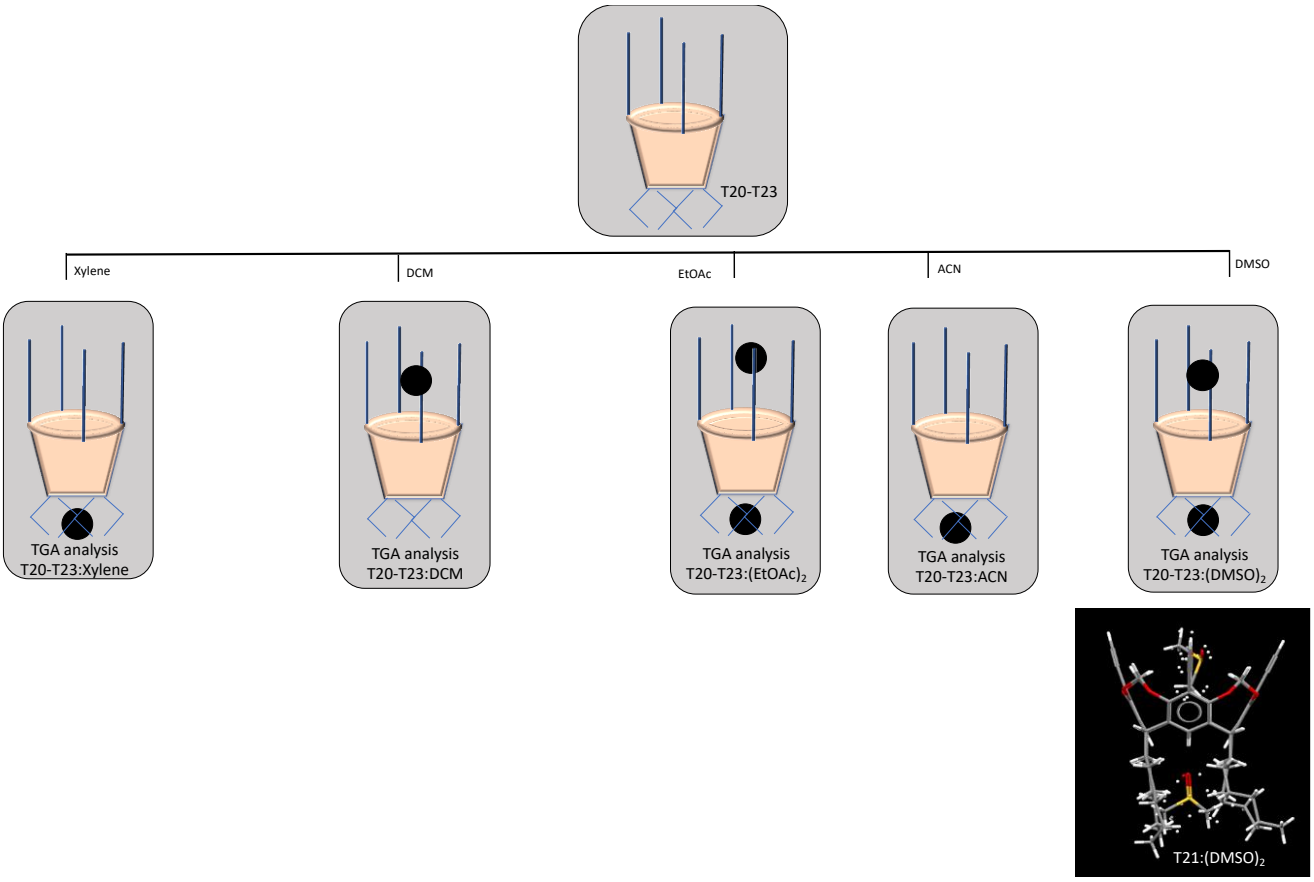

Figure 7.6. Crystal structures of **T20-T23** recrystallized from different solvents (color codes: red-oxygen, mustard -bromine, violet-iodine, yellow-sulfur, grey-carbon, white-hydrogen).

7.4. Discussions

7.4.1. Solvent-Xylene

The solvent xylene was present as a mixture of ortho, meta, para isomer. TGA analysis of **T18-T23** in combination with xylene displays 1:1 stoichiometry. We obtained single crystals of **T18** and **T19** with xylene, which also show a 1:1 stoichiometry. In **T18**, xylene was not present in the cavitand, rather it participates in the packing arrangement. **T18** specifically encapsulates ortho-xylene. For **T19**, xylene was present around the feet of the cavitand and specifically encapsulates meta-xylene, Figure 7.7.

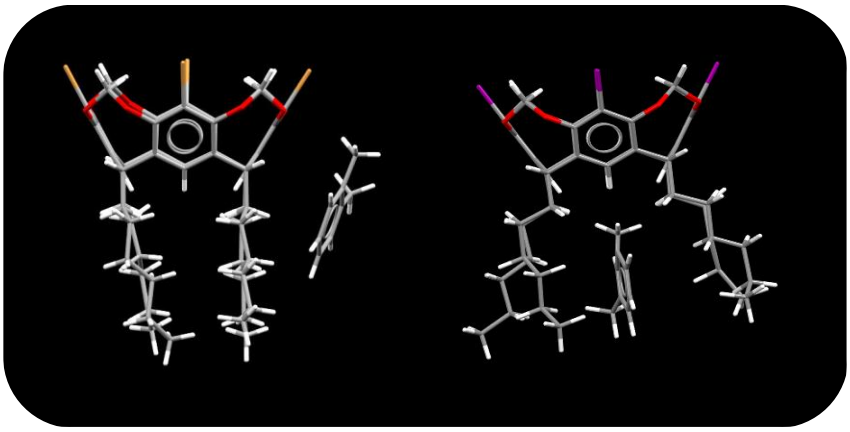

Figure 7.7. Packing of **T18** and **T19** with xylene (color codes: red-cavitands, green-xylene).

In **T18** since xylene interacted exocyclically, we observed "foot-in-the-mouth" kind of packing where foot of one cavitand was present in the mouth of other cavitand in order to fill the empty cavity space, Figure 7.8. For **T19**:xylene, xylene was present around the feet with empty space around the rim which was fulfilled by the foot of the neighboring cavitand molecule, Figure 7.8.

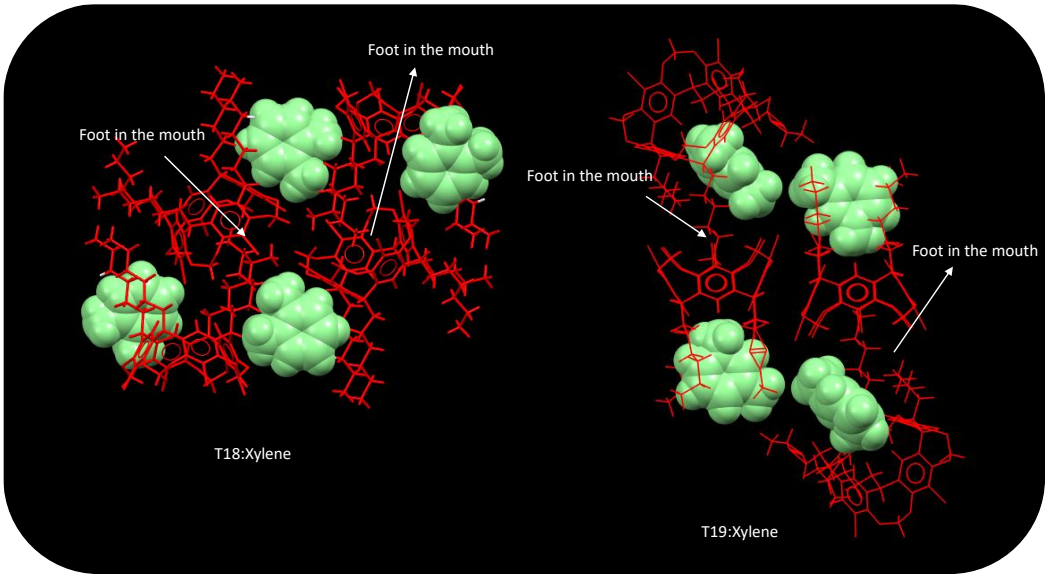

Figure 7.8. Packing of **T18** and **T19** with xylene (color codes: red-cavitands, green-xylene).

To understand the difference of the guest encapsulation between **T18**:xylene and **T19**:xylene, we measured the cavity size and overlay the structures. The size of the cavity for **T18** and **T19** were consistent with a negligible difference of 0.004 Å, Figure 7.9. However, the structure overlay shows that, the feet of **T18** has less space to accommodate xylene in comparison to **T19**, where

the feet curves out to make enough space for xylene encapsulation. Xylene is composed of carbon and hydrogen hence, it chooses to be around the feet, which is the non-polar part of the cavitand. TGA analysis of **T20-T23** also shows 1:1 stoichiometry with xylene. Although, we were unable to obtain single crystals, we assume that the structures will be similar to **T19**:xylene.

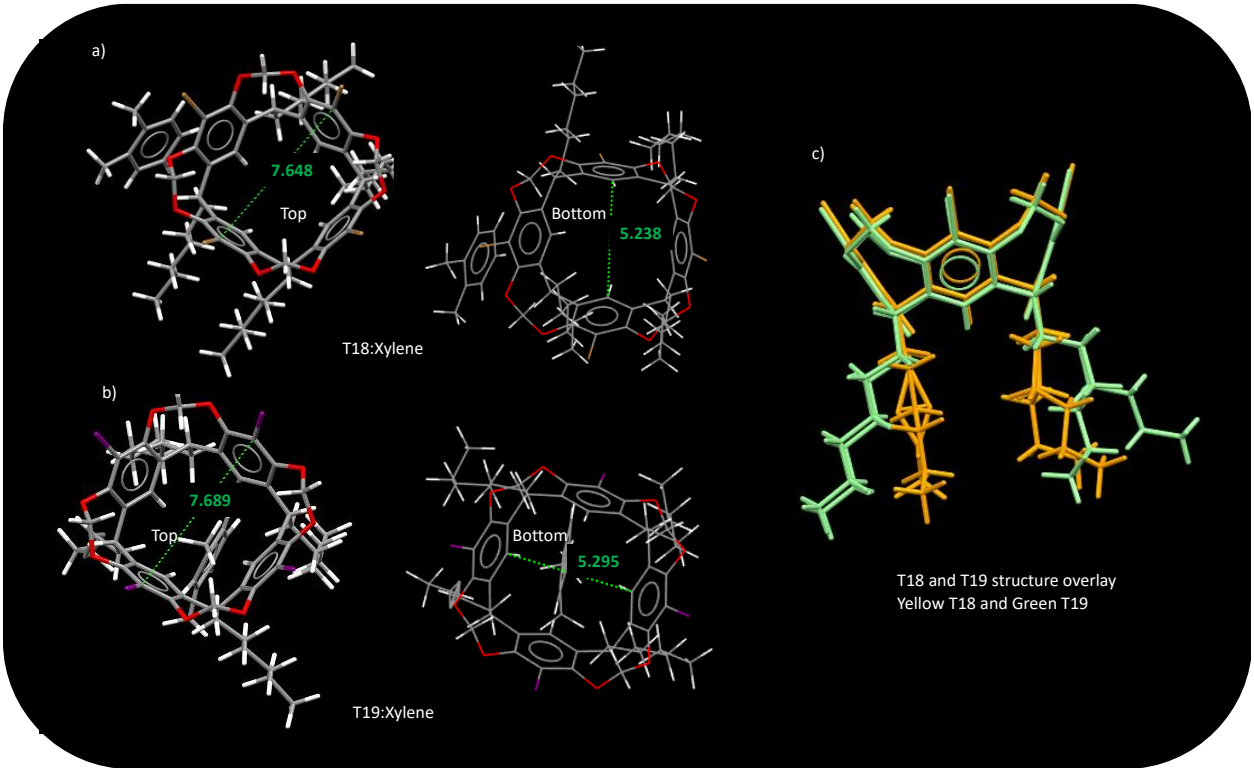

Figure 7.9. a) Top and bottom view of **T18**; b) Top and bottom view of **T19**; c) structure overlay of **T18** and **T19** (color codes: red-oxygen, yellowish green-boron, grey-carbon, white-hydrogen).

7.4.2. Solvent-dichloromethane (DCM)

TGA analysis of **T18** and **T19** with DCM shows no solvents in the cavitand, whereas with **T20-T23** gave 1:1 stoichiometry. We received crystal structures of **T18** and **T19** recrystallized from DCM. In both cases, the cavitands were vacant. The "foot-in-the-mouth" kind of packing remained consistent as we observed in **T18/T19**:xylene. For **T18**, the body was oriented at 180^{o} to each other, whereas for **T19** the body was at 90^{o}, Figure 7.10. The arrows at the bottom of the Figure 7.10, indicate the packing pattern observed in the crystal lattice. The arrowhead corresponds to the rim of the cavitand.

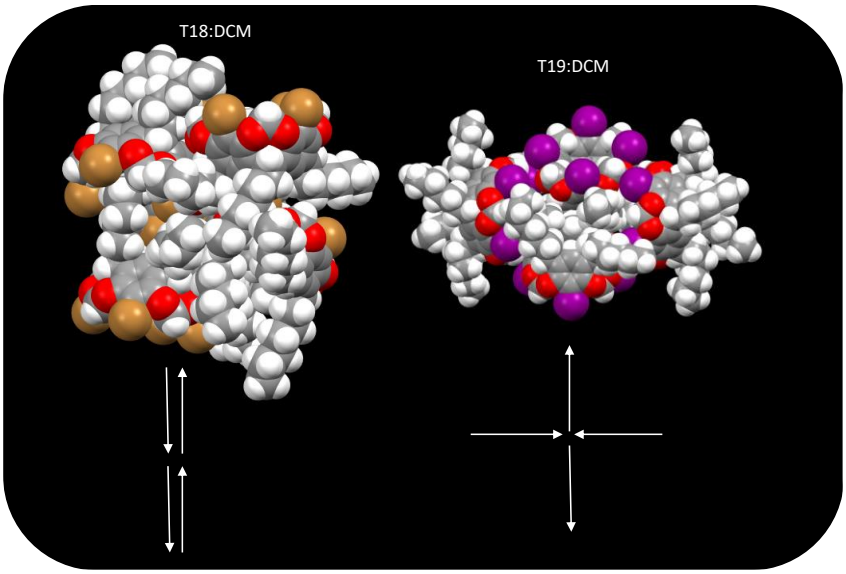

Figure 7.10. Packing of **T18**:DCM and **T19**:DCM (color codes: red-oxygen, brown-bromine, violet-iodine grey-carbon, white-hydrogen).

For the deeper cavitands, **T20-T23** we saw a 1:1 stoichiometry with DCM as indicated by TGA analysis. To examine the difference in the depth of the cavitands, we measured diagonally from top of the rim to the bottom of the body i.e. hydrogen on the aromatic ring, Figure 7.11. The difference between the depth of the **T18** and **T21** cavitands was around 2Å; for **T18** and **T20** was 2.06 Å; for **T21** and **T20** was same with negligible difference of 0.07 Å. Since the deeper cavitands has more rim space, we assume that in these cases, the solvent will most likely be located around the rim.

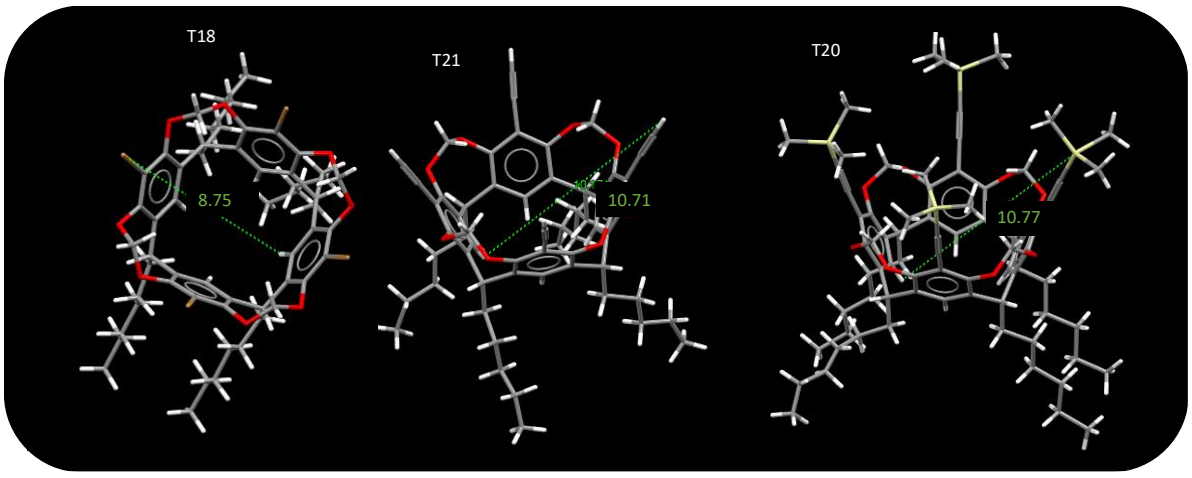

Figure 7.11. Difference in the depth of the cavitands **T18**, **T21** and **T20** (color codes: red-oxygen, brown-bromine, yellowish green-boron grey-carbon, white-hydrogen).

7.4.3. Solvent-ethyl acetate (EtOAc)

TGA analysis of **T18-T23** with EtOAc, shows 1:2 stoichiometry. The single crystal structure of **T18**:$(EtOAc)_2$ shows presence of two solvent molecules, one at the top of rim and the other at the feet of the cavitand. Since the rim of the cavitand was occupied by ethyl acetate, the molecular packing arrangement no longer follows "foot-in-the-mouth" kind of packing. The body is oriented at 180^o from each other, Figure 7.12. For all other combinations of cavitand and ethyl acetate, we were not able to get crystal structures. TGA analysis of **T19-T23** with EtOAc demonstrates 1:2 stoichiometry. In order to accommodate two EtOAc in the cavity it has to follow similar solvent encapsulation as we observed for **T18**.

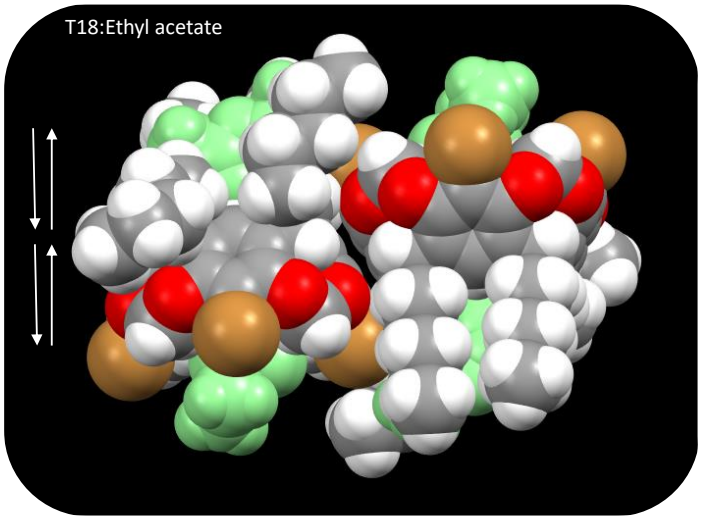

Figure 7.12. Packing of **T18**:$(EtOAc)_2$ (color codes: red-oxygen, brown-bromine, grey-carbon, white-hydrogen, green-EtOAc).

7.4.4. Solvent -acetonitrile (ACN)

TGA analysis of **T18-T23** with ACN indicates 1:1 stoichiometry. We obtained a crystal structure of **T18** recrystallized from ACN, Figure 7.7. In **T18**:ACN, the ACN was located around the feet of the cavitand. It formed CH(feet)•••N(ACN) interactions with the feet of the cavitand. It also forms a CH(ACN)•••O(rim) interaction with the rim of the neighboring cavitand. These interactions are commonly known as non-conventional hydrogen bonds.[36,37,38] The molecular packing still follows "foot-in-the-mouth" kind of packing. Although the packing is different from what we observed for **T18**:$(EtOAc)_2$, Figure 7.13.

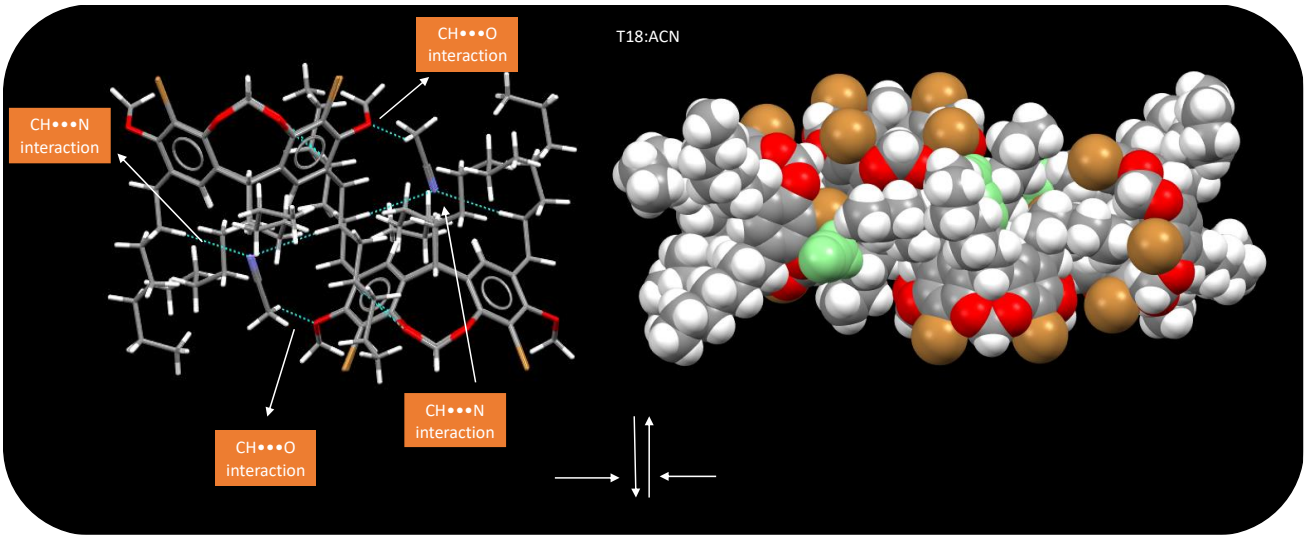

Figure 7.13. Packing of **T18**:ACN (color codes: red-oxygen, brown-bromine, grey-carbon, white-hydrogen, green-ACN).

7.4.5. Solvent -dimethyl sulfoxide (DMSO)

TGA analysis indicates 1:1 stoichiometry of **T18-T19** in combination with DMSO. With deeper cavitands **T20-T23**, we got 1:2 stoichiometry. Crystal structure of **T18**:DMSO shows DMSO encapsulation around the feet of the cavitand; **T19** encapsulates DMSO at the rim of the cavitand; and **T21** consists of two DMSO molecules located at the rim and feet of the cavitand, Figure 7.8. The molecular arrangement of **T18**:DMSO does not follow "foot-in-the-mouth" packing, although the rim was completely empty. We also observed a CH•••O non-conventional hydrogen-bond interaction between DMSO and **T18**, Figure 7.14.

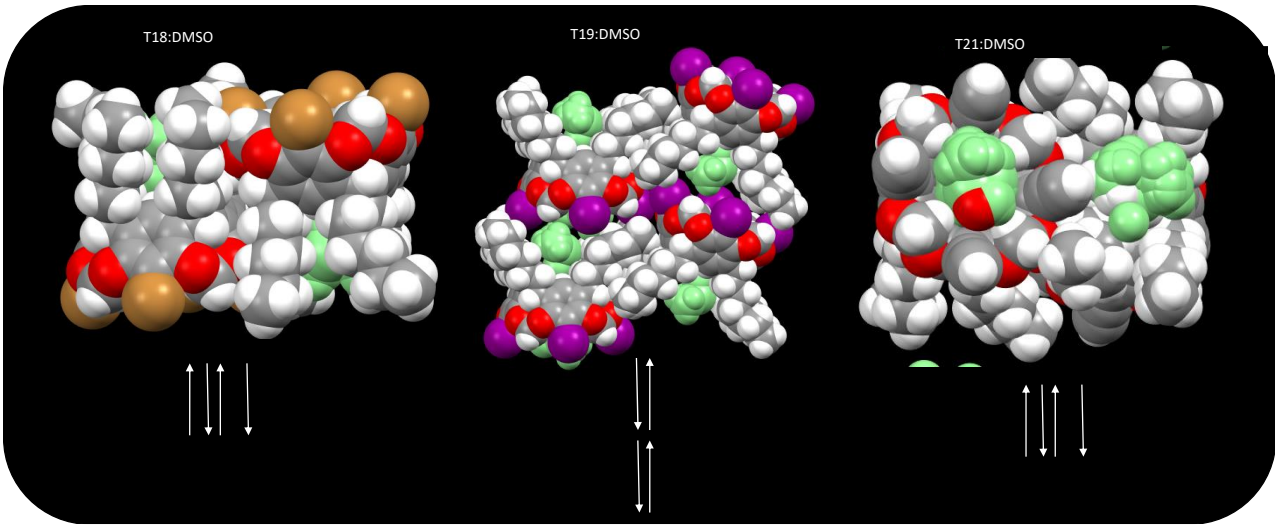

Figure 7.14. Packing of **T18**:DMSO, **T19**:DMSO, and **T21**:DMSO (color codes: red-oxygen, brown-bromine, violet-iodine, grey-carbon, white-hydrogen, green-DMSO).

In **T19**:DMSO, the solvent was located at the rim that interacts with another DMSO molecule, present at the feet of the cavitand, forming a parallel and anti-parallel chained pattern, Figure 7.15. With **T21**, we observed the presence of DMSO molecules both at the rim and feet of the cavitand.

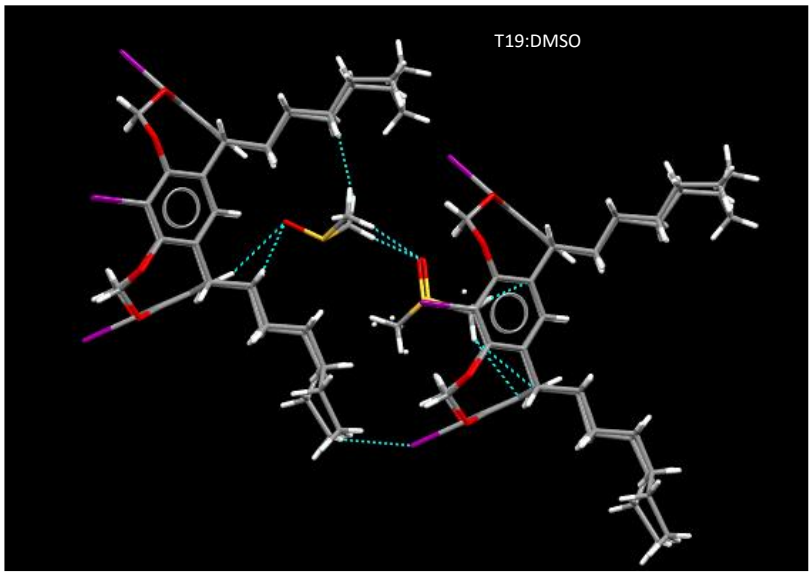

Figure 7.15. Packing of **T19**:DMSO (color codes: red-oxygen, violet-iodine, grey-carbon, white-hydrogen, green-ACN).

7.4.6. Solvent selectivity

We conducted selectivity studies by recrystallizing the cavitands from an equimolar mixture of solvents. We allowed crystal growth by slow evaporation technique followed by TGA and single crystal analysis. Among all the solvents, xylene/ DCM had the lowest dipole moment, and DMSO had the highest. Both xylene and DCM were not encapsulated in **T18**. For **T19**, xylene was present in 1:1 stoichiometry, but DCM was not encapsulated. Deeper cavitands **T20-T23** showed 1:1 stoichiometry with both xylene and DCM. EtOAc is present in the center of the dipole moment chart and showed 1:2 stoichiometry with all the cavitands. In **T18-T23**, ACN was present in 1:1 stoichiometry. Finally, DMSO exhibited 1:1 stoichiometry with **T18-T19** and 1:2 with **T20-T23**. **T18-T23** when subjected to a mixture of solvents, displayed a higher selectivity for DMSO as observed by TGA analysis and single crystal characterization. We also observed that the "foot-in-the-mouth" packing was found only with lower dipole moment solvents. With the increasing dipole moment other weak interactions such as CH•••O/ N stabilized the solvent encapsulation by the cavitand.

7.5. Conclusions

1. Overall the isostructural hosts showed similar stoichiometry for a given solvent. Although since the cavitands did not have a strong non-covalent interaction the location of the solvents within the cavitand were random, Figure 7.16.

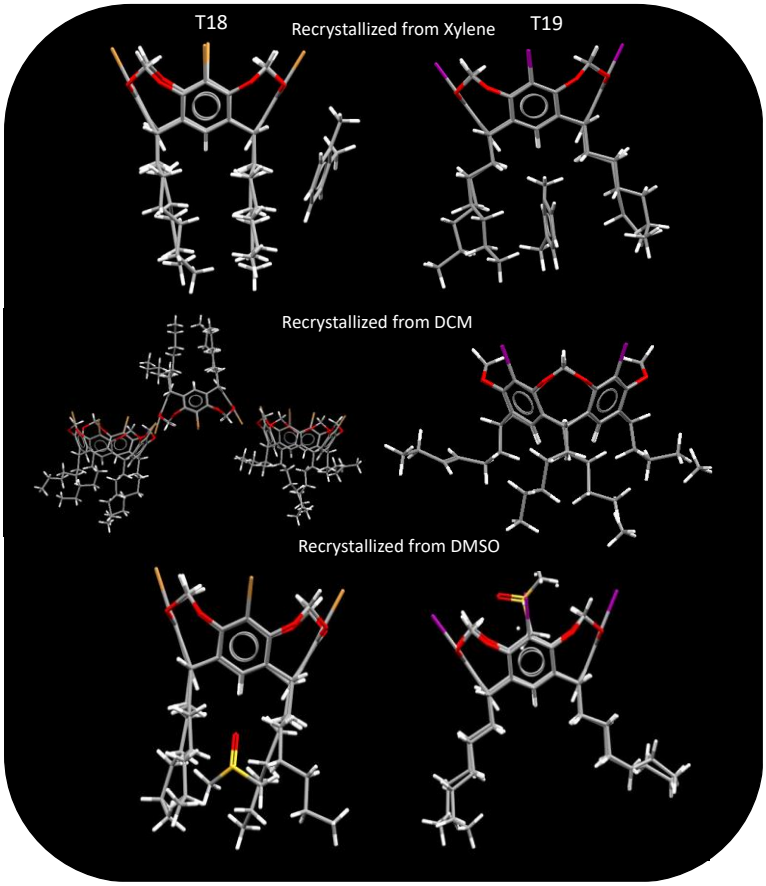

Figure 7.16. Comparison between **T18** and **T19** solvent encapsulation.

2. The difference in the depth of **T20-T23** displayed 1:1 stoichiometry with DCM and 1:2 with DMSO in comparison to no solvent molecules observed between **T18-T19** with DCM and 1:1 with DMSO.

3. DMSO had the highest dipole moment and was most selective in comparison to other solvent molecules, Figure 7.17.

Figure 7.17. Selectivity between the solvent molecules.

7.6. References

(1) Whitesides, G. M.; Mathias, J. P.; Seto, C. T. Molecular Self-Assembly and Nanochemistry: A Chemical Strategy for the Synthesis of Nanostructures. *Science* **1991**, *254* (5036), 1312–1319. https://doi.org/10.1126/science.1962191.

(2) Parkin, I. P. Supramolecular Chemistry. J.W. Steed and J.L. Atwood. John Wiley & Sons Ltd, Chichester, 2000. Xxvii + 745 Pages. £29.95 (Paperback). ISBN 0-471-98791-3. *Applied Organometallic Chemistry* **2001**, *15* (3), 236–236. https://doi.org/10.1002/aoc.125.

(3) Sanders, J. K. Supramolecular Chemistry. Concepts and Perspectives. Von J.-M. Lehn. VCH Verlagsgesellschaft, Weinheim, 1995. 271 S., Geb. 128.00 DM/Broschur 58.00 DM. - ISBN 3-527-29312-4/3-527-29311-6. *Angewandte Chemie* **1995**, *107* (21), 2617–2617. https://doi.org/10.1002/ange.19951072130.

(4) Rodriguez-Tenreiro, C.; Alvarez-Lorenzo, C.; Rodriguez-Perez, A.; Concheiro, A.; Torres-Labandeira, J. J. Estradiol Sustained Release from High Affinity Cyclodextrin Hydrogels. *Eur J Pharm Biopharm* **2007**, *66* (1), 55–62. https://doi.org/10.1016/j.ejpb.2006.09.003.

(5) Ghang, Y.-J.; Perez, L.; Morgan, M. A.; Si, F.; Hamdy, O. M.; Beecher, C. N.; Larive, C. K.; Julian, R. R.; Zhong, W.; Cheng, Q.; et al. Anionic Deep Cavitands Enable the Adhesion of Unmodified Proteins at a Membrane Bilayer. *Soft Matter* **2014**, *10* (48), 9651–9656. https://doi.org/10.1039/C4SM02347A.

(6) Axial binding and host-guest interactions of a phthalocyanine resorcinarene cavitand hybrid. - Abstract - Europe PMC https://europepmc.org/article/med/24276488 (accessed Mar 5, 2020).

(7) Moran, J. R.; Karbach, S.; Cram, D. J. Cavitands: Synthetic Molecular Vessels. *J. Am. Chem. Soc.* **1982**, *104* (21), 5826–5828. https://doi.org/10.1021/ja00385a064.

(8) Wiseman, A. Bioinorganic Chemistry: Inorganic Elements in the Chemistry of Life. An Introduction and Guide. By W. Kaim & B. Schwederski, Wiley, Chichester, 1994, Ix + 401 Pp., Price £19.95. ISBN 0 471 94369 X. *Journal of Chemical Technology & Biotechnology* **1995**, *63* (3), 297–297. https://doi.org/10.1002/jctb.280630318.

(9) Shao, C.; Yu, H.-J.; Wu, N.-Y.; Tian, P.; Wang, R.; Feng, C.-G.; Lin, G.-Q. Asymmetric Synthesis of β-Substituted γ-Lactams via Rhodium/Diene-Catalyzed 1,4-Additions: Application to the Synthesis of (*R*)-Baclofen and (*R*)-Rolipram. *Org. Lett.* **2011**, *13* (4), 788–791. https://doi.org/10.1021/ol103054a.

(10) Supramolecular Chemistry and Chemical Warfare Agents: From Fundamentals of Recognition to Catalysis and Sensing - Chemical Society Reviews (RSC Publishing).

(11) Tudisco, C.; Betti, P.; Motta, A.; Pinalli, R.; Bombaci, L.; Dalcanale, E.; Condorelli, G. G. Cavitand-Functionalized Porous Silicon as an Active Surface for Organophosphorus Vapor Detection. *Langmuir* **2012**, *28* (3), 1782–1789. https://doi.org/10.1021/la203797b.

(12) Djernes, K. E.; Padilla, M.; Mettry, M.; Young, M. C.; Hooley, R. J. Hydrocarbon Oxidation Catalyzed by Self-Folded Metal-Coordinated Cavitands. *Chem. Commun.* **2012**, *48* (94), 11576–11578. https://doi.org/10.1039/C2CC36236H.

(13) Tudisco, C.; Betti, P.; Motta, A.; Pinalli, R.; Bombaci, L.; Dalcanale, E.; Condorelli, G. G. Cavitand-Functionalized Porous Silicon as an Active Surface for Organophosphorus Vapor Detection. *Langmuir* **2012**, *28* (3), 1782–1789. https://doi.org/10.1021/la203797b.

(14) Cavitand-grafted silicon microcantilevers as a universal probe for illicit and designer drugs in water. - Abstract - Europe PMC https://europepmc.org/article/med/24909594 (accessed Mar 5, 2020).

(15) Biavardi, E.; Tudisco, C.; Maffei, F.; Motta, A.; Massera, C.; Condorelli, G. G.; Dalcanale, E. Exclusive Recognition of Sarcosine in Water and Urine by a Cavitand-Functionalized Silicon Surface. *PNAS* **2012**, *109* (7), 2263–2268. https://doi.org/10.1073/pnas.1112264109.

(16) Supramolecular Sensing with Phosphonate Cavitands | Accounts of Chemical Research https://pubs.acs.org/doi/10.1021/ar300178m (accessed Mar 5, 2020).

(17) Stabilization of Labile Carbonyl Addition Intermediates by a Synthetic Receptor | Science https://science.sciencemag.org/content/317/5837/493.abstract (accessed Mar 5, 2020).

(18) A Self-Assembled Cylindrical Capsule: New Supramolecular Phenomena through Encapsulation - Körner - 2000 - Chemistry – A European Journal - Wiley Online Library https://onlinelibrary.wiley.com/doi/10.1002/%28SICI%291521-3765%2820000103%296%3A1%3C187%3A%3AAID-CHEM187%3E3.0.CO%3B2-I (accessed Mar 5, 2020).

(19) Gas Behavior in Self-Assembled Capsules - Ajami - 2008 - Angewandte Chemie International Edition - Wiley Online Library https://onlinelibrary.wiley.com/doi/10.1002/anie.200802023 (accessed Mar 5, 2020).

(20) Nishimura, N.; Kobayashi, K. Self-Assembled Boronic Ester Cavitand Capsule as a Photosensitizer and a Guard Nanocontainer against Photochemical Reactions of 2,6-

Diacetoxyanthracene. *J. Org. Chem.* **2010**, *75* (18), 6079–6085. https://doi.org/10.1021/jo101255g.

(21) R. Samanta, S.; Parthasarathy, A.; Ramamurthy, V. Supramolecular Control during Triplet Sensitized Geometric Isomerization of Stilbenes Encapsulated in a Water Soluble Organic Capsule. *Photochemical & Photobiological Sciences* **2012**, *11* (11), 1652–1660. https://doi.org/10.1039/C2PP25115A.

(22) Tunstad, L. M.; Tucker, J. A.; Dalcanale, E.; Weiser, J.; Bryant, J. A.; Sherman, J. C.; Helgeson, R. C.; Knobler, C. B.; Cram, D. J. Host-Guest Complexation. 48. Octol Building Blocks for Cavitands and Carcerands. *J. Org. Chem.* **1989**, *54* (6), 1305–1312. https://doi.org/10.1021/jo00267a015.

(23) Mezo, A. R.; Sherman, J. C. Water-Soluble Cavitands: Synthesis of Methylene-Bridged Resorcin[4]Arenes Containing Hydroxyls and Phosphates at Their Feet and Bromomethyls and Thiomethyls at Their Rims. *J. Org. Chem.* **1998**, *63* (20), 6824–6829. https://doi.org/10.1021/jo980305k.

(24) Purse, B. W.; Rebek, J. Functional Cavitands: Chemical Reactivity in Structured Environments. *PNAS* **2005**, *102* (31), 10777–10782. https://doi.org/10.1073/pnas.0501731102.

(25) Purse, B. W.; Rebek, J. Self-Fulfilling Cavitands: Packing Alkyl Chains into Small Spaces. *Proceedings of the National Academy of Sciences* **2006**, *103* (8), 2530–2534. https://doi.org/10.1073/pnas.0511149103.

(26) Hooley, R. J.; Van Anda, H. J.; Rebek, J. Cavitands with Revolving Doors Regulate Binding Selectivities and Rates in Water. *J. Am. Chem. Soc.* **2006**, *128* (12), 3894–3895. https://doi.org/10.1021/ja058727g.

(27) Rj, H.; Jr, R. J. A Deep Cavitand Catalyzes the Diels-Alder Reaction of Bound Maleimides. *Org Biomol Chem* **2007**, *5* (22), 3631–3636. https://doi.org/10.1039/b713104f.

(28) Cram, D. J.; Choi, H. J.; Bryant, J. A.; Knobler, C. B. Host-Guest Complexation. 62. Solvophobic and Entropic Driving Forces for Forming Velcraplexes, Which Are 4-Fold, Lock-Key Dimers in Organic Media. *J. Am. Chem. Soc.* **1992**, *114* (20), 7748–7765. https://doi.org/10.1021/ja00046a022.

(29) Tucci, F. C.; Rudkevich, D. M.; Rebek, J. Deeper Cavitands. *J. Org. Chem.* **1999**, *64* (12), 4555–4559. https://doi.org/10.1021/jo990209z.

(30) Aoyama, Y.; Tanaka, Y.; Sugahara, S. Molecular Recognition. 5. Molecular Recognition of Sugars via Hydrogen-Bonding Interaction with a Synthetic Polyhydroxy Macrocycle. *J. Am. Chem. Soc.* **1989**, *111* (14), 5397–5404. https://doi.org/10.1021/ja00196a052.

(31) Bryant, J. A.; Blanda, M. T.; Vincenti, M.; Cram, D. J. Host-Guest Complexation. 55. Guest Capture during Shell Closure. *J. Am. Chem. Soc.* **1991**, *113* (6), 2167–2172. https://doi.org/10.1021/ja00006a040.

(32) El Moll, H.; Sémeril, D.; Matt, D.; Youinou, M.-T.; Toupet, L. Synthesis of a Resorcinarene-Based Tetraphosphine-Cavitand and Its Use in Heck Reactions. *Org. Biomol. Chem.* **2009**, *7* (3), 495–501. https://doi.org/10.1039/b813373e.

(33) Jude, H.; Sinclair, D. J.; Das, N.; Sherburn, M. S.; Stang, P. J. Self-Assembly of Supramolecular Platinum Complexes with Bis-4-Pyridyl Cavitands. *J. Org. Chem.* **2006**, *71* (11), 4155–4163. https://doi.org/10.1021/jo060133o.

(34) Topkaya, D.; Dumoulin, F.; Ahsen, V.; İşci, Ü. Axial Binding and Host–Guest Interactions of a Phthalocyanine Resorcinarene Cavitand Hybrid. *Dalton Trans.* **2013**, *43* (5), 2032–2037. https://doi.org/10.1039/C3DT52732H.

(35) Chopade, P. D. From Supramolecular Selectivity to Nanocapsules. **2012**.

(36) Dubey, R.; Lim, D. Weak Interactions: A Versatile Role in Aromatic Compounds. *COC* **2011**, *15* (12), 2072–2081. https://doi.org/10.2174/138527211795703667.

(37) Oruganti, M.; Khade, P.; Kumar Das, U.; R. Trivedi, D. The Hierarchies of Hydrogen Bonds in Salts/Cocrystals of Isoniazid and Its Schiff Base – a Case Study. *RSC Advances* **2016**, *6* (19), 15868–15876. https://doi.org/10.1039/C5RA14951G.

(38) Koch, U.; Popelier, P. L. A. Characterization of C-H-O Hydrogen Bonds on the Basis of the Charge Density. *J. Phys. Chem.* **1995**, *99* (24), 9747–9754. https://doi.org/10.1021/j100024a016.

Chapter 8 –Cavitands as Molecular Containers

8.1. Introduction

8.1.1. Background

Cavitands are organic macromolecules with bowl-shaped cavities capable of encapsulating cations, anions and solvents through a variety of intermolecular interactions[1,2,3,4]. There are various applications of cavitands as a molecular host[5,6,7,8,9,10,11,12] that are characteristic of the defined space, volume and functional groups[13,14,15,16,17]. The structural framework of the cavitands enables them to act as versatile molecular hosts where a large variation can be achieved without altering the integrity of the cavitand framework. In previous chapters, we used reversible non-covalent intermolecular interactions as tool[18] for exploring diversity in supramolecular assemblies. In this chapter we extend our understanding to hydrogen-bonding in cavitands, tailored towards molecular recognition[19] events for a wide range of guests. We focus our efforts on cavitands with two possible modes of host-guest binding, Figure 8.1.

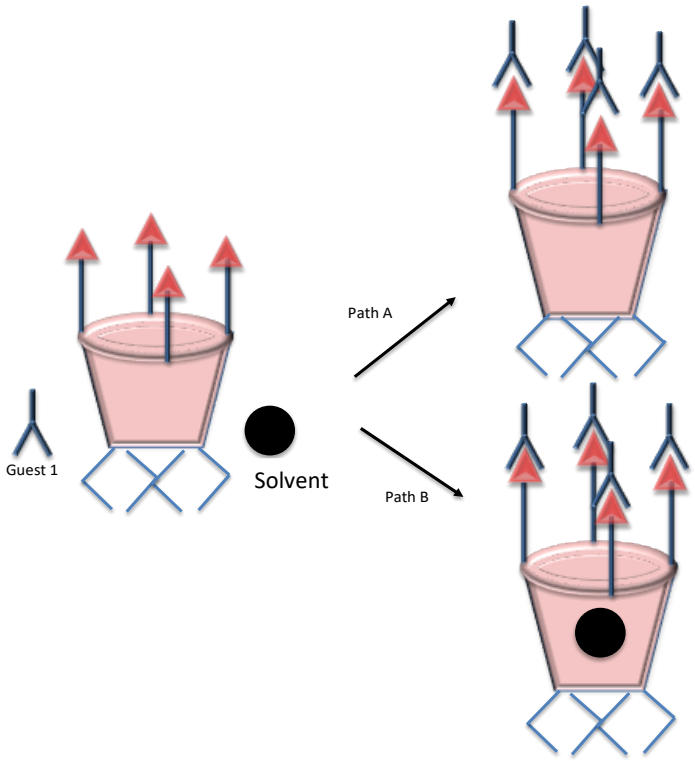

Figure 8.1. Cartoon representation of possible guest binding modes to the rim of a cavitand.

A major challenge in supramolecular chemistry is predicting the stoichiometry of host-guest interactions. Solid state techniques such as FTIR can provide proof for host-guest interactions but not the stoichiometry. Ideally analysis of the single crystal X-ray diffraction is the best possible route however, growing crystals of such large systems is rather difficult. The most common answer to this problem is by conducting NMR titrations[20]. In titration method, one component (i.e. guest) is incrementally titrated into the other component (i.e. host), by carefully monitoring the change in the chemical shift. The data acquired from the titration is fit into non-linear binding curves to obtain the value of association constant Ka which is the basic parameter for evaluating the host-guest recognition process. In addition, free energy, ΔG can be calculated as expressing the favorability of the complexation and also the stoichiometry of the binding event can be determined by means of a Jobs plot[21,22].

8.1.2. Choice of host and guest molecules

8.1.2.1. Fragrant compounds as guests

Fragrant compounds are organic compounds with characteristic strong odors that find applications in perfumes and perfumed products. The smell of fragrance compounds is often related to their highly volatility[23,24]. Therefore, molecular mass of these compounds is an important factor. The molecular mass of commonly used fragrant compounds range between 200 – 300 g/ mol. In this study we use three aliphatic carboxylic acid and two cyclic hydroxyl fragrant compounds frequently used as fragrant compounds, Figure 8.2.

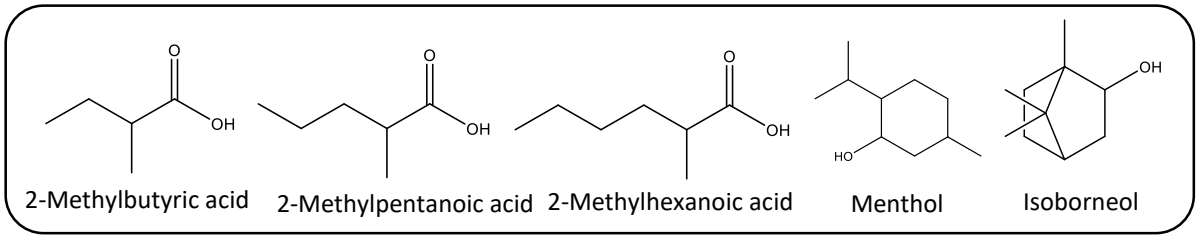

Figure 8.2. Fragrant compounds of choice.

The goal of this study is to use cavitands as a molecular container for fragrant compounds. The host-guest interactions between cavitands and guests will most likely change the volatility of the latter. In order to facilitate host-guest interactions we choose hydrogen-bond acceptor cavitands,

since all the guests have hydrogen-bond donor sites. We used three hydrogen-bond acceptor cavitands, where **T24** and **T25** are structural isomers Figure 8.3. **T26** had very similar molecular electrostatic potential surfaces (MEPS) as that of **T24** and **T25**.

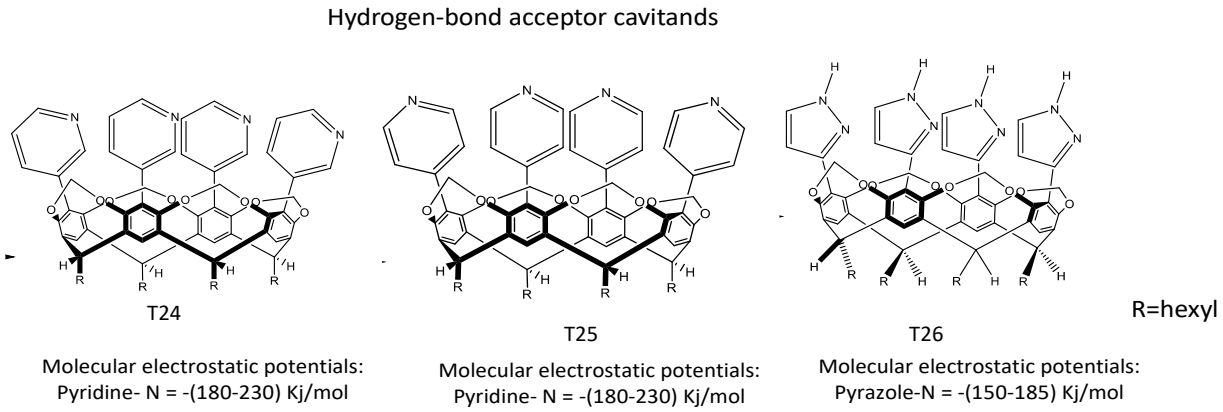

Figure 8.3. Choice of cavitands.

8.1.2.2. Heterocyclic N-oxides as guest

Heterocyclic-N-oxides were perceived as side products historically, of hepatic metabolism of N-heterocyclic therapeutic compounds[25]. Heterocyclic-N-oxides became a mainstream drug, during 1960s due to unusual discovery of antihypertensive and anti-alopecia agent *Minoxidil* by Upjohn[26]. Since then it has found various applications in anticancer, antiviral, anti-protozoal, and anti-fungal drug products in advanced discovery stage. Additionally, numerous heterocyclic-N-oxide compounds have found its applications in agrochemicals and cosmetics industry. In this study we use a series of N-oxides to study their binding ability with cavitands, Figure 8.4. The choice of hosts was hydrogen-bond donor cavitands since all the guests have hydrogen-bond acceptor sites.

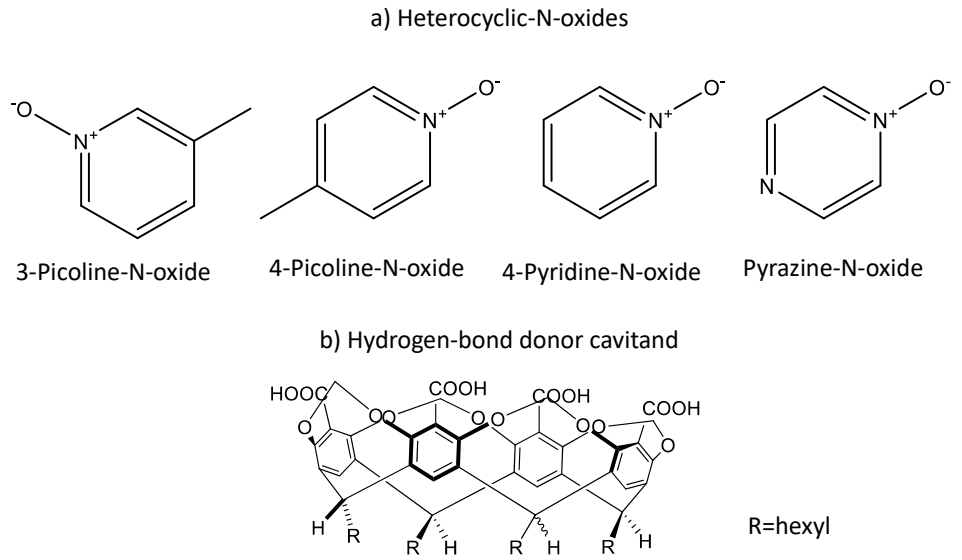

Figure 8.4. a) Heterocyclic-N-oxide guests of choice, b) Hydrogen-bond donor cavitand.

8.1.3. Goals

We will synthesize three hydrogen-bond acceptor and one hydrogen-bond donor cavitands to examine host-guest interactions via NMR titrations with fragrant compounds and heterocyclic-N-oxides. We will use TGA analysis in addition to NMR titrations, in order to analyze the resulting host-guest interactions. Hydrogen-bond propensity (HBP) calculations will be implemented to examine if host-guest interactions can be predicted for cavitands and guest compounds. We chose HBP, since it produced the highest reliability in comparison to other commercially available predictive methods, Chapter 4-5.

The study is done to answer the following questions:

1. Can HBP correctly predict the host-guest interactions?
2. Will the guests interact with the cavitands and if yes what will be the stoichiometry?

8.2. Experimental

All chemicals were purchased from Aldrich, Fischer, TCI America, Oakwood and Alfa Aesar which were used without further purification unless otherwise mentioned. Column chromatography was carried out using silica gel (150 Å pore size) from Analtech, Inc. ^{1}H and ^{13}C NMR spectra were recorded on Varian Unity plus 400 MHz spectrometer in $CDCl_3$ or DMSO.

The NMR data is in parts per million (ppm) with downfield shift from tetramethylsilane which is an internal reference. Nicolet 380 FT-IR was used for infrared spectroscopy and the data was analyzed using Omnic 8.0 Thermo Fischer Scientific Inc. software. DSC and TGA analysis were done using TA instruments Q20 and Q50, respectively.

8.2.1. Synthesis of hosts

*8.2.1.2. Synthesis of C-hexyltetra(3-pyridyl) cavitand, **T24***

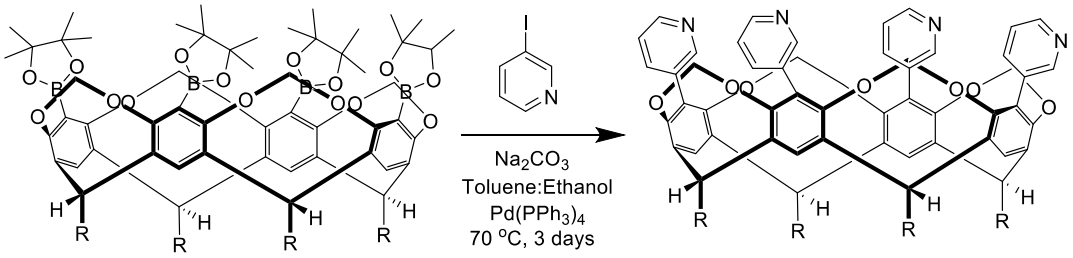

T 24

R= $(CH_2)_5CH_3$

A mixture of C- hexyltetraboronic acid dipinacolyl ester cavitand, **T23** (2.0 g, 1.77 mmol) and tetrakistriphenylphosphine palladium (0) (420 mg, 0.362 mmol) were placed in a round bottom flask under a stream of dinitrogen. To this was added a mixture of toluene (30 mL), ethanol (20 mL) and aqueous sodium bicarbonate (100 mg, 5 mL) purged with dinitrogen. Then 3-iodopyridyl (4.60g, 22.8 mmol) was added to the reaction mixture and refluxed for 72 hours under dinitrogen. Upon completion the reaction was cooled to room temperature and diluted with water (100 mL). The aqueous phase was washed with dichloromethane (3 x 100 mL) and dried with anhydrous magnesium sulfate. The solvent was removed on a rotary evaporator and the residue purified by column chromatography using an ethanol/ethyl acetate (1:2) mixture as the eluant. The product **T24** was isolated as a white crystalline solid, (1.44 g, 72%).

M.P.: > 280 ºC. ^{1}H NMR (400MHz, $CDCl_3$): 8.47 (d, 4H), 8.27 (s, 4H), 7.50 (d, 4H), 7.43 (s, 4H), 7.36 (s, 4H), 5.28 (d, J = 6.8 Hz, 4H), 4.95 (t, J = 7.2 Hz, 4H), 4.26 (d, J = 7.6 Hz, 4H), 2.34 (m, 8H), 1.43-1.35 (m, 72H), 0.93 (m, 12H).

8.2.1.1. Synthesis of C-hexyltetra(4-pyridyl) cavitand, ***T25***

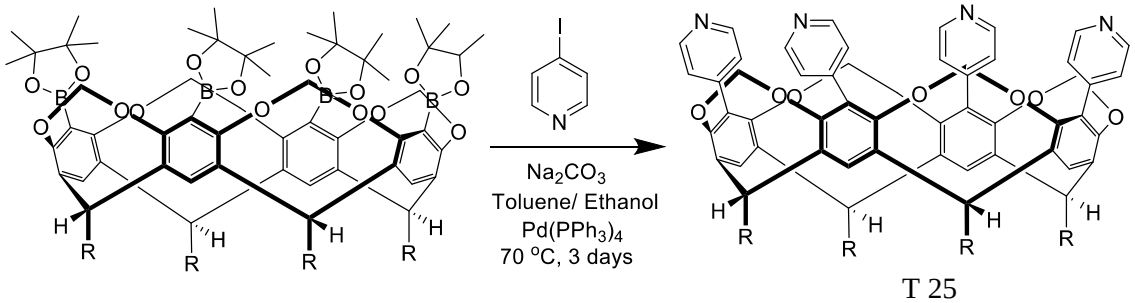

T 25

R= $(CH_2)_5CH_3$

A mixture of C- hexyltetraboronic acid dipinacolyl ester cavitand, **T23** (2.00 g, 1.77 mmol) and tetrakistriphenylphosphine palladium (0) (420 mg, 0.362 mmol) were placed in a round bottom flask under a stream of dinitrogen. To this was added a mixture of toluene (30 mL), ethanol (20 mL) and aqueous sodium bicarbonate (100 mg, 5 mL) purged with dinitrogen. Then 4-iodopyridyl (4.60g, 22.8 mmol) was added to the reaction mixture and refluxed for 72 hours under dinitrogen. Upon completion the reaction was cooled to room temperature and diluted with water (100 mL). The aqueous phase was washed with dichloromethane (3 x 100 mL) and dried with anhydrous magnesium sulfate. The solvent was removed on a rotary evaporator and the residue purified by column chromatography using an ethanol/ethyl acetate (1:2) mixture as the eluant. The product **T25** was isolated as a white crystalline solid, (1.53 g, 73%).

M.P.: > 280 ºC. ^{1}H NMR (400MHz, $CDCl_3$): 8.63 (d, 8H), 7.31 (s, 4H), 6.47 (d, 8H), 5.50 (d, J = 6.8 Hz, 4H), 5.23 (t, J = 7.2 Hz, 4H), 4.80 (d, J = 7.6 Hz, 4H), 2.30 (m, 8H), 1.36 (m, 72H), 0.93 (m, 12H).

8.2.1.3. Synthesis of C-hexyltetra(3-pyrazole) cavitand, ***T26***

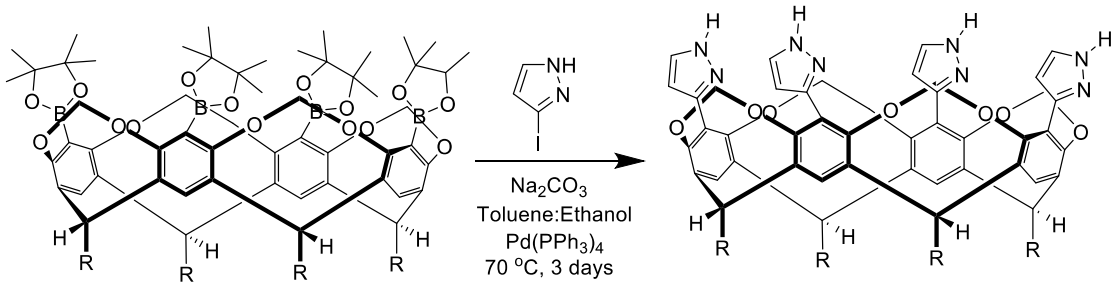

T26

R= $(CH_2)_5CH_3$

A mixture of C- hexyltetraboronic acid dipinacolyl ester cavitand, **T23** (2.00 g, 1.77 mmol) and tetrakistriphenylphosphine palladium (0) (420 mg, 0.362 mmol) were placed in a round bottom flask under a stream of dinitrogen. To this was added a mixture of toluene (30 mL), ethanol (20 mL) and aqueous sodium bicarbonate (100 mg, 5 mL) purged with dinitrogen. Then 3-iodopyrazole (4.44g, 22.8 mmol) was added to the reaction mixture and refluxed for 72 hours under a dinitrogen atmosphere. Upon completion the reaction was cooled to room temperature and diluted with water (100 mL). The aqueous phase was washed with dichloromethane (3 x 100 mL) and dried with anhydrous magnesium sulfate. The solvent was removed on a rotary evaporator and the residue purified by column chromatography using an ethanol/ethyl acetate (1:2) mixture as the eluant. The product **T26** was isolated as a white crystalline solid, (0.98 g, 54%).

M.P.: > 280 ºC. ^{1}H NMR (400MHz, $CDCl_3$): 7.43 (d, 4H), 7.33 (s, 4H), 7.04 (s, 4H), 5.97 (d, J = 6.8 Hz, 4H), 4.85 (t, J = 7.2 Hz, 4H), 4.38 (d, J = 7.6 Hz, 4H), 2.21 (m, 8H), 1.44-1.31 (m, 72H), 0.90 (m, 12H).

*8.2.1.4. Synthesis of C-hexyltetracarboxylic cavitand, **T27***

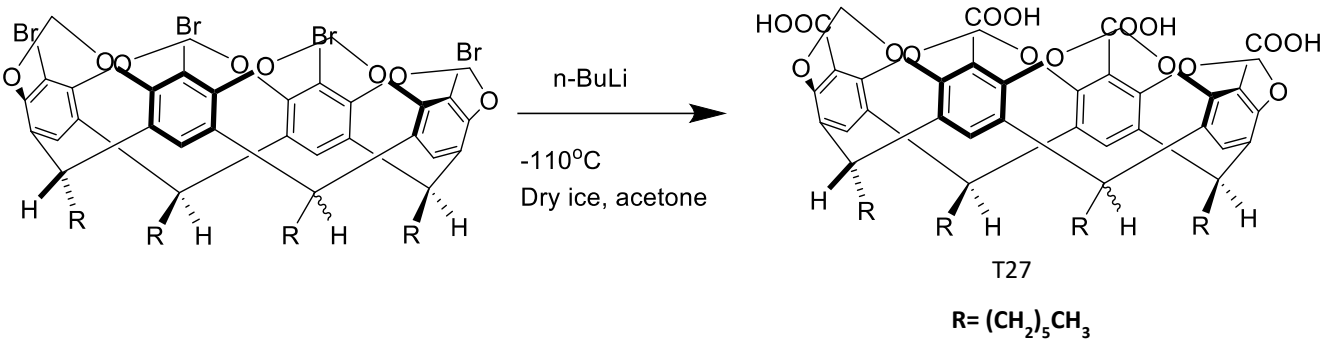

Dry freshly distilled tetrahydrofuran (20 mL) was added to C-hexyltetrabromocavitand, **T18** (2.16 g, 1.91 mmol), and then the solution was evaporated and dried at 80 °C (0.1 mmHg) for 2 h under a nitrogen atmosphere to get a rigorously dry solid. This procedure was repeated twice. At the end of the drying procedure, the solid, **T18** was dissolved in dry tetrahydrofuran (200 mL) and cooled to -78 °C using dry ice/ acetone bath under dinitrogen for 10 minutes. N- butyllithium (1.6 M in hexanes) (5.96 mL, 9.55 mmol) was slowly added dropwise to this solution upon which a milky solution begins to appear. After addition, the reaction mixture was stirred for 2 hours under nitrogen. Then the solution was added to a mixture of dry ice and diethyl ether. The reaction was left until it reached room temperature. Upon completion, a NaOH (1 M) aqueous solution (100 mL) was added to the reaction mixture at room temperature. THF was then removed under vacuum and the aqueous layer was washed with Et_2O (100 mL × 3), followed by acidifying with concentrated HCl at 0 °C. The resulted white solid of the product, **T27** was then extracted with Et_2O (100 mL × 3). The organic layer washed with water and brine, dried over anhydrous $MgSO_4$ and solvent removed under vacuum to yield **T27** as white solid (1.32 g, 74%). M.P. > 280℃; ^{1}H NMR (δH; 400 MHz, $CDCl_3$): 7.18 (s, 4H), 5.75 (d, J = 8.4Hz, 4H), 4.74 (t, J = 6.2Hz, 4H), 4.50 (d, J = 7.2Hz, 4H), 2.19 (m, 8H), 1.30 (m, 24H), 0.90 (t, 12H); IR: 3530, 3224, 2929, 2846, 1715, 1586, 1452, 1277, 1085, cm^{-1}.

8.2.2. Hydrogen bond propensity (HBP) calculations

The hydrogen-bond propensity[27,28,29,30,31] model was used to predict the host-guest interactions between the cavitands and guests molecules. A detailed description of HBP calculations is given

in section 2.2.3. We excluded the feet of the cavitands while performing HBP calculations, Figure 8.5.

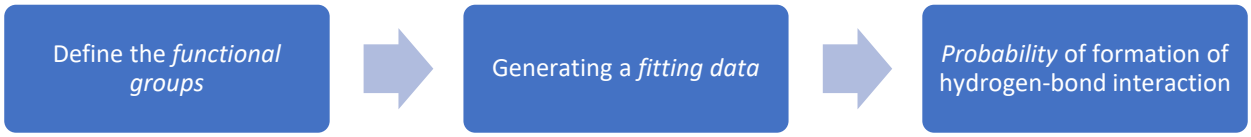

Figure 8.5. Schematic representation of the steps involved in HBP calculations.

8.2.3. Preparation of the host-guest complexes

The host-guest samples were prepared by dissolving the host and guest in 1:1 stoichiometry in a solvent. We used $CDCl_3$ as the solvent and kept it constant for all host-guest samples. The mixture was then heated, and the solvent was allowed to evaporate. The leftover solid residue was used for thermogravimetric analysis (TGA).

8.2.4. Thermogravimetric analysis (TGA) of target cavitands and guest molecules

TGA analysis of the host-guests complexes were performed to confirm the presence or absence of guest in the crystal lattice. Early weight loss (below 100 ^{o}C) suggests the presence of loosely bound guest molecules in the crystal lattice whereas, weight loss at a higher temperature corresponds to the presence of strong host-guest interaction. Figure 8.6. illustrates TGA analysis of **T24** with the aliphatic guests. The % weight loss in TGA corresponds to the number of guest molecules that are lost. This weight loss in TGA was compared with the NMR titration to examine if they display similar stoichiometry.

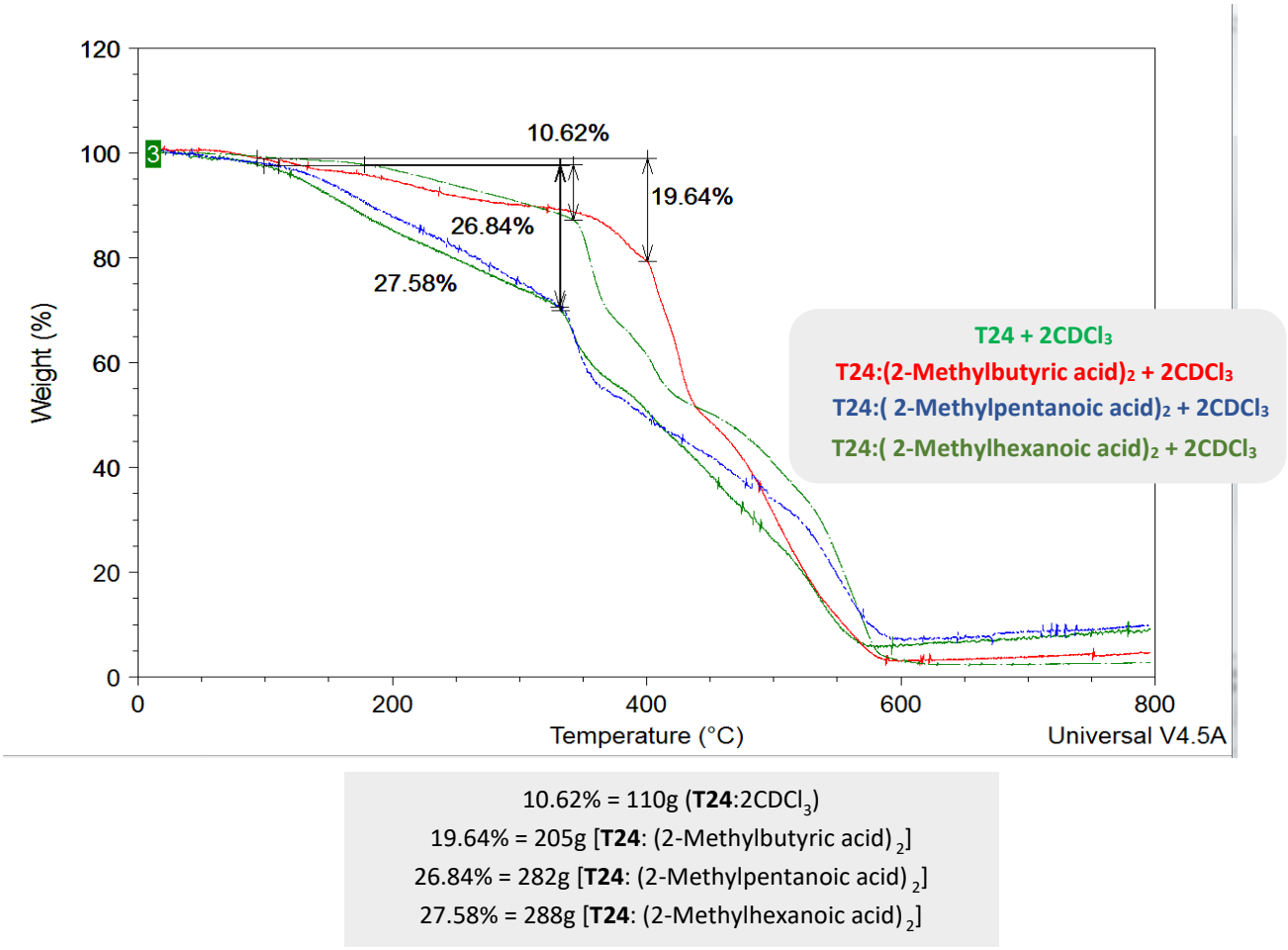

Figure 8.6. TGA analysis of **T25** with aliphatic guest and their corresponding weight losses.

8.2.5. NMR titration experiment

8.2.5.1. Preparation of the solutions

The host (cavitand) concentration [H] was kept constant throughout the titration while the guest (active ingredients) concentration [G] was varied gradually. A stock solution of the host cavitand was prepared from which a constant amount was added to each NMR sample. The concentration of each final sample was kept at 1.6 mM. A stock solution of the guest was prepared from which successive volumes were added into the host during the titration. The concentrations of the guest [G] in the final solution ranged between 0.25-12 mM, Table 8.1.

Table 8.1. Host-guest concentrations used in this study.

Host	Guest						
conc. mM	moles mmol	Volume	conc. mM	moles mmol	Volume	Solvent	Equivalence
1.6	0.0032	0.4	0.8	0.0016	0.1	1.5	0.5
1.6	0.0032	0.4	1.6	0.0032	0.2	1.4	1
1.6	0.0032	0.4	2.4	0.0048	0.3	1.3	1.5
1.6	0.0032	0.4	3.2	0.0064	0.4	1.2	2
1.6	0.0032	0.4	4.8	0.0096	0.6	1	3
1.6	0.0032	0.4	6.4	0.0128	0.8	0.8	4
1.6	0.0032	0.4	8	0.016	1	0.6	5
1.6	0.0032	0.4	9.6	0.0192	1.2	0.4	6
1.6	0.0032	0.4	12.8	0.0256	1.6	0	8

8.2.5.2. Binding constant determination

A solution of known concentration of the guest was successively added to the host until an equilibrium was reached in the host-guest binding event which is indicated by a constant value of the chemical shift in the NMR spectrum. All the spectra were run at 298 K in $CDCl_3$ unless otherwise noted. A series of 9-10 data points were recorded for each titration experiment. The changes in the chemical shifts acquired from the titrations were graphed against the guest concentration with non-linear mathematical approach based on Benesi-Hildebrand[32] analysis using Origin 8.1 software. The equation used for curve fitting is given below,

$$\boldsymbol{H + G \rightarrow HG}$$

$$Ka = \frac{[HG]}{[H]\,[G]}$$

$$\boldsymbol{\Delta\delta = \frac{\Delta\delta_{sat}}{2}\left[\left(\frac{[G]_0}{[H]_0} + 1 + \frac{1}{K_a[G]_0}\right) - \sqrt{\left(\frac{[G]_0}{[H]_0} + 1 + \frac{1}{K_a[H]_0}\right)^2 - 4\frac{[G]_0}{[H]_0}}\right]} \quad \textbf{Equation 8.1.}$$

$[H]_0$ is the host concentration
$[G]_0$ is the total guest concentration (bound and unbound)
Ka is the association constant
$\Delta\delta$ is the change in the chemical shift

8.3. Results

8.3.1. Hydrogen-bond propensity calculations

Following the scheme 2.2.3, hydrogen-bond propensity calculations was carried out for each host-guest pair. Table 8.2 summarizes the HBP values. A positive number indicates potential host-guest interactions and a negative HBP value suggests no host-guest interaction. **T24** and **T25** both consist of "pyridine" as the functional group in combination with OH. Hence all the HBP values are the same for both hosts.

Table 8.2. HBP values of cavitands and guest molecules.

Compounds	ΔHBP= Heteromeric-Homomeric
T24/**T25** + 2-Methylbutyric acid	0.73-0.21 = 0.52
T24/**T25** + 2-Methylpentanoic acid	0.73-0.21 = 0.52
T24/**T25** + 2-Methylhexanoic acid	0.73-0.21 = 0.52
T24/**T25** + Menthol	0.55-0.26= 0.29
T24/**T25** + Isoborneol	0.55-0.26= 0.29
T26 + 2-Methylbutyric acid	0.55-0.59 = -0.04
T26 + 2-Methylpentanoic acid	0.55-0.59 = -0.04
T26 + 2-Methylhexanoic acid	0.55-0.59 = -0.04
T26 + Menthol	0.61-0.67= -0.06
T26 + Isoborneol	0.61-0.67= -0.06
T27 + 3-Picoline-N-oxide	0.72-0.29= 0.43
T27 + 4-Picoline-N-oxide	0.72-0.29= 0.43
T27 + Pyridine-N-oxide	0.72-0.29= 0.43
T27 + Pyrazine-N-oxide	0.72-0.29= 0.43

8.3.2. Thermogravimetric analysis (TGA) of target cavitands and guest molecules

Table 8.3. summarizes the weight loss in TGA analysis and corresponding stoichiometry of the cavitands with the guests. **T24** and **T27** interacts with all the guests, **T25** shows host-guest interactions with only cyclic rigid guests, and **T26** does not interact with any of the guests. In all the instances, two solvent molecules ($CDCl_3$) were present.

Table 8.3. Host-guest stoichiometry from weight loss in TGA analysis.

Guest	2-methylbutyric acid	2-methylpentanoic acid	2-methylhexanoic acid	Isoborneol	Menthol
T24	21.88% = 2guests	26.89% = 2guests	29.74%= 2guests	27.67%= 2guests	28.73%= 2guests
T25	11.37% = 2$CDCl_3$	14.76% = 2$CDCl_3$	15.03% = 2$CDCl_3$	24.65%= 2guests	26.58%= 2guests
T26	15.32%= 2$CDCl_3$	14.54%= 2$CDCl_3$	14.63%= 2$CDCl_3$	15.64%= 2$CDCl_3$	15.42%= 2$CDCl_3$

Guest	3-Picoline-N-oxide	4-Picoline-N-oxide	Pyridine-N-oxide	Pyrazine-N-oxide
T27	17.32% = 2guests	19.27%= 2guests	18.26% = 2guests	17.56%= 2guests

8.3.3. NMR titrations

The binding affinity of the hosts, towards the guest were evaluated in solution using ^{1}H NMR spectroscopy. We expected an O-H•••N interaction to form in solution between the cavitands and guests. We focused our work on ^{1}H NMR titration as a way of quantifying this binding event, where the binding of the hydrogen-bond donor and acceptor was monitored by changes in the chemical shifts of the hydrogen atoms. An example of a positive and negative host-guest interaction is illustrated in Figure 8.7.

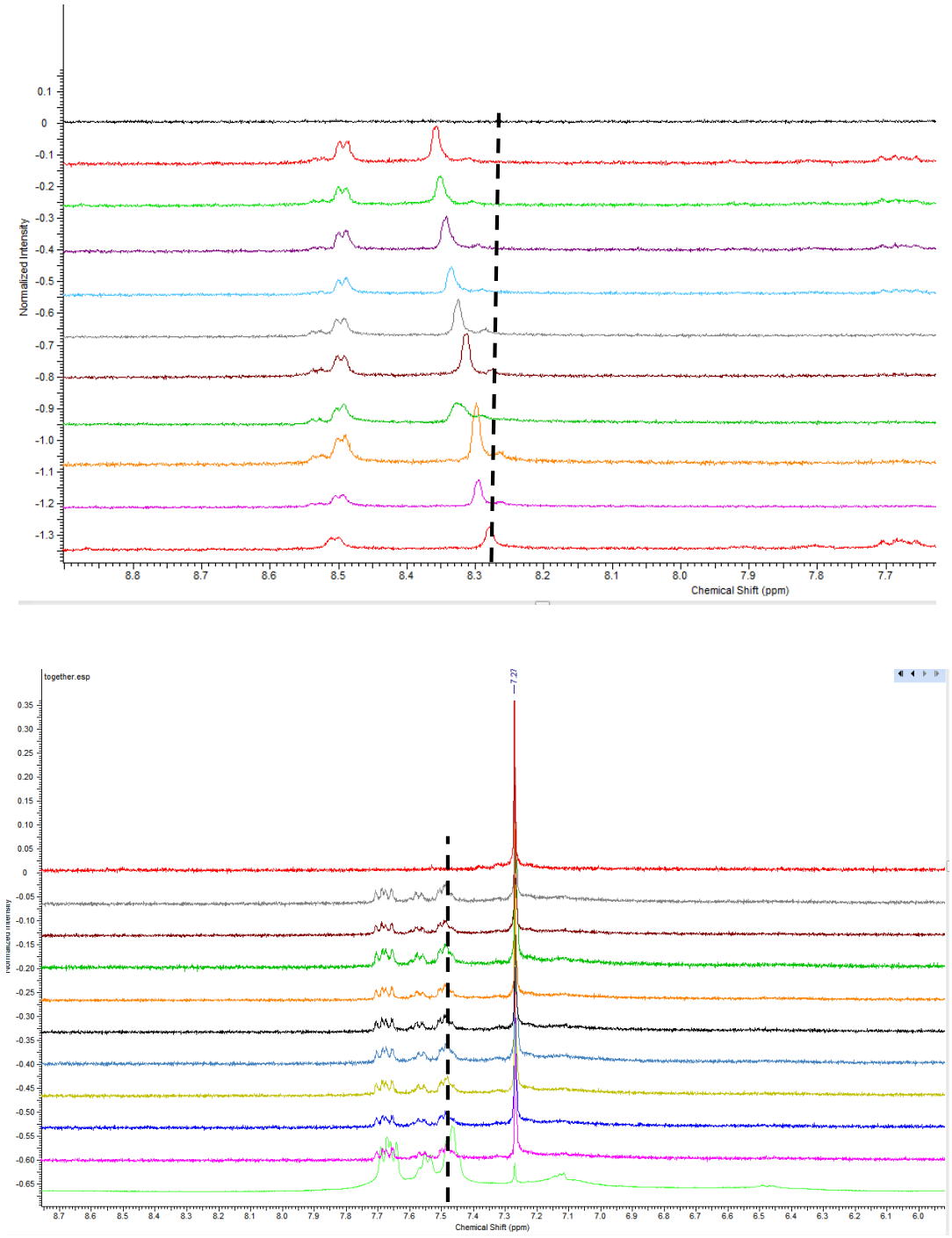

Figure 8.7. An example of positive (top) and negative (bottom) host-guest interactions.

The changes in δ ppm values ($\delta_{\text{bound host}} - \delta_{\text{free host}}$) obtained by titrating the guest (2-methylbutyric acid) with the host **T24** were plotted against the guest concentration and by non-linear curve fitting into equation 8.1 afforded Ka = 1412 M^{-1}, Figure 8.8. Jobs plot analysis of the results revealed 1:2

complexation which was consistent with TGA in the solid state. Similar analysis was done for all host-guest pairs and the results are summarized in Table 8.4.

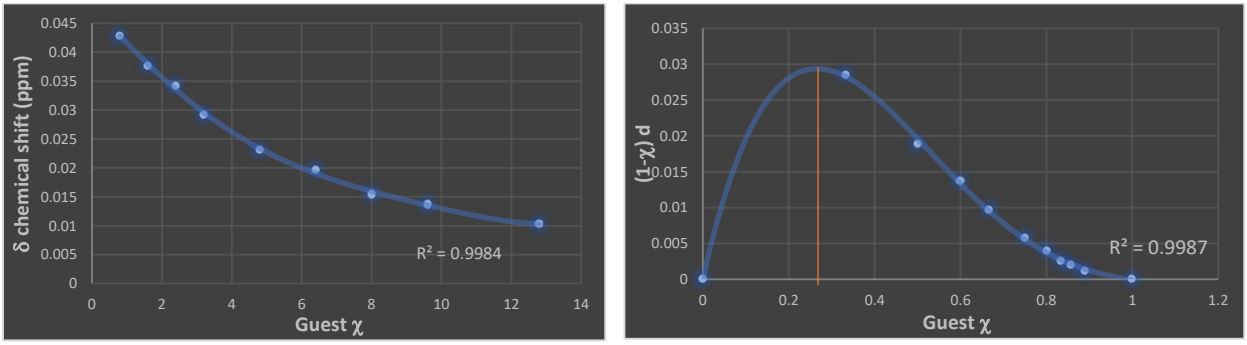

Figure 8.8. Titration curve of 2-methylbutyric acid into **T24** in $CDCl_3$ at 25 °C (left); Jobs plot of [**T24**: (2-Methylbutyric acid)$_2$] pair at 25 °C (right).

Table 8.4. Summary of host-guest interactions for **T24-T27.**

Guest	**T24**		**T25**		**T26**	
	Stoichiometry	Binding constant	Stoichiometry	Binding constant	Stoichiometry	Binding constant
2-Methylbutyric acid	**1:2**	1412 M^{-1}	No interaction	-	No interaction	-
2-Methylpentanoic acid	**1:2**	1552 M^{-1}	No interaction	-	No interaction	-
2-Methylhexanoic acid	**1:2**	1732 M^{-1}	No interaction	-	No interaction	-
Menthol	**1:2**	1638 M^{-1}	**1:2**	1680 M^{-1}	No interaction	-
Isoborneol	**1:2**	1750 M^{-1}	**1:2**	1786 M^{-1}	No interaction	-

Guest	**T27**	
	Stoichiometry	Binding constant
3-Picoline-N-oxide	**1:2**	2156 M^{-1}
4-Picoline-N-oxide	**1:2**	2765 M^{-1}
Pyridine-N-oxide	**1:2**	2635M^{-1}
Pyrazine-N-oxide	**1:2**	2743 M^{-1}

8.4. Discussions

8.4.1. Fragrant compounds

T24-T26 have similar MEPS for the acceptor-N site which suggests that they would demonstrate comparable host-guest interactions. The HBP calculations for **T24-T25** in combination with the fragrant compounds exhibit a positive value and for **T26** a negative value, Table 8.2. HBP is dependent on the statistical analysis of the defined functional groups of the host and guest present in the Cambridge Structural Database (CSD). The defined functional groups of **T24-T25** are pyridine-N and that of the guests are carboxylic acid-COOH/ alcohol-OH therefore, we observe same ΔHBP results for all **T24-T25** combinations.

*8.4.1.1. Host-guest interactions with **T24***

The TGA analysis for **T24** in combination with the guests indicates a consistent weight loss of ~21-29%. The weight loss corresponds to two guest molecules and two solvent molecules ($2CDCl_3$). Although **T24** had four arms where it could interact with the guests exhibiting a 1:4 stoichiometry. Due to the presence of steric cloud on the upper rim of the cavitands **T24** displays a 1:2 stoichiometry with the guests. In case of [**T24**:(2-Methyl butyric acid)$_2$] the weight loss in the TGA analysis starts at ~176 ^{0}C and is completed at 400 ^{0}C. The weight loss corresponds to 2 guest molecules, and the temperature at which the weight loss starts is the boiling point of the guest. The fact that it takes over 200 ^{0}C to completely loose the guest, suggests a strong host-guest binding. A similar trend was observed for **T24** and other fragrant molecules.

The NMR titrations for **T24** in combination with guests was varied from 1:0.5 to 1:8 stoichiometry. The host concentration was kept constant and we increased the guest concentration. With the increasing guest concentration, the ($\delta_{\text{bound host}} - \delta_{\text{free host}}$) value kept decreasing due to OH•••N interaction between host-guest. After a point the ($\delta_{\text{bound host}} - \delta_{\text{free host}}$) became constant, since host has completely reacted with the guest and any more addition of guest is extra unreacted guest. Hence the ($\delta_{\text{bound host}} - \delta_{\text{free host}}$) becomes constant, Figure 8.8. We plotted a Jobs plot which indicated a 1:2 stoichiometry for the **T24** combined with guest, Table 8.4. Additionally, we calculated the binding constants for all the combinations with **T24** and the results ranged between 1412-1750 M^{-1}.

Based on the TGA, ^{1}H NMR titrations and Job's plot, guest binding takes place on the upper rim of the cavitand via OH···N hydrogen bonds and one cavitand was capable of binding to two guest molecules.

*8.4.1.2. Host-guest interactions with **T25***

TGA analysis for **T25** in combination with aliphatic guests demonstrates a weight loss of 11-15%. This weight loss corresponds to the presence of two solvent molecules ($2CDCl_3$). The temperature at which the weight loss starts is below 100 °C and is completed by 200 °C which was much below than what we observed for **T24** and guest compounds (~200-400 °C), Figure 8.9.

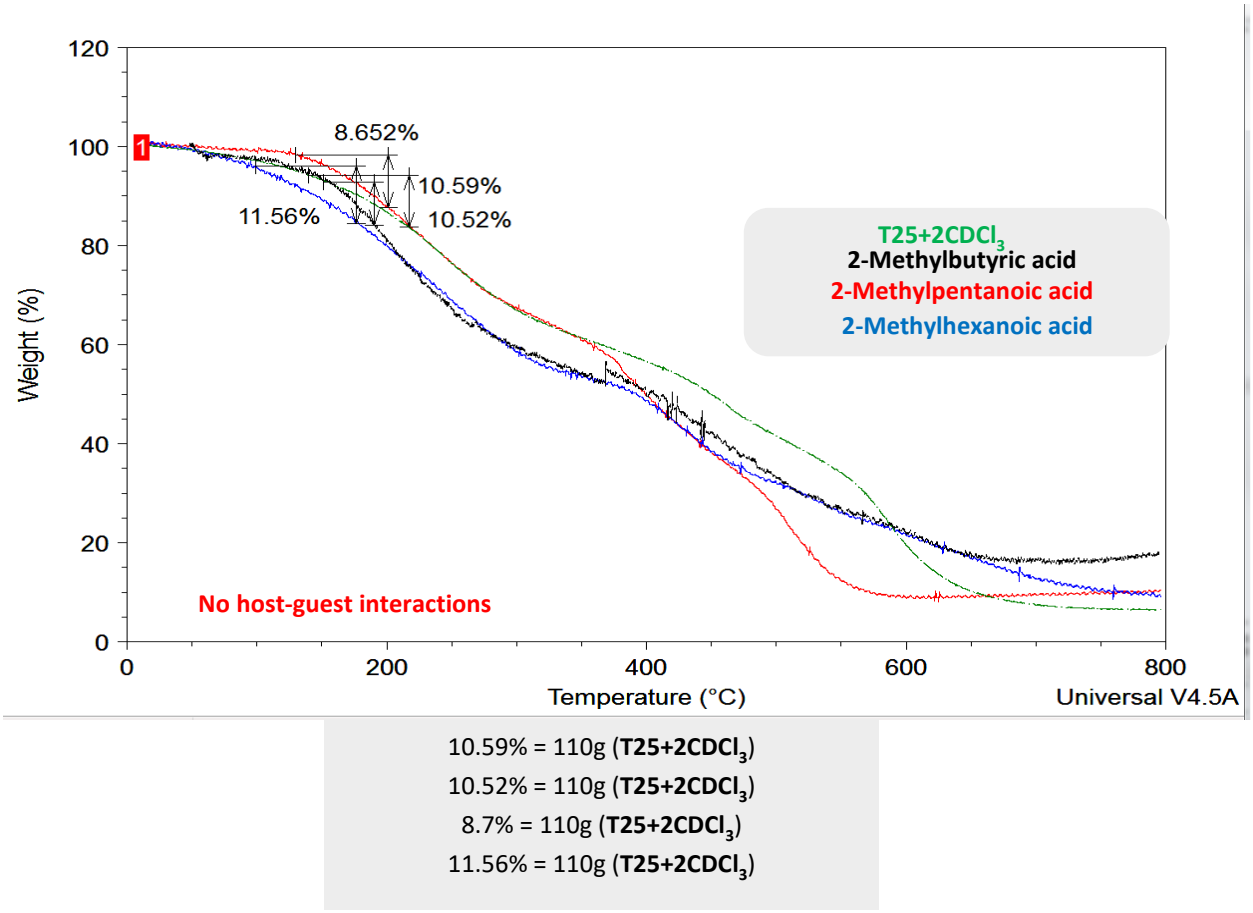

10.59% = 110g (**T25+2CDCl$_3$**)
10.52% = 110g (**T25+2CDCl$_3$**)
8.7% = 110g (**T25+2CDCl$_3$**)
11.56% = 110g (**T25+2CDCl$_3$**)

Figure 8.9. TGA analysis of **T25** with aliphatic guest and their corresponding weight losses.

For menthol and isoborneol the TGA weight loss was 24-26% at 200-400 °C, which is equivalent to two guest and two solvent molecules. The stoichiometry observed with menthol and isoborneol was 1:2. **T24** and **T25** are structural isomers. However, we see a difference in the host-guest interactions between them.

To further investigate the selectivity of **T25** towards rigid guests, we conducted experiments where **T25** was subjected to a mixture of aliphatic and cyclic guests. We prepared six different combinations of mixtures and analyzed them according to TGA weight loss. In each case the weight loss in TGA corresponded to cyclic guests and solvent molecules, Table 8.5.

Table 8.5. Summary of the selectivity outcome for **T25**.

Guest mixtures	TGA data analysis
2-Methylbutyric acid + Isoborneol	2Isborneol
2-Methylbutyric acid +Menthol	2Menthol
2-Methylpentanoic acid + Isoborneol	2Isborneol
2-Methylpentanoic acid + Menthol	2Menthol
2-Methylhexanoic acid + Isoborneol	2Isborneol
2-Methylhexanoic acid + Menthol	2Menthol

The NMR titrations for **T25** in combination with guests was also varied from 1:0.5 to 1:8 stoichiometry. With aliphatic guests, **T25** did not show any change in the ^{1}H NMR chemical shift. No change in the chemical shift corresponds to no formation of OH•••N interactions. However, **T25** in combination with isoborneol and menthol displays a 1:2 stoichiometry with binding constants of 1680 and 1786 M^{-1} respectively. The binding constants of **T25** with isoborneol and menthol is comparable to that of **T24**. The TGA analysis and NMR titrations display similar results.

The selectivity of the aliphatic guests to bind specifically with **T24** can be rationalized based on the following hypothesis:

a) We calculated the most stable structure of **T24** and **T25** using DFT calculations and basis set B3LYP and 6-31++G** (calculations were done excluding the hexyl feet), Figure 8.10. The calculations show that in **T24** the pyridine-N are facing away from each other and in **T25** the pyridine-N are facing upwards. Hence, in **T24** the pyridine-N have sufficient space for flexible aliphatic acids to make OH•••N interaction. In case of **T25** the pyridine-N available for binding are facing upwards which leads to steric hindrance between the non-bonding parts, hence these flexible guests cannot form any host-guest interactions.

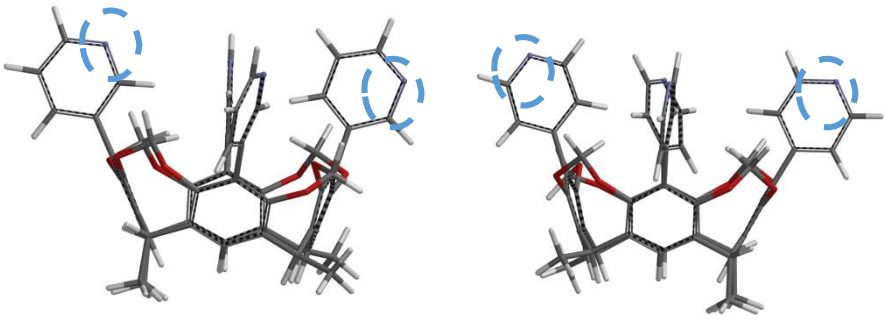

Figure 8.10. Most stable geometry of **T24** (left) and **T25** (right).

b) Our second hypothesis is that the cavitands are arranged in "foot in the mouth" type of packing which adds to the steric hindrance in the upper rim of the cavitands. Although we don't have a crystal structure at this point. However, based on the other existing crystal structures of cavitands in Chapter 7, where the upper rim does not participate in any interactions, such arrangements are frequently observed. Figure 8.11 illustrates an example of "foot in the mouth" type of packing.

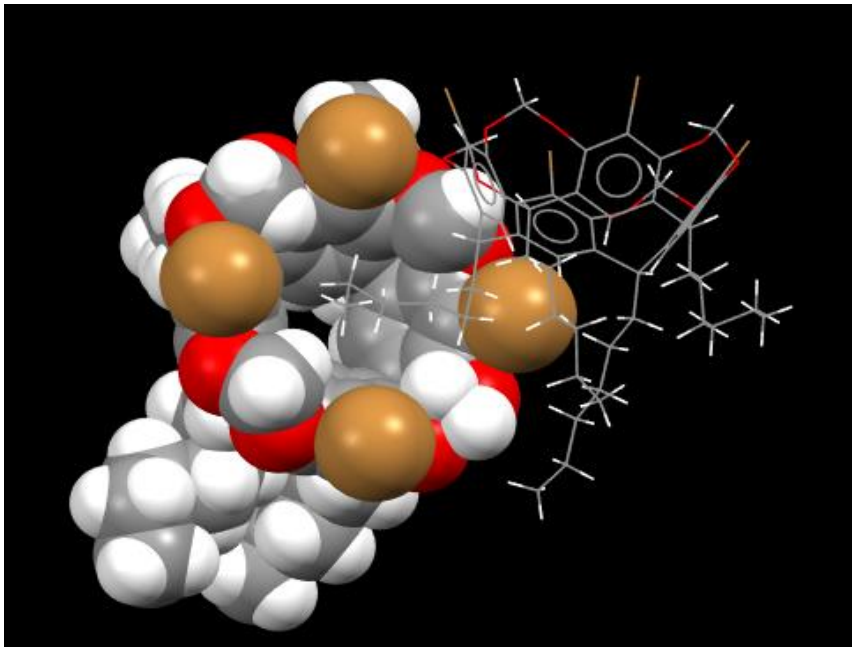

Figure 8.11. An example of **T11** with "foot in the mouth" packing.

c) Menthol and Isoborneol mimics the host-interaction in **T24** and **T25** because they are rigid and small. Hence, the donor OH can interact with pyridine-N even in the presence of the steric cloud.

A control experiment was conducted with **T24** and **T25** in combination with benzoic acid to confirm the formation of OH•••N interactions with rigid guests. We observed that benzoic acid interacts with both **T24** and **T25** in 1:2 stoichiometry and binding constants of 1856 M^{-1}, Table 8.6.

Table 8.6. Summary of host-guest interactions for **T24-T25** with benzoic acid.

Guest	**T24**		**T25**	
	Stoichiometry	Binding constant	Stoichiometry	Binding constant
Benzoic acid	**1:2**	1856 M^{-1}	**1:2**	1856 M^{-1}

*8.4.1.3. Host-guest interactions with **T26***

The NMR titrations and TGA analysis indicate that **T26** does not interact with any of the guests. This can be attributed to stronger homomeric interactions of pyrazole N-H•••N in **T26** than the heteromeric interaction O-H•••N. The HBP calculations attempted on **T26**, in combination with the guests, predicts that the homomeric interactions were preferred over heteromeric interactions, Table 8.2.

8.4.1.4. Improved stability of the fragrant compounds

The aliphatic guests used in this study are liquid at room temperature. Successful host-guest interactions resulted the final product as solid-glue like material. One of the goals of this study was to examine if we can improve the volatility of the fragrant compounds via host-guest interactions. Qualitative study was performed to test if the volatility of the compounds had improved. For the fragrant compounds by itself, it took 5-10 mins for a drop of guests to completely evaporate at room temperature. We followed that same process for cavitands containing guests, where the resulting solids were kept on a slide at room temperature. We performed NMR of the resulting solid every 6-7 days to check for the presence of guest peaks. We observed guest peaks in the NMR for 30 days after which we did not test it further. This analysis suggests that the volatility of the fragrant compounds was improved from 5-10mins to over a month.

8.4.2. Heterocyclic-N-oxides

HBP calculations predicted formation of a host-guest interaction between **T27** in combination with the guest compounds. TGA analysis and NMR titrations were carried out with **T27** in combination with heterocyclic-N-oxides. TGA analysis indicate a weight loss which corresponds to two guest molecules and presence of two solvent molecules, Table 8.3. The presence of two solvent molecules was consistent in all the host-guest interactions.

NMR titrations conducted with **T27** and N-oxide guests were varied from 1:0.5 stoichiometry to 1:8. The Job's plot calculations indicate a 1:2 stoichiometry in all the cases. A Job's plot of [**T27**:(Pyrazine-N-oxide)$_2$] is illustrated in Figure 8.12.

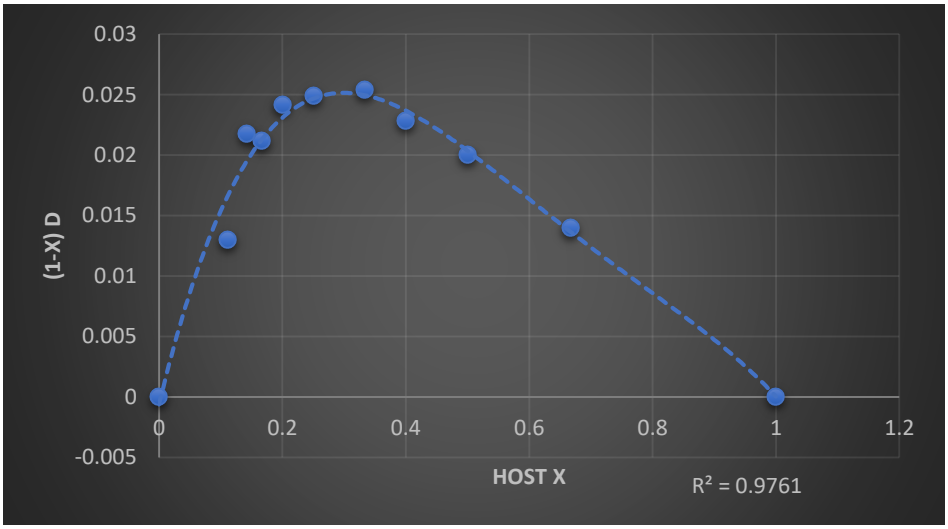

Figure 8.12. Jobs plot of [**T27**: (Pyrazine-N-oxide)$_2$] pair at 25 °C (right).

The binding constants of **T27** with guest compounds were observed between 2156-2743 M^{-1}, which is significantly higher than what we obtained for **T24-T25**. The ΔHBP values for **T27** were also significantly higher than **T24-T25**. The difference in the binding constants can be attributed to stronger OH•••O interaction than OH•••N. Since, oxygen is negatively charged in N-oxides and is a better Lewis base than pyridine-N contributing to higher binding constants.

8.5. Conclusions

1. HBP correctly predicted the host-guest interactions for **T24**, **T26** and **T27**. However, it fails to predict the selectivity of **T25** for rigid cyclic guests over aliphatic guests.
2. **T24** interacts in 1:2 stoichiometry with all fragrant guest compounds, **T25** interacts selectively with cyclic guest compounds in 1:2 stoichiometry, and **T26** does not participate in any host-guest interactions. Hydrogen-bond donor cavitand **T27** interacts with heterocyclic-N-oxides in 1:2 stoichiometry.

8.6. References

(1) Hooley, R. J.; Rebek, J. Chemistry and Catalysis in Functional Cavitands. *Chem Biol* **2009**, *16* (3), 255–264. https://doi.org/10.1016/j.chembiol.2008.09.015.

(2) Biros, S. M.; Rebek, Jr., J. Structure and Binding Properties of Water-Soluble Cavitands and Capsules. *Chem. Soc. Rev.* **2007**, *36* (1), 93–104. https://doi.org/10.1039/B508530F.

(3) Tucci, F. C.; Rudkevich, D. M.; Rebek, J. Deeper Cavitands. *J. Org. Chem.* **1999**, *64* (12), 4555–4559. https://doi.org/10.1021/jo990209z.

(4) Moran, J. R.; Karbach, S.; Cram, D. J. Cavitands: Synthetic Molecular Vessels. *J. Am. Chem. Soc.* **1982**, *104* (21), 5826–5828. https://doi.org/10.1021/ja00385a064.

(5) Ghang, Y.-J.; Perez, L.; Morgan, M. A.; Si, F.; Hamdy, O. M.; Beecher, C. N.; Larive, C. K.; Julian, R. R.; Zhong, W.; Cheng, Q.; et al. Anionic Deep Cavitands Enable the Adhesion of Unmodified Proteins at a Membrane Bilayer. *Soft Matter* **2014**, *10* (48), 9651–9656. https://doi.org/10.1039/C4SM02347A.

(6) Perez, L.; Mettry, M.; Hinman, S. S.; Byers, S. R.; McKeating, K. S.; Caulkins, B. G.; Cheng, Q.; Hooley, R. J. Selective Protein Recognition in Supported Lipid Bilayer Arrays by Tailored, Dual-Mode Deep Cavitand Hosts. *Soft Matter* **2017**, *13* (21), 3966–3974. https://doi.org/10.1039/c7sm00192d.

(7) Körner, S. K.; Tucci, F. C.; Rudkevich, D. M.; Heinz, T.; Jr, J. R. A Self-Assembled Cylindrical Capsule: New Supramolecular Phenomena through Encapsulation. *Chemistry – A European Journal* **2000**, *6* (1), 187–195. https://doi.org/10.1002/(SICI)1521-3765(20000103)6:1<187::AID-CHEM187>3.0.CO;2-I.

(8) Turunen, L.; Pan, F.; Beyeh, N. K.; Trant, J. F.; Ras, R. H. A.; Rissanen, K. Bamboo-like Chained Cavities and Other Halogen-Bonded Complexes from Tetrahaloethynyl Cavitands with Simple Ditopic Halogen Bond Acceptors. *Crystal Growth & Design* **2018**, *18* (1), 513–520. https://doi.org/10.1021/acs.cgd.7b01517.

(9) Adachi, T.; Ward, M. D. Versatile and Resilient Hydrogen-Bonded Host Frameworks. *Acc. Chem. Res.* **2016**, *49* (12), 2669–2679. https://doi.org/10.1021/acs.accounts.6b00360.

(10) MacGillivray, L. R.; Atwood, J. L. A Chiral Spherical Molecular Assembly Held Together by 60 Hydrogen Bonds. *Nature* **1997**, *389*, 469–472. https://doi.org/10.1038/38985.

(11) Gerkensmeier, T.; Iwanek, W.; Agena, C.; Fröhlich, R.; Kotila, S.; Näther, C.; Mattay, J. Self-Assembly of 2,8,14,20-Tetraisobutyl-5,11,17,23-Tetrahydroxyresorc[4]Arene. *European Journal of Organic Chemistry* **1999**, *1999* (9), 2257–2262. https://doi.org/10.1002/(SICI)1099-0690(199909)1999:9<2257::AID-EJOC2257>3.0.CO;2-H.

(12) Shivanyuk, A.; Rebek, J. Reversible Encapsulation by Self-Assembling Resorcinarene Subunits. *PNAS* **2001**, *98* (14), 7662–7665. https://doi.org/10.1073/pnas.141226898.

(13) Ghang, Y.-J.; Lloyd, J. J.; Moehlig, M. P.; Arguelles, J. K.; Mettry, M.; Zhang, X.; Julian, R. R.; Cheng, Q.; Hooley, R. J. Labeled Protein Recognition at a Membrane Bilayer Interface by Embedded Synthetic Receptors. *Langmuir* **2014**, *30* (34), 10161–10166. https://doi.org/10.1021/la502629d.

(14) Numanoğlu, U.; Şen, T.; Tarimci, N.; Kartal, M.; Koo, O. M. Y.; Önyüksel, H. Use of Cyclodextrins as a Cosmetic Delivery System for Fragrance Materials: Linalool and Benzyl Acetate. *AAPS PharmSciTech* **2007**, *8* (4), 34–42. https://doi.org/10.1208/pt0804085.

(15) Reinhoudt, D. N. Supramolecular Chemistry and Heterocycles. In *Reference Module in Chemistry, Molecular Sciences and Chemical Engineering*; Elsevier, 2013. https://doi.org/10.1016/B978-0-12-409547-2.05396-8.

(16) Fourmentin, S.; Crini, G.; Lichtfouse, E. *Cyclodextrin Applications in Medicine, Food, Environment and Liquid Crystals*; Springer, 2018.

(17) Otero-Espinar, F. J.; Torres-Labandeira, J. J.; Alvarez-Lorenzo, C.; Blanco-Méndez, J. Cyclodextrins in Drug Delivery Systems. *Journal of Drug Delivery Science and Technology* **2010**, *20* (4), 289–301. https://doi.org/10.1016/S1773-2247(10)50046-7.

(18) Parkin, I. P. Supramolecular Chemistry. J.W. Steed and J.L. Atwood. John Wiley & Sons Ltd, Chichester, 2000. Xxvii + 745 Pages. £29.95 (Paperback). ISBN 0-471-98791-3. *Applied Organometallic Chemistry* **2001**, *15* (3), 236–236. https://doi.org/10.1002/aoc.125.

(19) Florea, M.; Nau, W. M. Strong Binding of Hydrocarbons to Cucurbituril Probed by Fluorescent Dye Displacement: A Supramolecular Gas-Sensing Ensemble. *Angew. Chem. Int. Ed. Engl.* **2011**, *50* (40), 9338–9342. https://doi.org/10.1002/anie.201104119.

(20) Petroselli, M.; Angamuthu, V.; Rahman, F.-U.; Zhao, X.; Yu, Y.; Rebek, J. Radical Reactions in Cavitands Unveil the Effects of Affinity on Dynamic Supramolecular Systems. *J. Am. Chem. Soc.* **2020**, jacs.9b11595. https://doi.org/10.1021/jacs.9b11595.

(21) Hirose, K. A Practical Guide for the Determination of Binding Constants. *Journal of Inclusion Phenomena* **2001**, *39* (3), 193–209. https://doi.org/10.1023/A:1011117412693.

(22) Banjare, M. K.; Behera, K.; Satnami, M. L.; Pandey, S.; Ghosh, K. K. Host–Guest Complexation of Ionic Liquid with α- and β-Cyclodextrins: A Comparative Study by 1H-NMR, 13C-NMR and COSY. *New J. Chem.* **2018**, *42* (17), 14542–14550. https://doi.org/10.1039/C8NJ01840E.

(23) Fine Fragrance & Perfumes.Pdf.

(24) Dunkel, M.; Schmidt, U.; Struck, S.; Berger, L.; Gruening, B.; Hossbach, J.; Jaeger, I. S.; Effmert, U.; Piechulla, B.; Eriksson, R.; et al. SuperScent--a Database of Flavors and Scents. *Nucleic Acids Research* **2009**, *37* (Database), D291–D294. https://doi.org/10.1093/nar/gkn695.

(25) Mfuh, A. M.; Larionov, O. V. Heterocyclic N-Oxides – An Emerging Class of Therapeutic Agents. *Curr Med Chem* **2015**, *22* (24), 2819–2857.

(26) Ihsan, A.; Wang, X.; Tu, H.-G.; Zhang, W.; Dai, M.-H.; Peng, D.-P.; Wang, Y.-L.; Huang, L.-L.; Chen, D.-M.; Mannan, S.; et al. Genotoxicity Evaluation of Mequindox in Different Short-Term Tests. *Food and Chemical Toxicology* **2013**, *51*, 330–336. https://doi.org/10.1016/j.fct.2012.10.003.

(27) Macrae, C. F.; Bruno, I. J.; Chisholm, J. A.; Edgington, P. R.; McCabe, P.; Pidcock, E.; Rodriguez-Monge, L.; Taylor, R.; Streek, J. van de; Wood, P. A. Mercury CSD 2.0 – New Features for the Visualization and Investigation of Crystal Structures. *J Appl Cryst* **2008**, *41* (2), 466–470. https://doi.org/10.1107/S0021889807067908.

(28) Allen, F. H. The Cambridge Structural Database: A Quarter of a Million Crystal Structures and Rising. *Acta Crystallogr., B* **2002**, *58* (Pt 3 Pt 1), 380–388.

(29) Mapp, L. K.; Coles, S. J.; Aitipamula, S. Design of Cocrystals for Molecules with Limited Hydrogen Bonding Functionalities: Propyphenazone as a Model System. *Crystal Growth & Design* **2017**, *17* (1), 163–174. https://doi.org/10.1021/acs.cgd.6b01399.

(30) Vologzhanina, A. V.; Sokolov, A. V.; Purygin, P. P.; Zolotarev, P. N.; Blatov, V. A. Knowledge-Based Approaches to H-Bonding Patterns in Heterocycle-1-Carbohydrazoneamides. *Crystal Growth & Design* **2016**, *16* (11), 6354–6362. https://doi.org/10.1021/acs.cgd.6b00990.

(31) Wood, P. A.; Feeder, N.; Furlow, M.; Galek, P. T. A.; Groom, C. R.; Pidcock, E. Knowledge-Based Approaches to Co-Crystal Design. *CrystEngComm* **2014**, *16* (26), 5839–5848. https://doi.org/10.1039/C4CE00316K.

(32) Kuntz, I. D.; Gasparro, F. P.; Johnston, M. D.; Taylor, R. P. Molecular Interactions and the Benesi-Hildebrand Equation. *J. Am. Chem. Soc.* **1968**, *90* (18), 4778–4781. https://doi.org/10.1021/ja01020a004.

Chapter 9 – Summary

In our first study we examined, six different target molecules in combination with 25 possible co-formers and used the hydrogen-bond propensity (HBP) protocol for predicting if a co-crystal would form or not. The correct outcome was successfully predicated 92-95% of the time which indicates that for this series of small molecules, HBP is a very reliable indicator for determining if a co-crystal will form between a target molecule and a particular co-former, Figure 9.1.

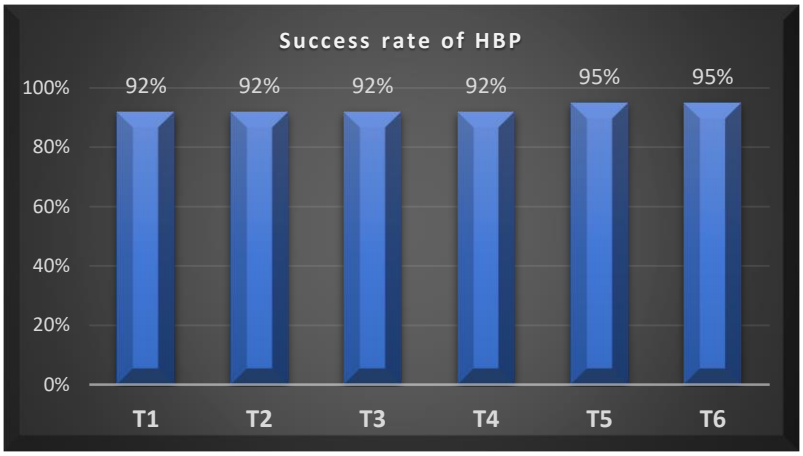

Figure 9.1. Validation study for HBP in predicting co-crystallization outcomes.

In our second study we used molecular electrostatic potential surfaces (MEPS) to rank the best donor-acceptor pair for predicting the most likely synthon formation, Figure 9.2. This study shows that, although hydrogen and iodine are far apart in the periodic table, if used in the same chemical environment then can mimic each other. This structural similarity could be significant in biomedical areas as halogen bonds are hydrophobic and lipophilic when compared to hydrogen bonds.

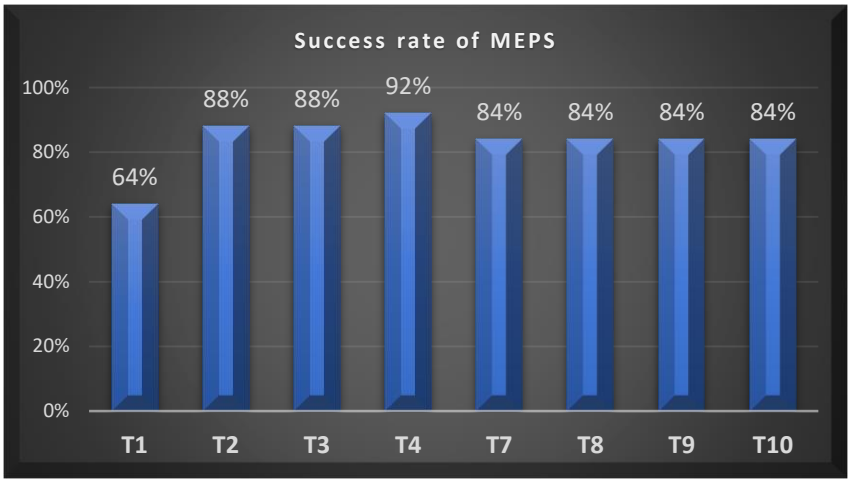

Figure 9.2. Validation study for MEPS in predicting co-crystallization outcomes.

Next, the predictive abilities of three different approaches were compared for predicting co-crystallization outcomes for two known drug molecules, Nevirapine and Diclofenac, and a series of potential co-formers. The hydrogen-bond propensity (HBP) tool gave the correct result in 26 out of 30 cases, whereas a hydrogen-bond coordination (HBC) method predicted the correct outcome in 22 out of 30 cases. Finally, calculated hydrogen-bond energies (HBE) using a simple electrostatic model, gave the correct result in 23 out of 30 experiments. In cases, where the crystal structure of a co-crystal of either Nevirapine or Diclofenac was known, we also examined how well the three methods predicted which primary hydrogen-bond interactions were present in the crystal structure. HBP correctly predicted 6 out of 6 cases, HBC could not predict any of the synthon formations correctly, and HBE successfully predicted 1 out of 6 cases, Figure 9.3.

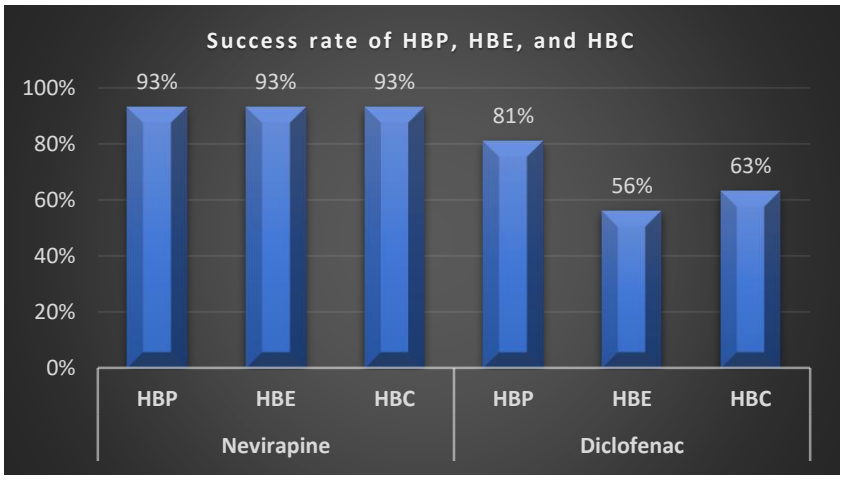

	Co-crystal	Experimental	HBP	HBC	HBE
Nevirapine	Yes	IV & V	IV & V	IV	II, IV & V
Diclofenac (Pyridines/Pyrimidines)	Yes	**VII**, XI & XII	**VII**, XI & XII	XI	**VII**, XI & XII
Diclofenac (Pyrazoles)	No	**X**	**X**	XV	XV

Figure 9.3. Validation study for HBP, HBE, and HBC in predicting co-crystallization outcomes (top) and synthon formations (bottom).

Although there is an abundance of studies reported on small and rigid targets, there is scarcity of reports based on large and flexible compounds for predicting co-crystallization screening experiments. Hence, in this study three predictive methods HBP, HBE, and molecular complementarity (MC) were employed on seven APIs in combination with 42 co-formers on the generally regarded as safe (GRAS) list. The targets used in this study have a molecular weight of 400-600 g/mol and have more than three rotatable bonds. The validation studies indicated that a combination of HBP and MC yielded the best results with an overall accuracy of 79%, Figure 9.4.

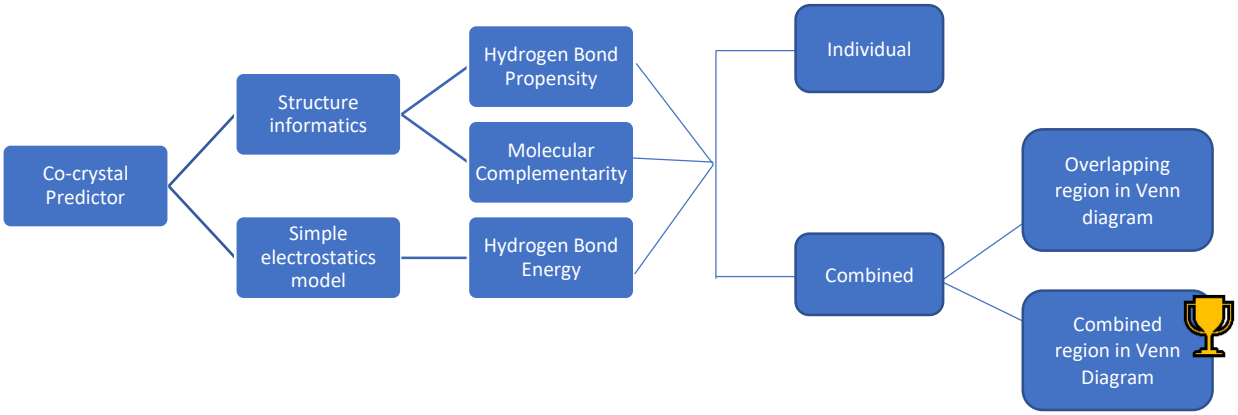

Figure 9.4. Strategies to predict co-crystallization outcomes.

The predictive approaches investigated thus far were complex and required in-depth knowledge of either theoretical, quantum-mechanical, or statistical data analysis. In order to address the growing demand of co-crystallization and co-crystallization-based approaches to access new solid forms in

various fields, we developed CoForm which is cheaper, faster, and more reliable for predicting the outcome of co-crystallization experiments, Figure 9.5.

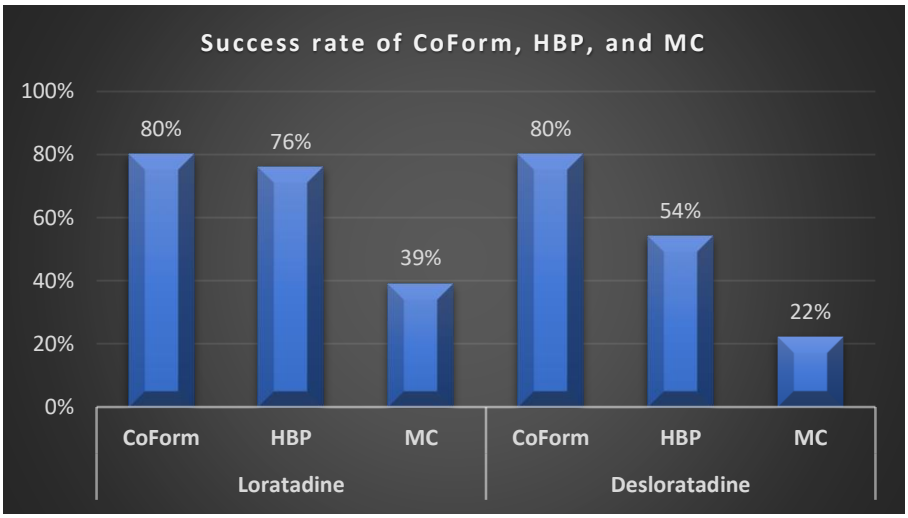

Figure 9.5. Validation study for CoForm in comparison to HBP and MC in predicting co-crystallization outcomes.

In order to investigate guest encapsulation via cavity inclusion we synthesized six cavitands where the rim did not participate in any conventional hydrogen/ halogen bonding. Five solvents (xylene, dichloromethane, ethyl acetate, acetonitrile, and dimethyl sulfoxide) with varied dipole moment were selected as guests. We found that cavitands encapsulated guests in a variety of arrangements with different stoichiometries as illustrated in Figure 9.6. In addition, selectivity study of equimolar mixtures of solvents suggested that the cavitands were selective towards dimethyl sulfoxide which had the highest dipole moment.

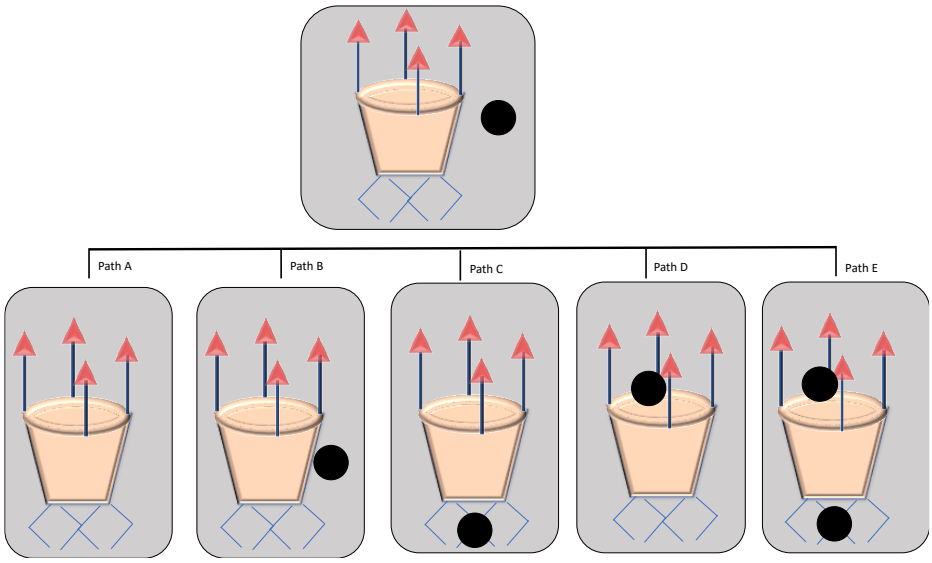

Figure 9.6. Cartoon representation of observed solvent binding modes to a cavitand.

Finally, we examined cavitands as molecular containers, for storage of volatile fragrant compounds and heterocyclic-N-oxides. The cavitands interacted with the fragrant compounds in 1:2 stoichiometry which was established by NMR titrations and TGA analysis. We found that the host-guest interactions improved the volatility of the fragrant compounds from 5-10 mins to over a month. The heterocyclic N-oxides was also observed to interact in 1:2 stoichiometry. The binding preferences of the guests are illustrated in Figure 9.7.

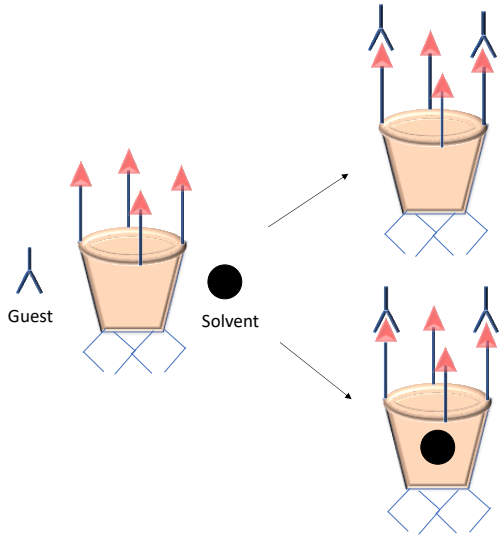

Figure 9.7. Cartoon representation of observed host-guest binding.

Appendix A – Design, develop and evaluate molecular complementarity as a predictive tool for co-crystal design.

A.1. Rationale

MC in the default setting, uses five descriptors, Scheme **A.1**. Each descriptor has a criterion to afford a "PASS" when it is predicted to form a co-crystal or a "FAIL" when it predicts not to form a co-crystal. For MC to predict a co-crystal formation, an overall "five PASS" from all the five descriptors is required.

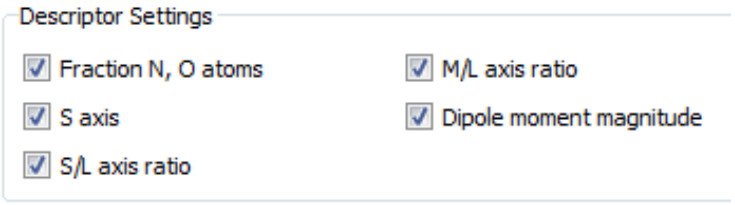

Scheme A.1. Default descriptor setting for molecular complementarity.

The compounds examined in this study are flexible. Therefore, it might exist in different conformations. To factor in the conformational insights, the five most stable conformations of both APIs and co-formers were incorporated in MC. The conformers were generated using Mercury and then passed through the five descriptors to afford a "PASS/ FAIL," Scheme **A.1**. Complementary shaped conformers of the API and co-former provided a "PASS," and the rest resulted in a "FAIL." Finally, the 125 (25 conformations X 5 descriptors) "PASS/ FAIL" combinations, contributed to yield a hit rate %. Hit rate% is the number of "PASS" over the total number of conformer combinations. If the hit rate ≥40%, it was assigned a "YES" to co-crystallization, and if hit rate <40%, it was designated as "NO" to co-crystallization.

Similar calculations were repeated, using the conformers generated using Spartan'14 Version 1.1.0, implementing molecular mechanics (conformer distribution in vacuum). The difference between the Spartan and Mercury conformer calculations is that the former calculates the conformers based on relative low energy, and the latter uses structure informatics. Subsequently, a comparison study employing both methods was investigated to comprehend the differences between them.

Seven APIs were used, Figure **A.1**, to explore the reliability of MC for predicting co-crystallization outcomes. We attempted co-crystal experiments on the seven APIs with 42 GRAS[36] list co-formers, Table **A.1**.

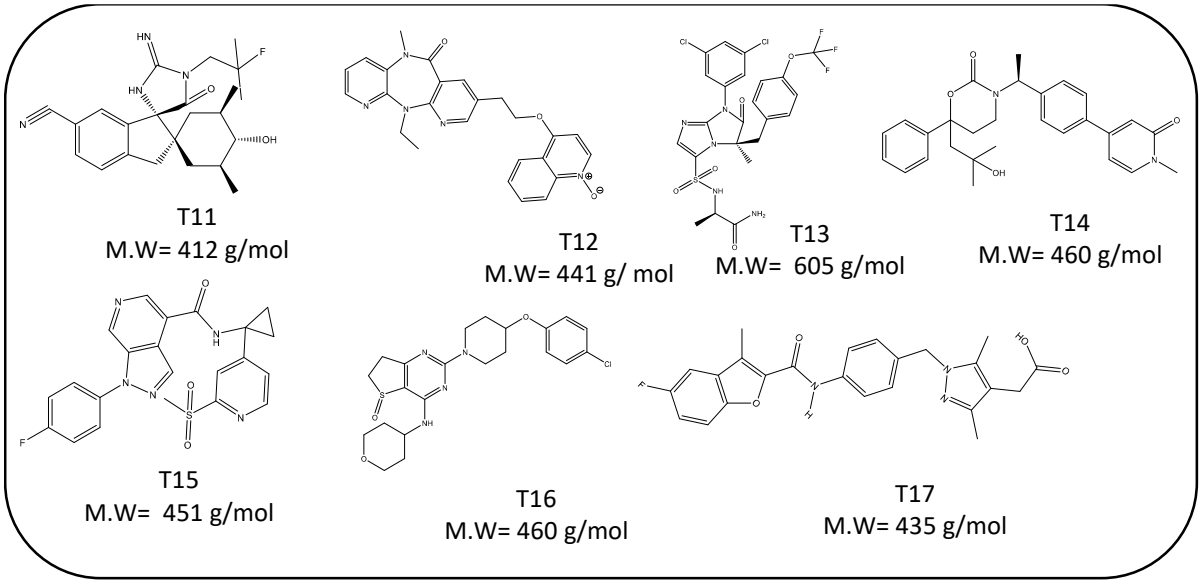

Figure A.1. Seven APIs of interest.

Table A.1. Selected potential co-formers.

Xanthine	Theophylline	Benzenesulfonic acid	Caffeine
Riboflavin	Piperazine	Methylparaben	Mannitol
Maltitol	Malic acid	L-tartaric acid	Glycolic acid
L-glutamic acid	Cholic acid	Glycine	D-Glucuronic acid
Folic acid	Hydro cinnamic acid	Apigenin	L-serine
EDTA	4-hydroxybenzoic acid	L-mandelic acid	Benzoic acid
Pamoic acid	Fumaric acid	Adipic acid	Glutaric acid
Citric acid	L-proline	Gentisic acid	Malonic acid
Isonicotinamide	Oxalic acid	Maleic acid	Sorbic acid
Nicotinamide	Urea	Saccharin	Phosphoric acid
Succinic acid	3-hydroxy-2-naphthoic acid		
Salicylic acid			

A.2. Predicting co-crystallization using MC

The first step to MC calculations is generating conformers of the APIs and co-formers. All the APIs and co-formers were sketched and auto edited individually. Under CSD materials, "conformer generator" was used to generate a maximum of five conformations for each of them.

Next, we selected co-crystal design followed by MC, under CSD materials to choose one target at a time (with its five conformations) against the 42 co-formers (each with five conformations). In the end, a table is generated with a hit rate% for each co-former and the defined API.

The calculations were repeated with the conformers generated using Spartan. The first step to calculate the conformers in Spartan is to sketch the API of interest. After that, energy minimization was done to obtain the lowest energy (most stable) conformation of the compound. We then applied molecular mechanics as implemented in Spartan 14 Version 1.1.0, to generate five conformers. These steps were repeated for each API and the 42 co-formers.

The first column in Table **A.2**, corresponds to default mercury settings with five conformations of API and that of co-formers generated using Mercury. The second column represents five conformations of both API and co-formers from Spartan. Third and fourth column is a mixture of Spartan and Mercury generated conformers. In the third column, API conformations were generated using Mercury, while the co-former conformations were calculated using Spartan. The fourth column corresponds to API conformations generated by Spartan and co-formers conformations generated from Mercury.

Accuracy of MC methodology was examined by calculating a success rate, which is the number of predictions match the experiments divided by the total number of experiments. The results of the success rates are summarized in Table **A.2**.

Table A.2. Success rates for MC-based predictions with default descriptor settings.

	Success Rate% Default-Mercury	Success Rate% Spartan	Success Rate% API mercury	Success Rate% API spartan
T11	43	40.5	38.1	45.2
T12	27	24.4	26.8	22.0
T13	25	N/A	N/A	N/A
T14	41	41.4	51.2	46.3
T15	57	41.5	41.5	48.8
T16	62	65.8	55.3	52.6
T17	70	65.9	73.2	68.3

A.3. Discussions

Firstly, the default descriptor settings for MC calculations resulted in poor success rates for **T11-T14** (success rates 25-43%) in Table **A.2**. Secondly, the results obtained from Spartan generated conformers were comparable to that of Mercury. The similarity in the Mercury and Spartan

calculations indicate that there is no significant difference between the conformers generated by both the methods. Hence, the lower accuracies for the co-crystal predictions could most likely be due to the descriptor settings. Taking a closer look into the descriptors of the default settings, we observed at first that, S-axis descriptor individually failed in almost all of the instances. S-axis is the short axis, which, by default, has a cut-off of δ< **3.23Å** for a "PASS." This cut-off "failed" in almost all the cases for the compounds examined in this study. To change most of the "FAIL" by this descriptor to a combination of both "PASS and FAIL," we varied the cut-off for **S axis** from **(**δ< **3.23-4.50) Å**. To find out if this modification would result in enhanced predictability of co-crystal formation, the success rates were calculated and are listed in Table **A.3**.

Table A.3. Success rate for S-axis with varied cut-off for co-crystal formation.

	S axis (Å) δ < 3.23 Å	S axis (Å) δ < 4.0 Å	S axis (Å) δ < 4.5 Å
T11	45%	55%	57%
T12	50%	62%	71%
T13	31%	45%	57%
T14	55%	62%	64%
T15	64%	52%	50%
T16	59%	59%	59%
T17	52%	40%	38%
Average	51%	54%	57%

To select the best S-axis cut-off, an average of the success rates across the seven compounds were calculated. The cut-off with 4.5 Å had the highest average success rate. Individually, this cut-off increased the prediction accuracies for five of the APIs (except for **T15andT17**). Since δ < 4.5 Å gave better results than the default; hence, all the further calculations were done using the new cut-off.

Additionally, to make effective and meaningful changes to the descriptor settings, we investigated the descriptor relationships and their significance. Figure **A.2** shows the correlation coefficients of the descriptors, where a positive sign indicates a higher significance.[21] Fábián et al., proposed that although *Fraction of polar volume* (FPV) has a higher positive correlation coefficient than *Fraction of nitrogen and oxygen* (FNO), FPV could be replaced by FNO in the calculations as an easier alternative.

Descriptor (molecule 1)	Descriptor (molecule 2)	ρ	r
FPV	*FPV*	0.41	0.37
S/L	*S/L*	0.40	0.38
Dipole	*Dipole*	0.39	0.28
S/M	*S/M*	0.38	0.38
M/L	*M/L*	0.38	0.41
PV	*FPV*	0.35	0.27
APV	*FPV*	-0.34	-0.32
ASAN	*Dplu*	-0.32	-0.29
PV	*APV*	-0.31	-0.28
ASAN	*Davg*	-0.31	-0.27
FNO	*FNO*	0.31	0.30
ASAN	*ASAP_P*	-0.31	-0.29
ASAN	*FASAP_P*	-0.31	-0.28
ASAN	*qHmax*	-0.30	-0.33
ASAN	*HBD2*	-0.30	-0.27
PV	*PV*	0.30	0.22
ASAN	*Aavg+Davg*	-0.30	-0.28
ASAN	*HBD1*	-0.30	-0.29

Figure A.2. Molecular descriptors and their significance[21].

In order to investigate if the replacement of FPV with FNO affects the MC success rate, we included FPV in the calculations. Moreover, *Polar Volume* (PV) also displayed a positive correlation and was, therefore, included as a descriptor in the updated/modified calculations.

To calculate the "polar volume" and "fraction polar volume," two different sources were used for the volume of the elements labeled as 'source **1**'[38] and 'source **2**'[39], respectively, Table A.4. Both FPV and PV were calculated for 42 co-formers and seven APIs. The difference between source 1 and 2 is that source 1 neglects hydrogen atom, whereas, in source 2, the volume of the elements is dependent on the number of neighboring hydrogen atoms.

Table A.4. Numerical values of volumes of elements used in calculations from two different sources.

Source 1	Atomic volume
Volume of N	17.3 cm^3 / mol
Volume of O	14.0 cm^3 / mol
Volume of S	15.5 cm^3 / mol
Volume of C	4.58 cm^3 / mol
Volume of F	17.1 cm^3 / mol

Source 2

O (2,1)	**O (1,0)**	**O(2,0)**	**N(3,0)**	**N(3,1)**	**N(2,0)**	**N(3,2)**	
15.764 Å^3	13.935Å^3	12.512Å^3	9.944Å^3	18.148Å^3	13.324Å^3	24.643Å^3	
C (3,0)	**C (4,1)**	**C(4,3)**	**C(4,2)**	**C(3,1)**	**C(4,0)**	**S(4,0)**	**P(4,0)**
12.119Å^3	18.13Å^3	33.468Å^3	24.409Å^3	21.02Å^3	10.286Å^3	17.531Å^3	22.161Å^3

All possible combinations of the descriptor settings were applied and tested against the experimental results. The different descriptor combinations were labeled as Data 1-5, Table A.5. Data-1 is the default five descriptor settings of MC with updated S-axis; Data-2 includes all the seven descriptors which were found to have positive correlations, Figure 2; Data-3 replaces FNO with FPV; Data-4 replaces FNO with PV; and finally Data-5 includes both FPV and PV as descriptors, replacing FNO. Data 2-5 were calculated using volumes from both sources. All the different combinations of the descriptors were examined to get the highest possible accuracy for MC prediction.

Table A.5. Different combinations of descriptor settings for MC calculations.

Data-1					
M/L axis ratio	S/L axis ratio	S-axis	Dipole Moment Magnitude	FNO	
Data-2					
M/L axis ratio	S/L axis ratio	S-axis	Dipole Moment Magnitude	FNO	PV	FPV
Data-3					
M/L axis ratio	S/L axis ratio	S-axis	Dipole Moment Magnitude	FPV	
Data-4					
M/L axis ratio	S/L axis ratio	S-axis	Dipole Moment Magnitude	PV	
Data-5					
M/L axis ratio	S/L axis ratio	S-axis	Dipole Moment Magnitude	PV	FPV

In addition to the descriptor settings, the requirement that an overall pass, requires 5pass/5 descriptors in the default settings seemed to us to be overly harsh. We, therefore, decided to explore if the match between prediction and experiment could benefit from introducing slightly less rigid

pass requirements. Hence, several "PASS/FAIL" criteria were also included in the updated calculations to identify the best possible combinations.

Once all the predictive calculations were done using the modified MC settings, the results were compared with the experimental outcomes. A success rate was calculated for all the different combinations, Table 6. An algorithm was designed and implemented (in groovy) to analyze a total of 1050,000 data points in this process to select the best combinations.

In order to select the best updated MC settings, we focused on combinations with the fewest number of poor performances (below 40%) or where the results were consistently above 40% throughout the seven APIs. This process of elimination allowed us to rule out Data-3, which had at least one API in each "PASS/FAIL" column where the success rate is below 40%. It gave the worst prediction match in comparison to other settings. Although, except for **T15** and **T17**, the accuracies of the other five APIs were increased in comparison to the default settings. These increased accuracies can be attributed to the fact that FPV had a higher positive correlation than FNO.

PV and FPV calculated from two separate sources (1and2) also affected the calculations, as we observed differences in the success rates. However, the observed differences were within the range of 2-4%. Despite that a winner between the source 1and2 was picked following similar guidelines, i.e., the results remain consistently above 40% for all the APIs.

The next step was to bring forward each descriptor settings with the most consistent (above 40%) "PASS/FAIL" criteria across the seven APIs to analyze the quality of the predictions between the different settings.

It was observed that the best success rates were achieved across the seven APIs with the following combinations, Table A.6.:

Data-1 with 3pass/ 5 descriptors;

Data-2 with 5 pass/7 descriptors calculated using source **2**;

Data-4 with 3pass/5 descriptors calculated using source **1** and

Data-5 with 4 pass 6 descriptors settings calculated using source **2**.

Table A.6. Comparison of prediction quality with different combinations of descriptors.

Data-1	5 Pass/5 descriptors Pass fail criteria (5X5) Complementarity Success rate	4 Pass/5 descriptors Pass fail criteria (5X5) Complementarity Success rate	3 Pass/5 descriptors Pass fail criteria (5X5) Complementarity Success rate

T11	55%	55%	45%
T12	55%	43%	50%
T13	69%	67%	50%
T14	55%	53%	50%
T15	21%	34%	64%
T16	52%	52%	52%
T17	24%	43%	60%

Data-2	7 Pass/7 descriptors Pass fail criteria (5X5) Complementarity Success rate		6 Pass/7 descriptors Pass fail criteria (5X5) Complementarity Success rate		5 Pass/7 descriptors Pass fail criteria (5X5) Complementarity Success rate		4 Pass/7 descriptors Pass fail criteria (5X5) Complementarity Success rate	
			Source 1	**Source 2**	**Source 1**	**Source 2**	**Source 1**	**Source 2**
T11	57%	55%	57%	57%	55%	57%	48%	45%
T12	55%	52%	55%	52%	50%	50%	55%	45%
T13	74%	69%	74%	69%	62%	64%	43%	45%
T14	55%	52%	53%	50%	50%	50%	40%	40%
T15	21%	29%	19%	21%	43%	64%	69%	74%
T16	52%	52%	52%	55%	55%	52%	50%	55%
T17	31%	38%	31%	40%	64%	64%	86%	81%

Data-3	5 Pass/5 descriptors Pass fail criteria (5X5) Complementarity Success rate		4 Pass/5 descriptors Pass fail criteria (5X5) Complementarity Success rate		3 Pass/5 descriptors Pass fail criteria (5X5) Complementarity Success rate	
	Source 1	**Source 2**	**Source 1**	**Source 2**	**Source 1**	**Source 2**
T11	55%	55%	57%	57%	38%	48%
T12	55%	55%	52%	52%	45%	55%
T13	71%	74%	71%	74%	50%	62%
T14	55%	55%	50%	52%	50%	50%
T15	52%	23%	52%	21%	52%	38%
T16	52%	52%	52%	48%	50%	52%
T17	24%	24%	24%	29%	57%	48%

Data-4	5 Pass/5 descriptors Pass fail criteria (5X5) Complementarity Success rate		4 Pass/5 descriptors Pass fail criteria (5X5) Complementarity Success rate		3 Pass/5 descriptors Pass fail criteria (5X5) Complementarity Success rate	
	Source 1	**Source 2**	**Source 1**	**Source 2**	**Source 1**	**Source 2**
T11	55%	57%	50%	55%	45%	45%
T12	55%	57%	50%	55%	52%	55%
T13	71%	71%	52%	57%	40%	45%
T14	55%	57%	52%	52%	50%	57%

T15	24%	24%	48%	38%	77%	69%
T16	52%	52%	48%	48%	60%	48%
T17	24%	24%	50%	43%	74%	60%

Data-5	6 Pass/6 descriptors Pass fail criteria (5X5) Complementarity Success rate		5 Pass/6 descriptors Pass fail criteria (5X5) Complementarity Success rate		4 Pass/6 descriptors Pass fail criteria (5X5) Complementarity Success rate	
	Source 1	**Source 2**	**Source 1**	**Source 2**	**Source 1**	**Source 2**
T11	55%	55%	52%	55%	45%	43%
T12	55%	48%	57%	50%	53%	52%
T13	71%	74%	71%	74%	50%	60%
T14	55%	54%	57%	54%	45%	55%
T15	24%	29%	24%	26%	45%	59%
T16	52%	52%	52%	52%	48%	50%
T17	24%	21%	24%	23%	55%	45%

Table A.7. Comparing the prediction using different descriptor combinations with the experimental outcomes.

	Data-1 3 Pass/5 descriptors	Data-2 5 Pass/7 descriptors (Source 2)	Data-4 3 Pass/5 descriptors (Source 1)	Data-5 4 Pass/6 descriptors (Source 2)
T11	45%	57%	45%	43%
T12	50%	50%	52%	52%
T13	50%	64%	40%	60%
T14	50%	50%	50%	55%
T15	64%	64%	77%	59%
T16	52%	52%	60%	50%
T17	60%	64%	74%	45%
Average	53%	57%	56%	52%

We identified that Data-2 with 5pass/ 7descriptors offered marginally better results than the other three combinations. Table A8 exhibits a comparison between the success rate obtained from the new and default settings.

Table A.8. Comparison between the default and modified MC settings with the experimental outcomes for co-crystal formation.

	Where we started (Default)	New setting Data-2
T11	43%	57%
T12	27%	50%
T13	25%	64%

T14	41%	50%
T15	57%	57%
T16	62%	52%
T17	70%	64%

By carefully modifying the default setting of the MC calculations, we were able to improve the prediction success for four APIs, one remained the same and decreased the accuracy for two of them. The efficiency improved from 27% to 50% for **T12** and 25% to 64% for **T13** in comparison to the decrease from 62% to 52% for **T16** and 70% to 64% for **T17**. Overall the accuracy of MC increases many fold times when the default settings are adjusted to the new settings. Although the reliability of MC, when compared to other predictive studies reported[27] is low, however, there are very few significant studies reported on large and flexible compounds. Furthermore, the average molecular weight of organic structures reported in CSD is ~400 g/mol.[40] Hence, the structure informatics studies for compounds with a molecular weight greater than 400 g/mol might not reflect the same high accuracies as that of small compounds. Nonetheless, it opens a whole new area for studying APIs, which might not be restricted to small and rigid compounds.

It is worth noting that structure-informatics methods such as HBP and HBC[27,25] predict the co-crystallization outcomes based on hydrogen bonds, whereas MC is dependent on shape and polarity factors. Therefore, it will be interesting to compare and combine the different methodologies, which might provide significant insight into the predictive methods and its reliability.

A.4. Conclusions

We attempted to predict co-crystallization for seven APIs against 42 potential co-formers using MC. The predicted outcomes were compared with the experimental results. The seven APIs investigated in this study were significantly larger (molecular weight 400 - 600 g/ mol) and flexible (rotatable bonds > 3) than the compounds reported in CSD (average molecular weight ~400 g/ mol). The default MC settings in Mercury afforded a success rate ranging from 27-70%.

A total of 1050,000 data points was analyzed to introduce updated and modified MC settings, which concluded that Data-2 with 5pass/ 7descriptors (using source 2) increases the overall

accuracy. The reliability of the updated MC ranges from 50-64%, which was found to be more consistent across the seven APIs than the default settings.

A.5. References

1 G. E. Wnek, *J. Chem. Educ.*, 2017, **94**, 1647–1654.

2 S. Li, T. Yu, Y. Tian, C. P. McCoy, D. S. Jones and G. P. Andrews, *Mol. Pharmaceutics*, 2016, **13**, 3054–3068.

3 D. D. Gadade and S. S. Pekamwar, *Adv Pharm Bull*, 2016, **6**, 479–494.

4 T. Friščić and W. Jones, *Crystal Growth & Design*, 2009, **9**, 1621–1637.

5 S. Cherukuvada, R. Kaur and T. N. G. Row, *CrystEngComm*, 2016, **18**, 8528–8555.

6 S. Basavoju, D. Boström and S. P. Velaga, *Pharm Res*, 2008, **25**, 530–541.

7 A. O. Surov, A. P. Voronin, A. N. Manin, N. G. Manin, L. G. Kuzmina, A. V. Churakov and G. L. Perlovich, *Mol. Pharmaceutics*, 2014, **11**, 3707–3715.

8 W. Jones, W. D. S. Motherwell and A. V. Trask, *MRS Bulletin*, 2006, **31**, 875–879.

9 P. Vishweshwar, J. A. McMahon, J. A. Bis and M. J. Zaworotko, *Journal of Pharmaceutical Sciences*, 2006, **95**, 499–516.

10 The role of cocrystals in pharmaceutical science - ScienceDirect, https://www.sciencedirect.com/science/article/pii/S1359644608000779?via%3Dihub, (accessed May 12, 2019).

11 J. Berger, J. D. Dunn, M. M. Johnson, K. R. Karst and W. C. Shear, *Am J Manag Care*, 2016, **22**, S487–S495.

12 C. Aakeröy, *Acta Cryst B*, 2015, **71**, 387–391.

13 D. Musumeci, C. A. Hunter, R. Prohens, S. Scuderi and J. F. McCabe, *Chem. Sci.*, 2011, **2**, 883.

14 C. A. Hunter, *Angewandte Chemie International Edition*, 2004, **43**, 5310–5324.

15 B. Sandhu, A. McLean, A. S. Sinha, J. Desper, A. A. Sarjeant, S. Vyas, S. M. Reutzel-Edens and C. B. Aakeröy, *Crystal Growth & Design*, 2018, **18**, 466–478.

16 N. Blagden, M. de Matas, P. T. Gavan and P. York, *Advanced Drug Delivery Reviews*, 2007, **59**, 617–630.

17 A. J. Cruz-Cabeza, *CrystEngComm*, 2012, **14**, 6362–6365.

18 M. A. Mohammad, A. Alhalaweh and S. P. Velaga, *International Journal of Pharmaceutics*, 2011, **407**, 63–71.

19 N. Issa, P. G. Karamertzanis, G. W. A. Welch and S. L. Price, *Crystal Growth & Design*, 2009, **9**, 442–453.

20 C. F. Macrae, I. J. Bruno, J. A. Chisholm, P. R. Edgington, P. McCabe, E. Pidcock, L. Rodriguez-Monge, R. Taylor, J. van de Streek and P. A. Wood, *J Appl Cryst*, 2008, **41**, 466–470.

21 L. Fábián, *Crystal Growth & Design*, 2009, **9**, 1436–1443.

22 R. Chakrabarty, P. S. Mukherjee and P. J. Stang, *Chem. Rev.*, 2011, **111**, 6810–6918.

23 C. B. Aakeröy, P. D. Chopade and J. Desper, *Crystal Growth & Design*, 2011, **11**, 5333–5336.

24 P. A. Wood, N. Feeder, M. Furlow, P. T. A. Galek, C. R. Groom and E. Pidcock, *CrystEngComm*, 2014, **16**, 5839.

25 P. T. A. Galek, F. H. Allen, L. Fábián and N. Feeder, *CrystEngComm*, 2009, **11**, 2634.

26 P. T. A. Galek, J. A. Chisholm, E. Pidcock and P. A. Wood, *Acta Crystallogr B Struct Sci Cryst Eng Mater*, 2014, **70**, 91–105.

27 N. Sarkar, A. S. Sinha and C. B. Aakeröy, *CrystEngComm*, , DOI:10.1039/C9CE01196J.

28 E. Arunan, G. R. Desiraju, R. A. Klein, J. Sadlej, S. Scheiner, I. Alkorta, D. C. Clary, R. H. Crabtree, J. J. Dannenberg, P. Hobza, H. G. Kjaergaard, A. C. Legon, B. Mennucci and D. J. Nesbitt, *Pure Appl. Chem.*, 2011, **83**, 1619–1636.

29 A. D. Buckingham, J. E. Del Bene and S. A. C. McDowell, *Chemical Physics Letters*, 2008, **463**, 1–10.

30 J.-M. Lehn, *Science*, 2002, **295**, 2400–2403.

31 B. Moulton and M. J. Zaworotko, *Chem. Rev.*, 2001, **101**, 1629–1658.

32 E. Bosch, *CrystEngComm*, 2007, **9**, 191–198.

33 C. B. Aakeröy, D. J. Salmon, M. M. Smith and J. Desper, *Crystal Growth and Design*, 2006, **6**, 1033–1042.

34 M. A. Siegler, Y. Fu, G. H. Simpson, D. P. King, S. Parkin and C. P. Brock, *Acta Cryst Sect A Found Cryst*, 2007, **63**, 912–925.

35 H.-J. Schneider, *New J. Chem.*, 2019, **43**, 15498–15512.

36 R. Shaikh, R. Singh, G. M. Walker and D. M. Croker, *Trends in Pharmacological Sciences*, 2018, **39**, 1033–1048.

37 H. G. Brittain, *Crystal Growth & Design*, 2009, **9**, 2492–2499.

38 Periodic Table of the Elements, http://hyperphysics.phy-astr.gsu.edu/hbase/pertab/pertab.html#c1, (accessed August 25, 2019).

39 S. Beaucamp, D. Mathieu and V. Agafonov, *Acta Crystallogr B Struct Sci*, 2007, **63**, 277–284.

40 C. R. Groom, I. J. Bruno, M. P. Lightfoot and S. C. Ward, *Acta Crystallographica Section B*, 2016, **72**, 171–179.

Appendix B – NMR of synthetized compounds

B.1. Synthesis of 4-((4-bromo-1H-pyrazol-1-yl)methyl)benzonitrile (**T5**)

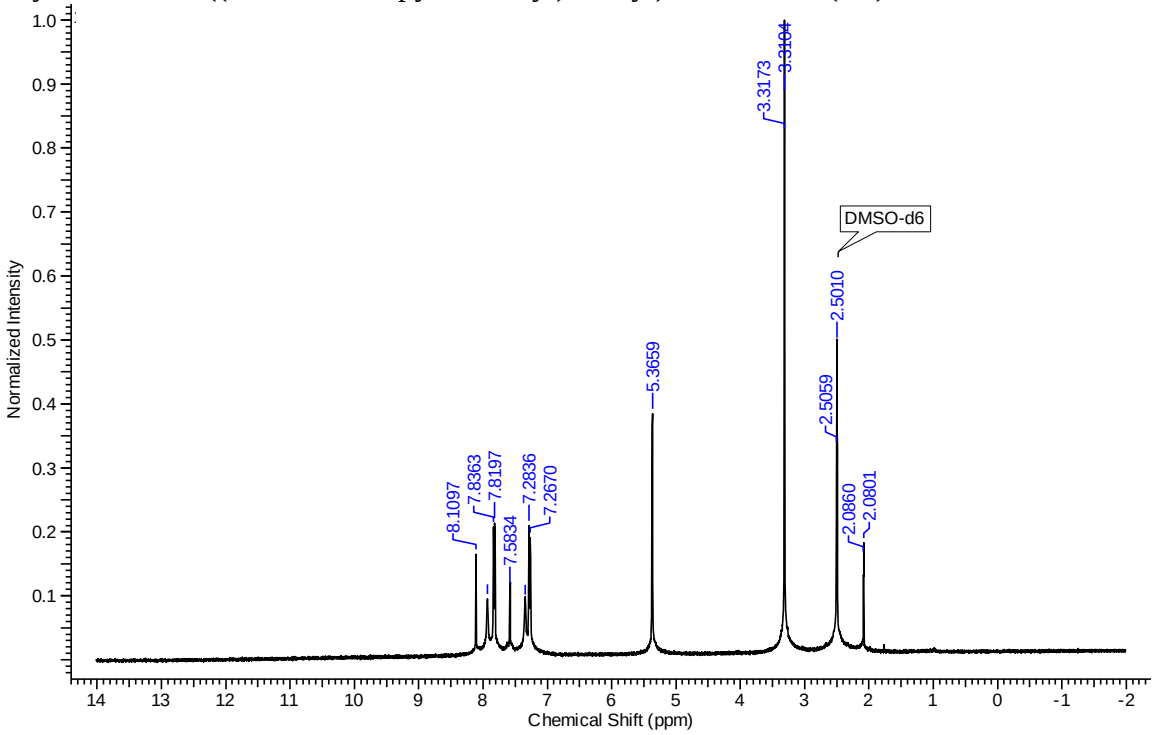

B.2. Synthesis of 4-((3-bromocyclopenta-2,4-dien-1-yl)methyl)benzamide

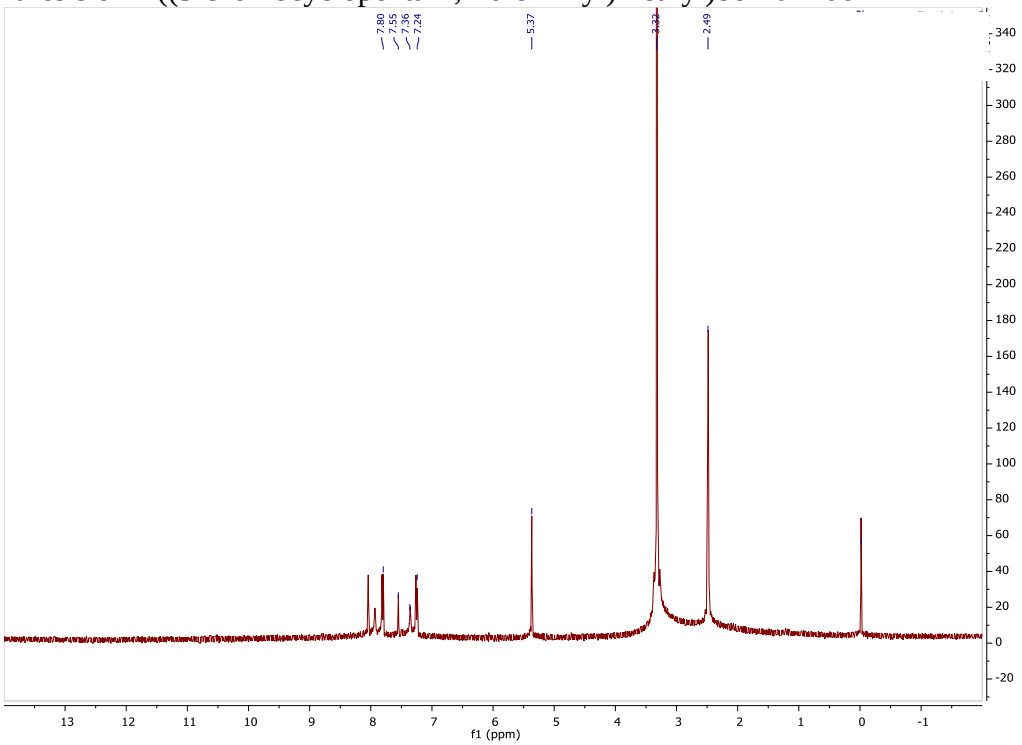

B.3. Synthesis of 4-((4-((trimethylsilyl)ethynyl)-1H-pyrazol-1-yl)methyl)benzamide

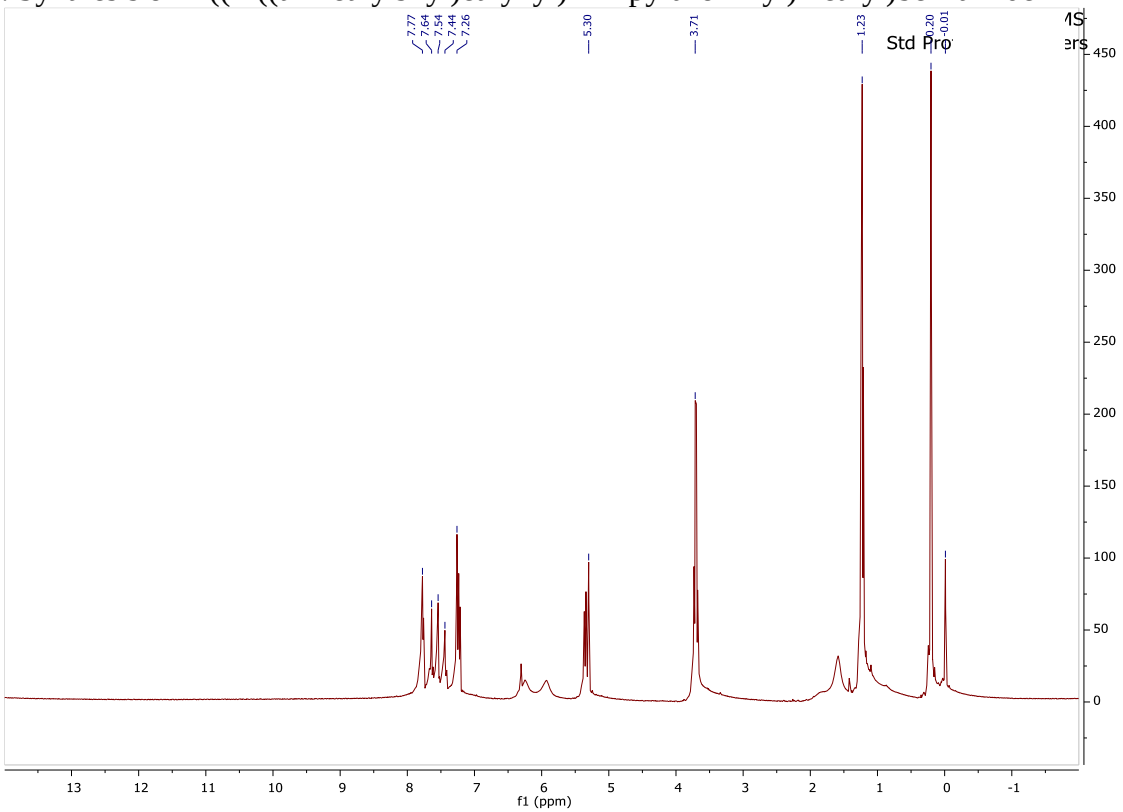

B.4. Synthesis of 4-((4-ethynyl-1H-pyrazol-1-yl)methyl)benzamide (**T1**)

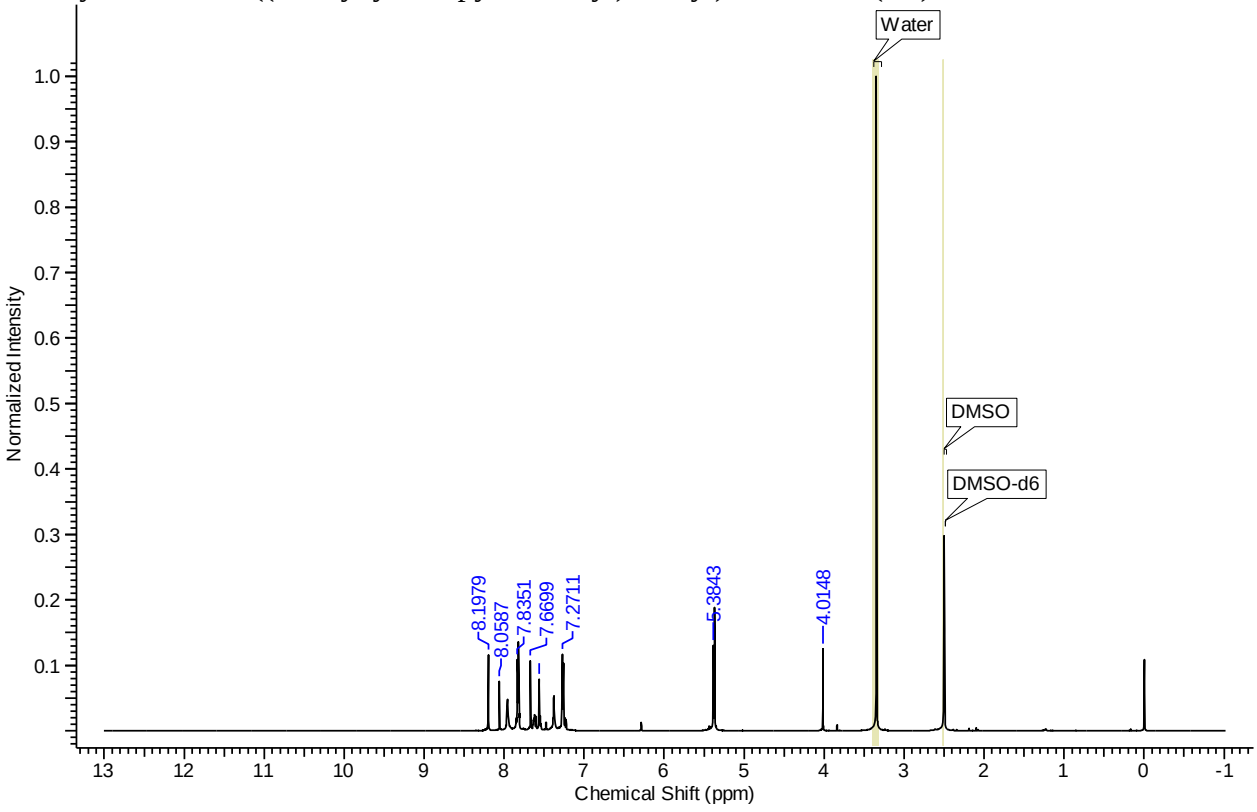

B.5. Synthesis of 3-((4-bromo-1H-pyrazol-1-yl)methyl)benzonitrile (**T6**)

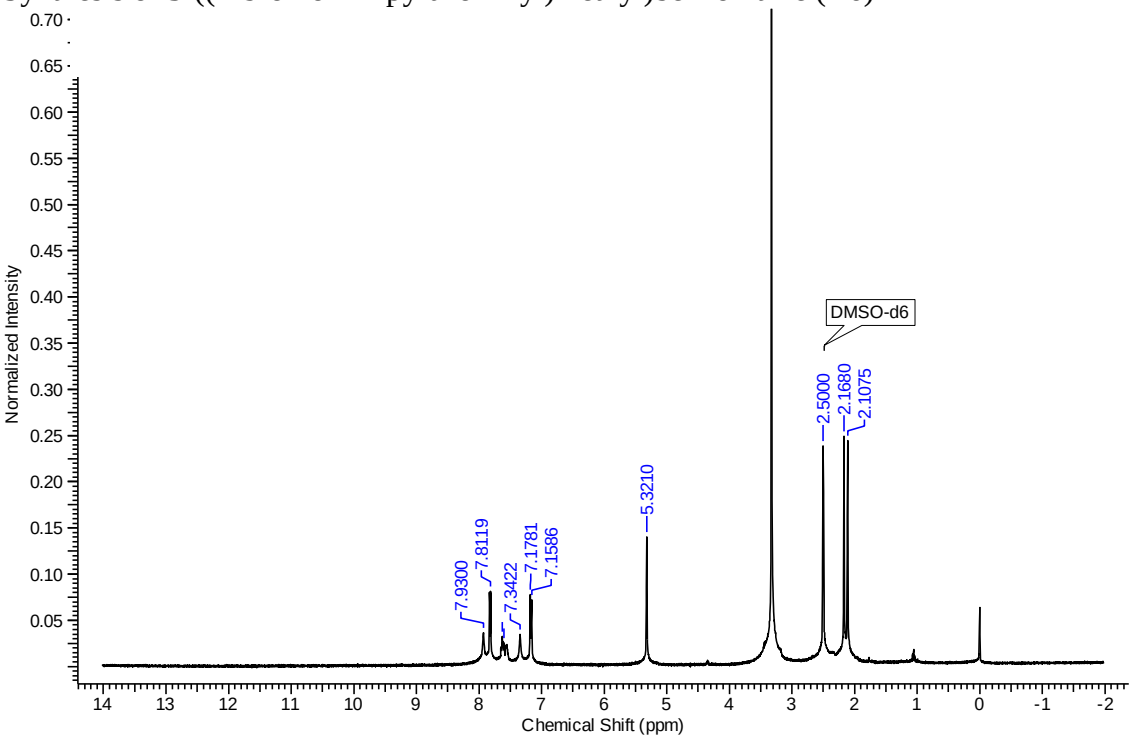

B.6. Synthesis of 3-((3-bromocyclopenta-2,4-dien-1-yl)methyl)benzamide

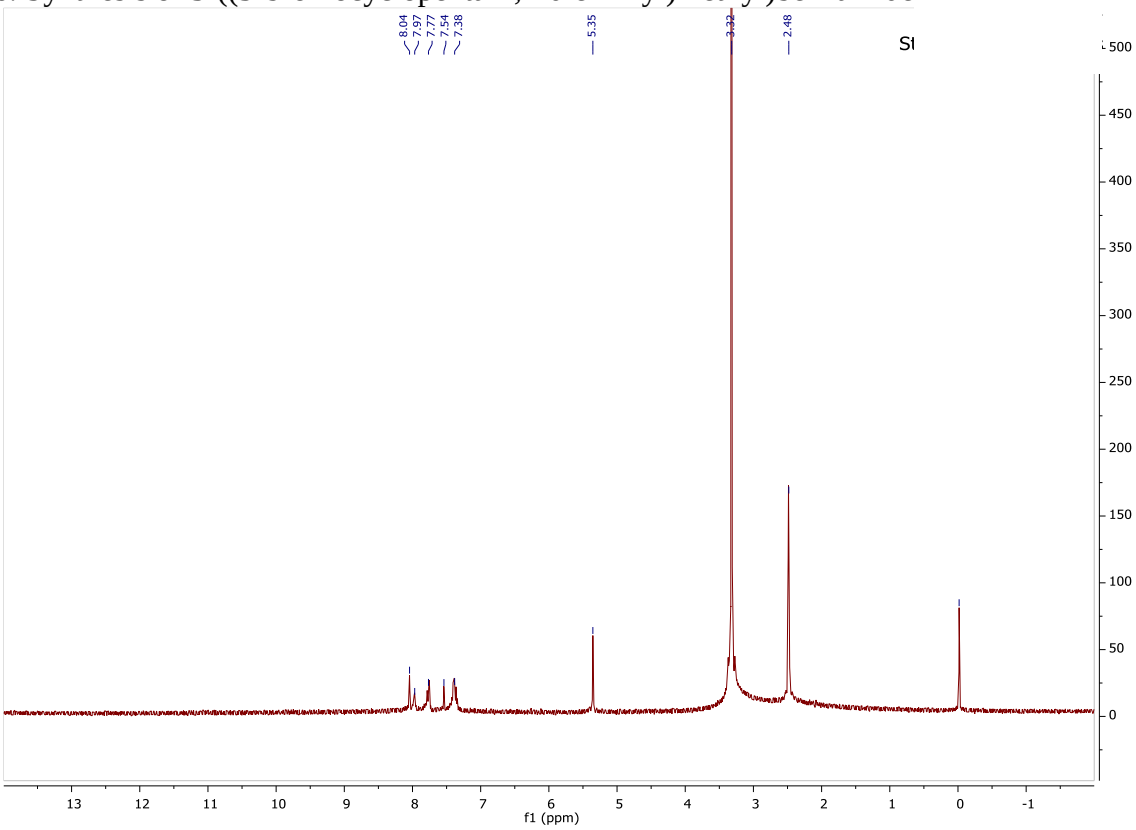

B.7. Synthesis of 3-((3-((trimethylsilyl)ethynyl)cyclopenta-2,4-dien-1-yl)methyl)benzamide

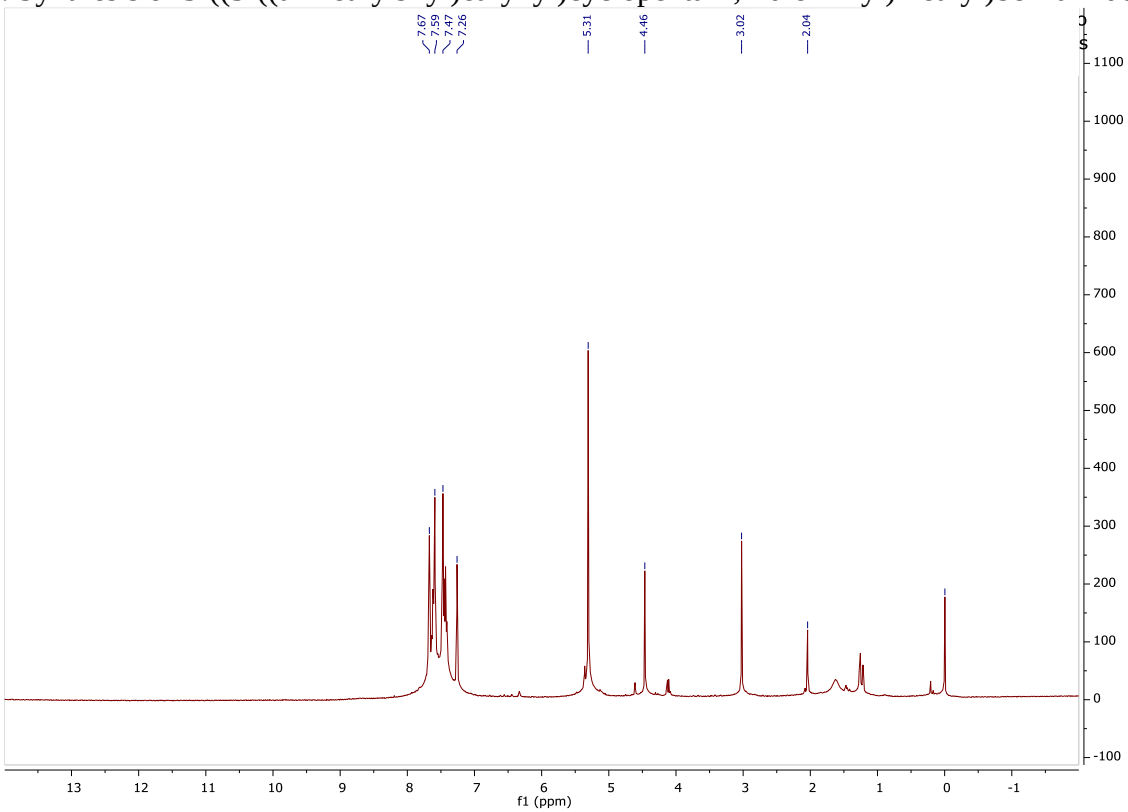

B.8. Synthesis of 3-((3-ethynylcyclopenta-2,4-dien-1-yl)methyl)benzamide (**T2**)

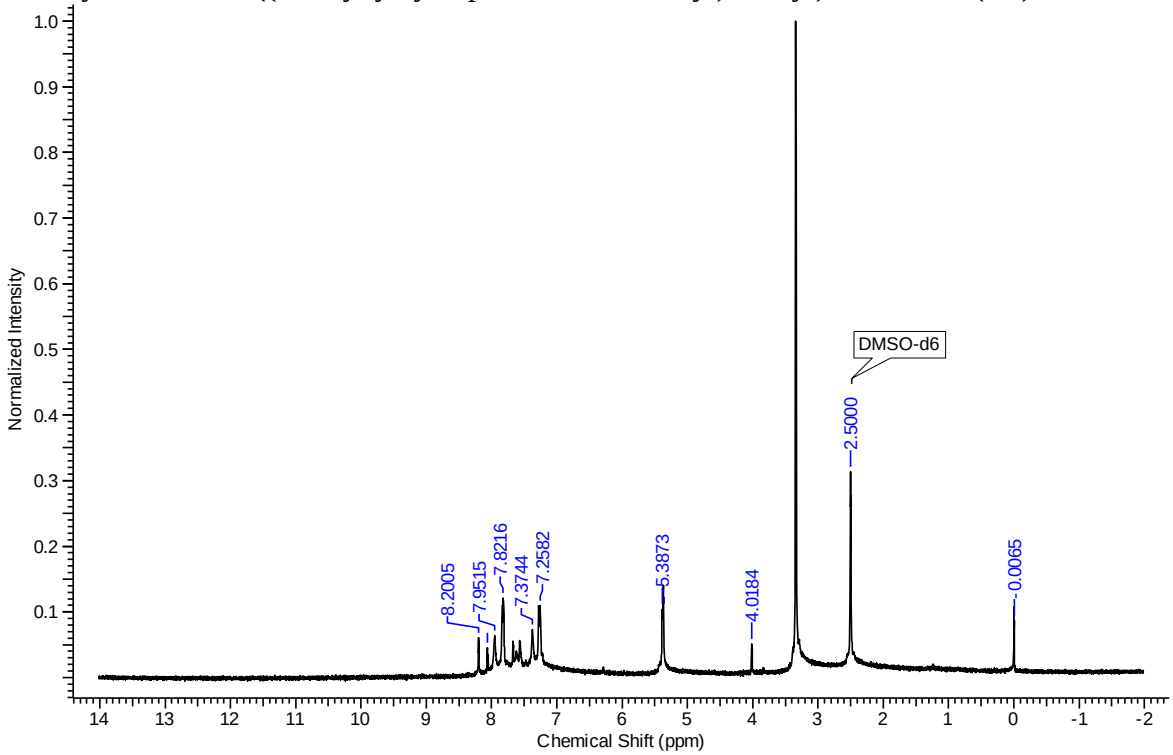

B.9. Synthesis of 4-((4-bromo-1H-pyrazol-1-yl)methyl)benzonitrile

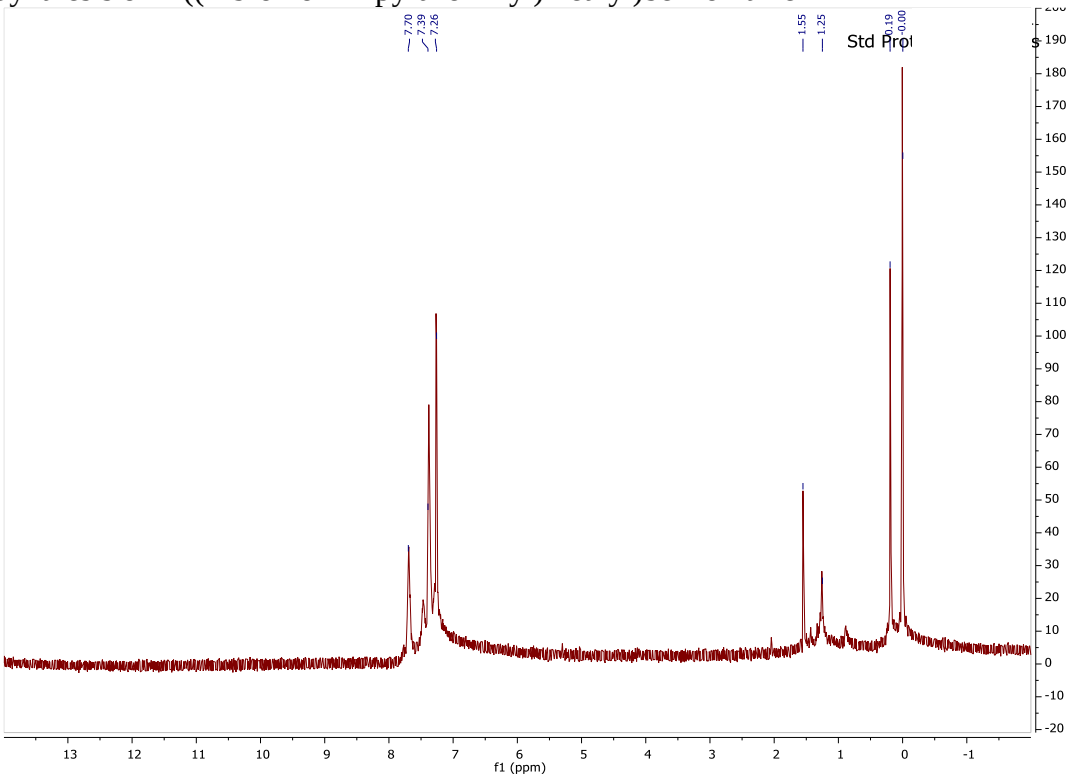

B.10. Synthesis of 4-((3-bromocyclopenta-2,4-dien-1-yl)methyl)benzamide

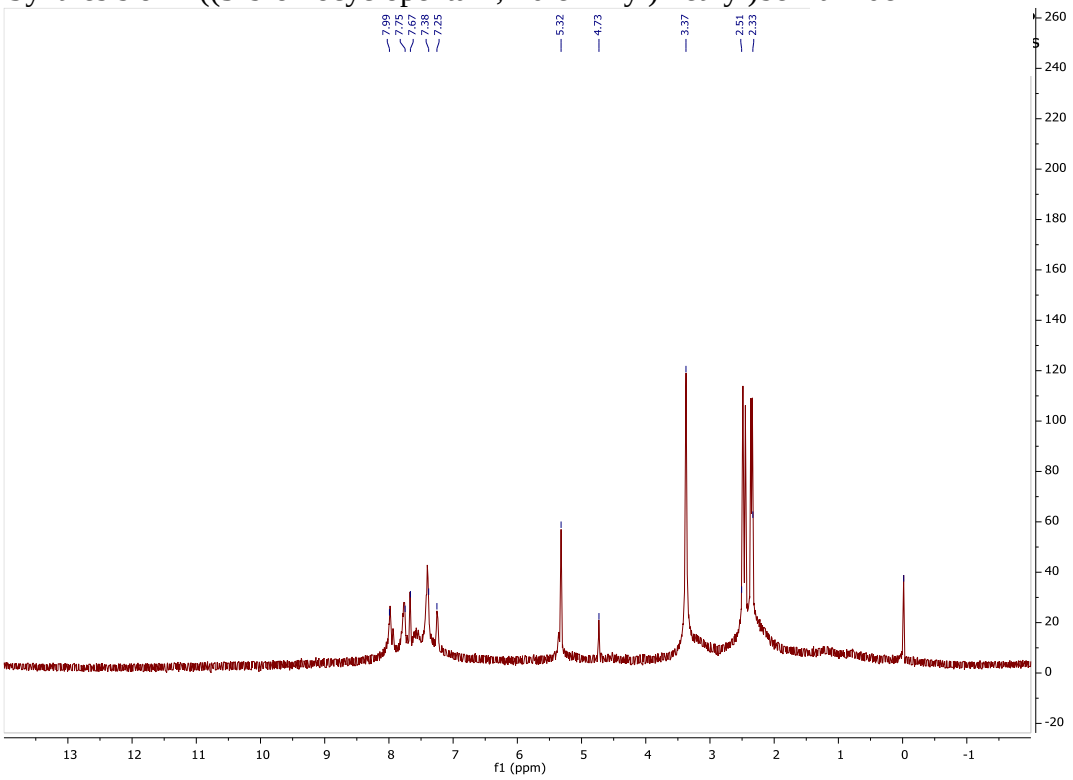

B.11. Synthesis of 4-((3,5-dimethyl-4-((trimethylsilyl)ethynyl)-1H-pyrazol-1-yl)methyl)benzamide

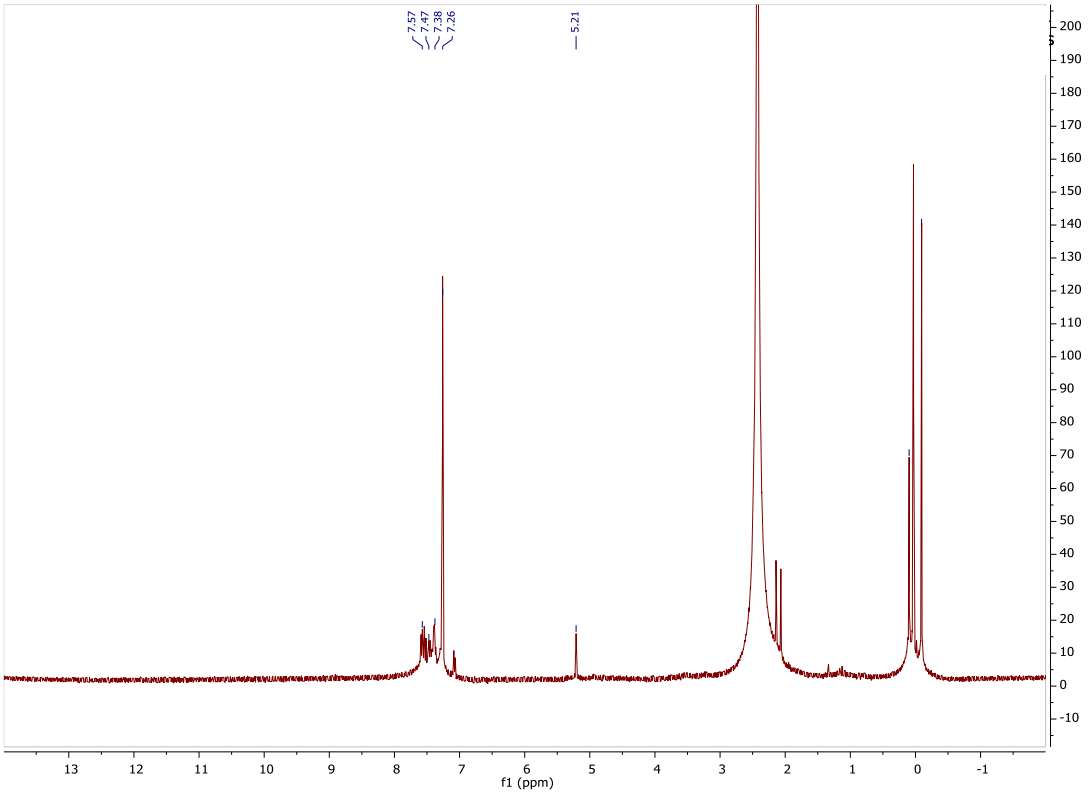

B.12. Synthesis of 4-((3-ethynyl-2,4-dimethylcyclopenta-2,4-dien-1-yl)methyl)benzamide (**T3**)

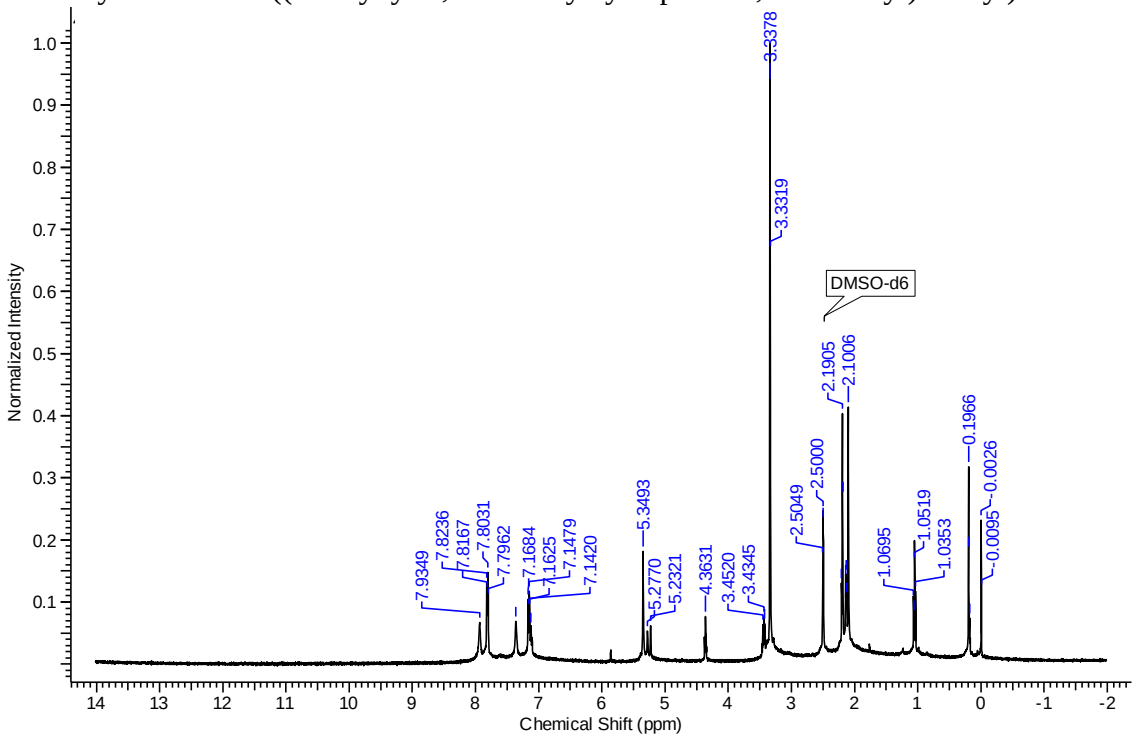

B.13. Synthesis of 3-((4-bromo-3,5-dimethyl-1H-pyrazol-1-yl)methyl)benzonitrile

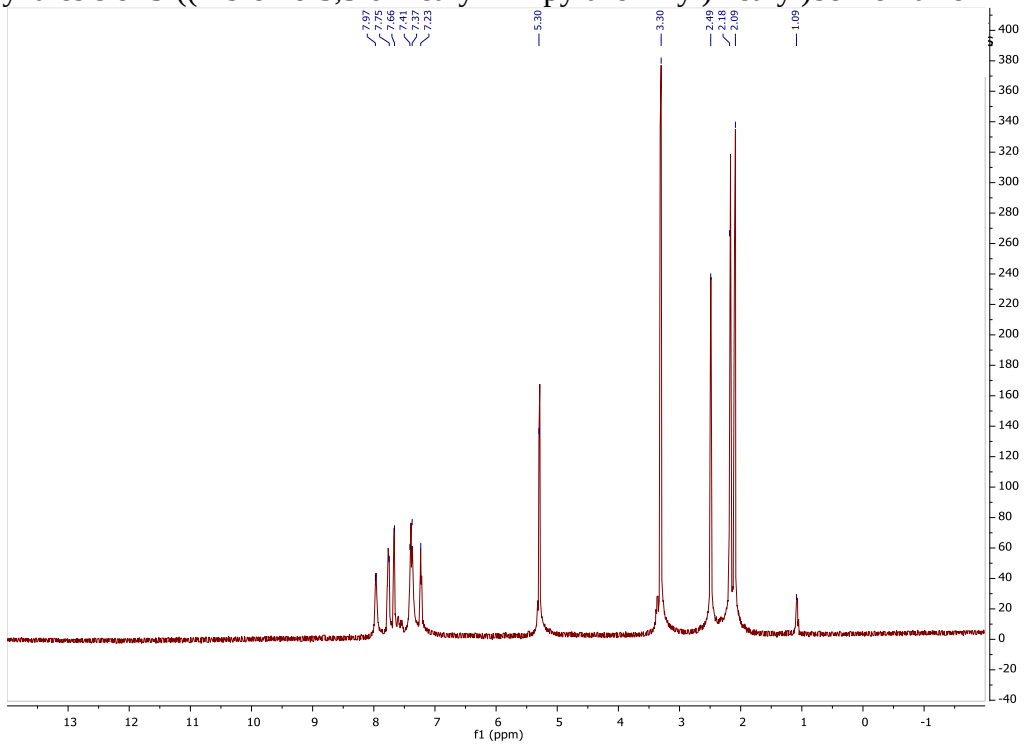

B.14. Synthesis of 3-((3-bromo-2,4-dimethylcyclopenta-2,4-dien-1-yl)methyl)benzamide

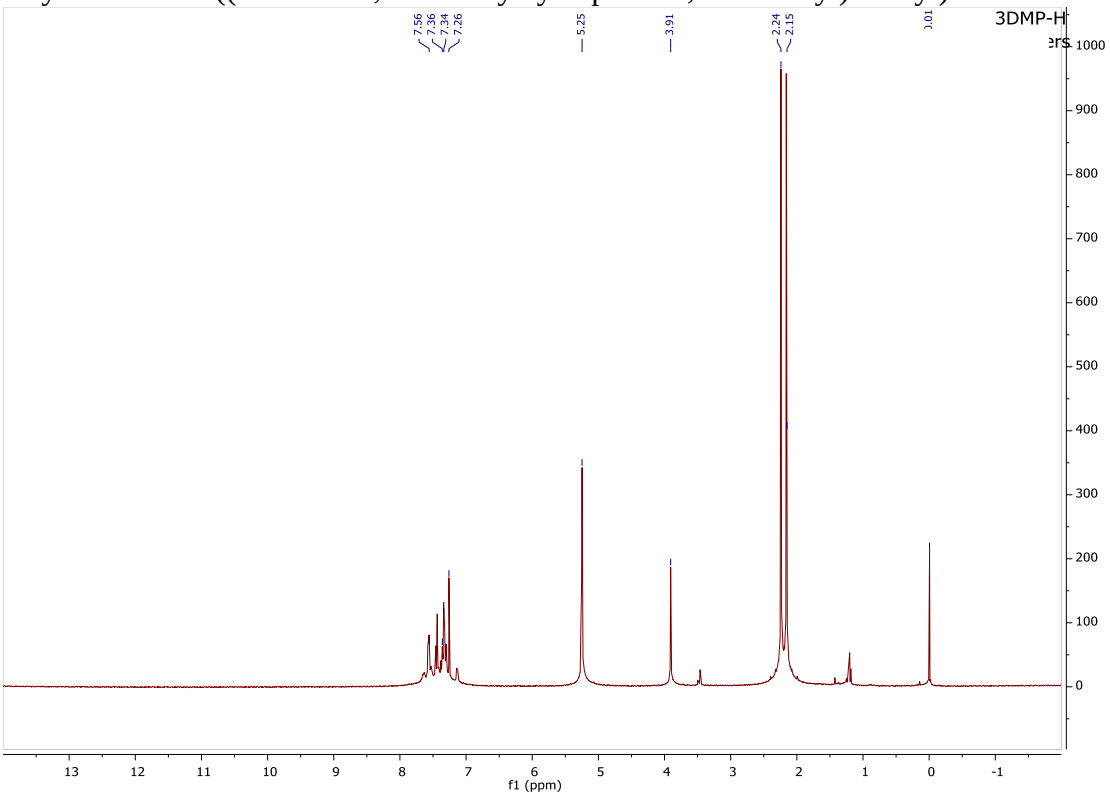

B.15. Synthesis of 3-((3,5-dimethyl-4-((trimethylsilyl)ethynyl)-1H-pyrazol-1-yl)methyl)benzamide

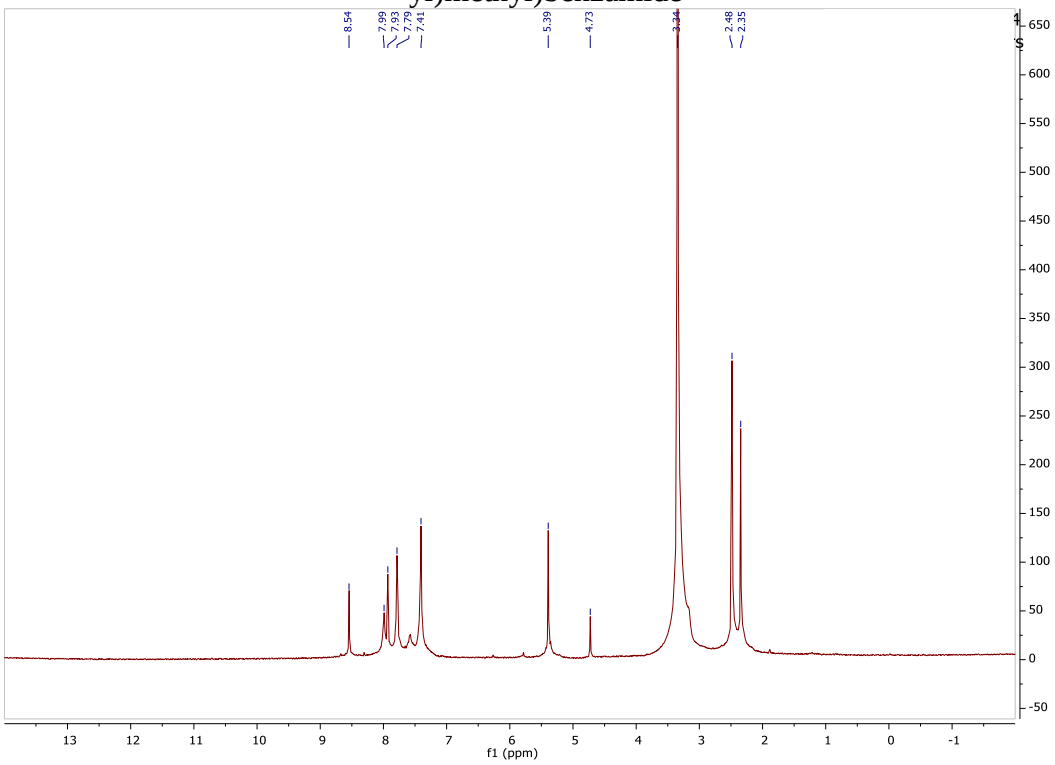

B.16. Synthesis of 3-((3-ethynyl-2,4-dimethylcyclopenta-2,4-dien-1-yl)methyl)benzamide (**T4**)

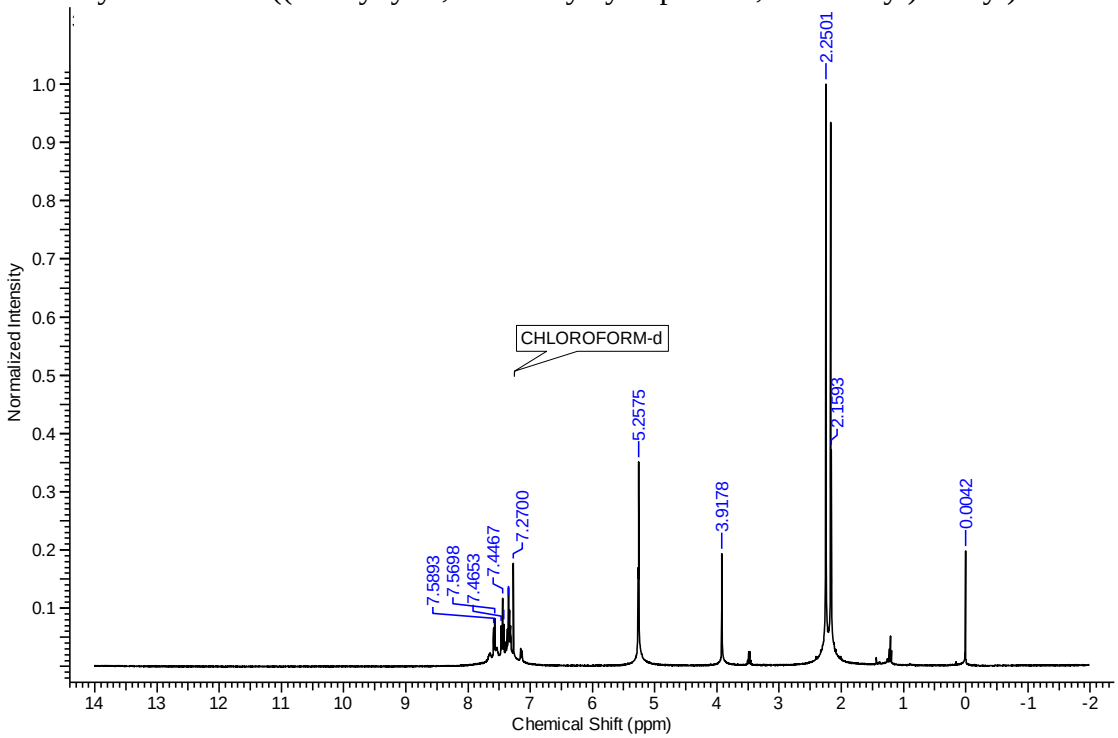

B.17. Synthesis of 4-((4-(iodoethynyl)-1H-pyrazol-1-yl)methyl)benzamide (**T7**)

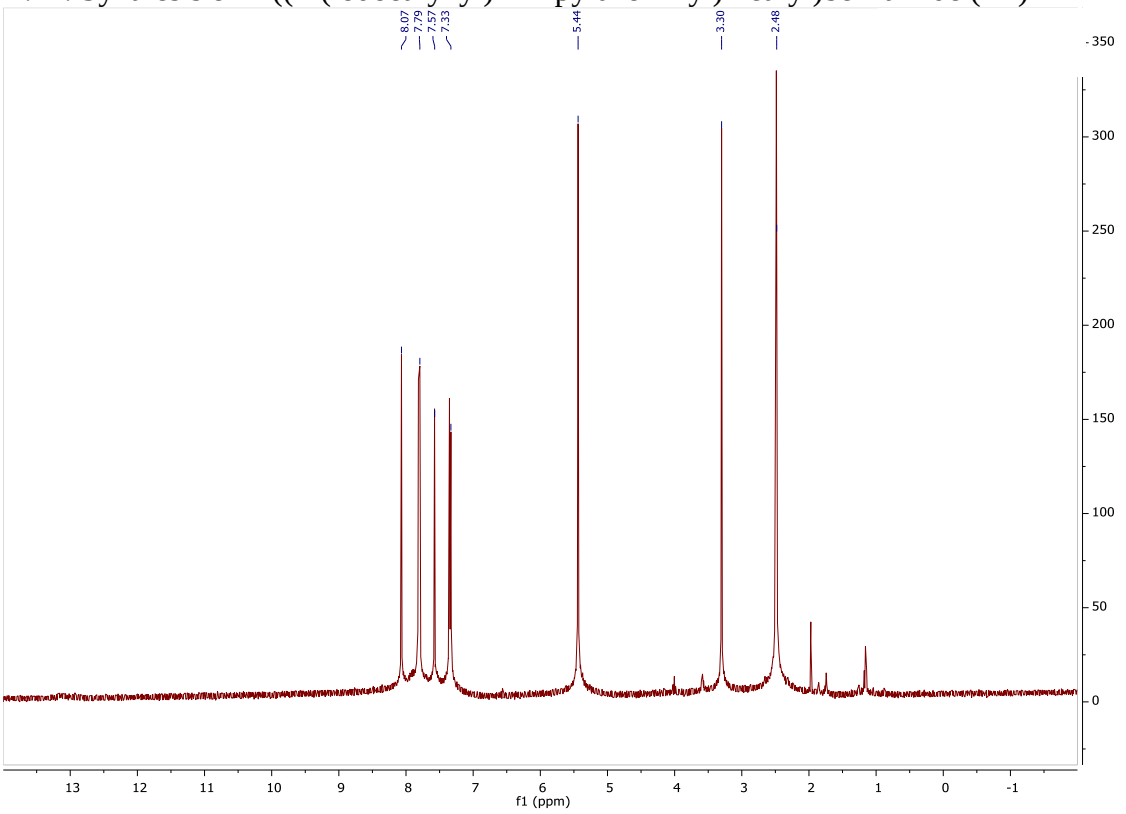

B.18. Synthesis of 3-((4-(iodoethynyl)-1H-pyrazol-1-yl)methyl)benzamide (**T8**)

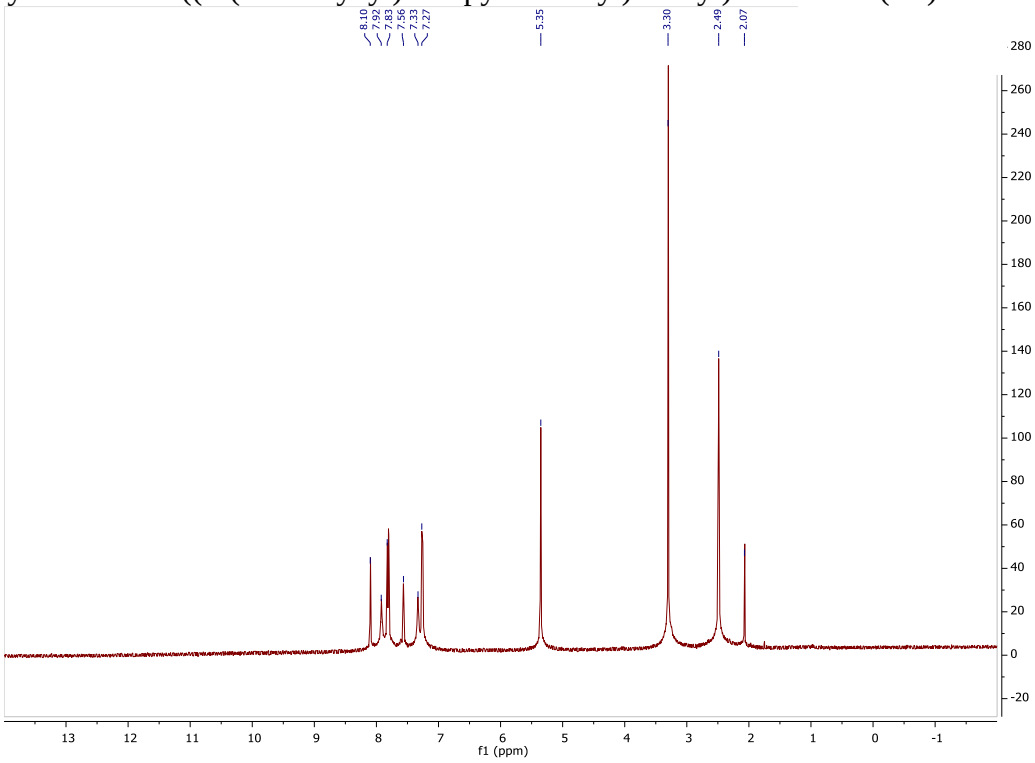

B.19. Synthesis of 4-((4-(iodoethynyl)-3,5-dimethyl-1H-pyrazol-1-yl)methyl)benzamide (**T9**)

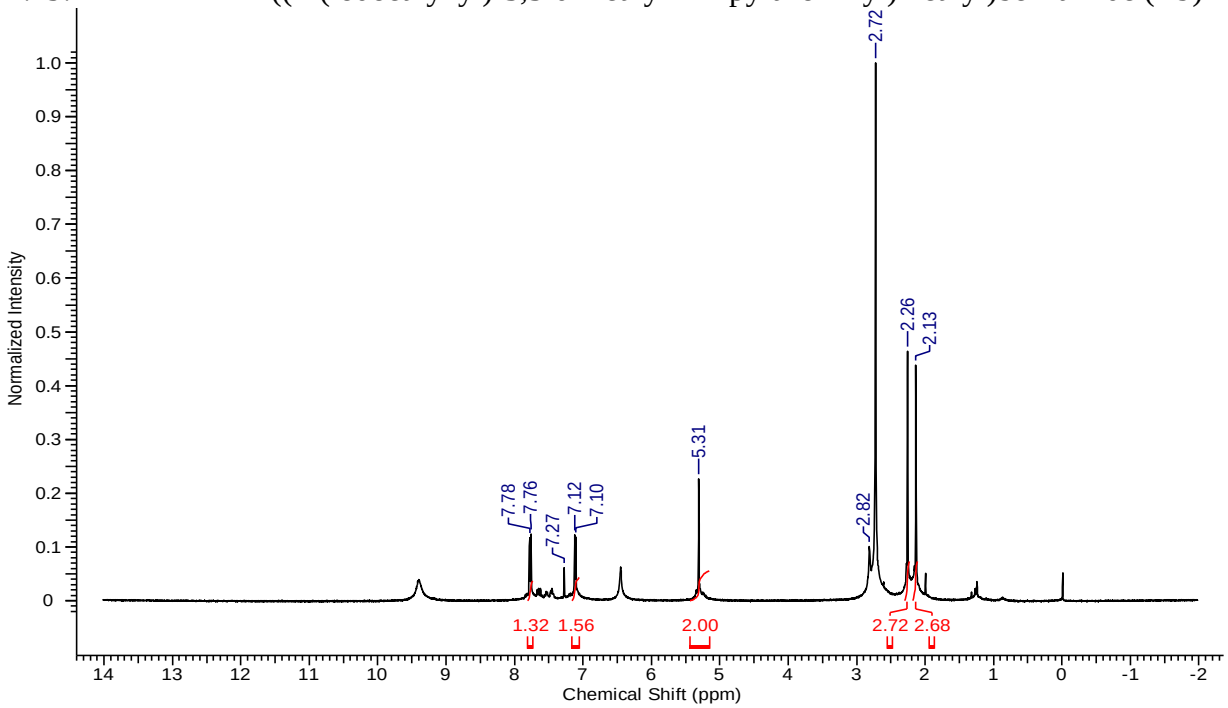

B.20. Synthesis of 3-((4-(iodoethynyl)-3,5-dimethyl-1H-pyrazol-1-yl)methyl)benzamide (**T10**)

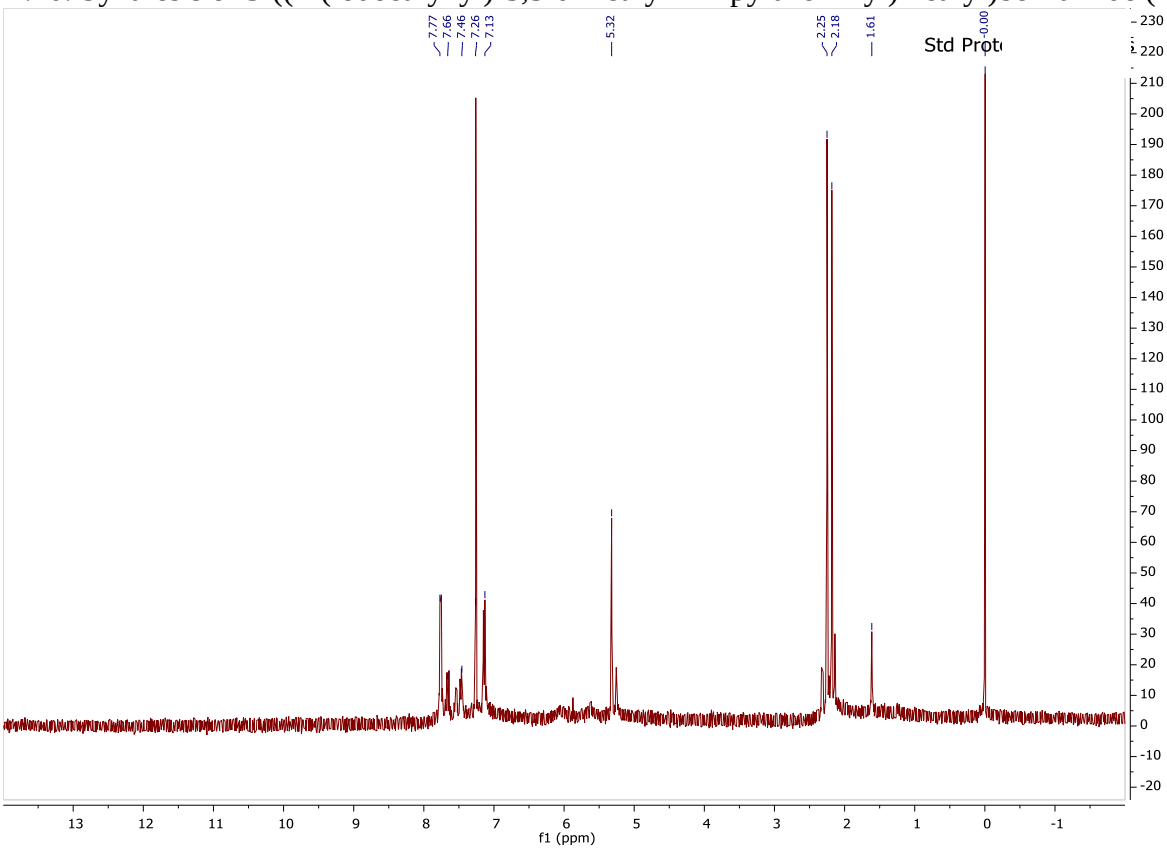

B.21. Synthesis of C-hexylcalix[4]resorcinarene, **1**

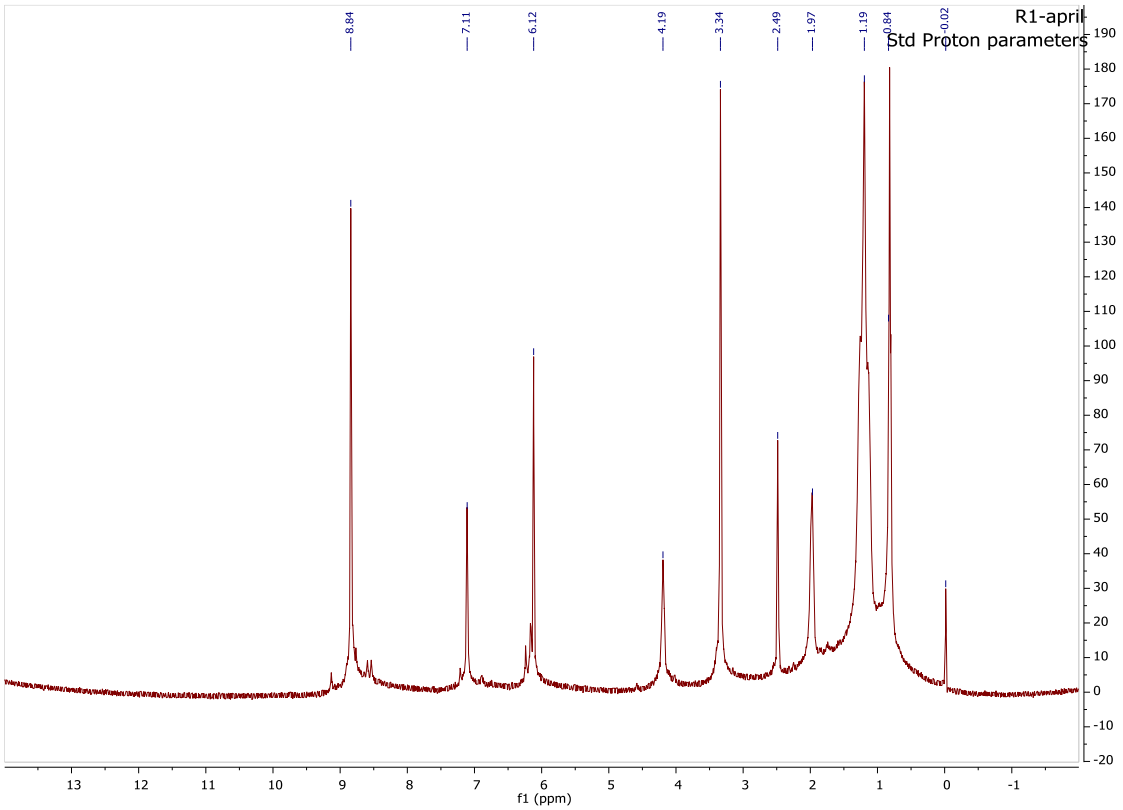

B.22. Synthesis of C-hexyltetrabromocalix[4]resorcinarene, **2**

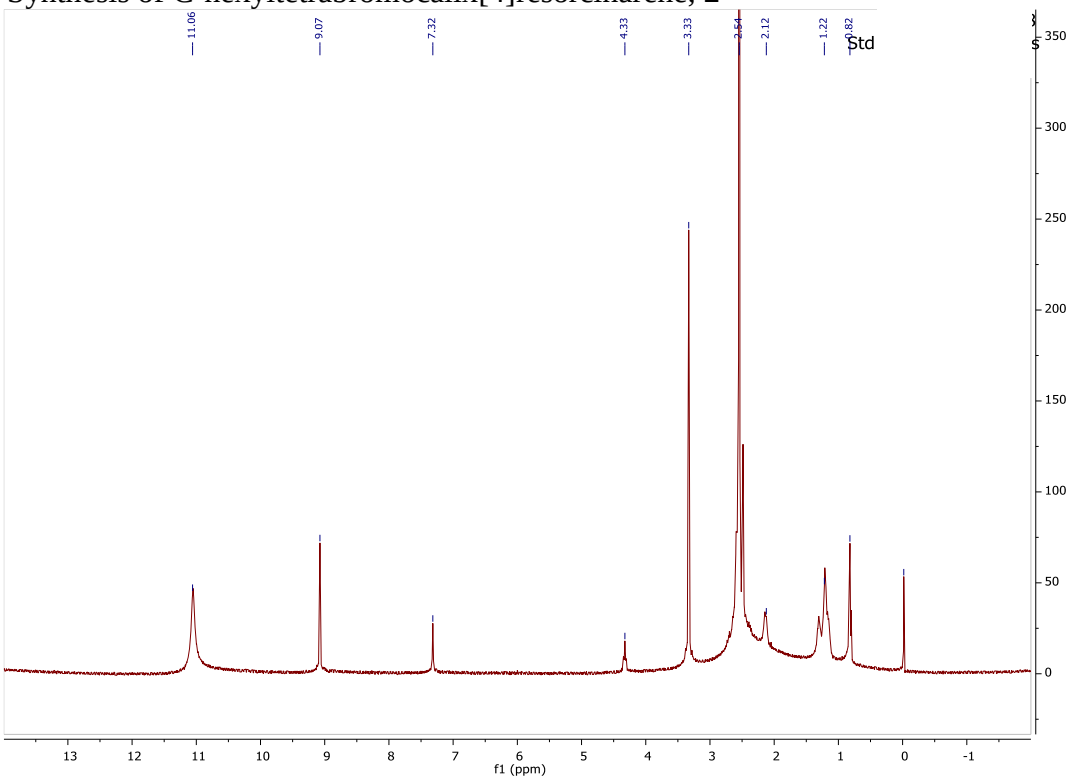

B.23. Synthesis of C-hexyltetrabromocavitand, **T18**

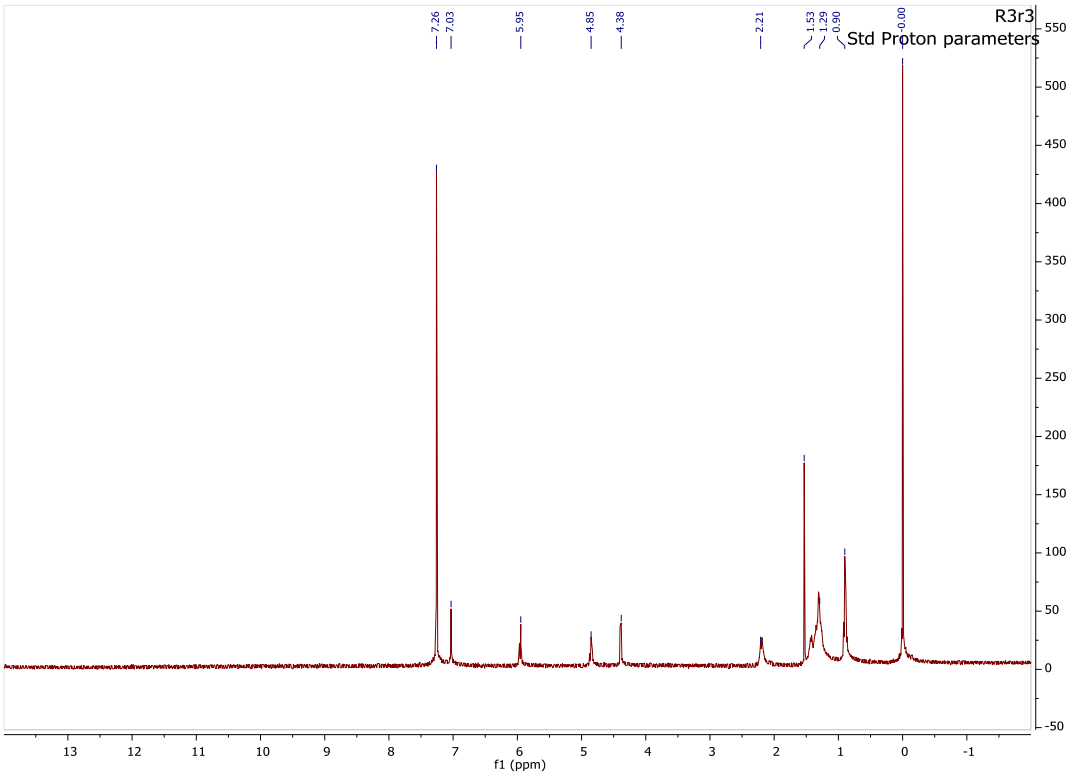

B.24. Synthesis of C-hexyltetraiodocavitand, **T19**

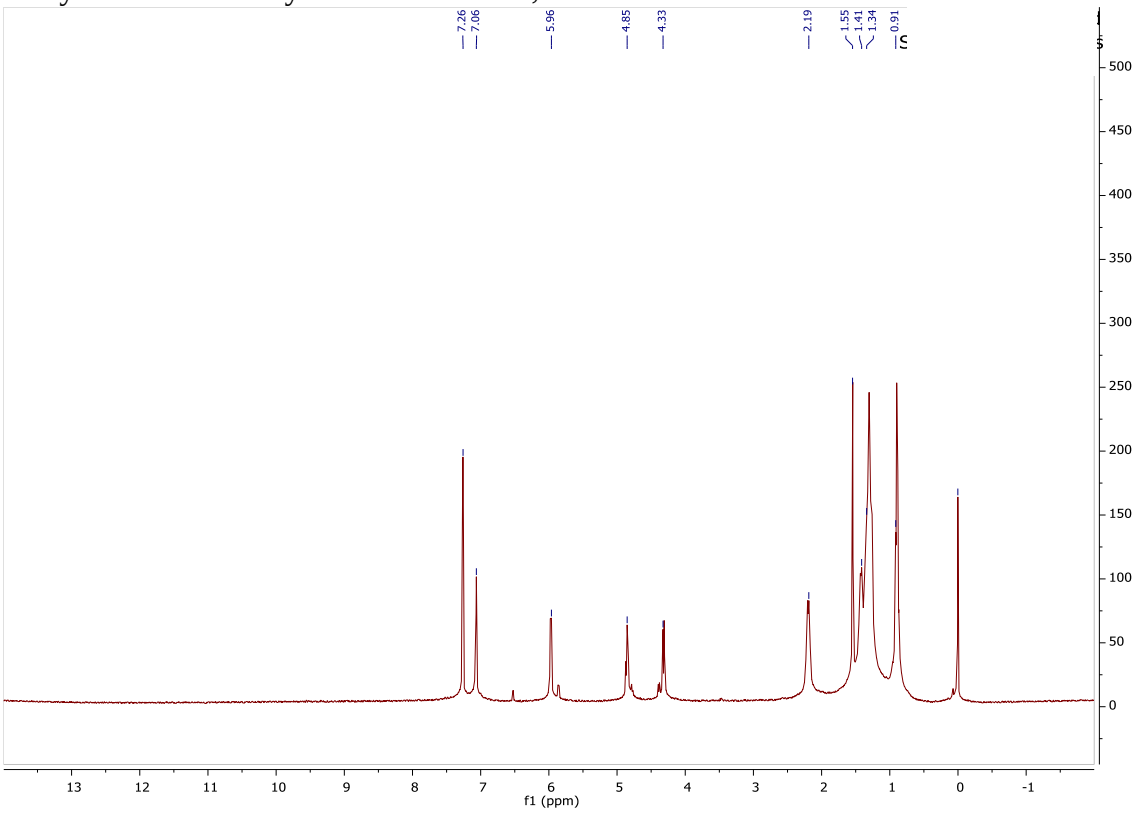

B.25. Synthesis of C-hexyltetra((trimethylsilyl)ethynyl)cavitand, **T20**

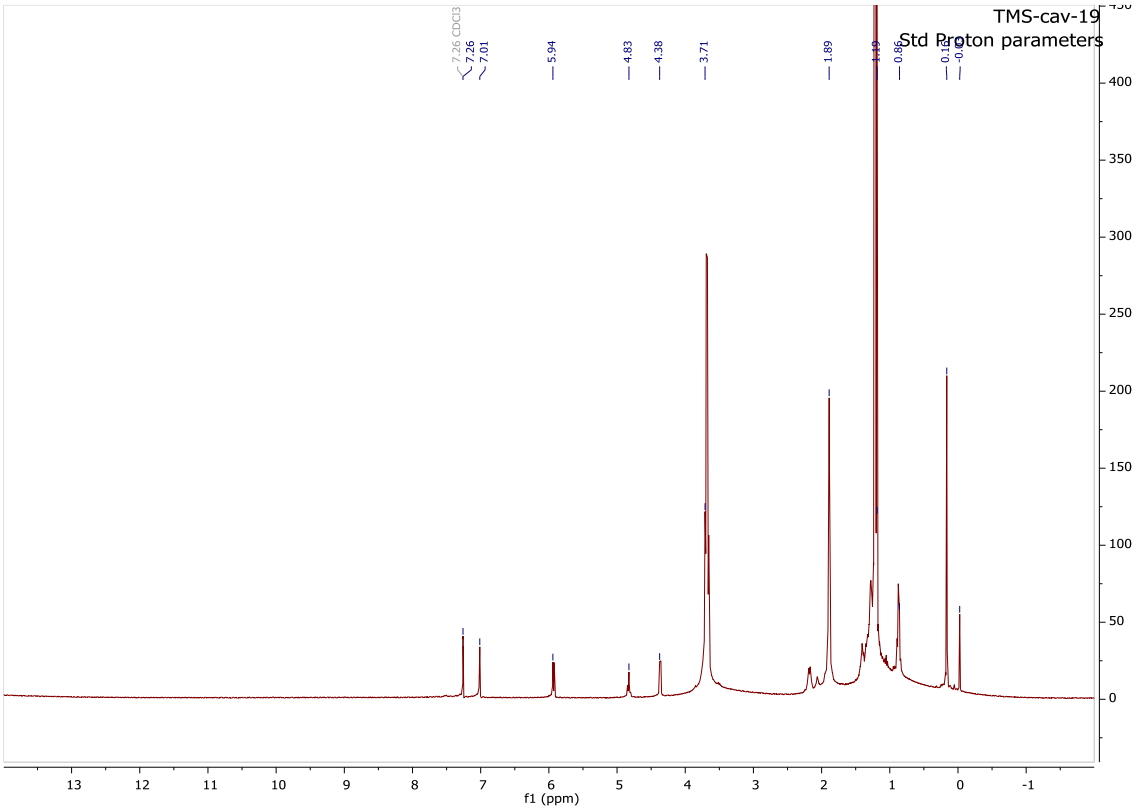

B.26. Synthesis of C-hexyltetra(ethynyl)cavitand, **T21**

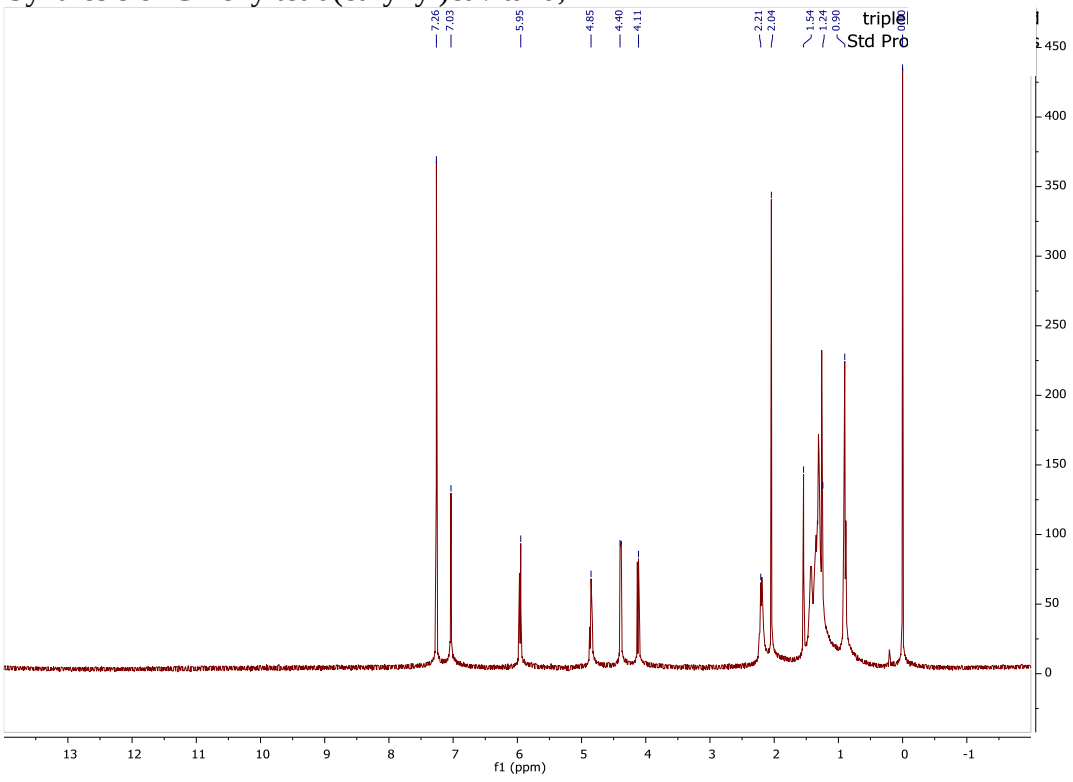

B.27. Synthesis of C-hexyltetra(iodoethynyl)cavitand, **T22**

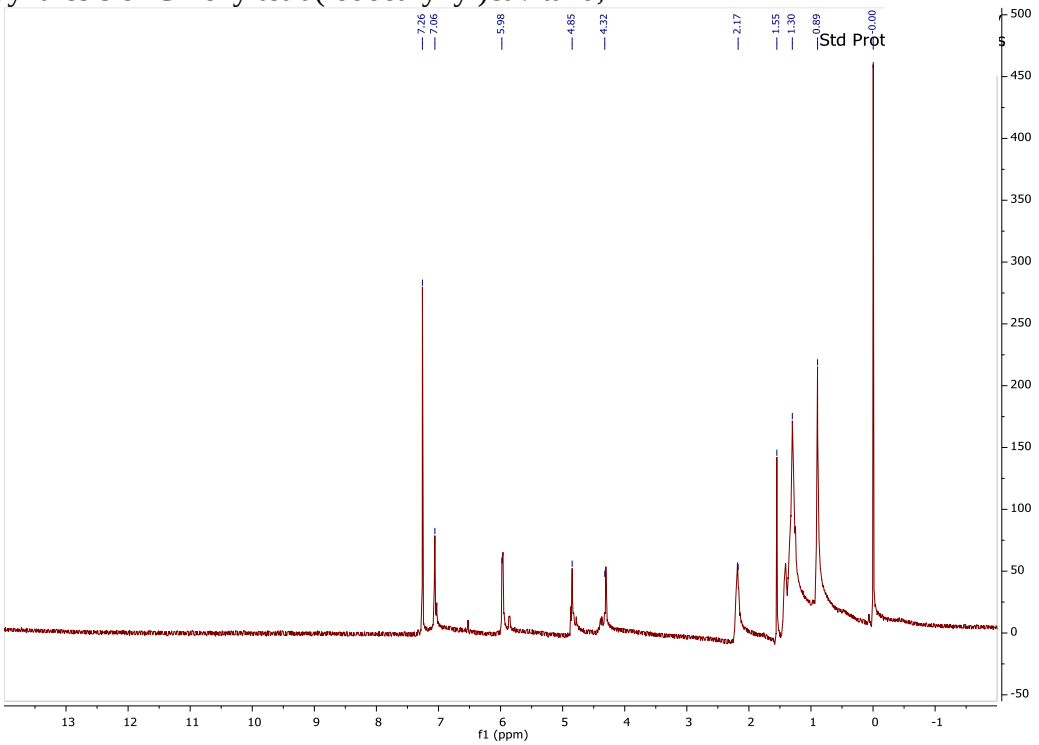

B.28. Synthesis of C-hexyltetra(iodoethynyl)cavitand, **T22**

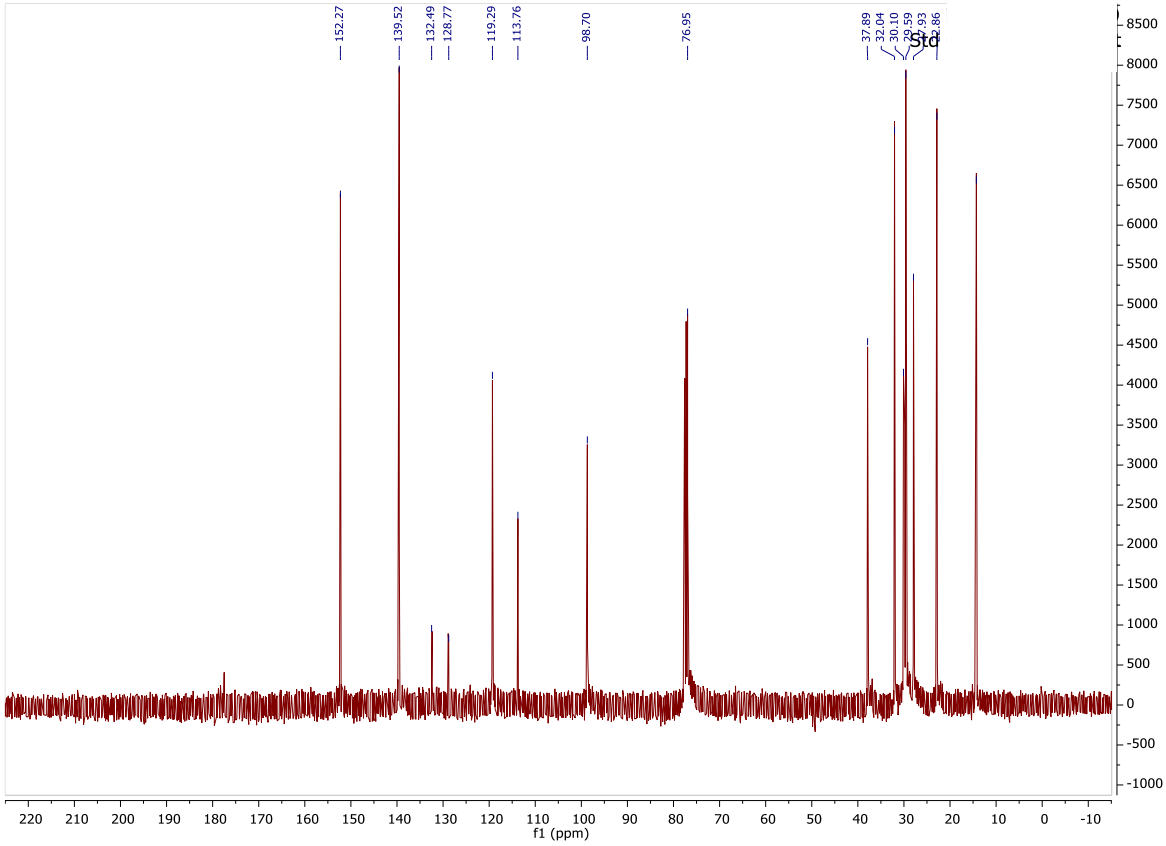

B.29. Synthesis of C- hexyltetraboronic acid dipinacolyl ester cavitand, **T23**

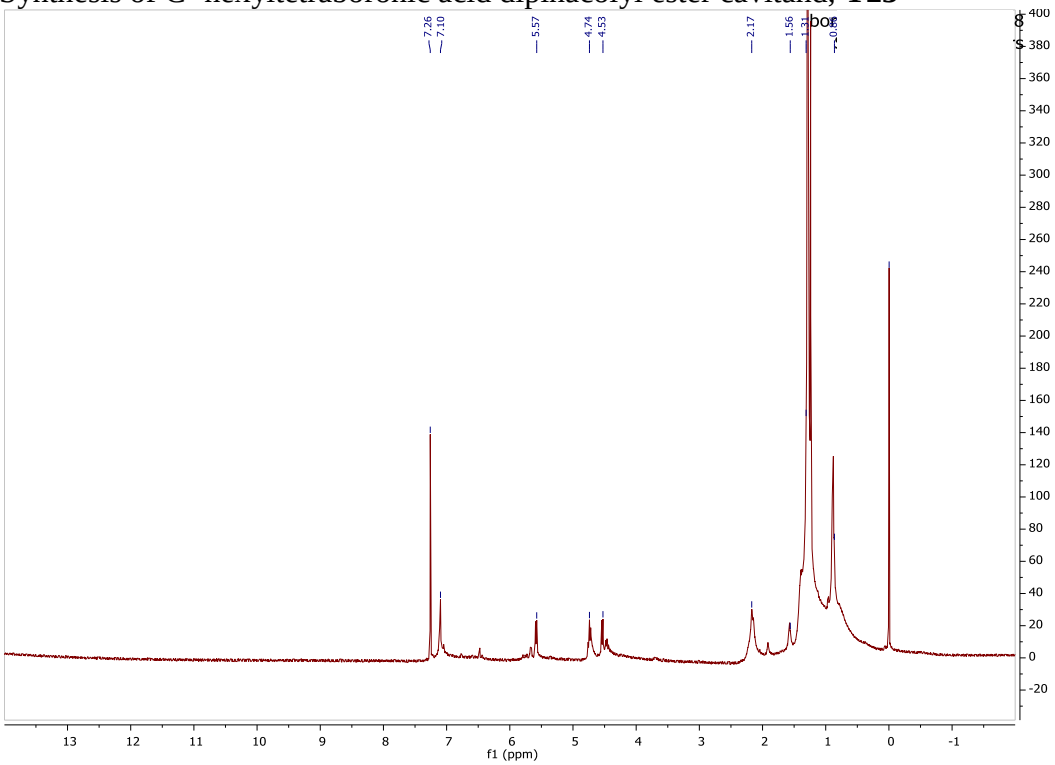

B.30. Synthesis of C-hexyltetra(3-pyridyl) cavitand, **T24**

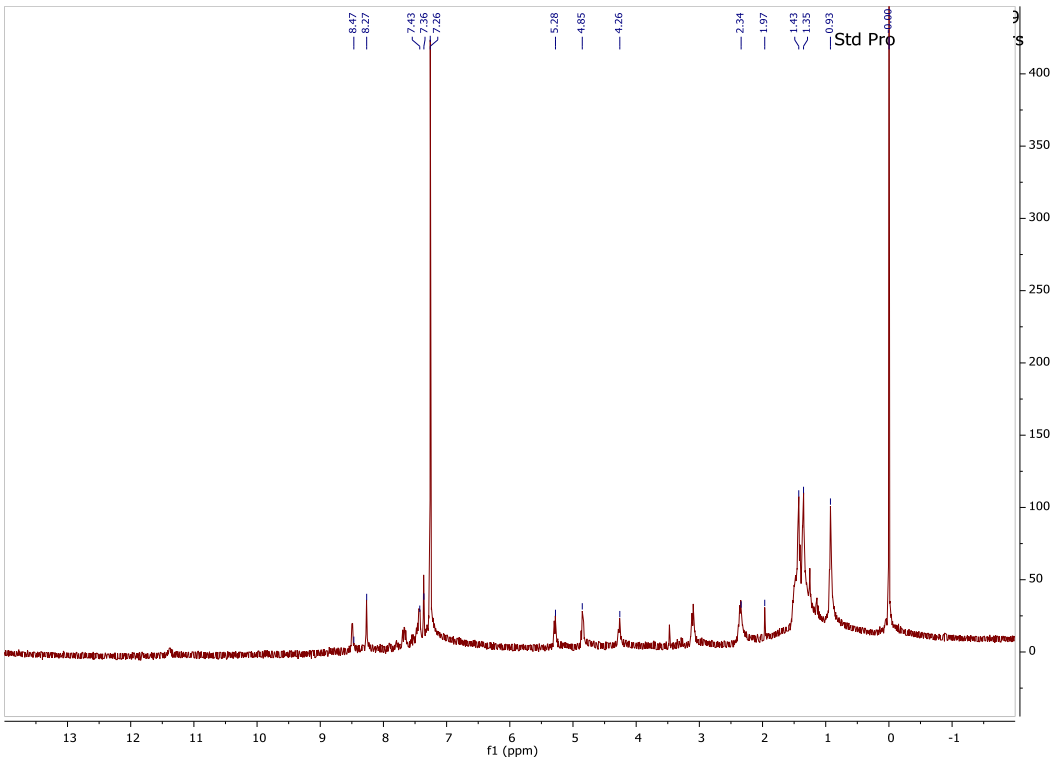

B.31. Synthesis of C-hexyltetra(4-pyridyl) cavitand, **T25**

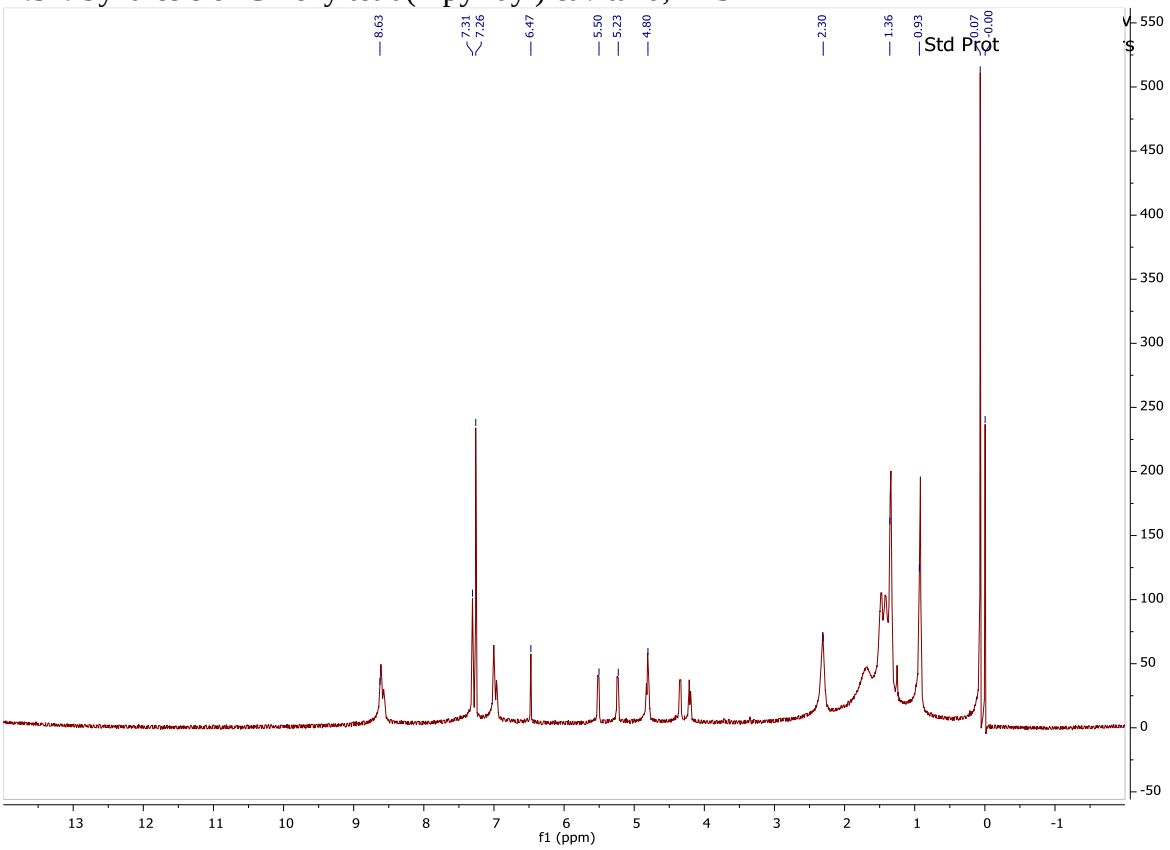

B.32. Synthesis of C-hexyltetra(3-pyrazole) cavitand, **T26**

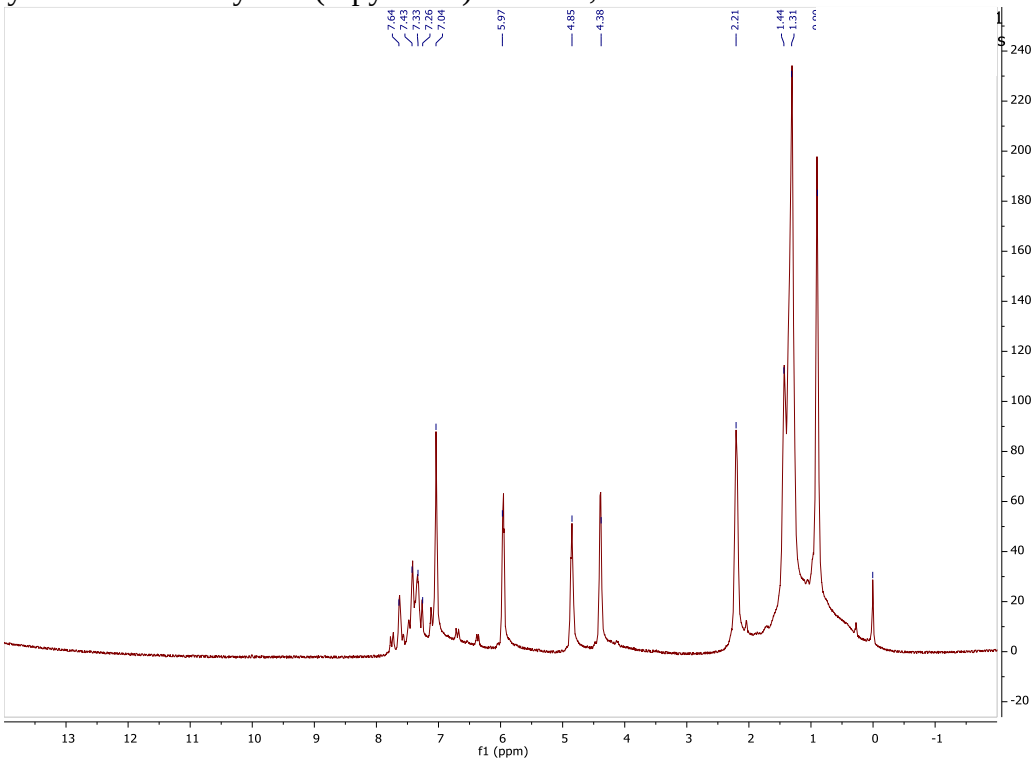

B.33. Synthesis of C-hexyltetracarboxylic cavitand, **T27**

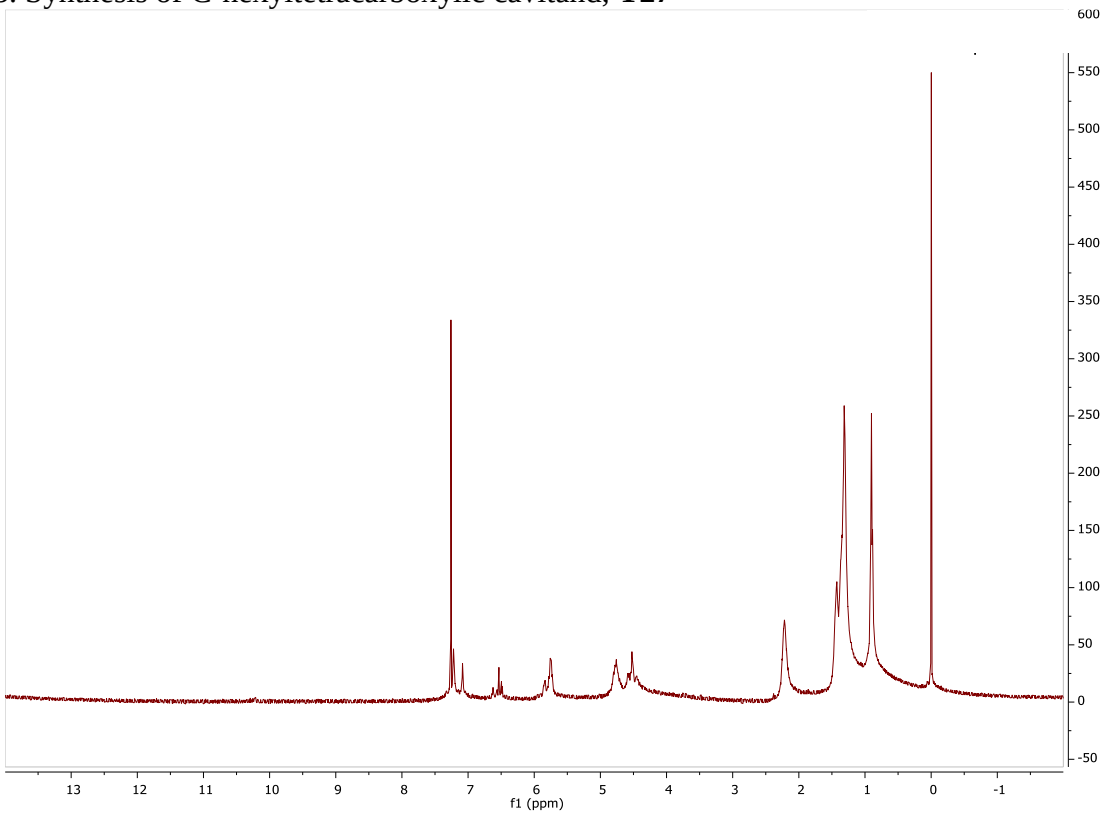

B.34. Synthesis of C-hexyltetracarboxylic cavitand, **T27**

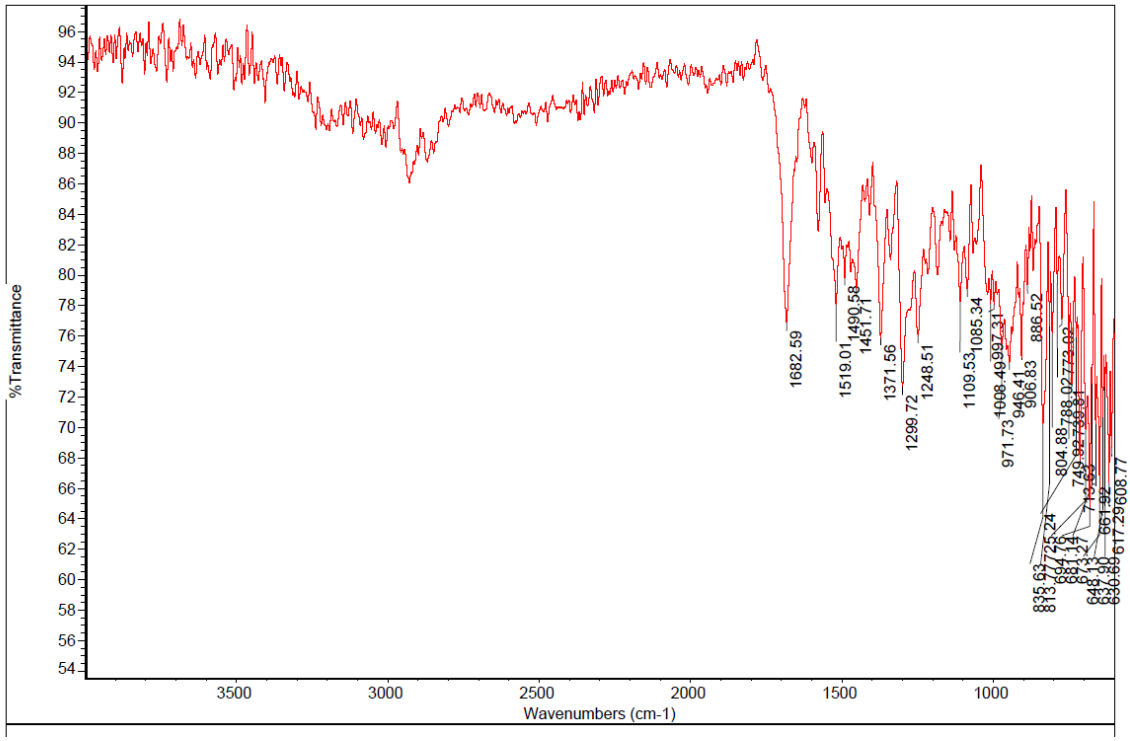

Appendix C – TGA analysis

C1. **T18** recrystallized from xylene

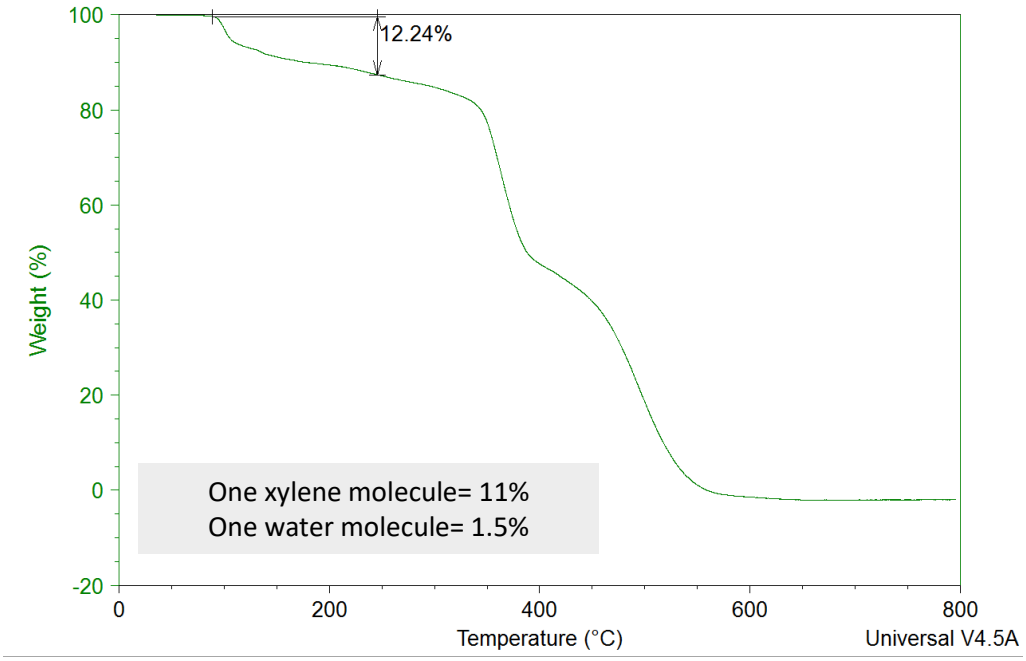

C.2. **T18** recrystallized from dichloromethane (DCM)

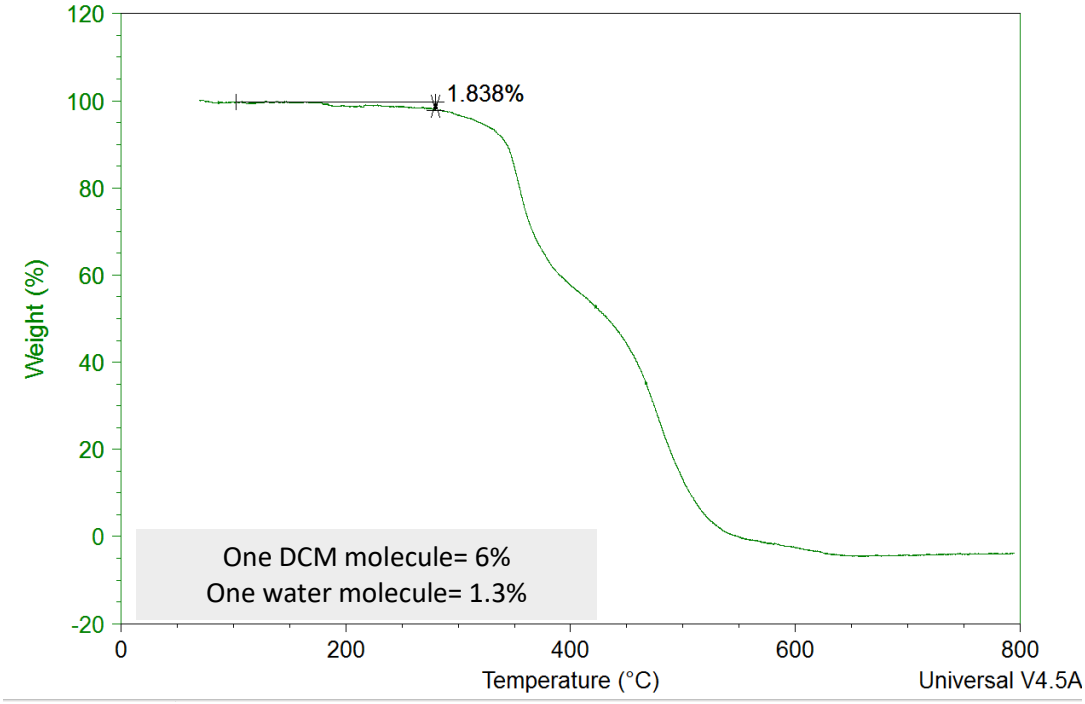

C3. **T18** recrystallized from ethyl acetate (EtOAc)

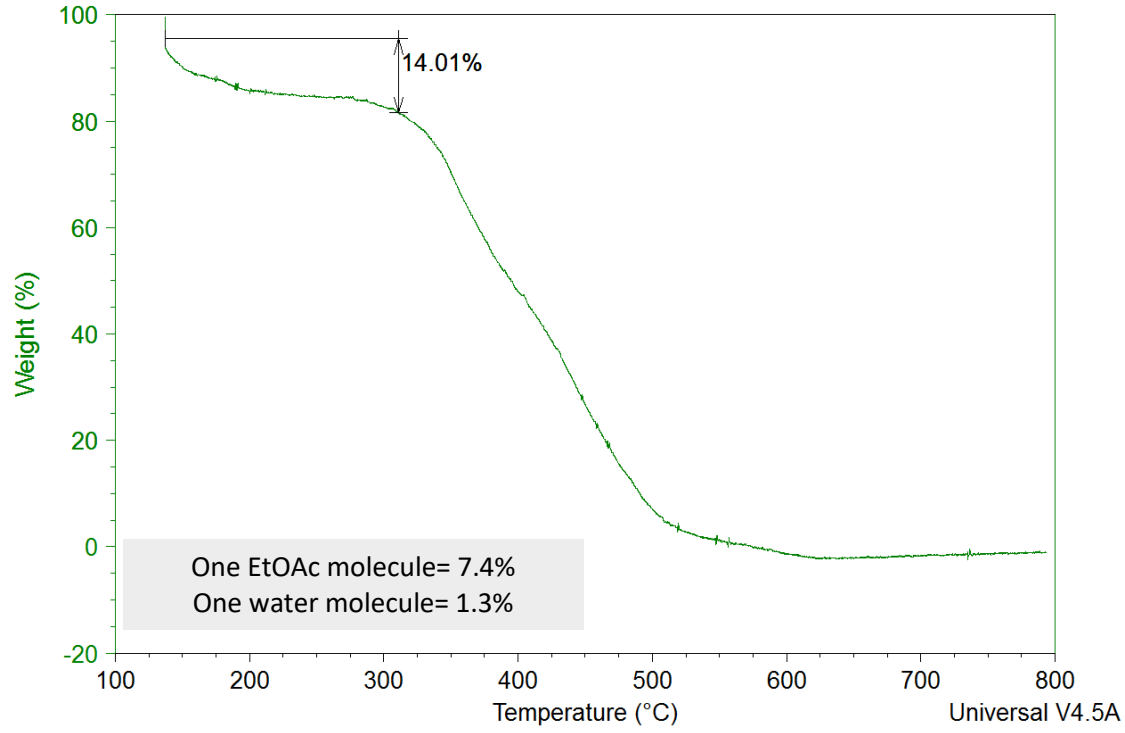

C4. **T18** recrystallized from acetonitrile (ACN)

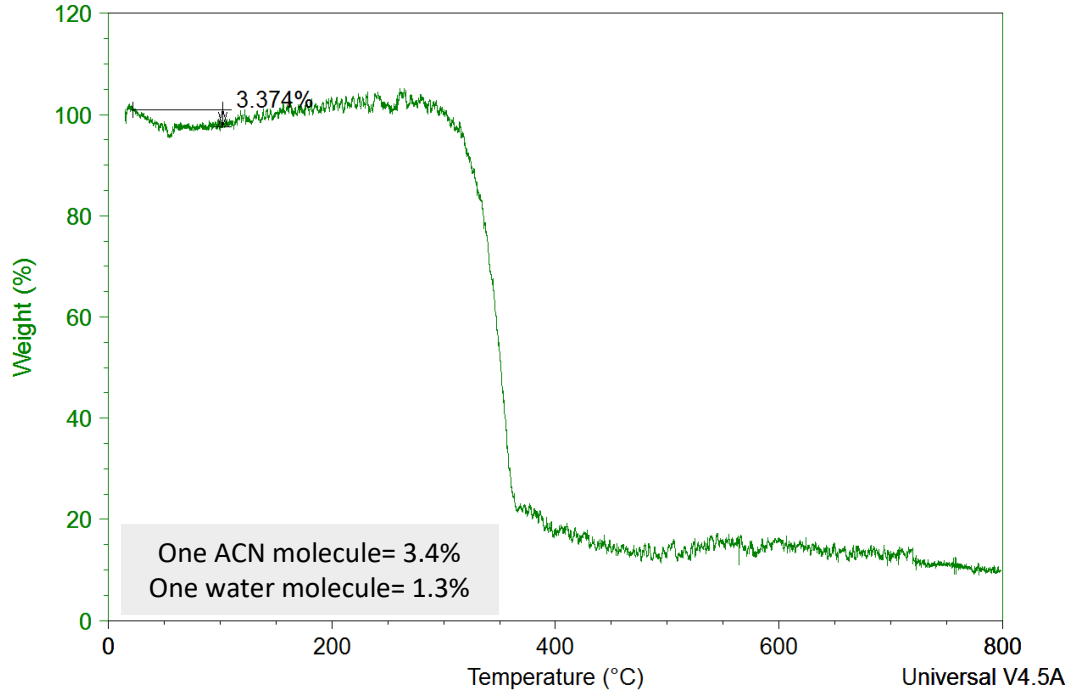

C5. **T18** recrystallized from dimethyl sulfoxide (DMSO)

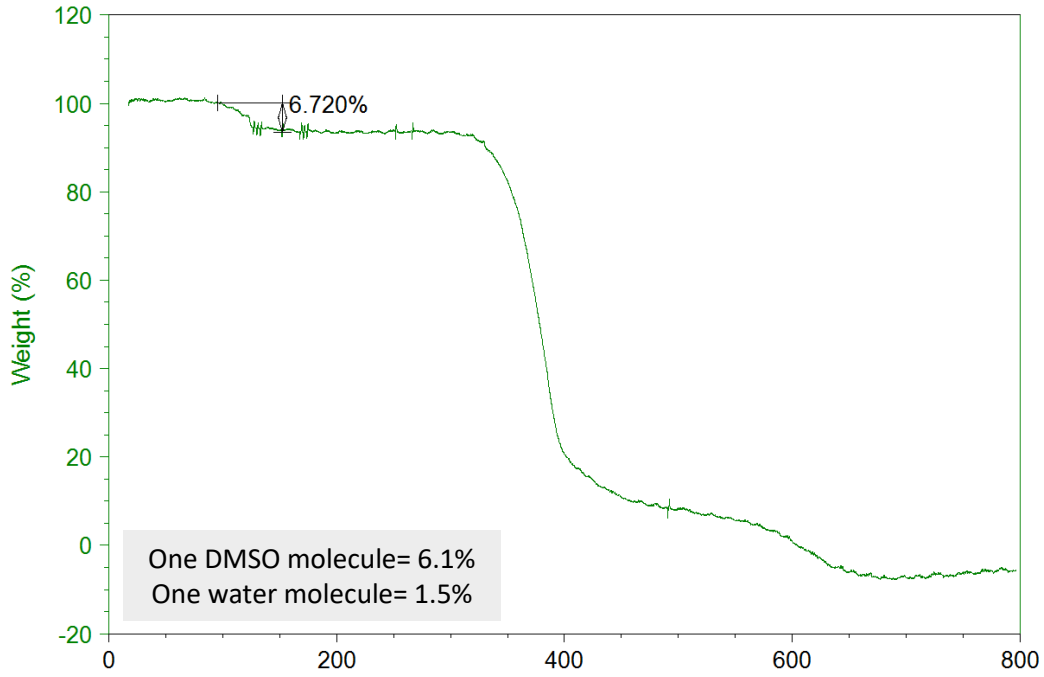

C6. **T18** recrystallized from equimolar mixture of solvents

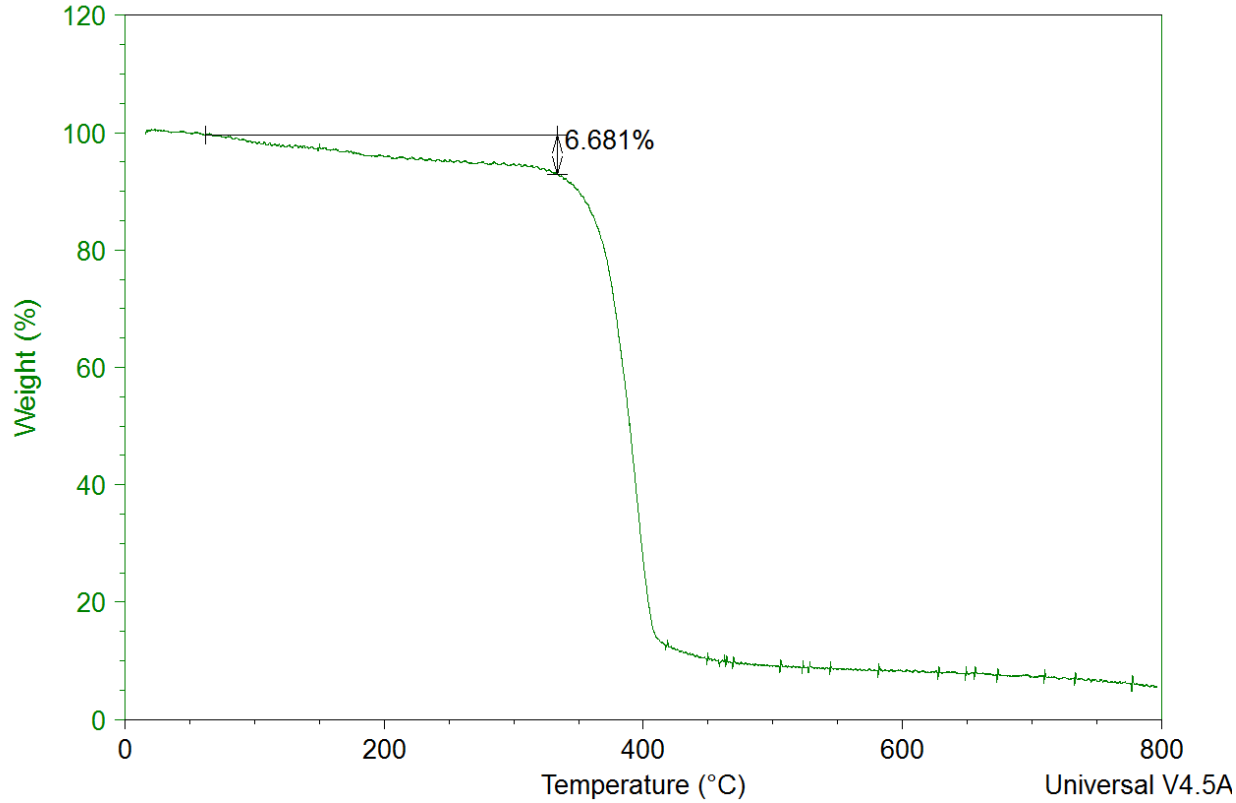

C7. **T19** recrystallized from xylene

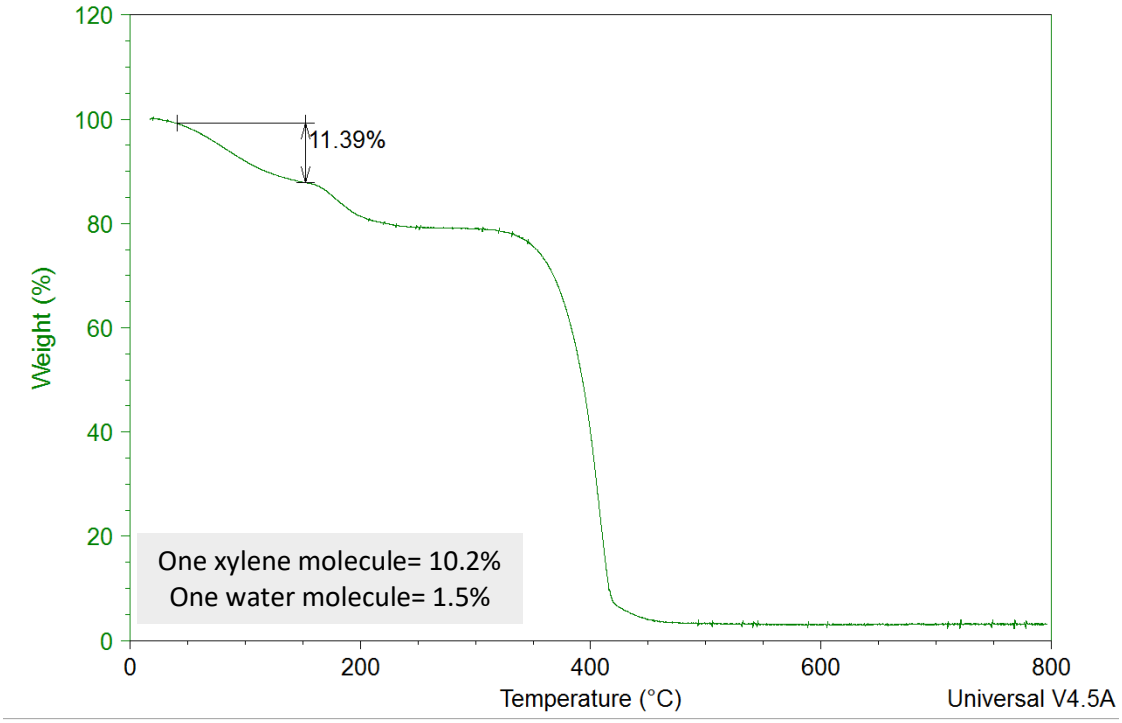

C8. **T19** recrystallized from dichloromethane (DCM)

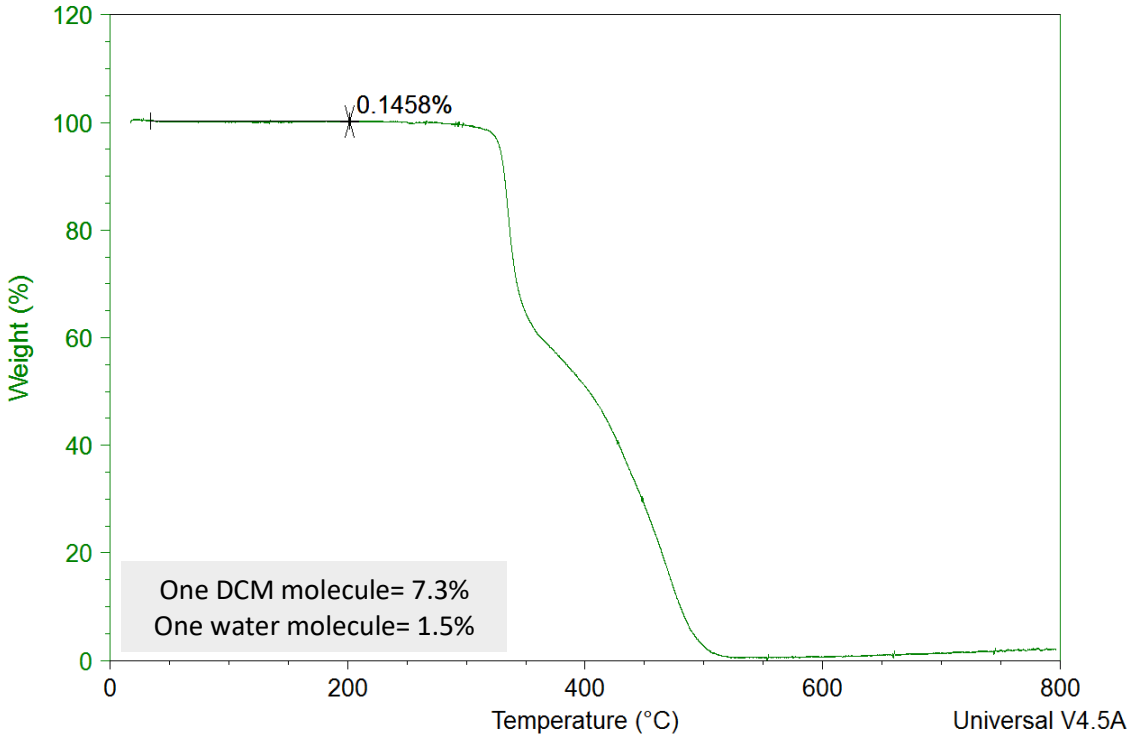

C9. **T19** recrystallized from ethyl acetate (EtOAc)

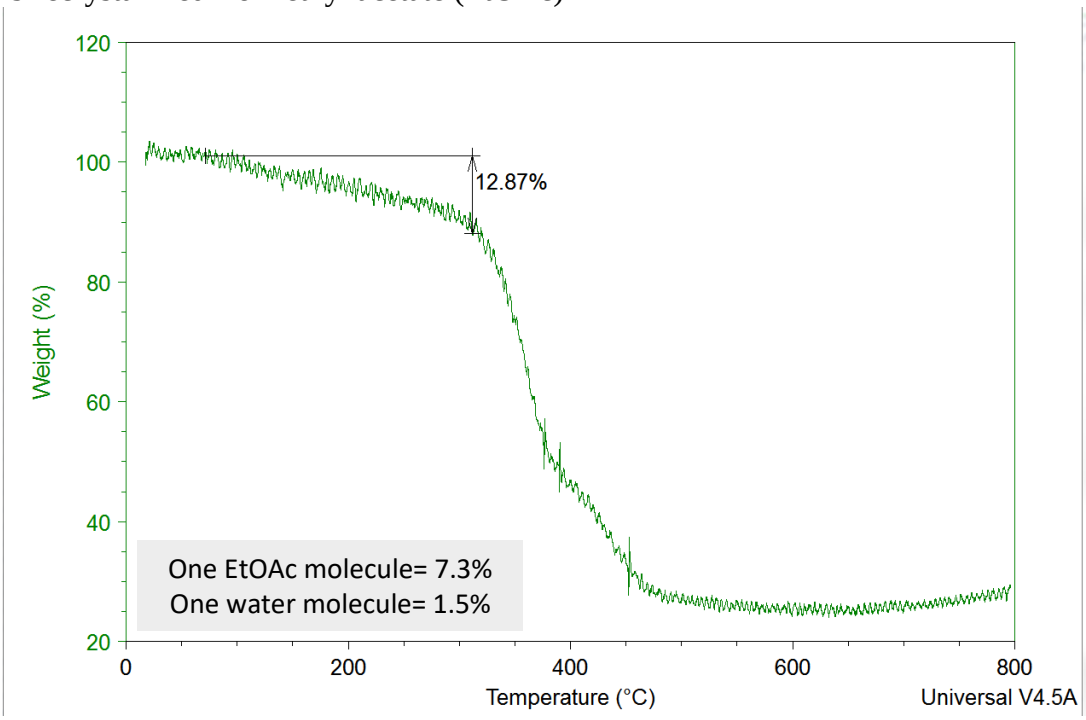

C10. **T19** recrystallized from acetonitrile (ACN)

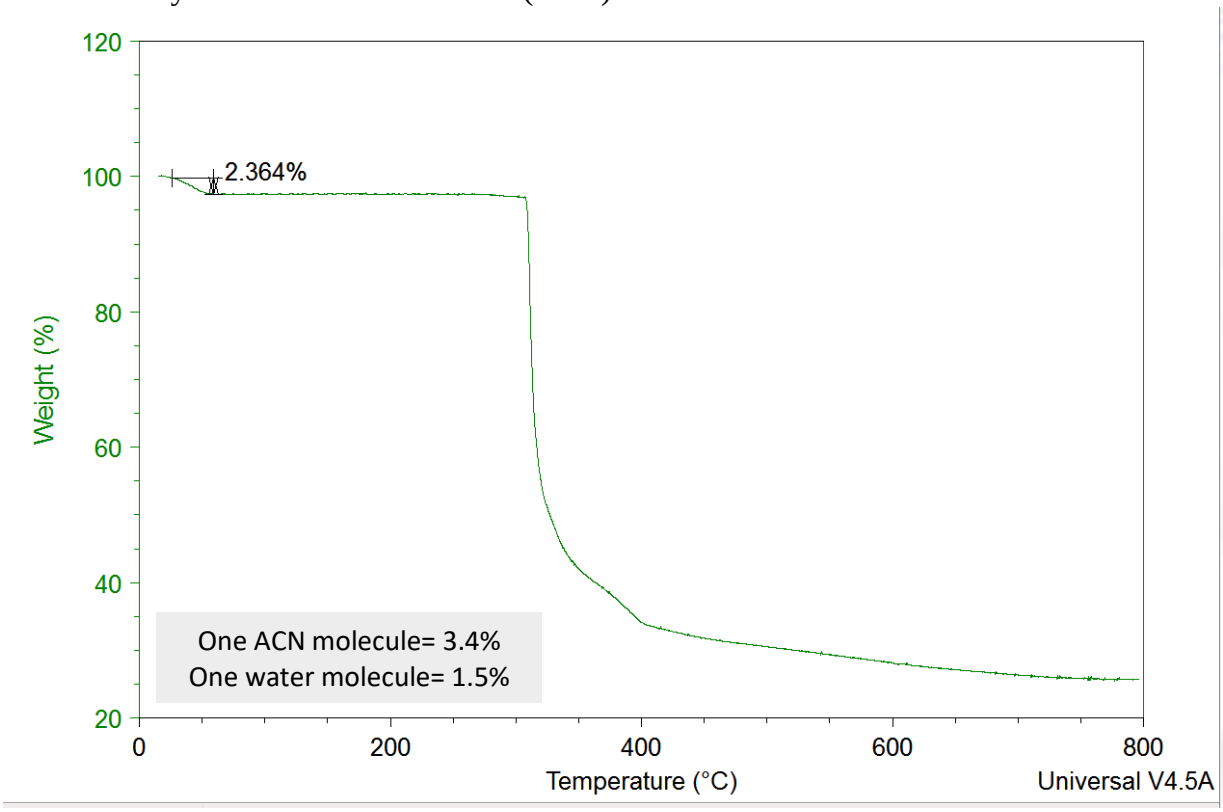

C11. **T19** recrystallized from dimethyl sulfoxide (DMSO)

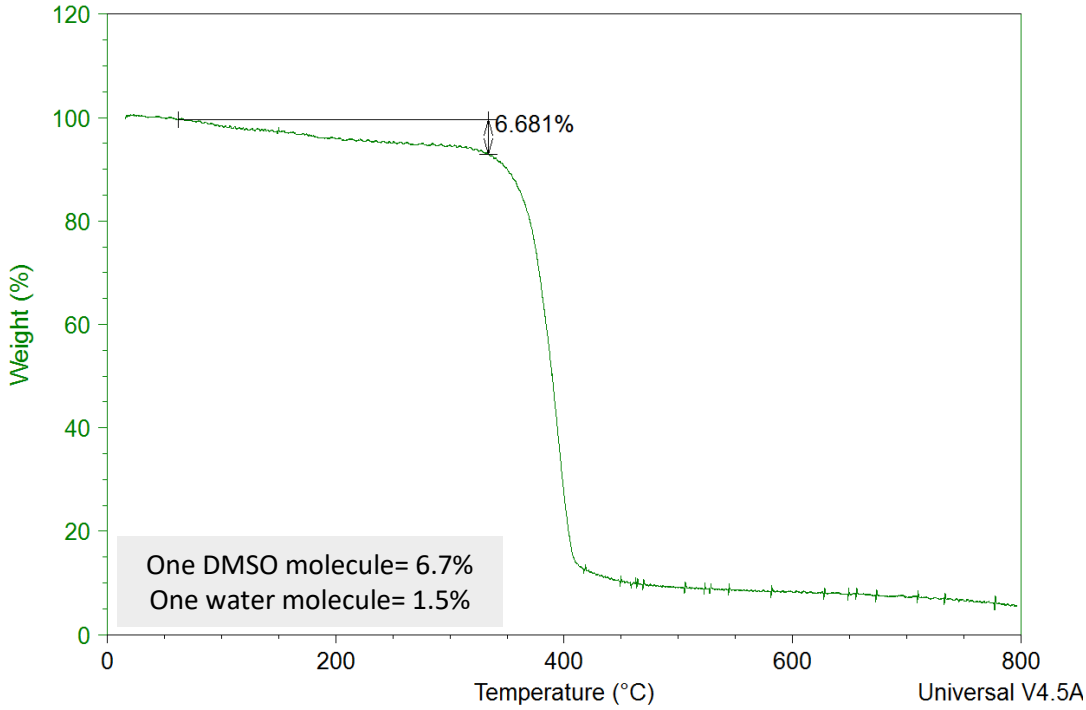

C12. **T19** recrystallized from equimolar mixture of solvents

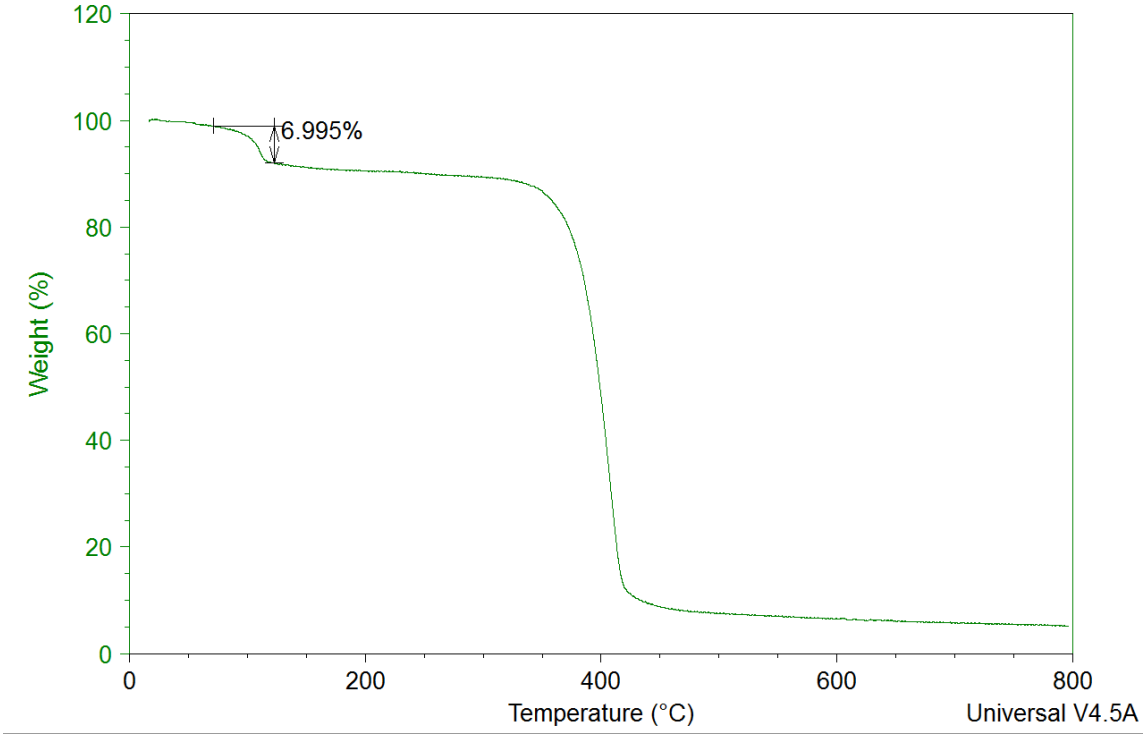

C13. **T20** recrystallized from xylene

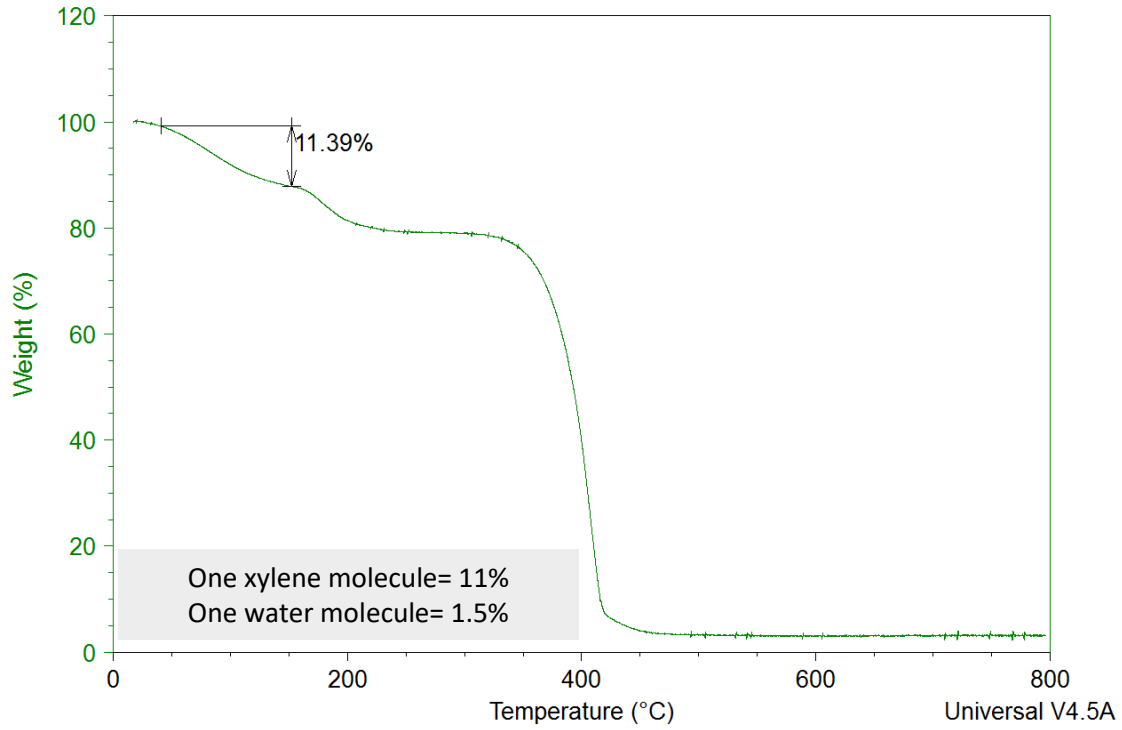

C14. **T20** recrystallized from dichloromethane (DCM)

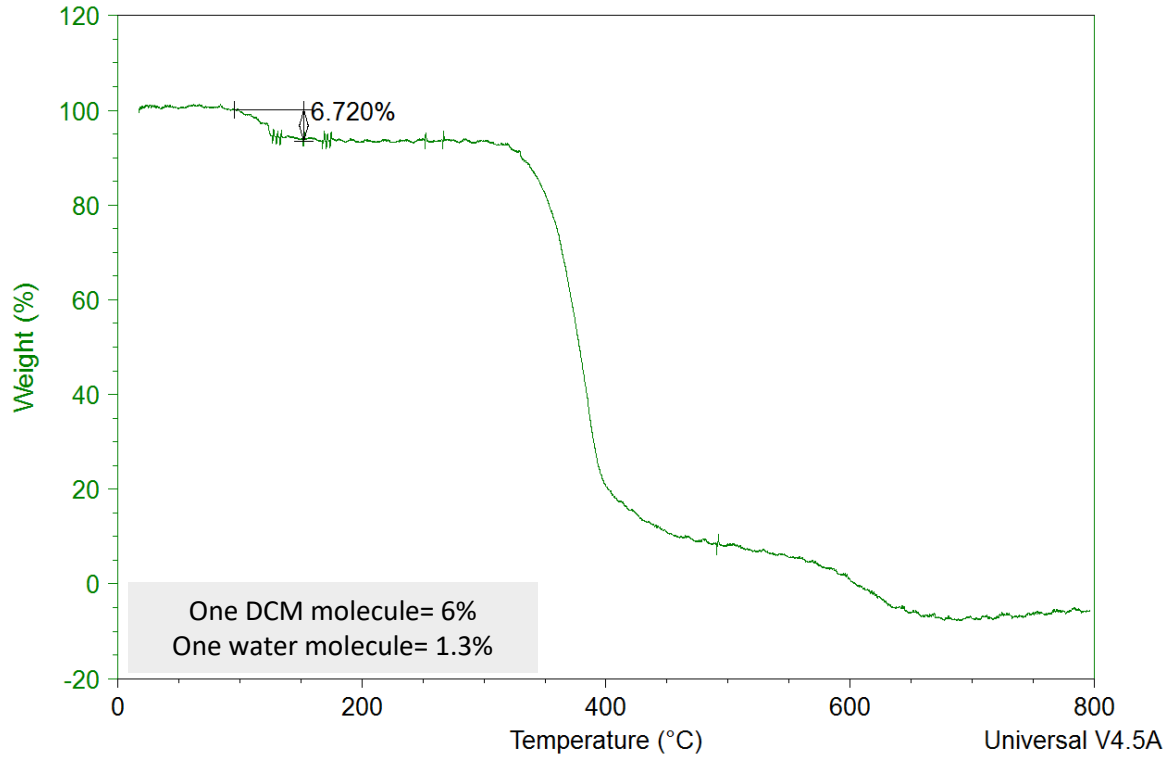

C15. **T20** recrystallized from ethyl acetate (EtOAc)

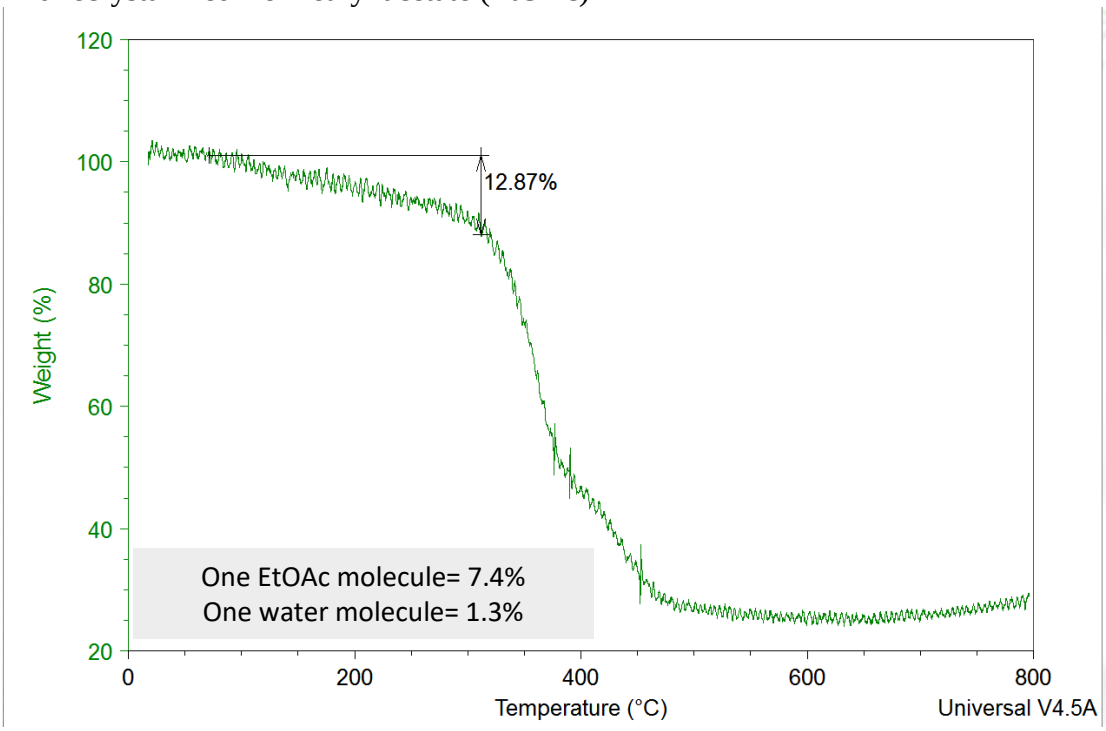

C16. **T20** recrystallized from acetonitrile (ACN)

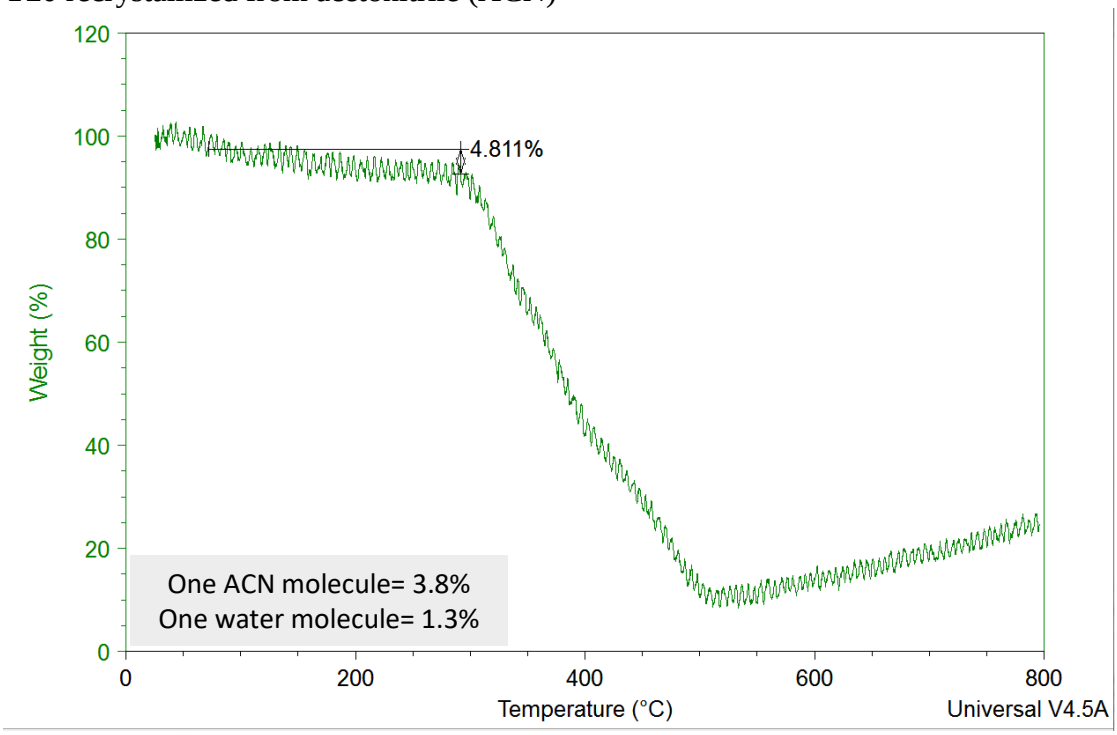

C17. **T20** recrystallized from dimethyl sulfoxide (DMSO)

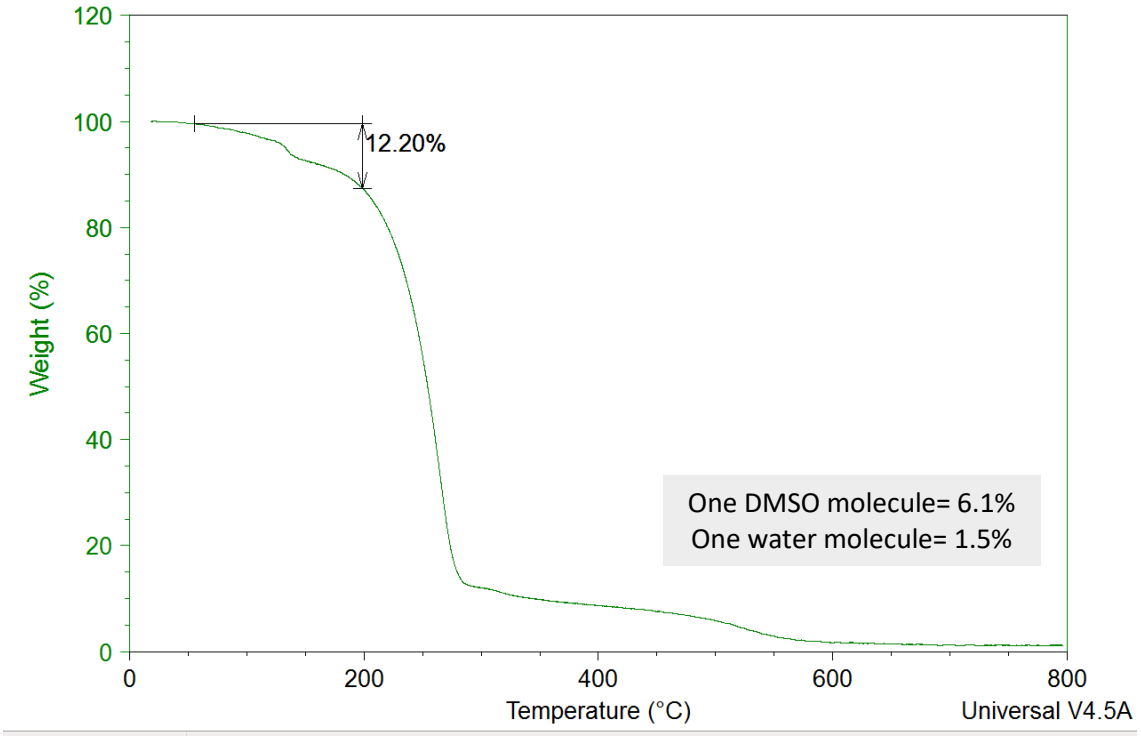

C18. **T20** recrystallized from equimolar mixture of solvents

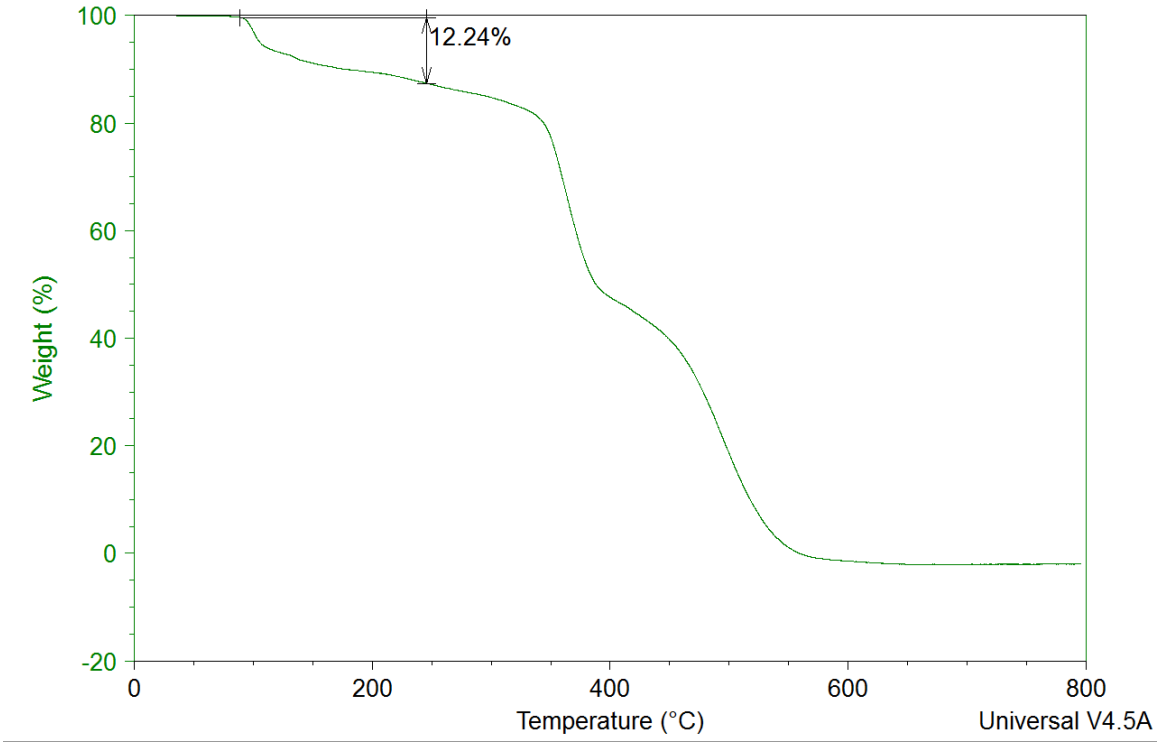

C19. **T21** recrystallized from xylene

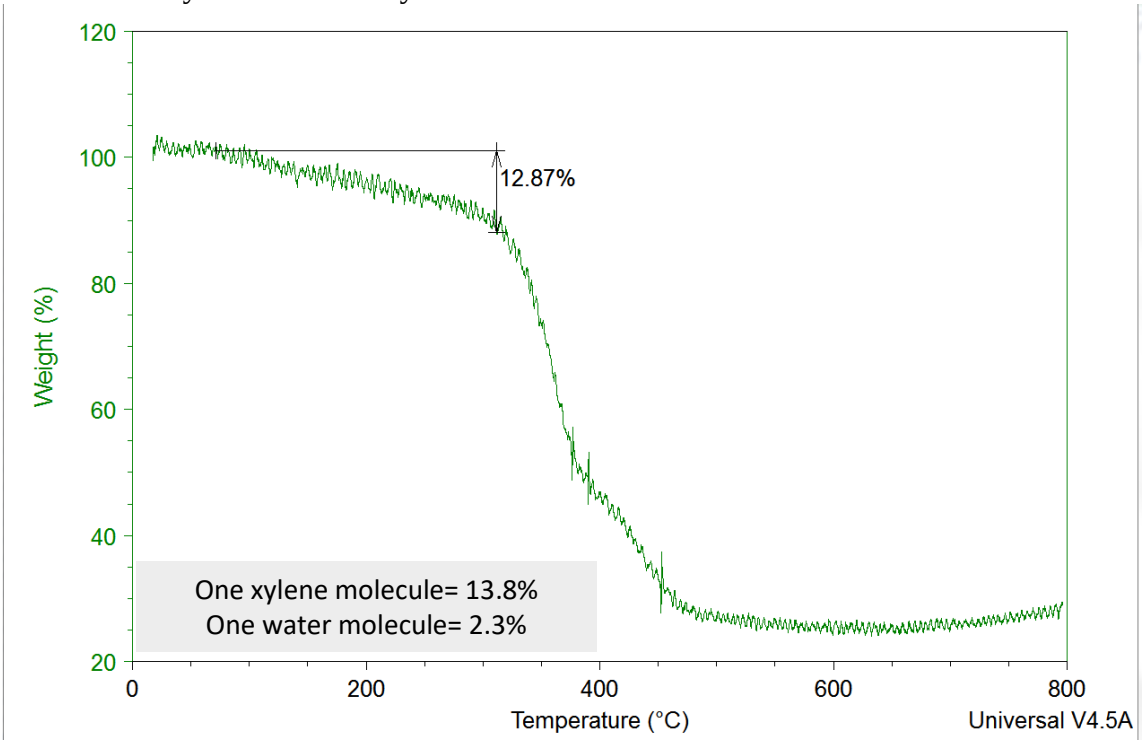

C20. **T21** recrystallized from dichloromethane (DCM)

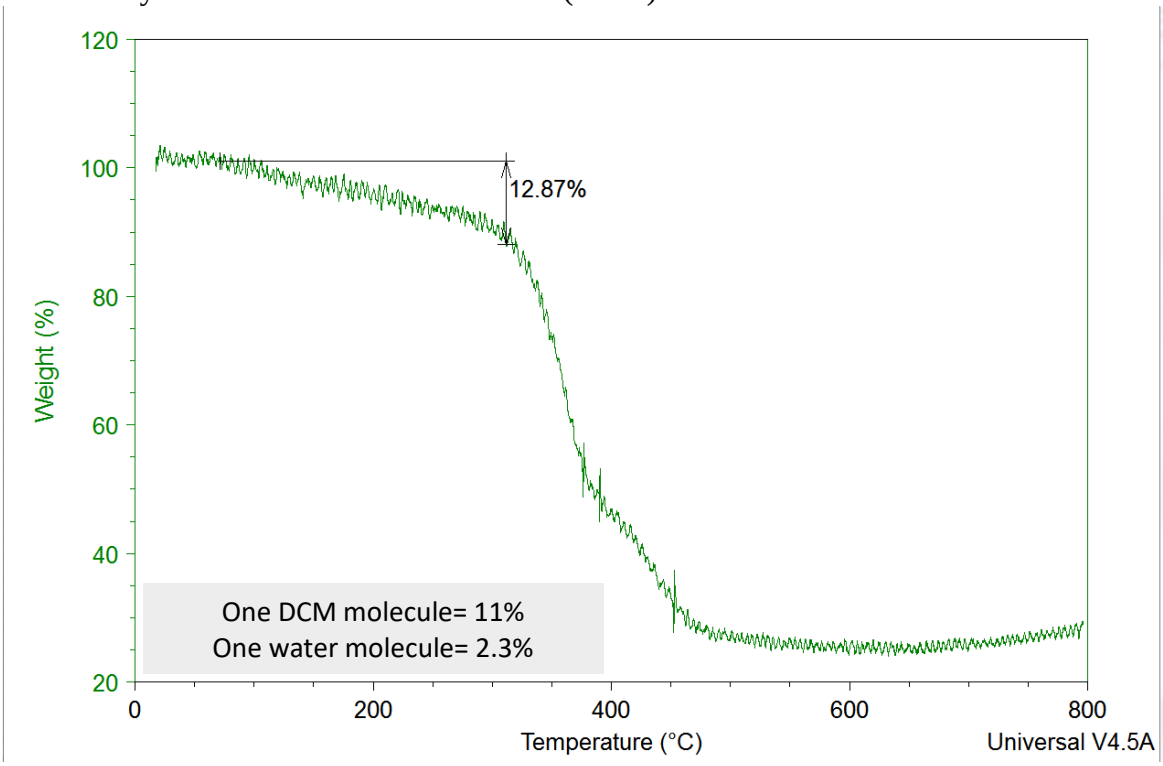

C21. **T21** recrystallized from ethyl acetate (EtOAc)

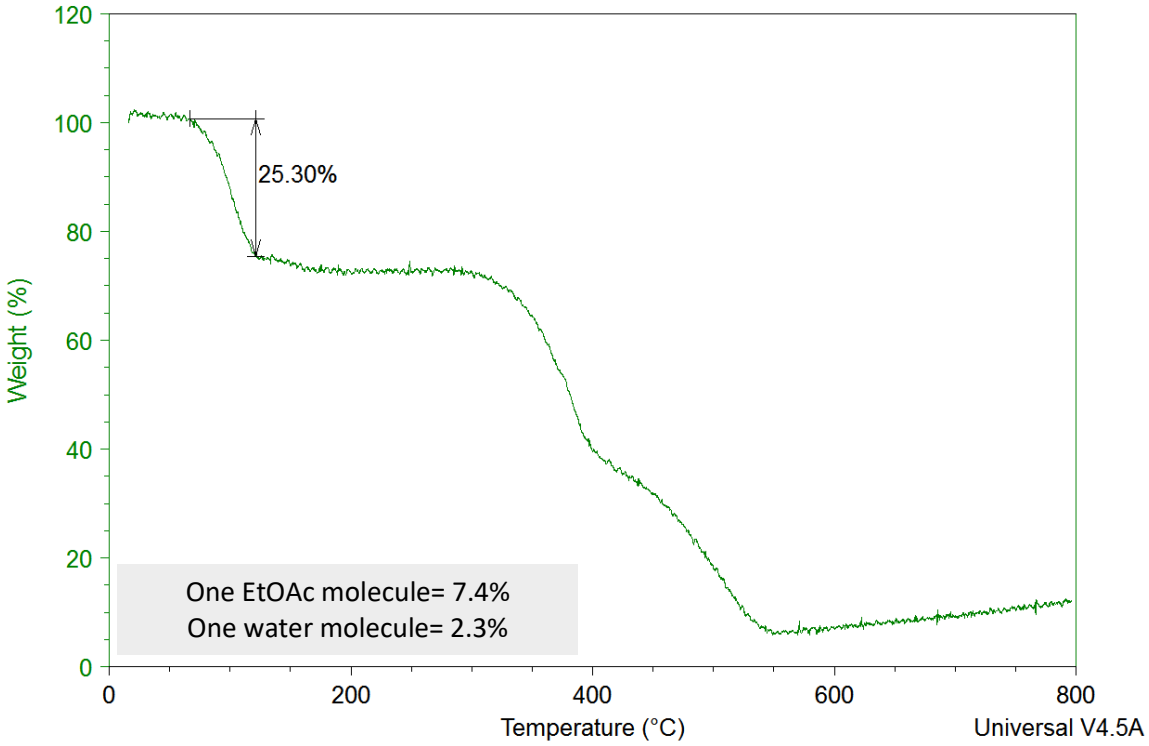

C22. **T21** recrystallized from acetonitrile (ACN)

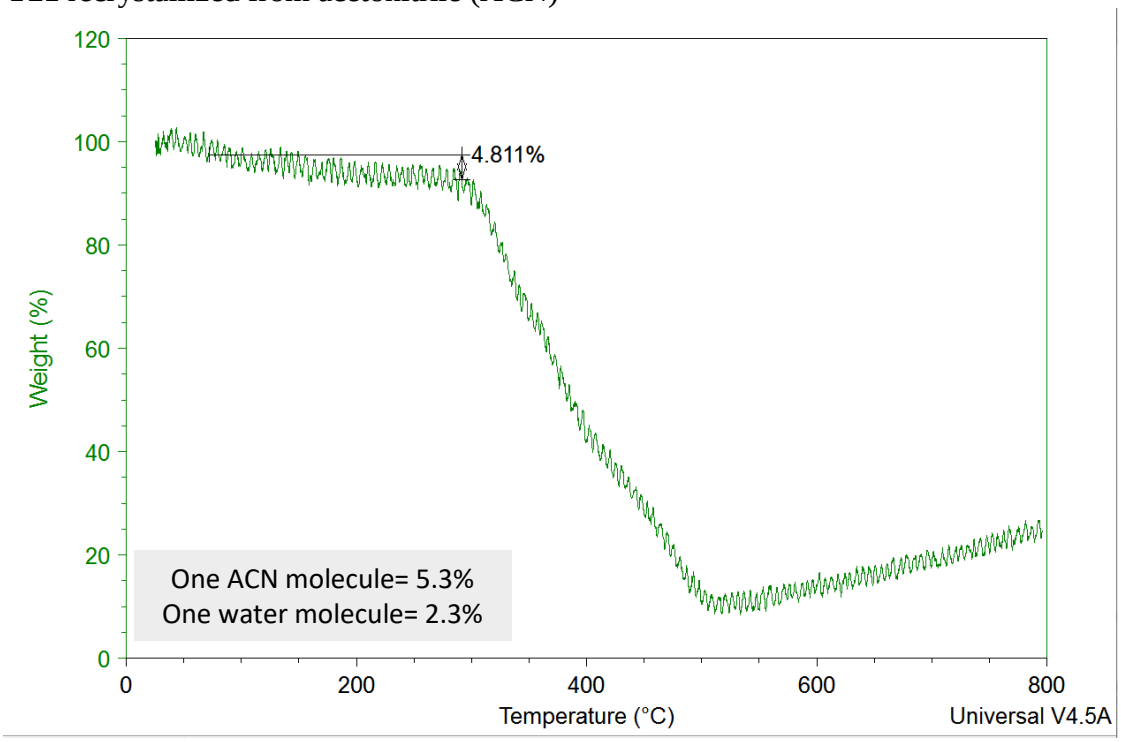

C23. **T21** recrystallized from dimethyl sulfoxide (DMSO)

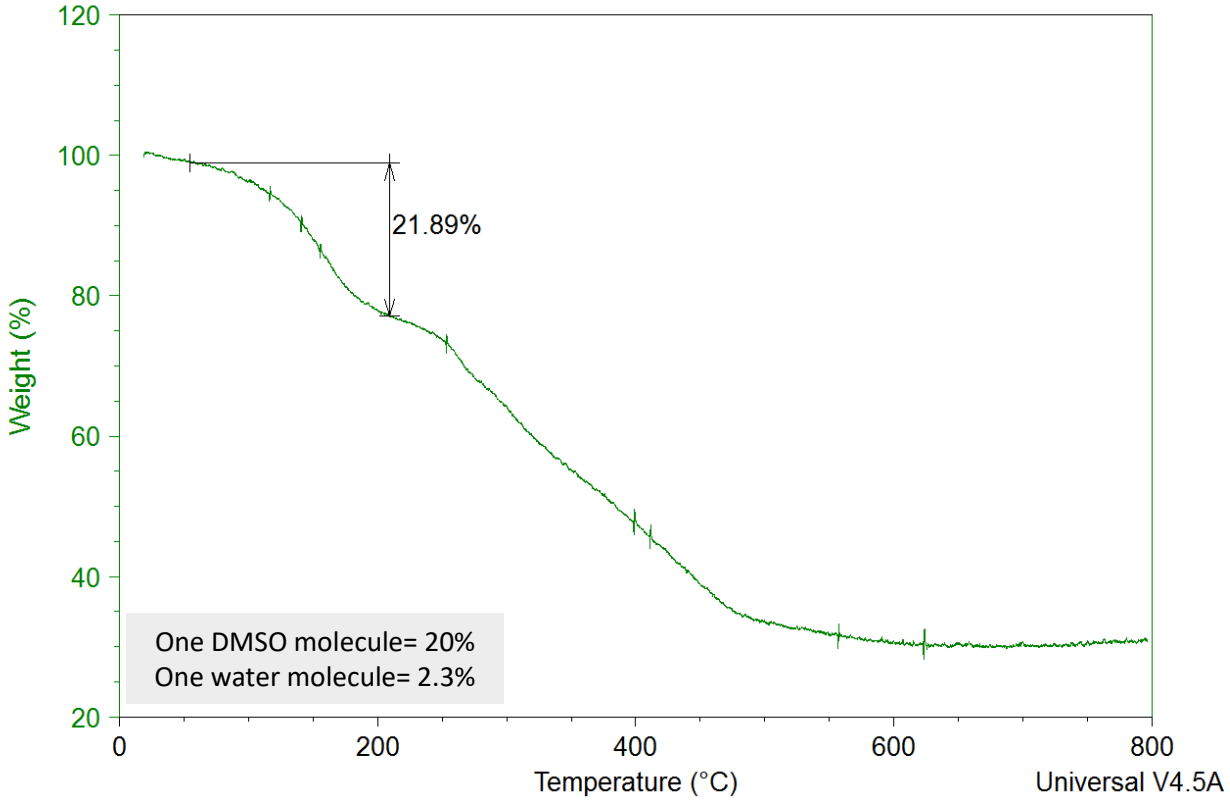

C24. **T21** recrystallized from equimolar mixture of solvents

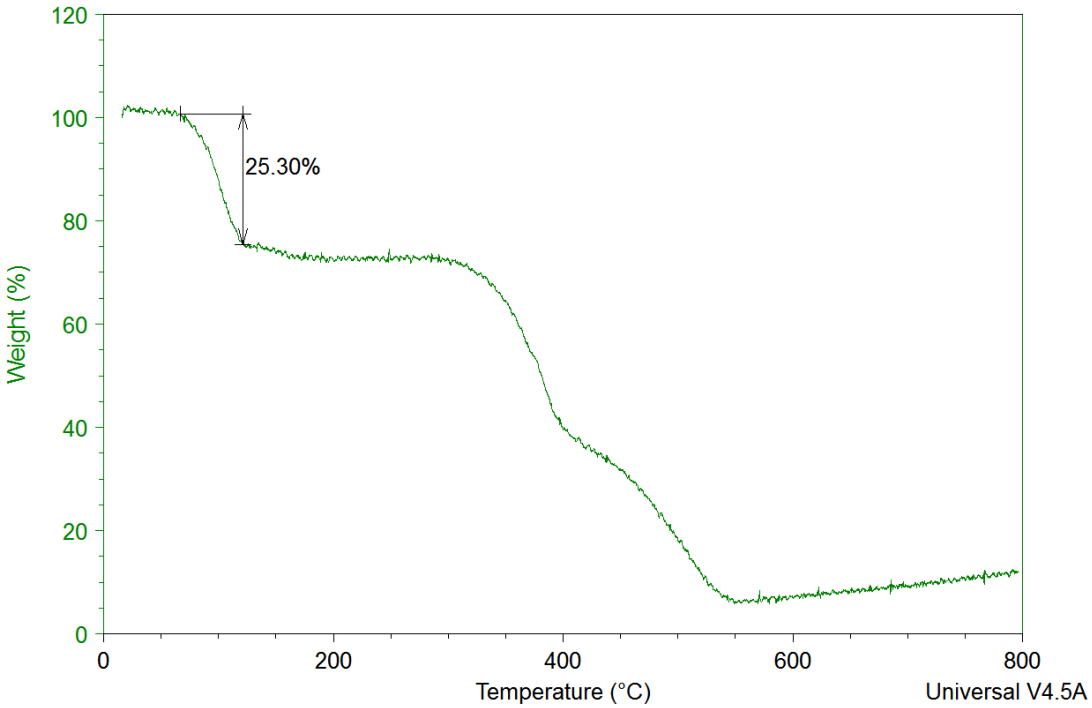

C25. **T22** recrystallized from xylene

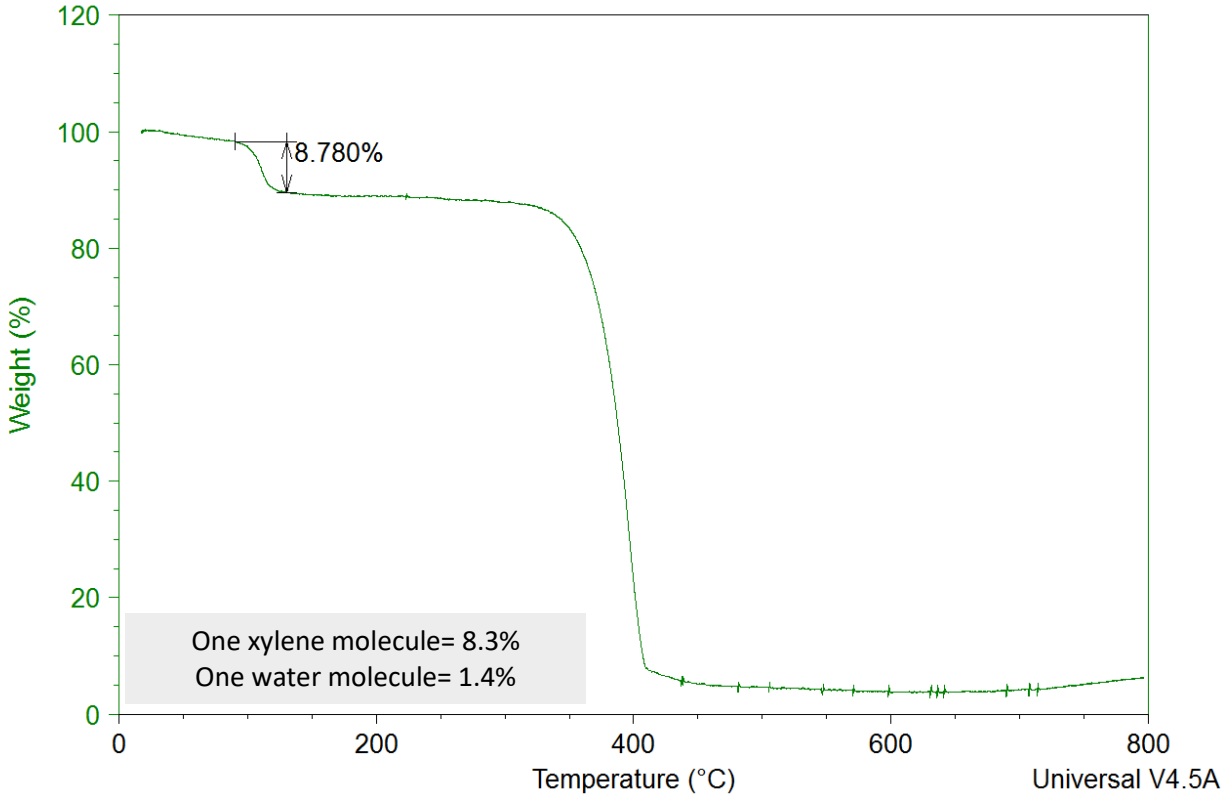

C26. **T22** recrystallized from dichloromethane (DCM)

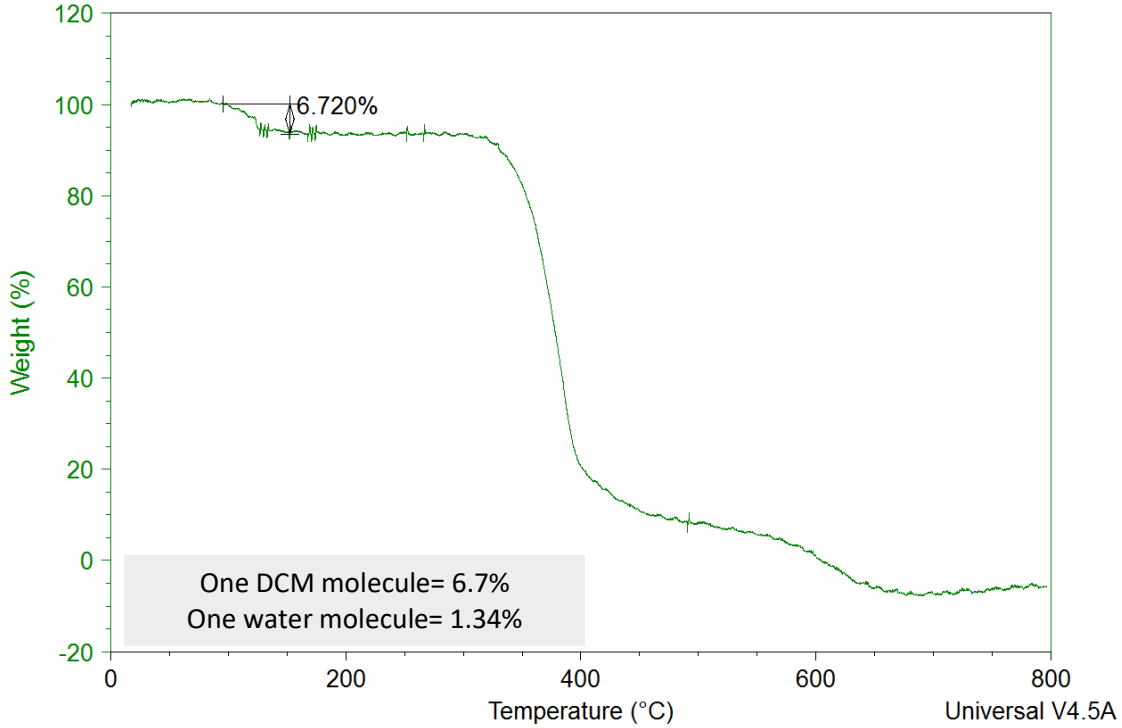

C27. **T22** recrystallized from ethyl acetate (EtOAc)

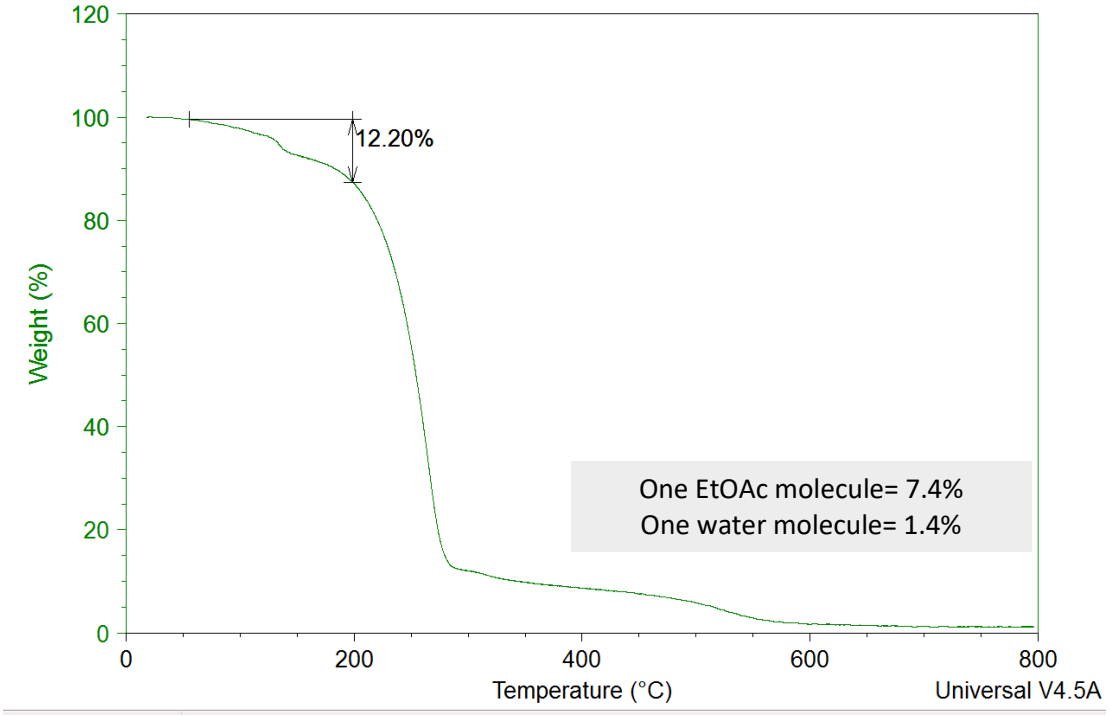

C28. **T22** recrystallized from acetonitrile (ACN)

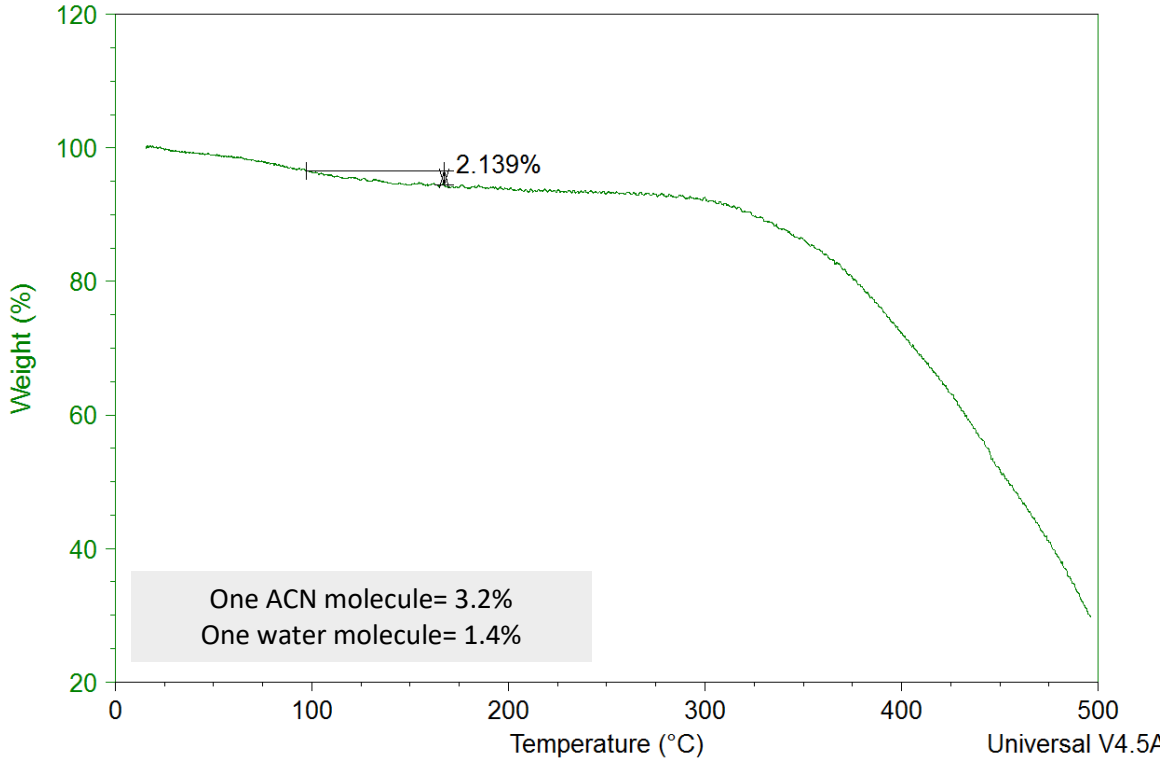

C29. **T22** recrystallized from dimethyl sulfoxide (DMSO)

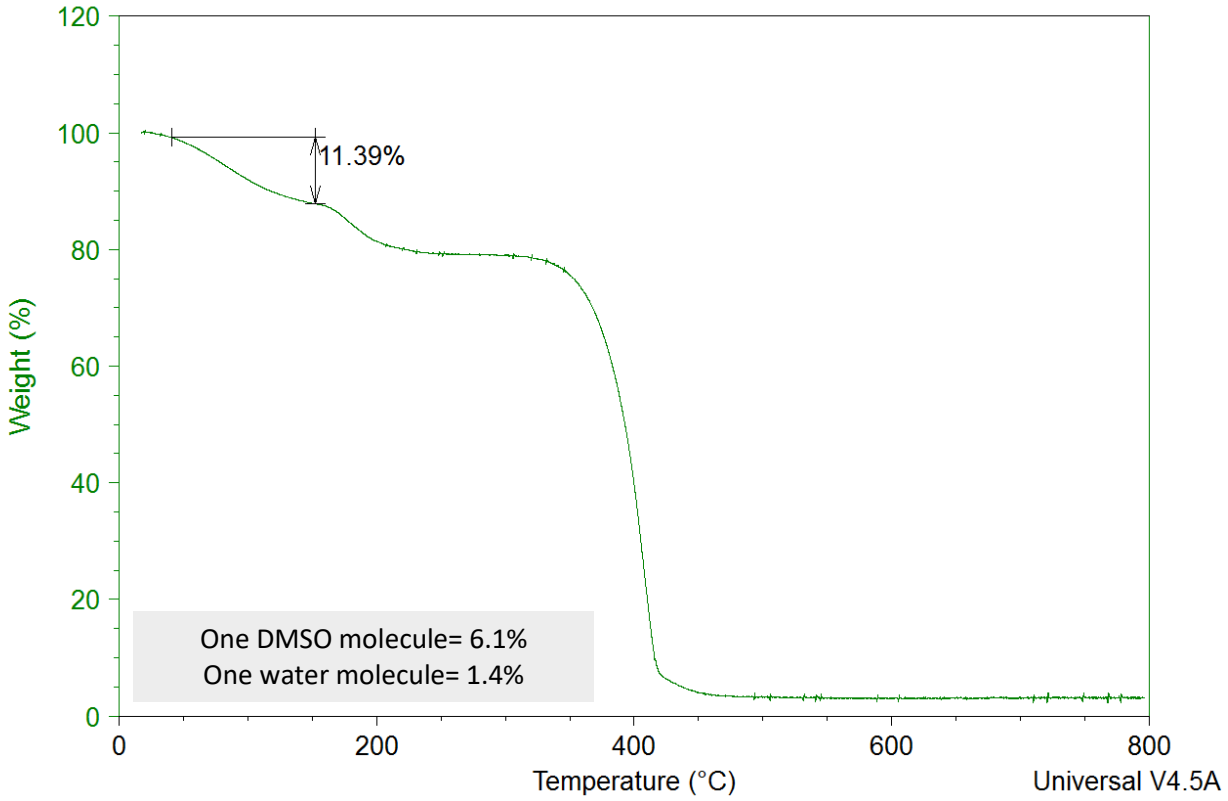

C30. **T22** recrystallized from equimolar mixture of solvents

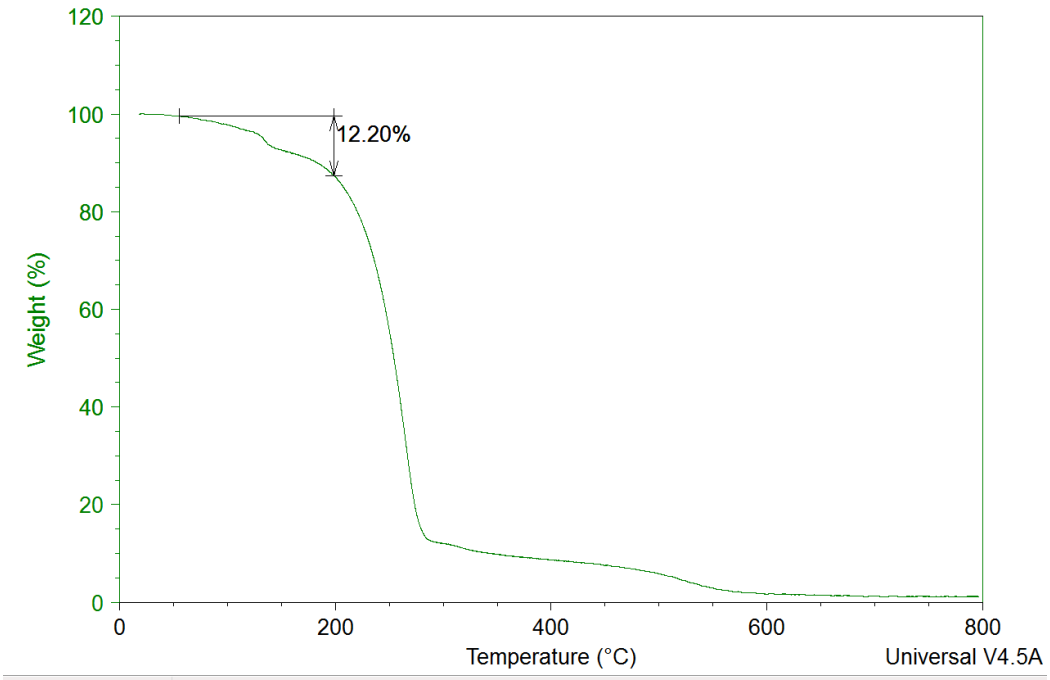

C31. **T23** recrystallized from xylene

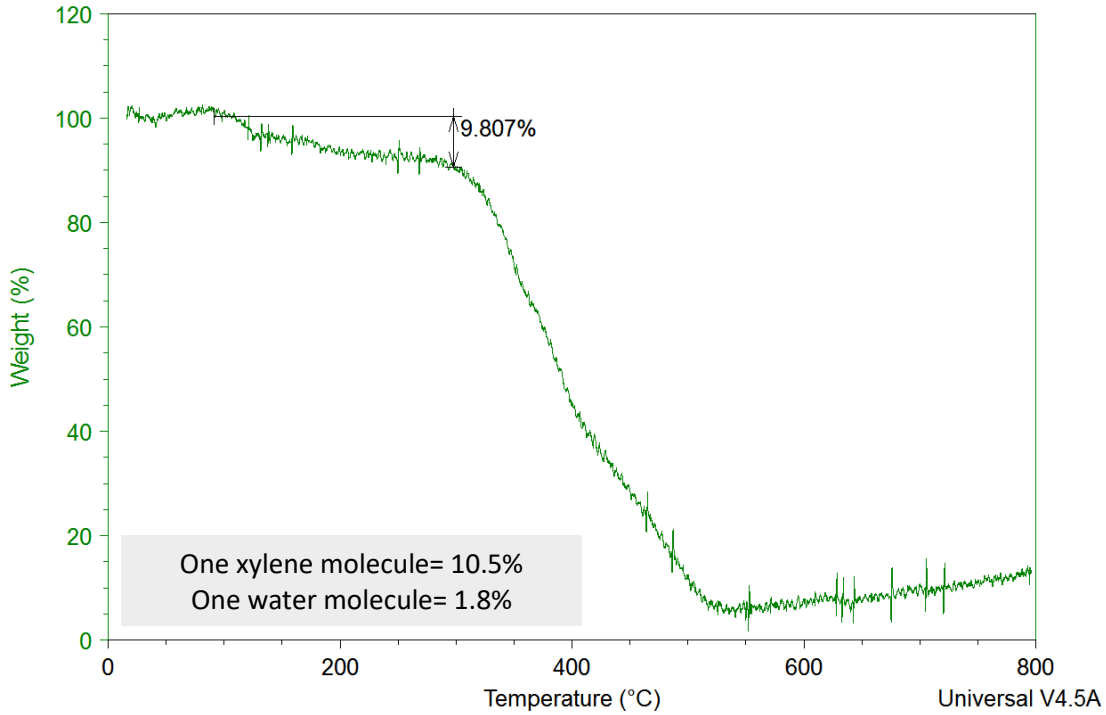

C32. **T23** recrystallized from dichloromethane (DCM)

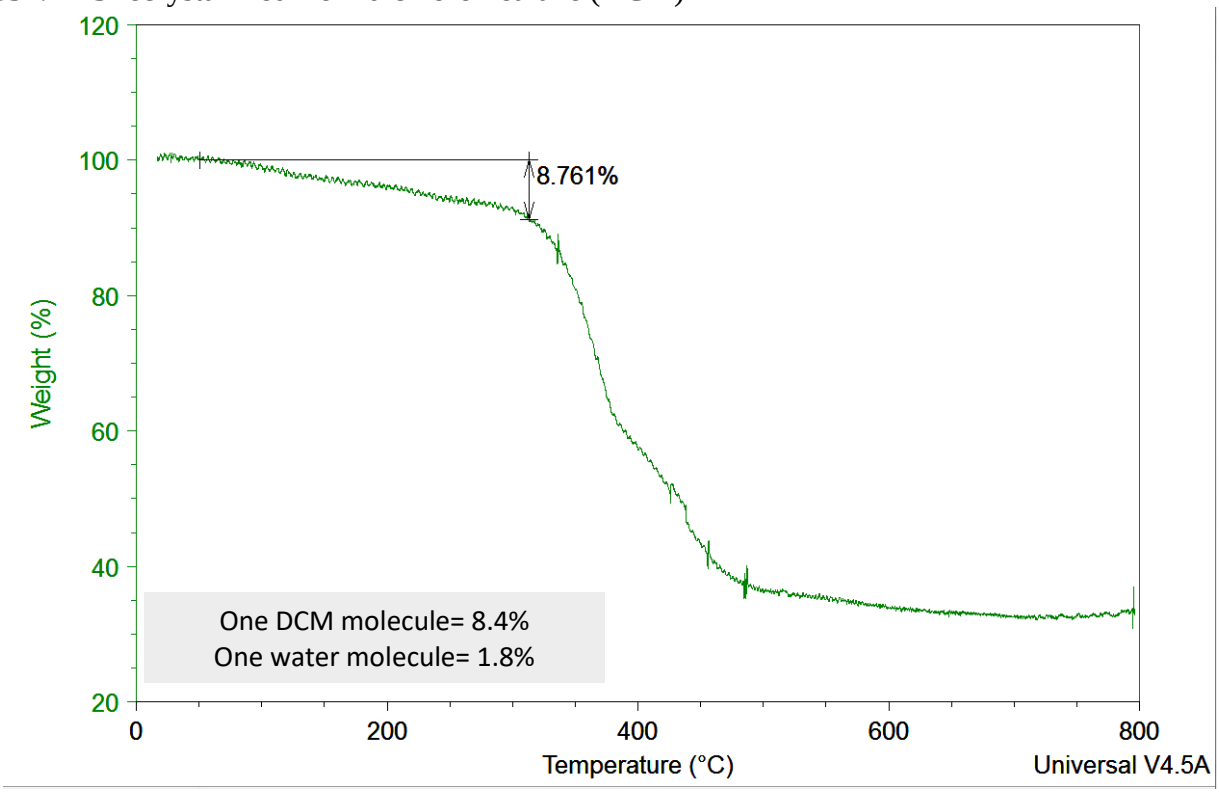

C33. **T23** recrystallized from ethyl acetate (EtOAc)

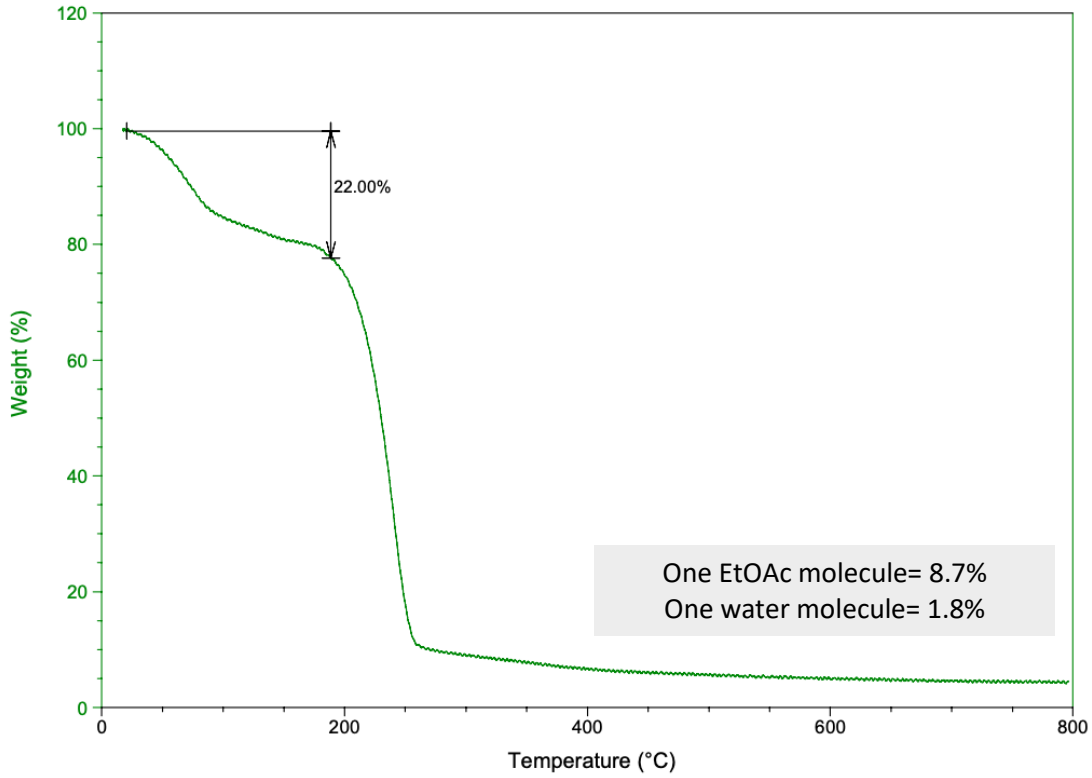

C34. **T23** recrystallized from acetonitrile (ACN)

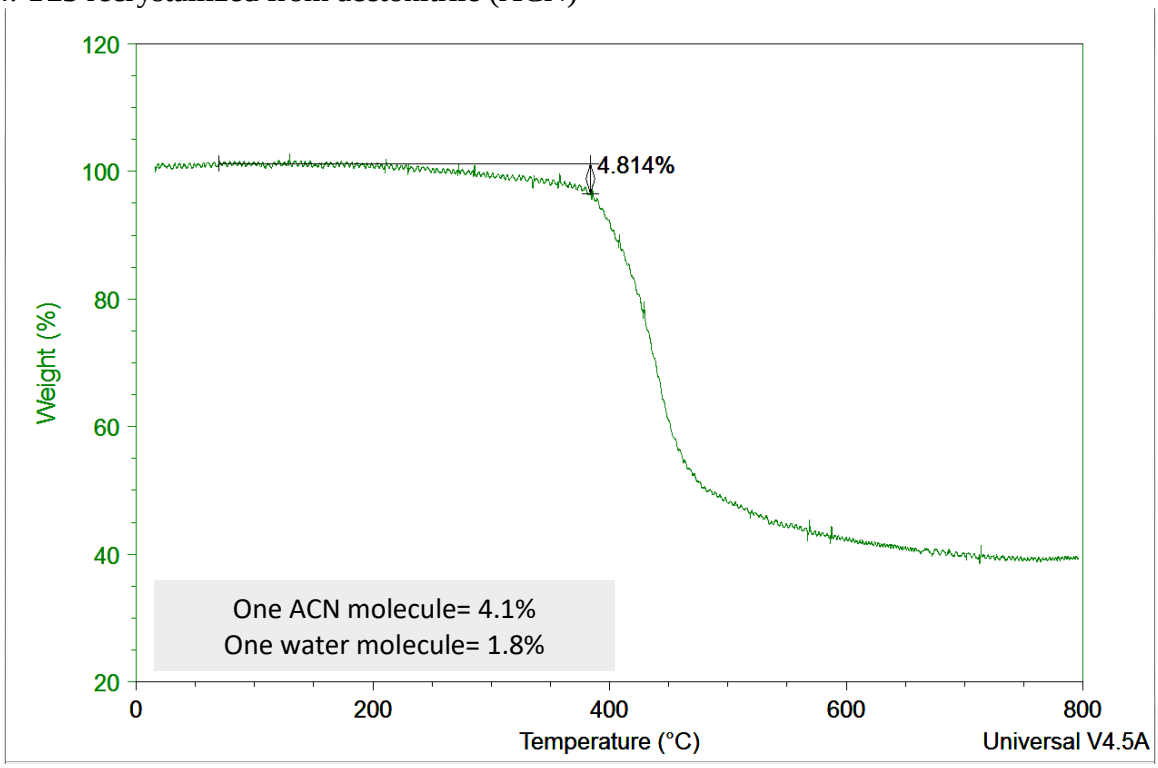

C35. **T23** recrystallized from dimethyl sulfoxide (DMSO)

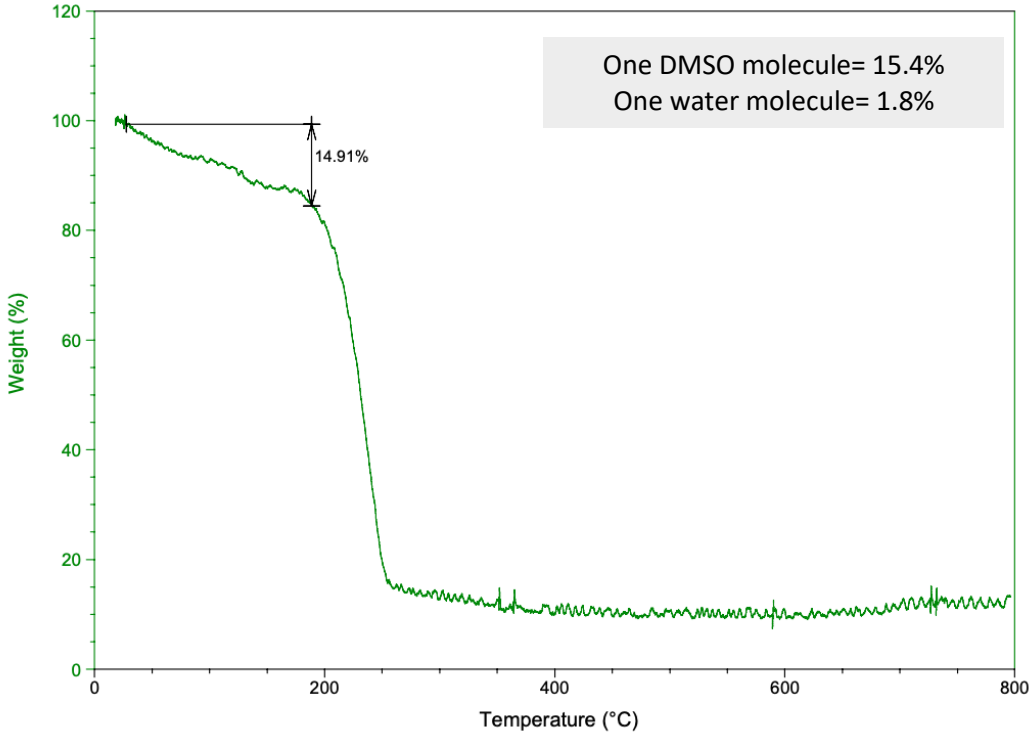

C36. **T23** recrystallized from equimolar mixture of solvents

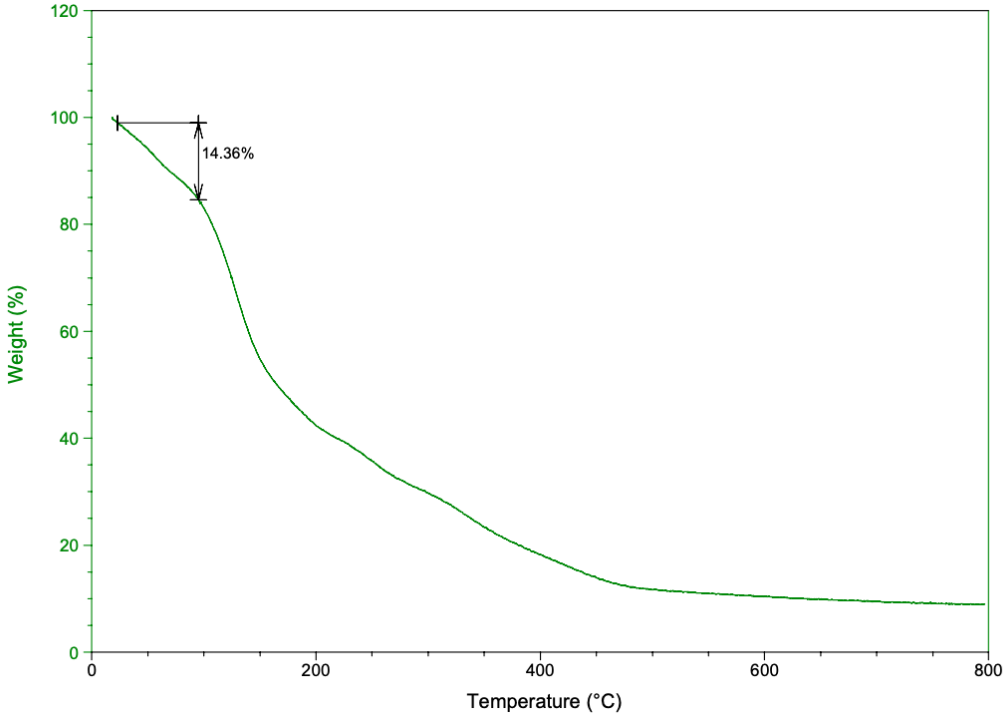

C37. **T24** with Isoborneol

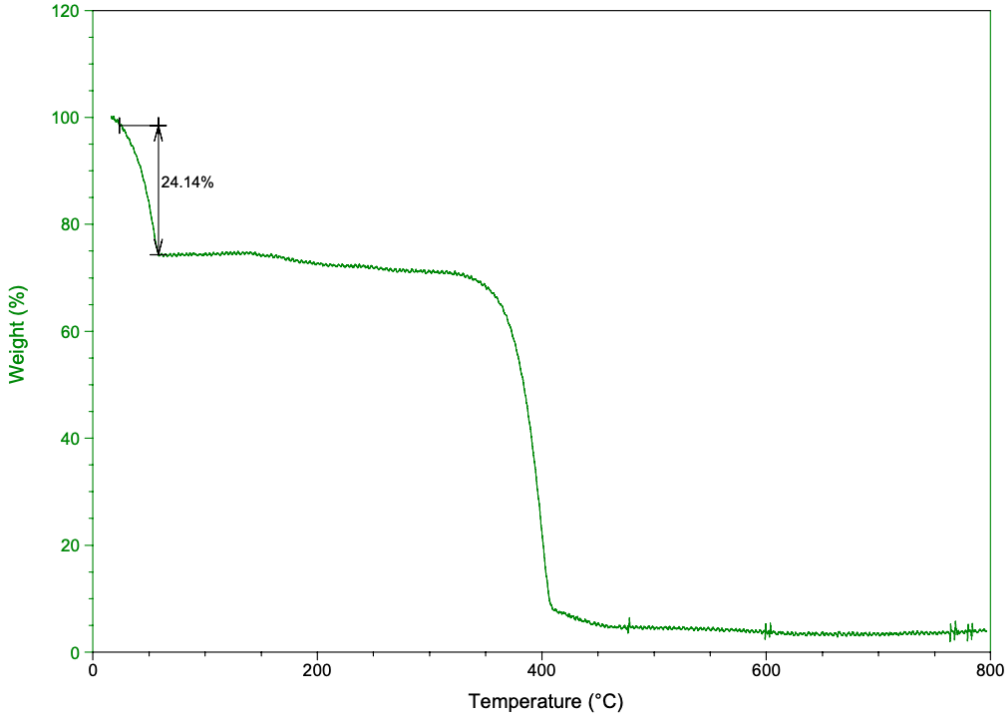

C38. **T24** with Menthol

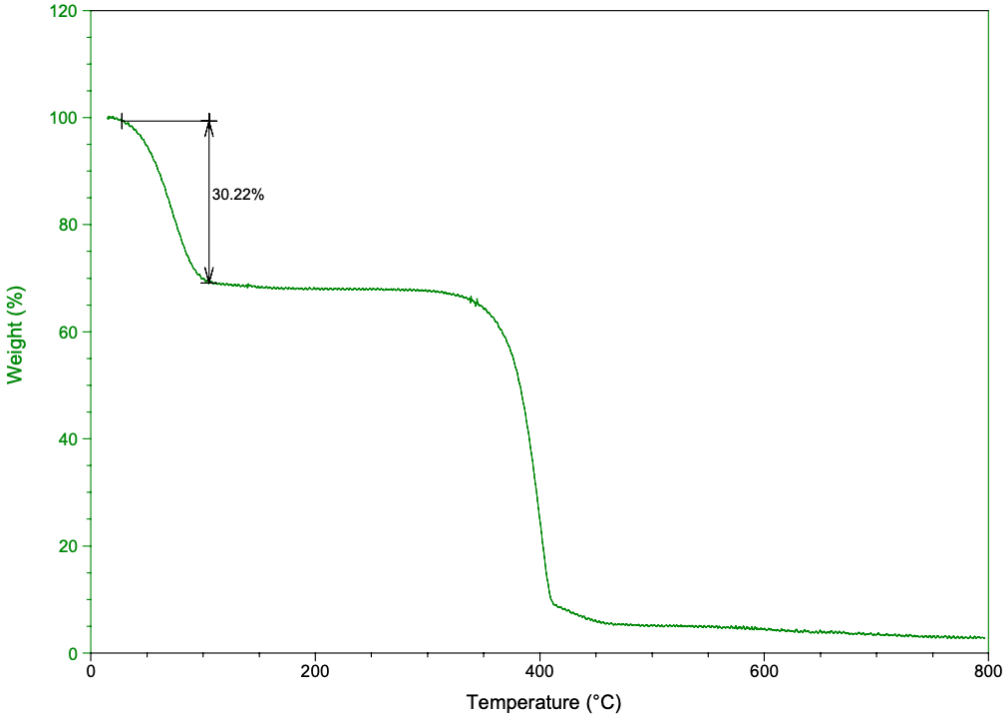

C39. **T25** with Isoborneol

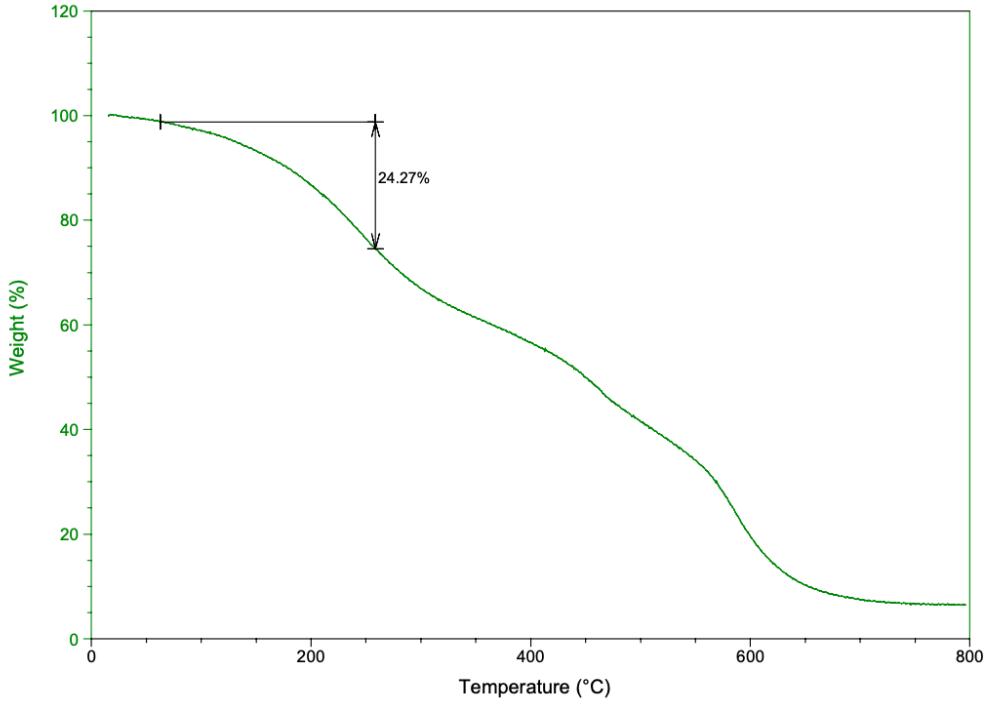

C40. **T25** with Menthol

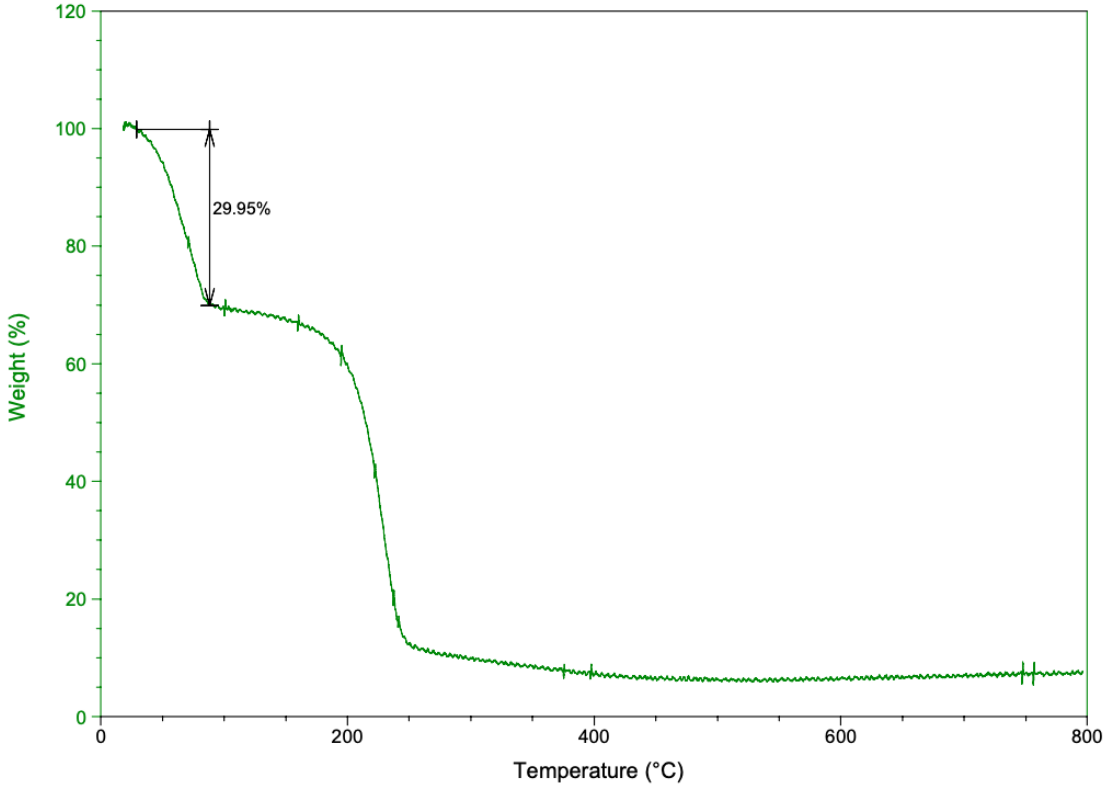

C41. Selectivity of **T25** between Menthol and 2-Methylbutyric acid

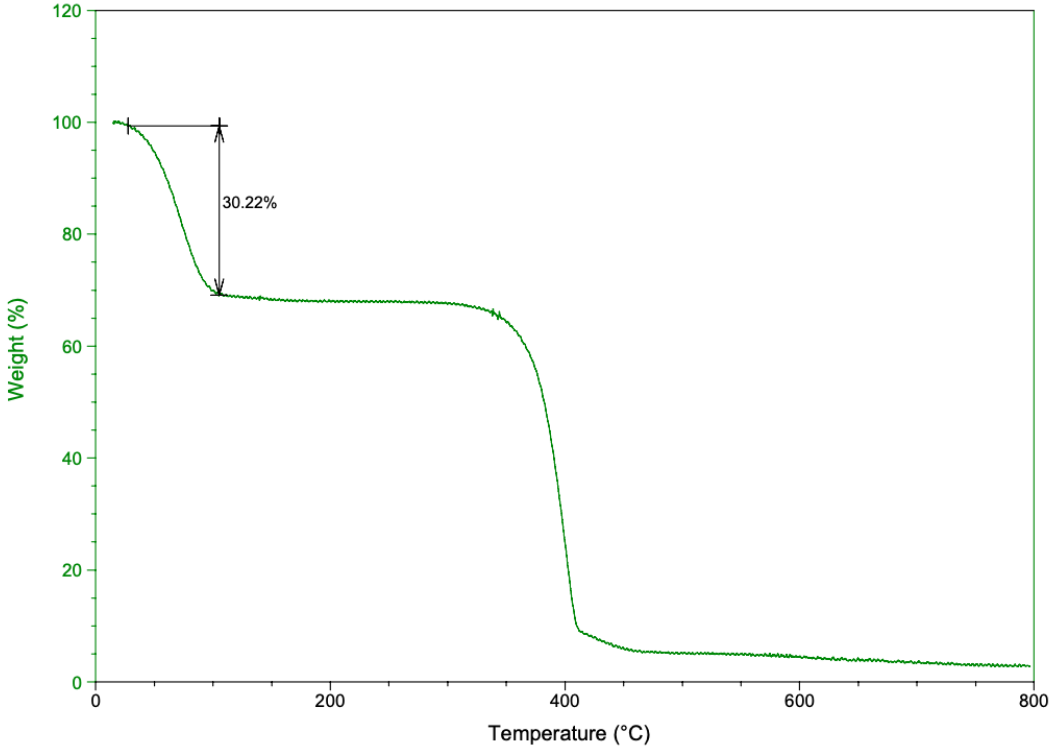

C42. Selectivity of **T25** between Menthol and 2-Methylpentanoic acid

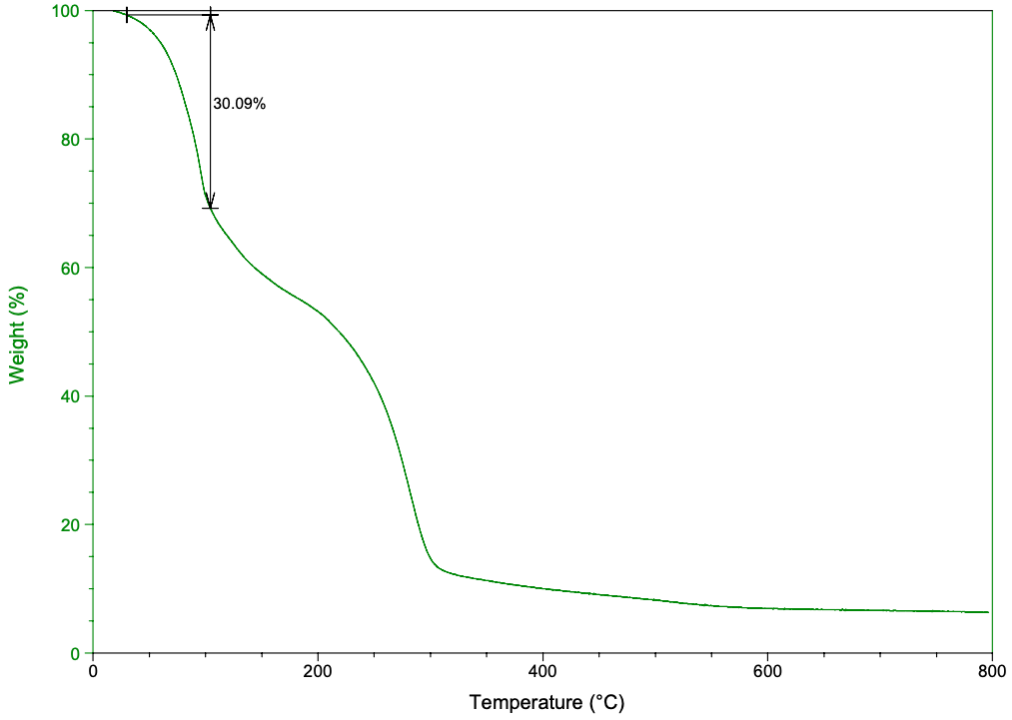

C43. Selectivity of **T25** between Menthol and 2-Methylhexanoic acid

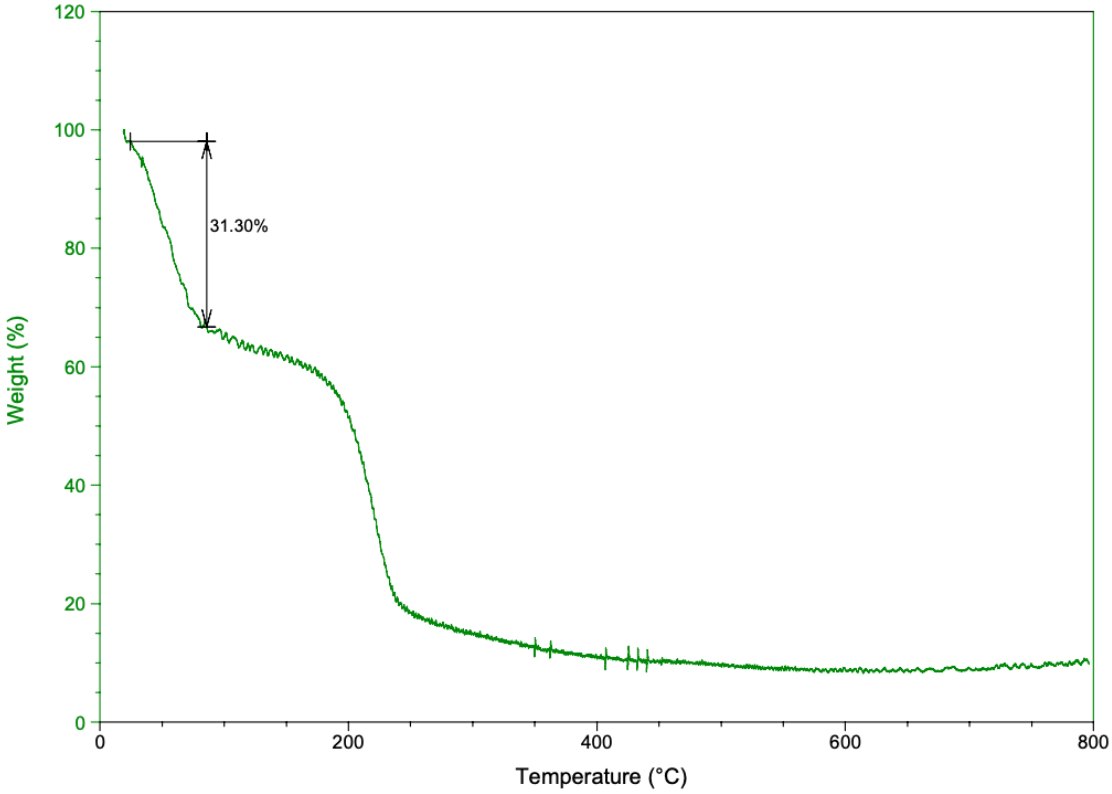

C44. Selectivity of **T25** between Isoborneol and 2-Methylbutyric acid

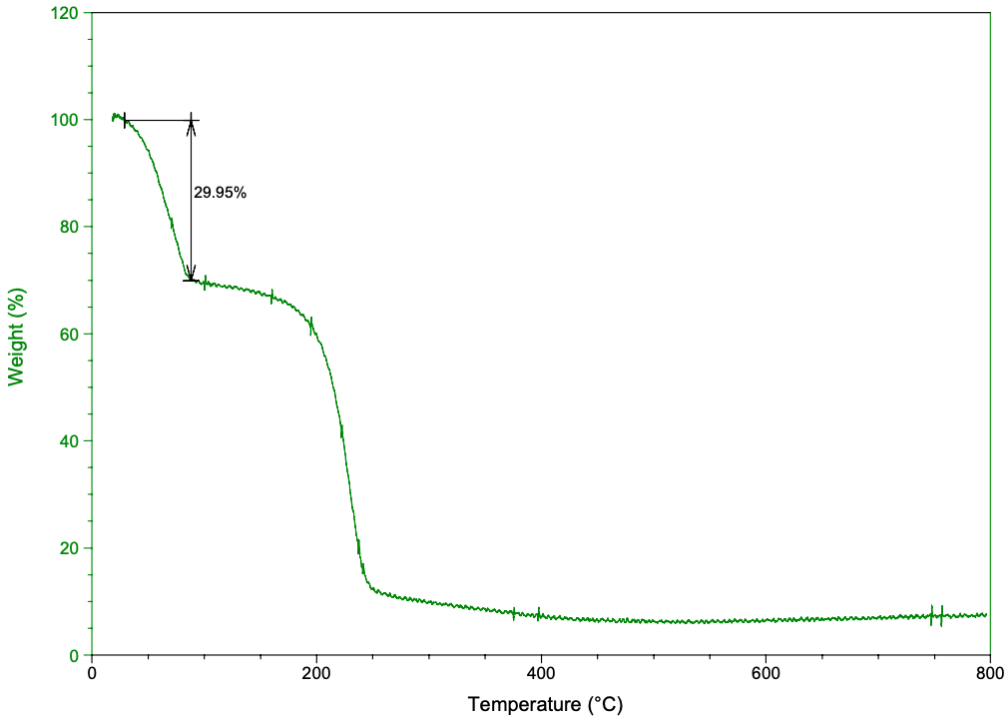

C45. **T27** with 3-Picoline-N-oxide

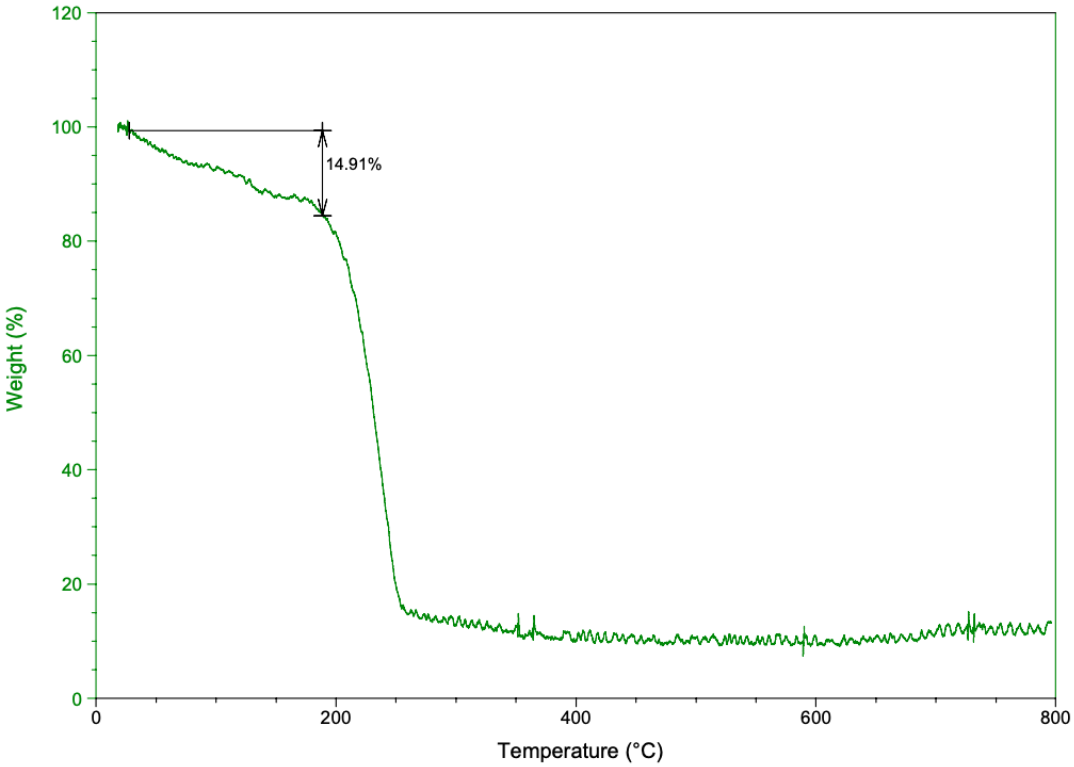

C46. **T27** with 4-Picoline-N-oxide

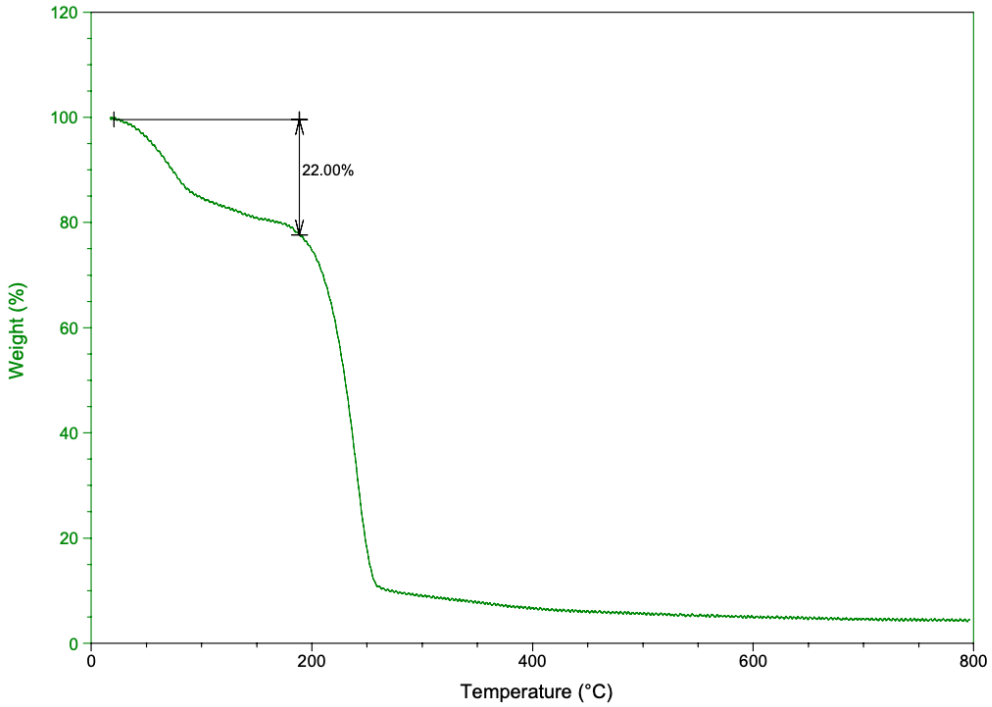

C47. **T27** with Pyridine-N-oxide

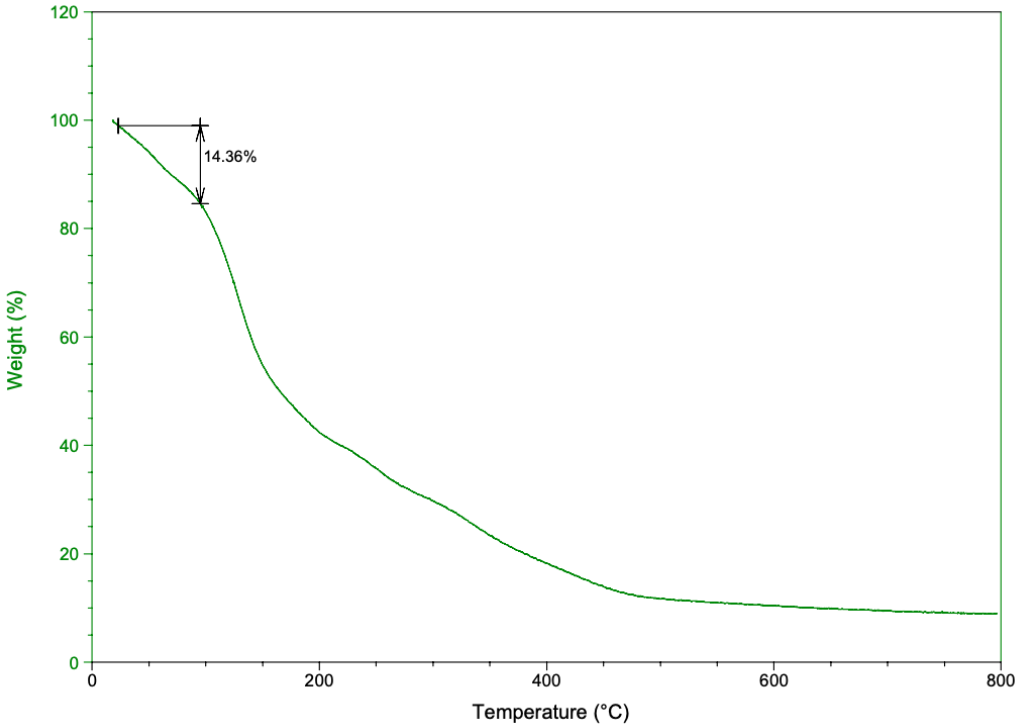

C48. **T27** with Pyrazine-N-oxide

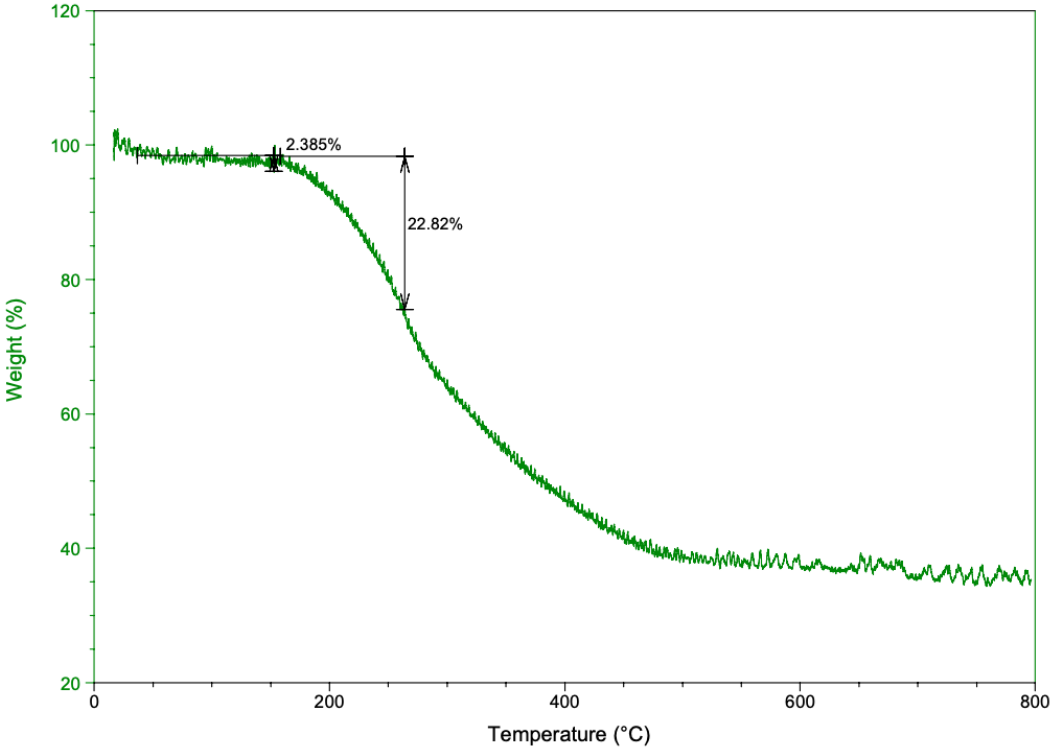

Appendix D – Jobs Plot

D1. **T24** in combination with 2-Methylbutyric acid.

1:2 host-guest stoichiometry

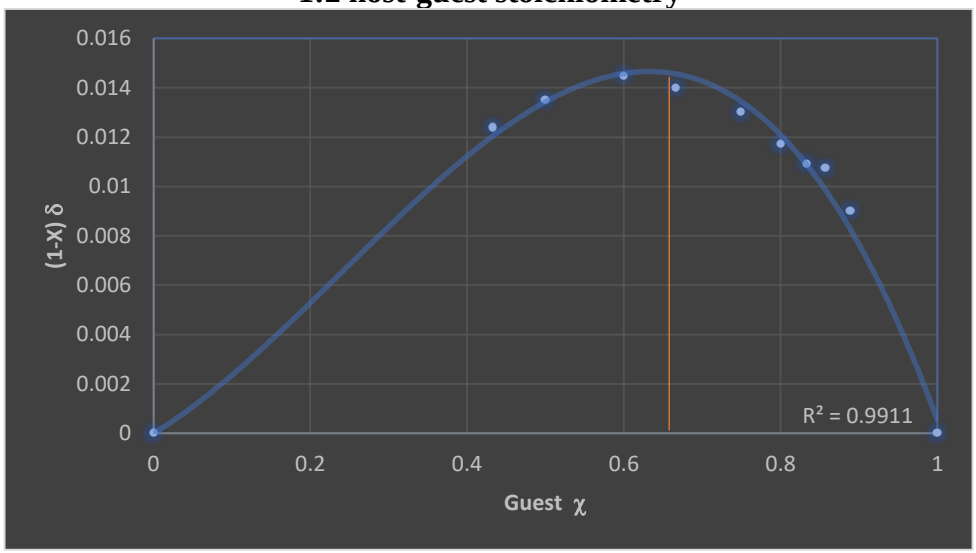

D2. **T24** in combination with 2-Methylpentanoic acid.

1:2 host-guest stoichiometry

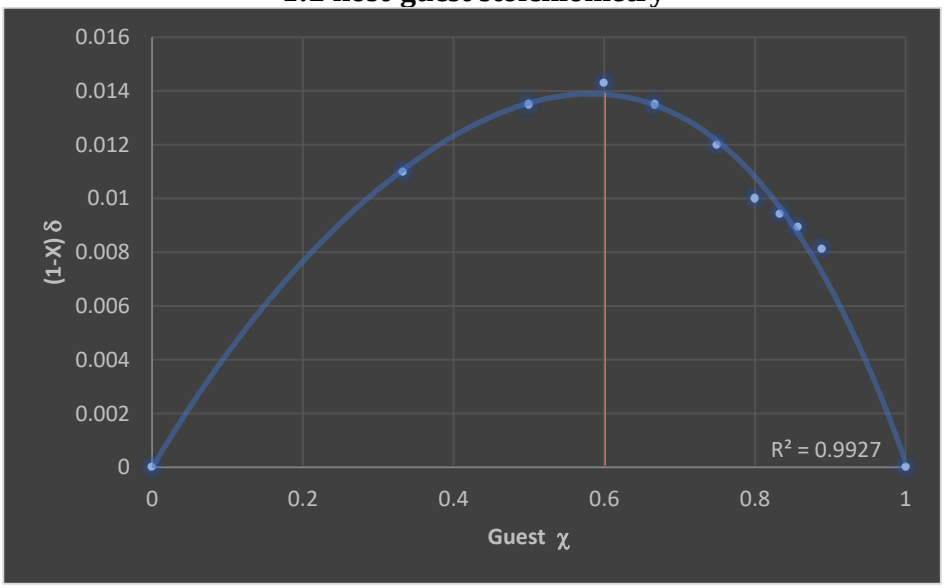

D3. **T24** in combination with 2-Methylhexanoic acid.

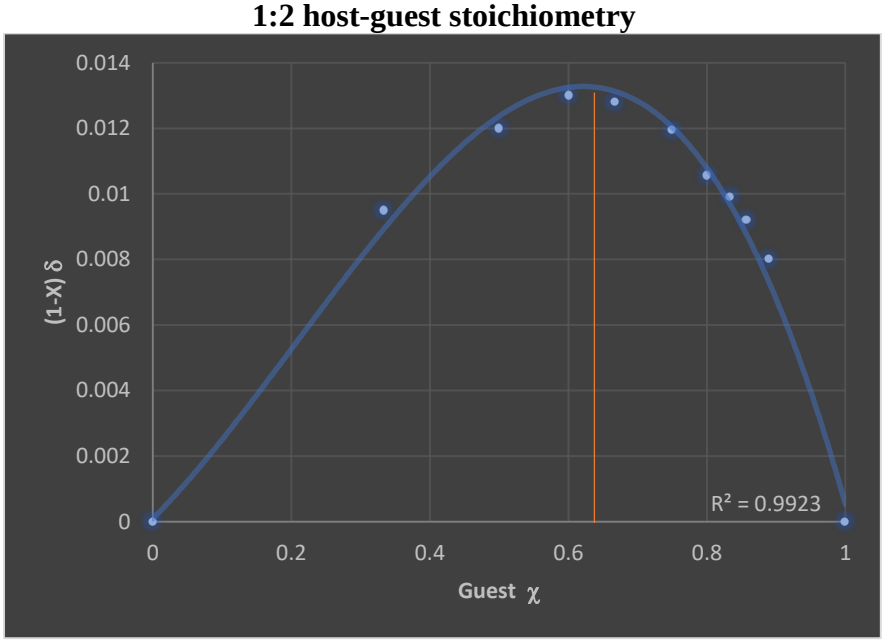

D4. **T24** in combination with Menthol.

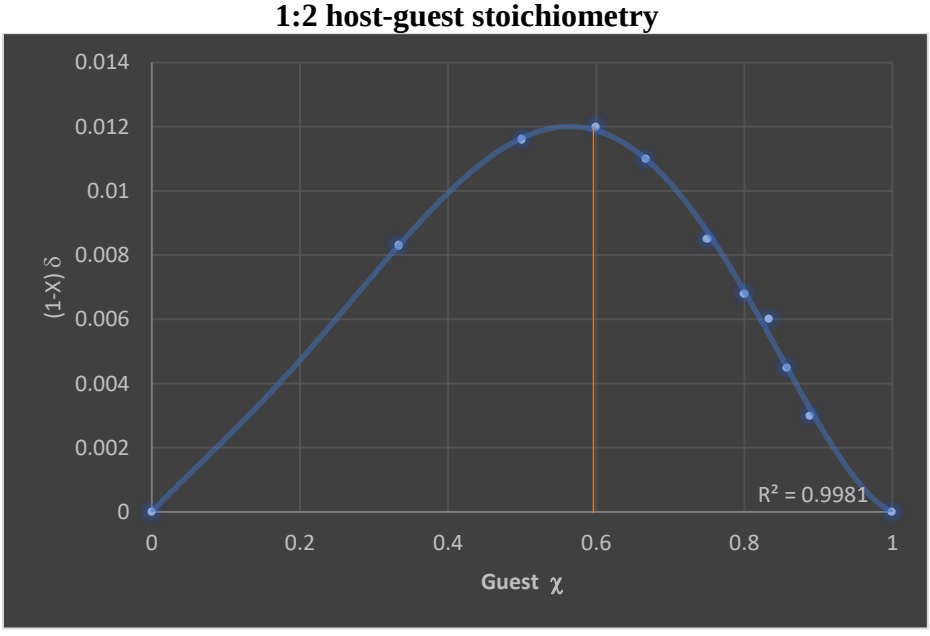

D5. **T24** in combination with Isoborneol.

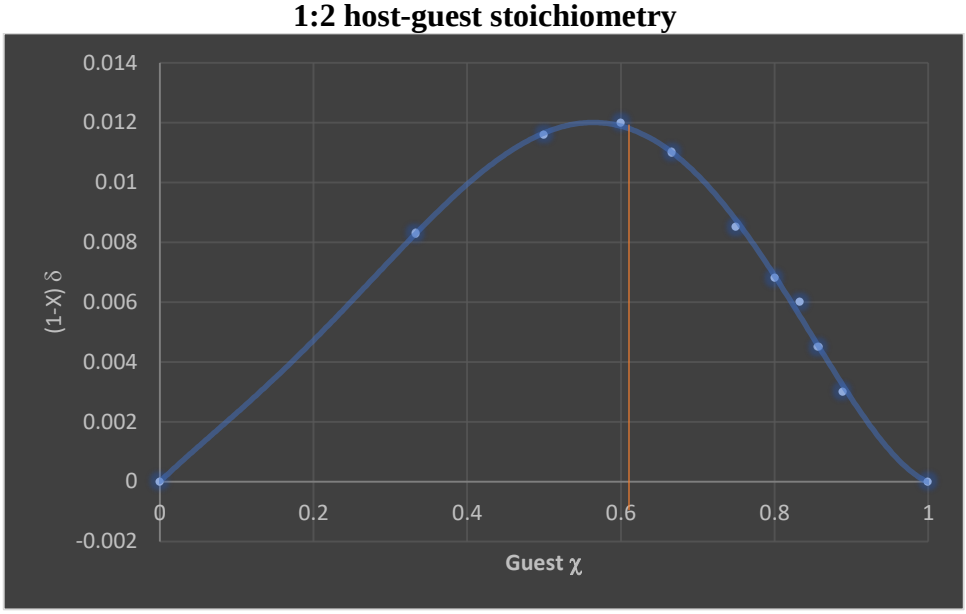

D6. **T24** in combination with Benzoic acid.

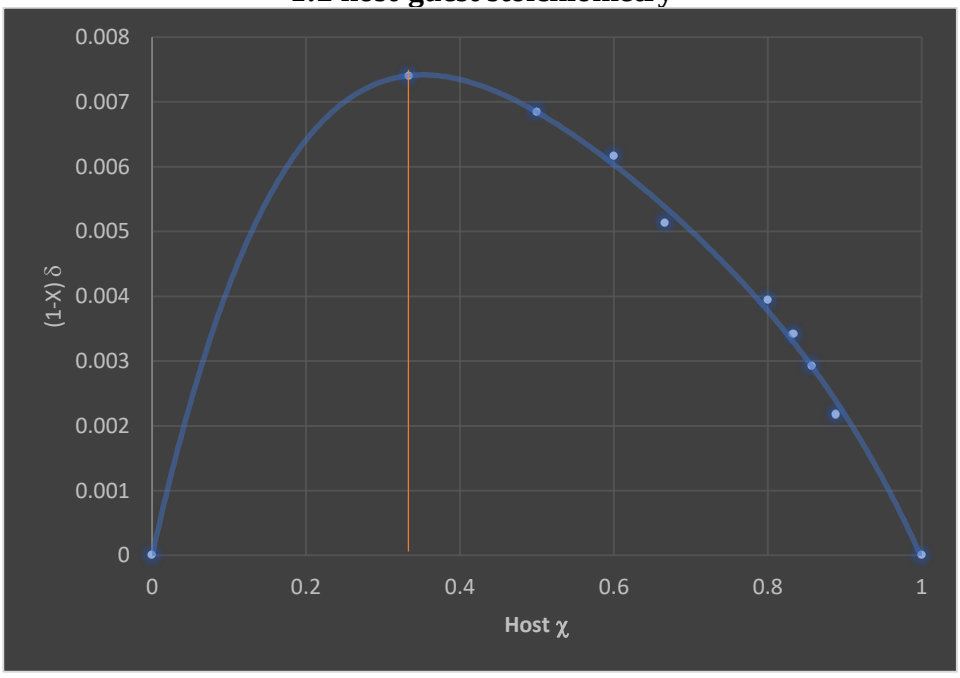

D7. **T25** in combination with Menthol.

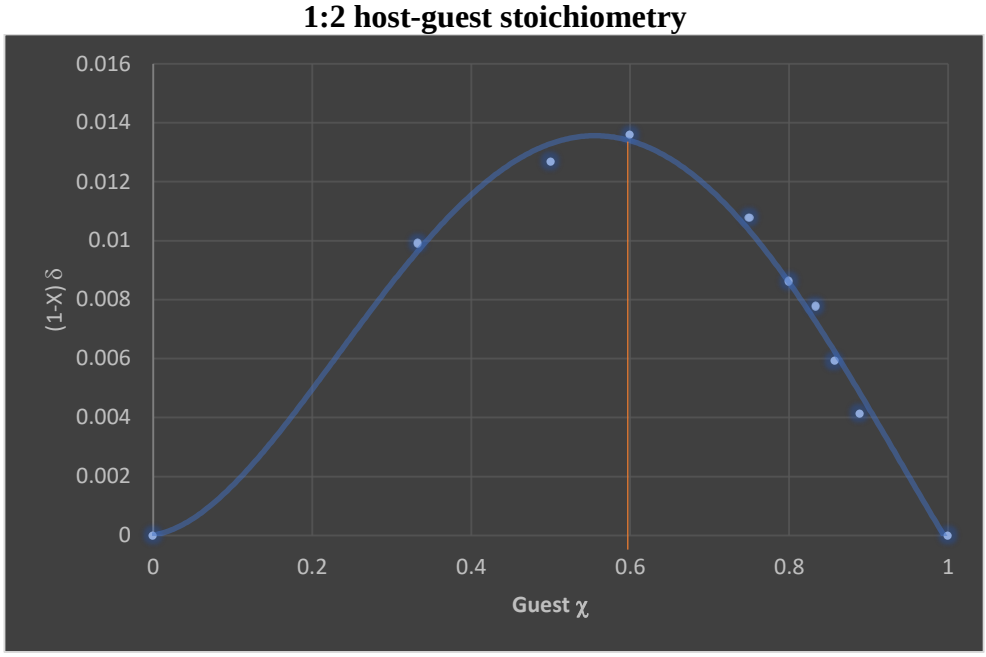

D8. **T25** in combination with Benzoic acid.

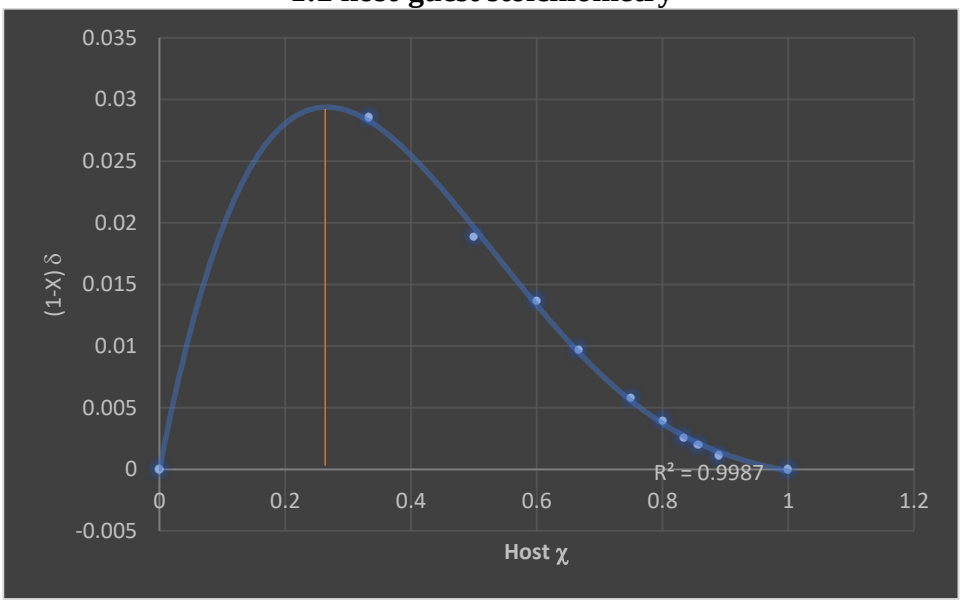

D9. **T27** in combination with 3-Picoline-N-oxide.

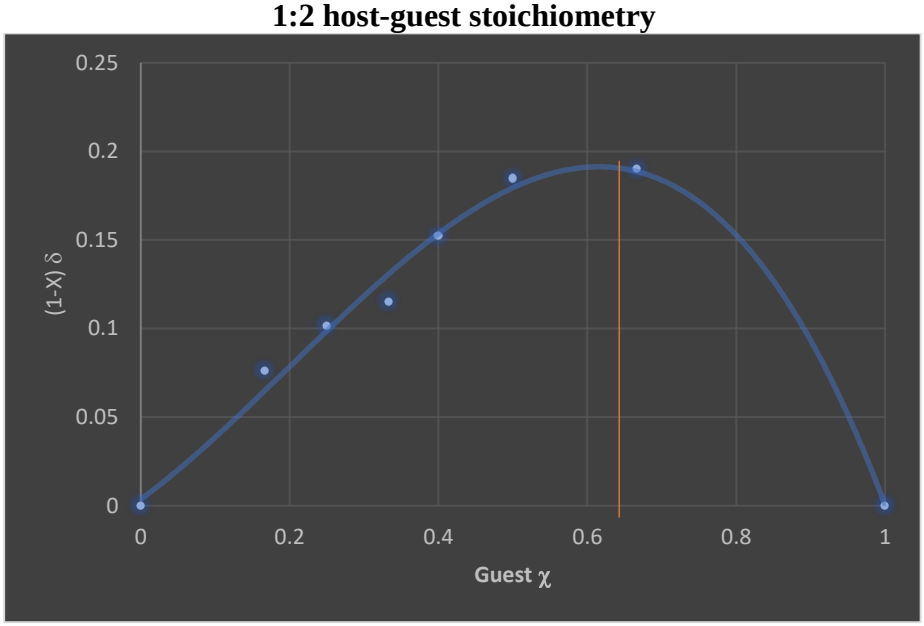

D10. **T27** in combination with 4-Picoline-N-oxide.

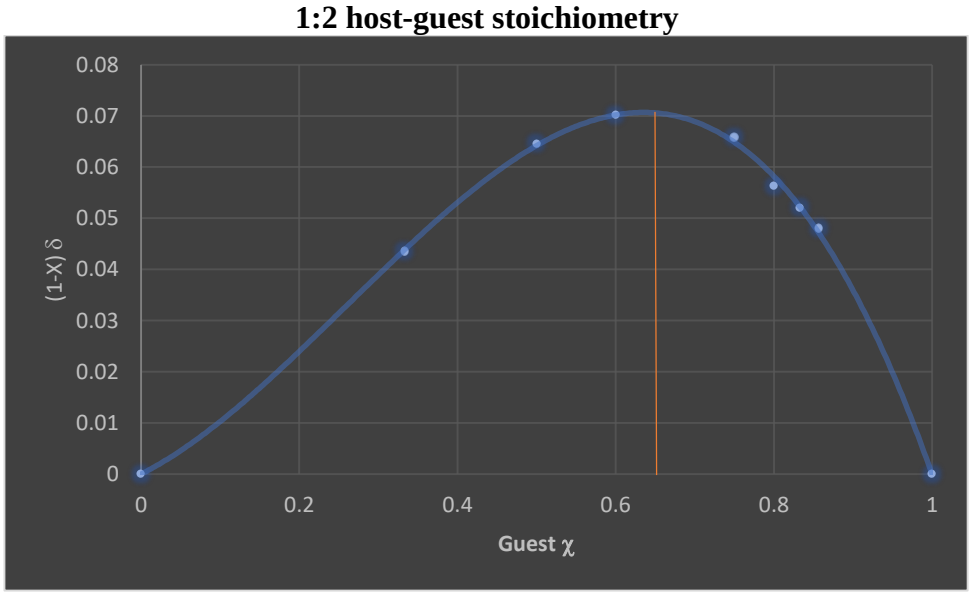

D11. **T27** in combination with 4-Pyridine-N-oxide.

1:2 host-guest stoichiometry

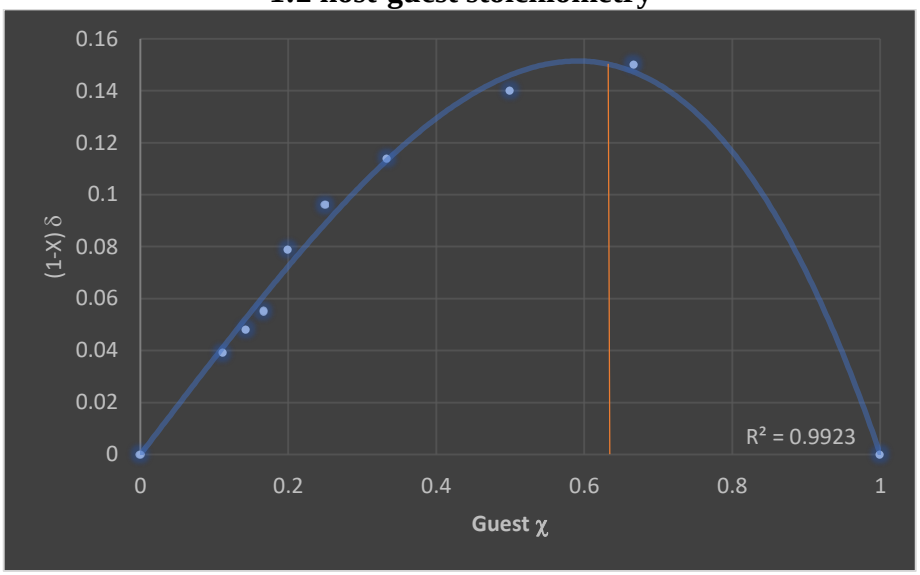

D12. **T27** in combination with 4-Pyrazine-N-oxide.

1:2 host-guest stoichiometry

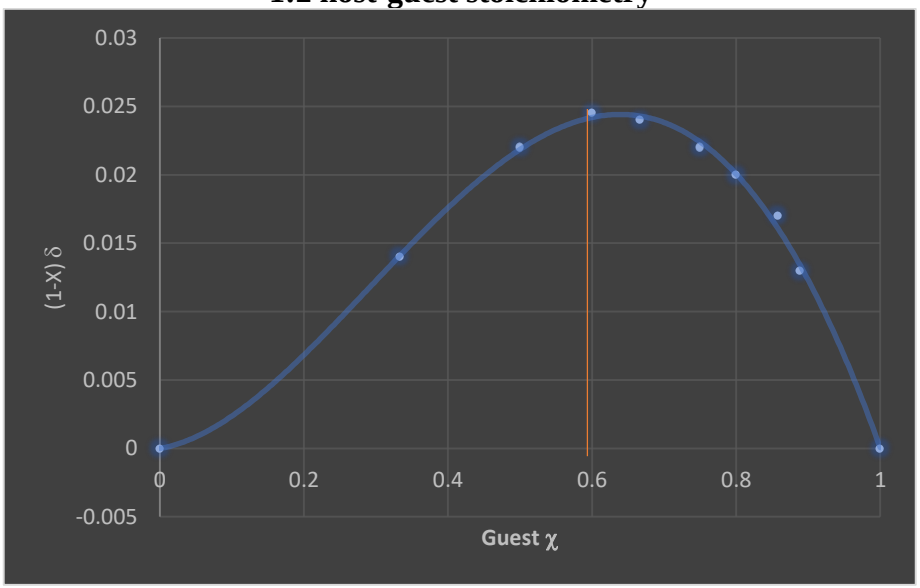

Appendix E – Crystallography Table

Code	**T18:xylene**	**T18**	**T18:$(EtOAc)_2$**	**T18:ACN**	**T18:DMSO**
Formula moiety	$C_{56}H_{68}Br_4O_8$, C_8H_{10}	$C_{56}H_{68}Br_4O_8$	$(C_{64}H_{84}Br_4O_{12})$ $(C_4H_8O_2)_{0.5}$	$C_{56}H_{68}Br_4O_8$, C_2H_3N	$C_{56}H_{68}Br_4O_8$, C_2H_6OS
Empirical formula	$C_{64}H_{78}Br_4O_8$	$C_{56}H_{68}Br_4O_8$	$C_{64}H_{84}Br_4O_{12}$	$C_{58}H_{71}Br_4NO_8$	$C_{56}H_{68}Br_4O_8$
Molecular weight	1294.90	1188.74	1364.95	1229.79	1266.87
Color, Habit	Colorless, Rectangular	Colorless, Needles	Colorless, Plates	Colorless, Rectangular	Colorless, Rectangular
Crystal system	Monoclinic	Orthorhombic	Monoclinic	Monoclinic	Monoclinic
Space group, *Z*	*P121/n1*, 4	*Pbca*, 4	*P121/c1*, 4	*P121/c1*,4	*P121/c1*,4
a, Å	11.9255(7)	29.4357(12)	15.5083(4)	18.2598(7)	18.730(2)
b, Å	17.9854(10)	17.4607(7)	23.6111(6	17.4497(7)	25.524(3)
c, Å	27.7020(16)	61.265(3)	18.3214(5)	18.8784(7)	12.8330(14)
α, º	90	90	90	90	90
β, º	94.3430(10)	90	107.8770(10)	111.954(2)	91.112(6)
γ, º	90	90	90	90	90
Volume, $Å^3$	5924.6(6)	31488(2)	6384.8(3)	5579.0(4)	6133.9(12)
Density, g/cm^3	1.452	1.505	1.420	1.464	1.372
T, ºK	199.99	199.99	273.(2)	296.(2)	296.15
Crystal size, min x mid x max	0.28 x 0.24 x 0.13	0.48 x 0.19 x 0.09	0.325 x 0.105 x 0.070	0.390 x 0.100 x 0.090	0.23 x 0.12 x 0.10
X-ray wavelength, Å	1.54178	1.54178	1.54178	1.54178	1.54178
μ, mm^{-1}	3.743	4.170	3.549	3.948	3.924
Trans min / max	0.7531 / 0.6098	0.239 / 0.705	0.639/ 0.79	0.39/ 0.72	0.466/ 0.695
θ_{min}, º	2.932	2.081	2.99	2.61	2.359
θ_{max}, º	68.210	68.251	69.97	69.92	67.586
Reflections					
collected	53980	169575	62416	70021	35608

independent	10556	28264	11530	10015	9931
observed	10300	24204	10627	9306	7916
R_{int}	0.0284	0.0571	0.0480	0.1295	0.0516
Threshold expression	> 2σ(I)	> 2σ(I)	> 2σ(I)	> 2σ(I)	> 2σ(I)
No. parameters	679	1849	730	645	655
No. restraints	7	0	0	0	0
R_1 (observed)	0.0372	0.0756	0.0558	0.0634	0.2405
wR_2 (all)	0.0957	0.1860	0.1435	0.1664	0.6116
Goodness of fit (all)	1.065	1.141	1.085	1.040	3.107
ρ_{max}, ρ_{min}, e Å^{-3}	1.066, -0.801	0.002, 0.000	1.411, -1.566	1.637, -1.761	3.242, -2.130
Completeness to 2θ limit	0.974	0.981	0.952	0.949	0.896

Code	**T19:xylene**	**T19**	**T19:DMSO**	**T21:DMSO**
Formula moiety	$C_{56}H_{68}I_4O_8$, C_8H8	$C_{56}H_{68}I_4O_8$	$C_{56}H_{68}I_4O_8$ $2(C_2H_6OS)$	$C_{64}H_{72}Br_4O_8$, $2(C_2H_6OS)$
Empirical formula	$C_{56}H_{68}I_4O_8$	$C_{56}H_{68}I_4O_8$	$C_{56}H_{68}I_4O_8$	$C_{64}H_{72}Br_4O_8$
Molecular weight	1472.78	1376.70	1532.96	1125.47
Color, Habit	Colorless, Rectangular	Colorless, Needles	Colorless, Rectangular	Colorless, Rectangular
Crystal system	Monoclinic	Monoclinic	Monoclinic	Monoclinic
Space group, Z	*C12/c1*, 4	*P 21/c1*, 4	*P121/c*, 4	*P121/c1*,4
a, Å	36.3616(16)	18.8079(14)	19.9328(5)	18.9835(6)
b, Å	14.9480(7)	16.3640(11)	12.3491(3)	25.5744(8)
c, Å	23.2062(10)	18.9127(13)	26.6063(6)	12.7022(4)
α, º	90	90	90	90
β, º	101.6480(10)	109.738(2)	105.2720(10)	92.5190(10
γ, º	90	90	90	90
Volume, Å^3	12353.6(10)	5478.8(7)	6317.9(3)	6160.9(3)

Density, g/cm^3	1.584	1.669	1.612	1.213
T, ºK	199.99	199.99	199.99	199.99
Crystal size, min x mid x max	0.22 x 0.19 x 0.17	0.33 x 0.17 x 0.075	0.125 x 0.06 x 0.05	0.55 x 0.17 x 0.07
X-ray wavelength, Å	1.54178	1.54178	1.54178	1.54178
μ, mm^{-1}	16.256	18.275	16.539	1.243
Trans min / max	0.7530 / 0.6150	0.065/ 0.341	0.1766/ 0.5685	0.7531/ 0.5181
θ_{min}, º	3.206	2.496	2.298	2.330
θ_{max}, º	68.506	68.545	70.046	68.386
Reflections				
collected	35657	26870	31840	45296
independent	11003	9473	11437	11002
observed	9731	7255	9768	8929
R_{int}	0.0361	0.0892	0.0690	0.0362
Threshold expression	> 2σ(*I*)	> 2σ(*I*)	> 2σ(*I*)	> 2σ(*I*)
No. parameters	686	617	703	807
No. restraints	9	4	2	108
R_1 (observed)	0.1054	0.1572	0.0742	0.0554
wR_2 (all)	0.3157	0.4267	0.1903	0.1556
Goodness of fit (all)	2.675	1.750	1.069	1.025
ρ_{max}, ρ_{min}, e Å^{-3}	2.468, -1.314	4.173, -2.365	2.932, -2.466	0.352, -0.365
Completeness to 2θ limit	0.968	0.937	0.947	0.972